OPTIMIZATION OF USE OF FOURIER TRANSFORM INFRARED TO MEASURE THE COMPOSITION OF FINE PARTICULATE MATTER

by

VILMA MARIA ARRIARAN LA TORRE

A dissertation submitted to the Graduate Faculty in Engineering in partial fulfillment of the requirements for the degree of Doctor of Philosophy, The City University of New York

2011

This manuscript has been read and accepted for the
Graduate Faculty in Engineering in satisfaction of the
dissertation requirement for the degree of Doctor of Philosophy.

Prof. Beth Wittig

April 25, 2011 _____

Date Chair of Examining Committee

Prof. Mumtaz K. Kassir

April 25, 2011 _____

Date Executive Officer

Prof. Vasil Diyamandoglu

Prof. Reza Khanbilvardi

Prof. Urs Jans

Supervisory Committee

THE CITY UNIVERSITY OF NEW YORK

Abstract

OPTIMIZATION OF USE OF FOURIER TRANSFORM INFRARED TO MEASURE THE COMPOSITION OF FINE PARTICULATE MATTER

by

Vilma Maria Arriaran La Torre

Adviser: Professor Beth Wittig

The goal of this dissertation is to evaluate the feasibility of, and develop and optimize a method that uses FTIR to measure the detailed chemical composition of organics and inorganics in ambient fine particulate matter, $PM_{2.5}$. The use of FTIR will lead to the analysis of a $PM_{2.5}$ sample using a single technique, without the need for extraction, nondestructively and free of analysis artifacts.

This method has been used quantitatively despite issues that may limit its accuracy. This research has developed and evaluated optimal approaches of the FTIR operation, spectra interpretation and data reduction. Each component is addressed in a separate chapter of this dissertation, in terms of the challenges and issues, prior work to address the issue, the goal and proposed research to address the issue, and the results that have been obtained.

An algorithm that does not depend on path length and uses all parameters calculated during the spectral analysis was developed in order to determine the concentrations of the functional groups present in the sample and in the actual ambient air. For accurate quantitation results, all issues related with the spectral interpretation must be solved first before inserting them into the algorithms developed.

Sample analysis experiments were designed to effectively handle the sample analysis in the FTIR spectrometer. These experiments will help to get sample spectra free of interferents that may obscure the sample interpretation. FTIR may use two different techniques for analyzing the sample that may affect the signal to noise ratio if light does not penetrate through the whole sample, therefore aerosol samples collected on the optimal substrates must be analyzed by both techniques.

Experiments for sample interpretation were designed to select the best approach to interpret the IR spectra of aerosol samples. These spectra can be difficult to interpret since the samples contain billions of particles, each of which can contain millions of chemicals. Functional groups in the aerosol spectra has to be identified and their ABS areas accurately measured by defining the correct baselines and end points of the functional group peaks. ABS measurements of targeted functional group at different concentrations were evaluated to determine the linearity of ABS and their relative molar absorptivities. This information will be used to identify, evaluate and determine the correct approaches to split overlapping functional group peaks.

Acknowledgments

I want to thank God for his guidance, love and protection and for giving me the opportunity to accomplish one of the goals of my life.

Thanks to my grandparents who are the angels that always protect me and give me the strength to accomplish my goals.

Thanks to my parents, brothers and all my family for all the support they gave me during these years of study, they were my motivation for continuing my professional and personal development.

Thanks to all people I have met during these years of study, for their friendship, and all the support received from them.

Thanks to my adviser for believe in my capacity to do research with her and to pursue my doctoral degree.

TABLE OF CONTENTS

LIST OF TABLES

LIST OF FIGURES

CHAPTER 1 INTRODUCTION

The goal of this work is to investigate the feasibility of using FTIR to measure the composition of particles in the ambient air, and to develop and optimize a method for its use in the process.

1.1. $PM_{2.5}$ CHARACTERISTICS

The focus of this work is on particulate matter suspended in the ambient air that is smaller than 2.5μm in aerodynamic diameter. These particles are interchangeably known as $PM_{2.5}$, fine particles, or fine aerosols.

Not all fine particles are the same size. The typical size distribution of ambient particles in an urban area is shown in **Figure 1-1**.

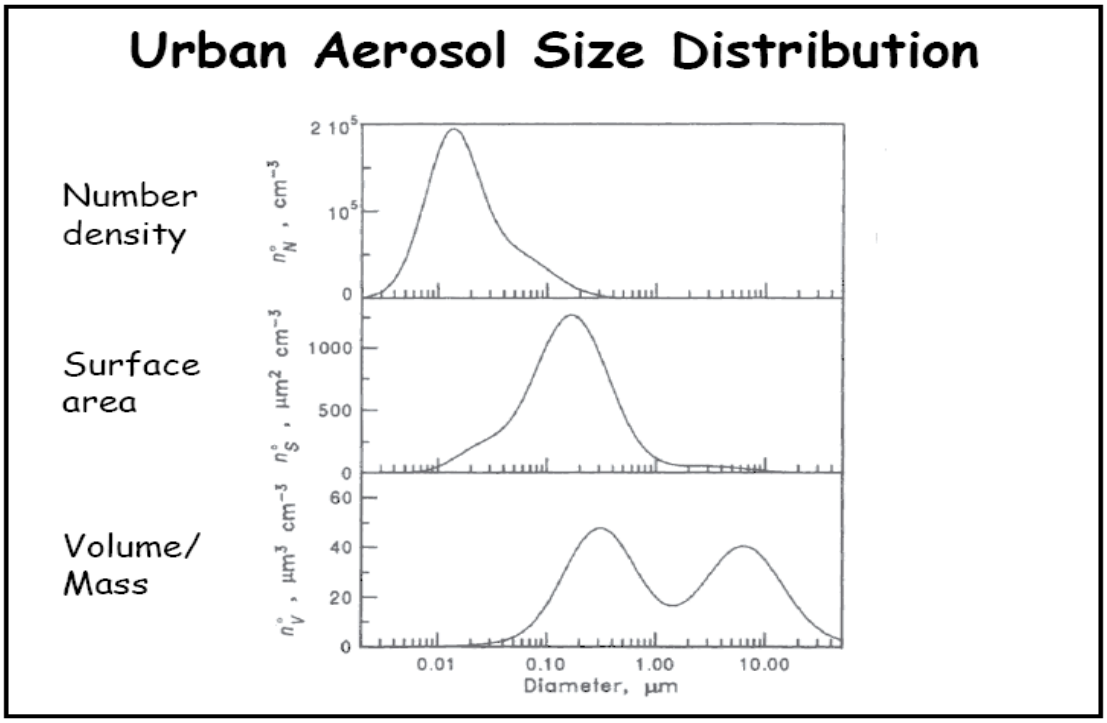

Figure 1- 1 Urban aerosol size distribution (Seinfield and Pandis, 1998)

Particles are usually described by their size. Ultrafine particles have aerodynamic diameters from 0.002 to 0.1 micrometers and usually comprise the largest number of particles. Fine particles have aerodynamic diameters from 0.1 to 2.5 micrometers and usually make up the largest amount of surface area, and to some extent mass, of particles. Course particles have aerodynamic diameters from 2.5 to 10 micrometers and account for the majority of the mass of urban particles.

There are two different types of sources of fine particles: primary and secondary. Primary particles are directly released from a source or suspended as particles. Most coarse particles are primary (e.g. dust, pollen, plant and insect parts). Some fine particles are primary: suspended dust from roads or emissions from combustion activities. Ultrafine particles are rarely primary.

Secondary particles are formed in the atmosphere from other particles or by photochemical reaction of precursor gases. Most ultrafine particles are formed by the homogeneous nucleation of gases to form particles or by the condensation of semi-volatile gases onto smaller particles. Some ultrafine and many fine particles are formed by the coagulation of smaller particles with each other. Reactions of volatile gas phase precursors such as SO_2, NOx, VOCs and NH_3 form semi-volatile chemicals which then condense onto smaller particles, allowing them to gradually grow in size. Since particles smaller than 2.5 μm can be transported on the wind over thousands of kilometers from upwind areas, there is much opportunity for the secondary formation of particles. Many of these reactions are influenced by atmospheric meteorology such as temperature, solar irradiation and humidity. Since these particles are transported on the wind, they are also affected by wind speed and direction. During transport, they may be wet or dry deposited to the ground, and removed from the suspended phase. The various phenomena that affect particle composition and concentration are illustrated in **Figure 1-2.**

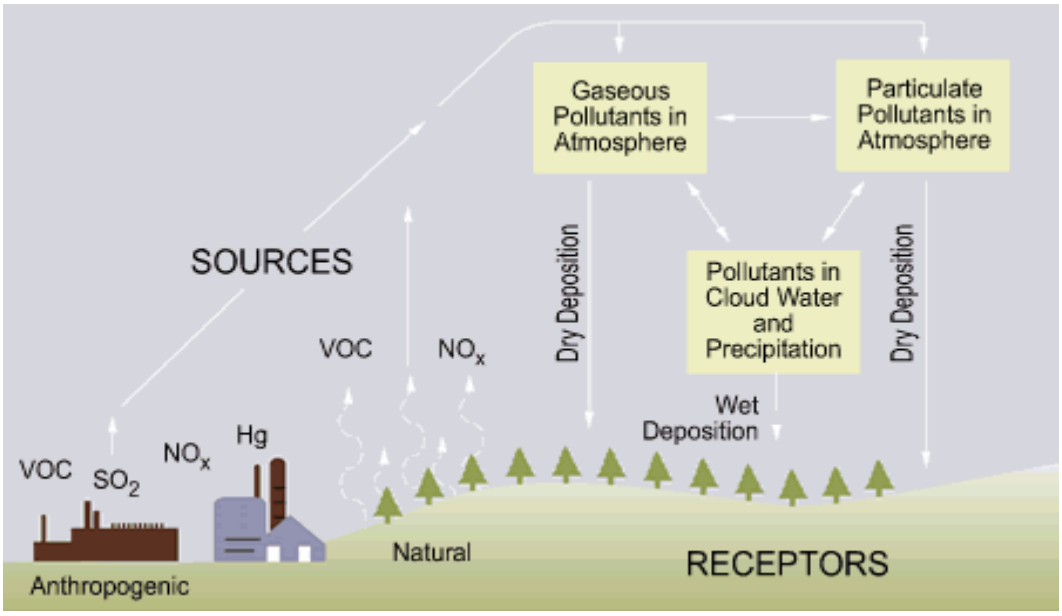

Figure 1- 2 Secondary sources of fine particles in the ambient air (EPA, June 8th 2007)

The diversity in the sources of fine particles causes great differences in chemical composition from particle to particle, from time to time, and from location to location. Some pure particles are possible but less likely in an urban area because of all of the secondary processes that create fine particles. Fine particles usually contain many different chemical components that can be broadly classified as inorganics, organics, and elements, as well as particle-bound water (Seinfield and Pandis, 1998). The ambient $PM_{2.5}$ in NYC measured in the summer of 2001 contained 60% inorganics (i.e., 30% sulfate, 15% nitrate and 15% ammonium), 36% organics, and 5% elements (i.e., metals and crustal material) and particle-bound water, on a mass basis (Schwab et al., 2004). The specific chemicals that are usually present in fine particles are given below.

Inorganic species	Organic species	Elemental species
Ammonium NH_4^+	Carbonate CO_3^{-2}	Aluminum Al
Bromide Br^-	Thousands of different molecules that contain Elemental Carbon (black carbon, graphitic carbon or soot)	Arsenic As
Chloride Cl^-		Bromine Br
Fluoride F^-		Cadmium Cd
Nitrate NO_3^-		Calcium Ca
Nitrite NO_2^-		Chlorine Cl
Phosphate PO_4^{3-}	Thousands of different molecules that contain Organic Carbon	Chromium Cr
Potassium K^+		Copper Cu
Sodium Na^+		Iron Fe
Sulfate SO_4^{2-}		Lead Pb
		Manganese Mn
		Nickel Ni
		Phosporus P
		Potassium K
		Selenium Se
		Silicon Si
		Sodium Na
		Sulfur S
		Titanium Ti
		Uranium U
		Vanadium V
		Zinc Zn

Table 1- 1 Chemical components typically found in ambient PM2.5

This work will develop and evaluate a method to measure $PM_{2.5}$ speciation which can be used to answer many pressing questions that pertain to environmental and human health.

1.2 AFFECTS OF $PM_{2.5}$ EXPOSURE

1.2.1. Human Health Impact

Exposure to ambient fine particulate matter can cause serious problems to public health. Fine particles may penetrate in the tracheobronchial and pulmonary region, shown in **Figure 1-3**, causing a range of respiratory system responses from sneezing, coughing, broncho-constriction, rapid, shallow breathing (Boudel et al, 1994) to lung cancer and cardiopulmonary disease (Lall et al, 2004) and even death.

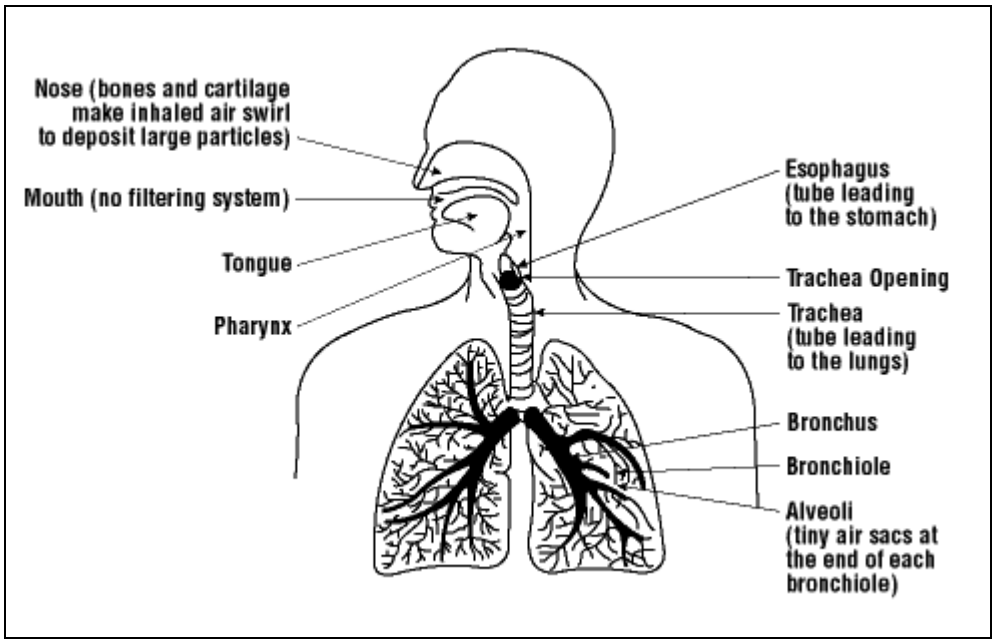

Figure 1- 3 Parts of the respiratory system affected by particulate matter inhalation (CCOHS, March 22 1999)

For example, in London in 1952, about 4000 people were killed in four days due to inhalation of excessive concentration of particles and sulfur that accumulated in the air due to stagnant weather conditions (Boudel et al, 1994).

Despite the clear association between fine particle exposure and health, epidemiologists do not know which components in the fine particles cause the observed health effects. To date, epidemiologists link chemicals species in $PM_{2.5}$ such as lead with anemia, high blood pressure and cancer; mercury with impaired memory, cerebral palsy and emotional instability (EPA, January 29th 2010), sulfur with some cases of eye irritation, chest tightness, lung damage and anemia, high blood pressure, brain and kidney damage, and

cancer (EPA, January 29th 2010), however there are other cases with no clear association to a specific fine particle component.

Detailed fine particle composition data is needed on a regular basis for epidemiologists to identify which of the thousands of possible fine particle species cause a statistically significant number of the public health cases.

1.2.2 Environmental Health Impact

The same fine particles that affect public health can also adversely affect the environment. The type of environmental effect depends on where the particles are and the components present in the fine particles. Particles that deposit to the earth can cause damage to the cellular structure of plants, corrode stone work of buildings and structures, and acidify entire ecosystems when the particles contain acidic components.

In suspension they cause the air to take on an aesthetically unpleasing character and can impair visibility. **Figure 1-4** illustrates the effect of $PM_{2.5}$ on visibility.

Figure 1- 4 Comparison of visibility on good versus bad days: the picture on the left is of a clear day in April 5, 2004; and the picture on the right is of smog resulting from heavy pollution in February 1, 2005 (CAMNET, 2008).

The USEPA reports that visibility has decreased about 70% across the U.S.; in the east, a natural visibility of 90 miles has decreased to 14-24 miles, while in the west a natural visibility of 140 miles has decreased to 33-90 miles (EPA, March 6th 2008). PM containing inorganic components affects visibility more because these components are more hygroscopic and so they attract water and grow in size more than particles that do not contain inorganic components. This allows them to scatter more light and impair visibility more (EPA, January 29th 2010).

1.3. FEDERAL REGULATION OF $PM_{2.5}$

Although epidemiologists have not been able to conclusively identify the chemical components in fine particles that cause the observed health effects, the Clean Air Act requires the USEPA to set the National Ambient Air Quality Standards (NAAQS) for pollutants considered to be harmful for public health and the environment which includes particles.

The earliest particle NAAQS was established in 1971 for total filterable particulate matter, or total suspended particles (TSP). Later research suggested that smaller particles penetrate the respiratory system farther than larger particles, and therefore would be more likely to cause health problems. Thus in 1988, the USEPA replaced the NAAQS for TSP with one for PM_{10}. This prompted more studies. As a result of these studies, in 1997, the USEPA promulgated a new (and additional) NAAQS for $PM_{2.5}$. NAAQS set the maximum permissible concentration for fine particulate matter at 15μg/m^3 on an annual basis and 35μg/m^3 on a 24 hour basis (EPA, May 9th 2008). All of these standards are based on total mass of particles and not their chemical composition, in part because it is easier to measure mass than composition, and because the specific components in $PM_{2.5}$ that cause health problems are unknown.

In February 2004, the USEPA designated the first set of $PM_{2.5}$ "non attainment" areas where $PM_{2.5}$ levels exceeded the primary ambient air quality standards and could potentially cause health problems, as well as counties that may be in "attainment" but that contribute to the poor air quality of downwind "non-attainment" areas. As shown in **Figure 1-5**, counties in New York that are designated as non-attainment include Bronx, Kings, Nassau, New York, Orange, Queens, Richmond, Rockland, Suffolk, Westchester counties (EPA, June 19th, 2008).

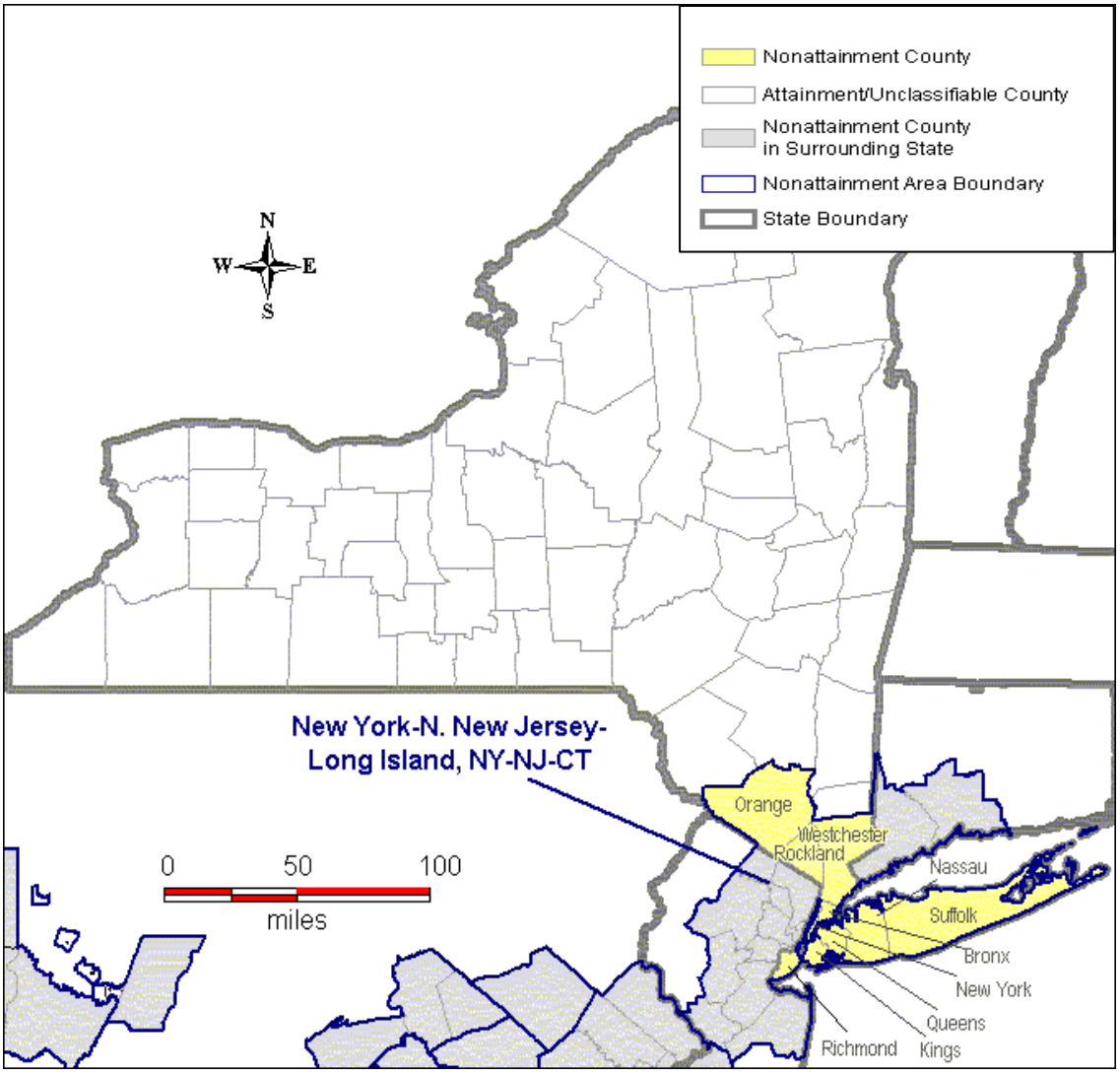

Figure 1- 5 $PM_{2.5}$ NAAQS designation of counties in the New York airshed (EPA, June 19th 2008).

1.4. WHY DETAILED $PM_{2.5}$ CHEMICAL SPECIATION IS NEEDED

Areas that do not comply with the NAAQS must develop State Implementation Plans (SIPs) that identify the schedule and magnitude of reductions from the key sources of $PM_{2.5}$ and its precursors that affect their particular region. Developing an effective SIP is challenging and its implementation can be quite expensive. The cost arises from the regulatory controls on the public, private or industrial sectors to reduce emissions of $PM_{2.5}$ or its gaseous precursors released by anthropogenic sources. Confounding factors

in the analysis include reasonable knowledge of the sources of primary and secondary fine particles and the ambient meteorology which can modify the production rate of many of these sources.

SIPs are developed based on knowledge of the baseline ambient air quality, meteorology, and source strength and distribution in an area. In regions without their own monitoring network, SIPs depend on measurements of $PM_{2.5}$ mass and its approximate composition from existing nationwide monitoring networks. The most effective SIPs are developed by using these measurements in receptor models, or in chemical transport models.

Receptor models are statistical models which use $PM_{2.5}$ chemical speciation to identify the sources that contributed to the observed air quality levels (Wittig et al., 2008). Examples include Positive Matrix Factorization (PMF) and Chemical Mass Balances (CMB) both of which solves the following balance for the values of S_{kj}:

Equation 1- 1 $C_{ij} = \sum \left(a_{ik} \times S_{kj} \right)$

where *i* is the chemical species measured in the air quality sample at the receptor site, *j* is the air quality sample of $PM_{2.5}$ collected at a particular location and time; C_{ij} is the concentration of the species in the air quality sample, a_{ik} is the mass fraction of chemical species in the emission from source *k*; and S_{kj} is the mass of source *k* that contributed to the species observed in air quality sample *j*.

The successful use of receptor models requires accurate and detailed $PM_{2.5}$ speciation of both the fine particle species in the air sample, C_{ij}, and the fine particle species released by the source, a_{ik}.

Chemical transport models predict air quality levels across a region (e.g. transport models like PMCAMX based on knowledge of the sources that contribute to the air quality. These models mathematically represent the key physical and chemical atmospheric processes which affect particle size, composition and concentration: horizontal and vertical advection, horizontal and vertical dispersion, wet and dry deposition, gas phase chemistry and secondary formation of particles through inorganic aerosol growth, aqueous-phase chemistry and secondary organic aerosol formation and growth (Gaydos et al., 2007). They require source emission composition and rates and meteorological conditions as inputs. An example is the Particulate Matter Comprehensive Air Quality Model with extensions (PMCAMx), which solves the following material balance for the values of C_i:

$$\frac{\partial C_i}{\partial t} = \left.\frac{\partial C_i}{\partial t}\right|_{Advection} + \left.\frac{\partial C_i}{\partial t}\right|_{Dispersion} + \left.\frac{\partial C_i}{\partial t}\right|_{\substack{Gas-phase\\Chemistry}} + \left.\frac{\partial C_i}{\partial t}\right|_{Emission} - \left.\frac{\partial C_i}{\partial t}\right|_{\substack{Wet/Dry\\Deposition}} + \left.\frac{\partial C_i}{\partial t}\right|_{Aerosol} + \left.\frac{\partial C_i}{\partial t}\right|_{\substack{Aqueous-phase\\Chemistry}}$$

Equation 1- 2

Where *i* is the chemical species resulting from $PM_{2.5}$ speciation in a given section, C_i is the change in concentration over time for a given specie.

PMCAMx is a three dimensional Eulerian model that uses a sectional representation to model the aerosol species based in particle size distribution, where a uniform mass concentration is assumed for the particles in a given section. The advection term represents the change in concentration due to transport of pollutants by wind effects. The dispersion term represents the change in concentration also due to transport of pollutants by local mixing that varies the air flow velocity. The gas-phase chemistry term represents the change in concentration due to the production of secondary aerosols. The emission term represents the change in concentration due to low level anthropogenic emissions or elevated point sources emissions. The wet and dry deposition change in concentration is due to the removal of species mass from the entire sample volume. The aerosol term represents the change in concentration due to effects of condensation and evaporation and the coagulation and nucleation upon particle size distribution.

In general, the chemical transport models and receptor models approach the same problem from opposite directions. Both types of models require detailed chemical speciation information, either for the emission sources or for the existing air quality. However, it is important to note that both use functional groups to describe the chemical speciation since it gives a better representation of how the PM behaves in the atmosphere.

These models are still being refined and need speciation data that is more detailed than what is commonly measured to improve their accuracy in identifying key sources (i.e., receptor models) or to predict the effect of emissions reductions on ambient air quality levels of fine particles (i.e., transport models).

More detailed $PM_{2.5}$ chemical speciation is also needed so that epidemiologists can reveal which of the chemical species present in ambient particles cause adverse public health, so that the SIPs to improve air quality can target their sources in specific.

1.5. EXISTING $PM_{2.5}$ MONITORING NETWORKS IN THE US

Measurements of fine particulate matter chemical speciation are routinely made around the country. However, these measurements are typically only for a subset of the species present in fine particulate matter, or with little chemical detail (e.g., organic carbon as a lump sum).

In order to demonstrate compliance with the NAAQS for $PM_{2.5}$ mass, areas need only measure fine particle mass with a EPA Federal Reference Method (FRM). These samples are rarely analyzed for chemical speciation information.

Chemical speciation is measured at several networks across the country: NCore, PM Chemical Speciation Network (including STN sites), IMPROVE, CASTNET, NADP, and select locations in NY and NYC to support the development of SIPs.

The USEPA National Core (NCore) is a new multi-pollutant monitoring network, intended to provide data to demonstrate compliance with the NAAQS and to characterize regional and urban patterns of air pollution. NCore stations are located at ~55 representative urban and ~20 rural sites across the United States. In addition to speciated

$PM_{2.5,}$ speciated $PM_{10-2.5}$, $PM_{2.5}$ and $PM_{10-2.5}$ mass, ozone O_3, sulfure dioxide SO_2, carbon monoxide CO, nitrogen oxides (NO, NO_2, NO_y) and basic meteorology will be measured at NCore sites. The available information of $PM_{2.5}$ speciation will be maximized by EPA and its partners in order to improve the basis for future health studies, the NAAQS revisions, validate air quality models, and study the impact of fine particles in ecosystems.

The USEPA PM Chemical Speciation Network is intended to provide data to determine the time-based spatial trends in $PM_{2.5}$ speciation. It consists of about 300 monitoring sites across the United States, 54 of which are known officially as the Speciation Trends Network (STN), and some of which are also NCore sites. $PM_{2.5}$ speciation is measured at all STN sites; however the speciation is incomplete and only targets select ions and elements, and organic and elemental carbon as lump sums. Concentration trends of $PM_{2.5}$ speciation is expected over a period of three years, and this data will be used by decision-makers as input to models and for development of emission control strategies. This data will also be used for epidemiological studies.

The Federal and Regional-State Interagency Monitoring of Protected Visual Environments (IMPROVE) network is intended to provide data to monitor and protect visibility in Class I remote areas, such as national parks and wildness, which are protected under the EPA's regional haze rule. There are 110 IMPROVE sites across the United States. In addition to $PM_{2.5}$ speciation, PM_{10} and $PM_{2.5}$ mass, light scattering and meteorological conditions are measured at all IMPROVE sites. The $PM_{2.5}$ speciation,

however, is limited to elements heavier than sodium, select anionic inorganics, and lump sums of organic and elemental carbon.

The USEPA/NOAA Clean Air Status and Trends Network (CASTNET) is intended to provide data to monitor acidic air pollutants which acidify ecosystems when they dry deposit to the ground. This network has 80 sites across the United States. In addition to limited $PM_{2.5}$ speciation (sulfate, nitrate and ammonium only), at each CASTNET site, sulfur dioxide, nitric acid and the meteorological variables needed to calculate dry deposition rate is measured.

The SAES National Atmospheric Deposition Network (NADP) purpose is to provide data that supports informed decisions on air quality issues which center around aqueous-phase chemistry. The NADP network includes sites in several other networks, including 250 National Trends Network (NTN) sites, 7 Atmospheric Integrated Research Monitoring Network (AIRMoN) sites, and 100 Mercury Deposition Network (MDN) sites. At NADP sites, limited $PM_{2.5}$ speciation of only sulfate, nitrate, chloride, ammonium, calcium, magnesium, sodium, potassium, pH and mercury are measured.

There are several STN and IMPROVE sites located in New York, as shown in **Figure 1-6**, where limited $PM_{2.5}$ speciation measurements are made routinely.

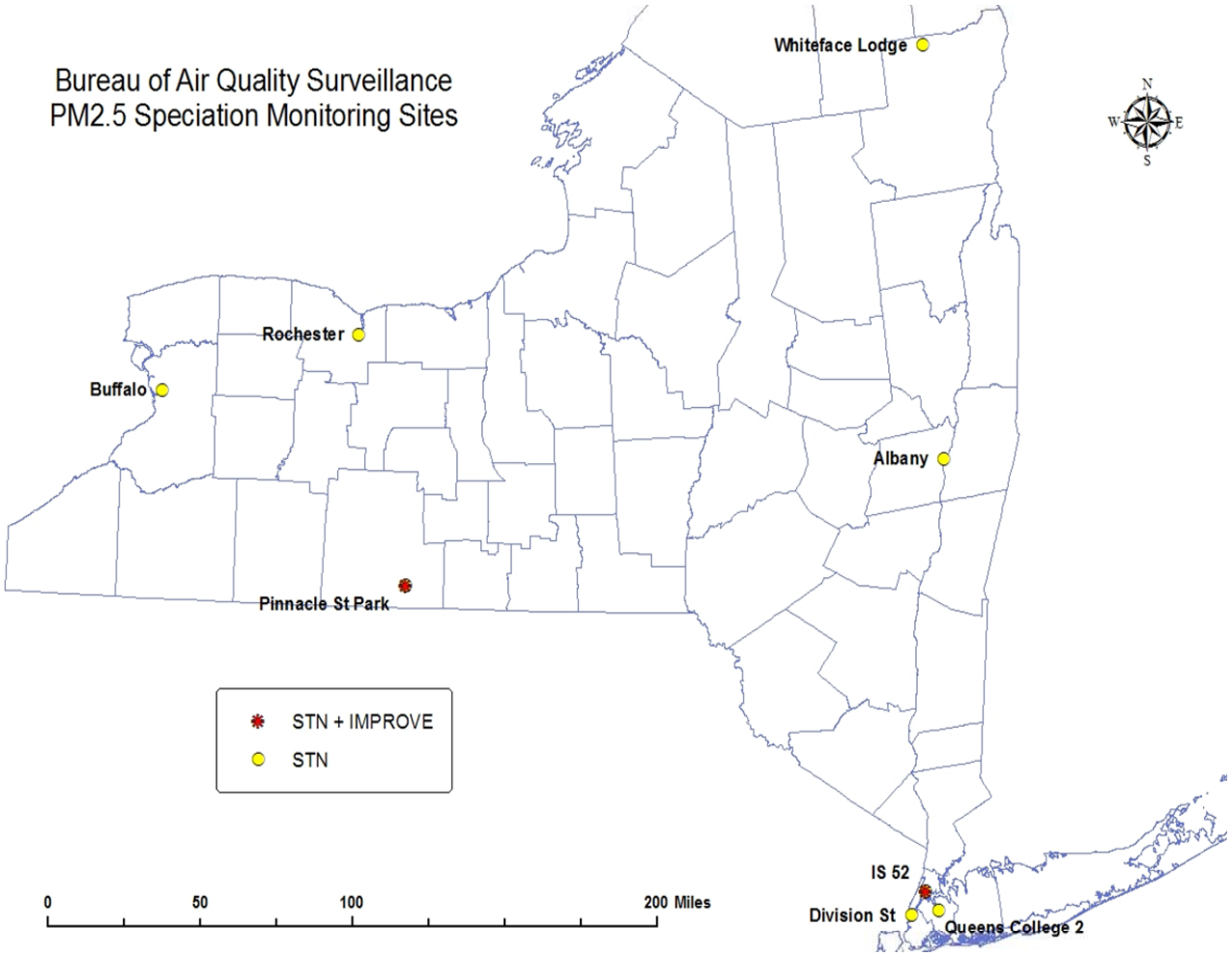

Figure 1- 6 $PM_{2.5}$ speciation monitoring sites in NYS (Department of Environmental Conservation)

In summary, while there are many networks at which $PM_{2.5}$ speciation is measured routinely across the country and in New York, the $PM_{2.5}$ speciation is limited to a subset of the species actually present in the particles, or is lacking in chemical detail. This is illustrated in **Table 1-2**.

$PM_{2.5}$ Monitoring Networks			
Network	**$PM_{2.5}$ components that are measured**	**Frequency of measurement**	**Duration of sample**
NCORE	Sulfate and nitrate	Every 3 days	24 hours
STN	Sulfate, nitrate and ammonium Aluminum, silicon, calcium, iron and titanium Organic and Elemental carbon as a lump	Every 3 days	24 hours
IMPROVE (All sites have speciation monitoring)	Sulfate, nitrate and ammonium; Organic and Elemental carbon concentration as a lump; $PM_{2.5}$ elements heavier than sodium	Every 3 days	24 hours
CASTNET	Sulfate, nitrate and ammonium	Weekly	24 hours
NADP	Sulfate, nitrate, ammonium, chloride, calcium, magnesium, sodium, potassium	NTN: one week precipitation sample AIRMoN: daily precipitation samples	

Table 1- 2 Monitoring Networks for $PM_{2.5}$ chemical speciation and mass concentration.

The networks described above provide limited data on $PM_{2.5}$ speciation. This is in part due to the cost to maintain a nationwide network, which is modest even for the limited speciation that is done. However, this is also because their goals do not support the need for complete and detailed $PM_{2.5}$ speciation. For example, the NCore network collects limited $PM_{2.5}$ speciation data but detailed criteria pollutant data, because its purpose is to demonstrate compliance, not support the development of SIPs to reach compliance.

In order to develop a SIP to reach compliance with the NAAQS for $PM_{2.5,}$ nonattainment areas will need to reduce the emissions of $PM_{2.5}$ and its precursors, which in turn will require receptor modeling to identify key sources to reduce and transport modeling to

evaluate the effectiveness of reductions, which in turn require $PM_{2.5}$ speciation data that is complete and detailed.

1.6. METHODS COMMONLY USED TO MEASURE AMBIENT AEROSOL COMPOSITION

The methods used by the nationwide networks are reliable and have been used for decades: Ion Chromatography for inorganics, Gas Chromatography with FID for organics, and XRF for elements.

There are many other methods that can be applied to $PM_{2.5}$ speciation. Some provide more detail than the methods used by the networks and some less. All are less advantageous than FTIR, the approach which will be developed in this research, in one way or another.

There are four criteria used to evaluate each method relative to FTIR. The first is what level of chemical detail is provided by the measurement. Some methods such as IC and indophenol colorimetry and flash volatilization only measure the inorganic species in aerosol samples. Some such as aethalometry, thermal evolution, GC/MS, MALDI, DRIFT and supercritical fluids only measure the organic species in aerosol samples. And others such as XRF and PIXE only measure element species in aerosol samples. The second is whether the sample must be extracted or converted into another form for analysis. Some methods such as IC, flame atomic absorption, indophenol colorimetry, GC/MS, MALDI, supercritical fluids and PIXE need the sample in liquid form therefore

samples have to be extracted with solvents before analysis. The third is whether it is destroyed during analysis. All methods mentioned in previously destroyed sample during analysis limiting the ability of reanalyzing the sample by using other methods. The fourth and final criteria is whether the method is quantitative for the $PM_{2.5}$ chemical species. Most of the methods mentioned are quantitative, but they are not able to do it for the entire aerosol chemical species. These methods are discussed below, organized by the groups of chemicals present in $PM_{2.5}$ they are able to measure.

1.6.1. Inorganic speciation

As given in **Table 1-1**, inorganic species include ammonium, bromide, chloride, fluoride, nitrate, nitrite, phosphate, potassium, sodium and sulfate. According to Schwab et al. (2004), approximately 60% of the fine particle mass measured in NYC in 2001 was inorganic in nature.

Possible methods used to measure inorganic ions in ambient $PM_{2.5}$ samples include ion chromatography, indophenol colorimetry, and flash volatilization.

Ion chromatography (IC) uses ion exchange resins to separate atomic or molecular ions in a liquid sample based on their interaction with the resin, and a conductivity detector to measure the concentration of the separated ions. The ions are identified by evaluating the elution time of the peaks in the spectrum. When applied to ambient aerosol analyses, this method can be used to measure concentrations of ammonium, bromide, chloride, fluoride, nitrate, nitrite, phosphate and sulfate ions present in a $PM_{2.5}$ sample. This

approach requires a liquid sample and so the $PM_{2.5}$ must be extracted from the sampling substrate before analysis. Also, the sample is destroyed during analysis (Hildemann et al., 1991) and so repeat analyses are not possible.

Indophenol colorimetry measures the concentration of ammonium in a liquid sample by converting it with alkaline phenol and NaDTT to form indophenol blue and then measuring its absorbance at 640nm. When applied to ambient aerosols, this method is only able to measure a single inorganic ion in the aerosol, ammonium. The method requires extraction, and it destroys the sample upon analysis (Bolleter et al., 1961).

Flash volatilization applies a charge to a metal strip holding a liquid or solid sample, reducing and volatilizing select chemicals in the sample to the gas phase, where they are measured by a chemically specific gas detector. This method is able to measure nitrate and sulfate in ambient $PM_{2.5}$ by flash volatilizing the nitrate and sulfate in the particles to NO and SO_2 in the gas phase, and then measuring the evolved gas using commercially available NOx and SO_2 gas monitors (Stolzenburg et al., 2000). This method does not require extraction, but the sample is destroyed during analysis.

1.6.2. Organic speciation

Organic species include carbonate, thousands of different chemicals classified as "elemental carbon" (black carbon, graphitic carbon or soot) and thousands of different chemicals classified as "organic carbon". According to Schwab et al. (2004), 36% of the fine particle mass in NYC in 2001 is organic in nature. While many of the methods to

measure inorganic composition are well documented and used, there is much ongoing research to develop methods to identify and quantify organic species.

Possible methods used to measure organic species in ambient $PM_{2.5}$ samples include Aethalometry, Thermal Evolution, Gas Chromatography, High-Resolution Gas Chromatography, High-Resolution Gas Chromatography with Mass Spectrometry, Matrix Assisted Laser Desorption/Ionization with Mass Spectrometry, Diffuse Reflectance Infrared Fourier Transform Spectrometry, and Supercritical Fluid Chromatography.

Aethalometry measures the attenuation of a light beam that is transmitted through ambient aerosol particles collected from the atmosphere onto a substrate. This method has been used to measure the concentration of "black" carbon in aerosol particles as a lump sum and as a surrogate for elemental carbon which is the primary light absorbing species in fine particles (Hansen et al., 1984). This method does not require extraction since the sample can be analyzed while on the filter, and the sample is not destroyed as a result of the analysis.

Thermal Evolution gradually heats a solid or liquid sample, volatilizing the semi-volatile components in the sample to the gas phase, and then measures them using an appropriate gas detector. When combined with flash volatilization, the method can measure non-volatile components of a sample as well. This method can be used to measure organic and elemental carbon as a lump sum in ambient $PM_{2.5}$ using a flame ionization detector or the

lump sum of both organic and elemental carbon when using nondispersive infrared CO_2 gas detector (Stoltzenburg et al., 2000). This method does not require extraction, but the sample is destroyed during the analysis.

Thermal optical analysis is based on oxidation of organic carbon and elemental carbon at different temperatures. The analyzer liberates carbon compounds under different temperatures and oxidation environments, then convert these compounds to carbon dioxide by passing the volatilized compounds through an oxidizer and reducing it to methane and quantifying methane through a flame ionization detector. This method measures organic and elemental carbon as thermally based lump sums in ambient $PM_{2.5}$. This method does not require extraction but the sample is destroyed during the analysis.

Gas Chromatography (GC) and High-Resolution Gas Chromatography (HRGC) are methods which inject a liquid sample into the instrument and vaporize it, allowing it to bond to a fused silica capillary column. As temperature is gradually increased, an inert gaseous mobile phase elutes the gases bonded to the column in order of volatility. Use when paired with a Flame Ionization Detector, components that can be burned such as those that contain carbon and hydrogen are detected and counted. Chemicals are identified by their retention time on the column. When applied to fine particle analysis, this method can be used to identify and quantify a limited number of the molecules classified as “organic carbon” and “elemental carbon”. This limit can be explained by the overlap of many molecules with similar volatility, the inefficiency of the extraction process for organic compounds from fine particles, and the inability of polar species to

bond to the capillary column without derivatization, another very inefficient process (Mazurek et al., 1987). This method does require extraction as well as derivatization, and the sample is destroyed during the analysis.

When HRGC is coupled with Mass Spectrometry (MS), eluted chemicals are ionized and detected using a MS which uses the mass to charge ratio of the ionized sample to identify the compounds present in the sample (Mazurek et al., 1987). When applied to aerosol analysis, HRGC with MS has the same limitations as identified for HRGC on its own, as well as a new one: the ionization process often breaks apart chemicals into unrecognizable ions. It also requires extraction and derivatization, and the sample is destroyed during the analysis.

When Matrix Assisted Laser Desorption/Ionization (MALDI) is coupled with Mass Spectrometry (MS), some of the fragmentation described for HRGC with MS is avoided. MALDI is a soft ionization technique which uses a matrix that absorbs light energy causing a small part of the sample to vaporize. Once the sample molecules are vaporized and ionized they are transferred into a mass spectrometer where they are separated from the matrix ions and detected individually. To date, this method has only been used to measure biomolecules and large organic molecules in fine particles, but is able to provide a detail composition of molecules classified as organic carbon, as well as the size and shape of the molecules. However, quantitation is not consistently accurate due to poor reproducibility of the MALDI signal intensity (Mansoori et al., 1996). This method also requires extraction and derivatization, and the sample is destroyed during the analysis.

Diffuse Reflectance Infrared Fourier Transform Spectrometry (DRIFT) is a method which directs infrared radiation through powder and solid samples. Chemicals in the sample scatter, absorb and diffusely reflect the radiation. The detected radiation is Fourier transformed and quantified using a standard infrared detector. While this method may be able to measure more chemical species, it has only been used to date, to measure polar organic species in fine particles (Gordon et al, 1988). This method does not require extraction, and the sample is not destroyed during the analysis.

Supercritical fluids are substances which can exist at temperatures and pressures above their thermodynamic critical points, such as carbon dioxide and water. Supercritical Fluid Extraction (SFE) is used to separate one component from another using a supercritical fluid as the solvent. The sample and supercritical fluid are heated to supercritical conditions in into a extraction vessel, where it dissolves the material to be extracted. The dissolved material is swept from the extraction cell into a separator at lower pressure, and the extracted material settles out. The SF can be cooled, recompressed and recycled. Supercritical Fluid Chromatography (SFC) uses supercritical fluids as the mobile phase in a chromatography capillary column to elute components in the sample from the column. The sample is eluted from the column in unique bands based on the interaction of the SF and the stationary phase of the column. The bands leave the column and are identified and quantified by the detector. The detectors used are compatible with GC detectors . When applied to ambient aerosol analysis, these methods are able to measure the composition of low to moderate molecular weight semi-volatile molecules (e.g.

Lundanes et al., 1985). However, mixtures of compounds typical in aerosol samples are more difficult to analyze since the method may not separate them efficiently before analysis. Both SFE and SFC require extraction of the sample, and the sample is destroyed during the analysis.

1.6.3. Elemental speciation

By most air quality literature, elements are not considered to be inorganics. $PM_{2.5}$ speciation for elemental species include 20 elements from sodium to lead on the Periodic Table and listed in **Table 1-1**.

Possible methods used to analyze elements include Ion Chromatography, Flame Atomic Absorption, X-Ray Fluorescence, Proton Induced X-Ray Emission.

In addition to select inorganics, ion chromatography can also be used to measure the select elements potassium, calcium, magnesium, and sodium commonly found in $PM_{2.5}$.

Flame atomic absorption is a method that measures select elements sodium, potassium, calcium, magnesium, copper, aluminum, cadmium in a liquid sample by converting them to their atomic state using a flame, and then measuring the light absorbed by the converted sample (Hildemann et al, 1991). This method requires extraction, and the sample is destroyed during the analysis.

X-Ray Fluorescence (XRF) and Proton Induced X-Ray Emission (PIXE) are methods which irradiate a liquid or solid sample, and then measure the emission characteristics to identify and quantify the elements in the sample (Dzubay and Stevens, 1975). XRF irradiates the sample with x-rays and measures the fluorescence emissions, while PIXE excites the sample with protons and alpha particles and then measures the x-ray emission (Cahill and Surovik, 1990). When applied to fine particle analysis, these approaches can be used to quantify the concentration of most elements from sodium through lead on the Periodic Table. These methods are limited to measure only elements, a portion of the whole chemical species present in fine particulate matter. These methods do not require extraction, and the sample is not destroyed during the analysis.

Table 1-3 presents all the different methods used by many researches to analyze the different chemical species present in fine particulate matter.

	IC	Flame Atomic Absorption	Indophenol Colorimetry	Flash Volatilization	Aethalometer	Thermal Evolution	TOA
Inorganics ammonium, bromide chloride, fluoride, nitrate, nitrite, phosphate, potassium, sodium, sulfate	All	None	Some (ammonium)	Some (nitrate and sulfate)	None	None	None
Organics Carbonate Thousands of different molecules that contain elemental carbon (black carbon, graphitic carbon or soot) Thousands of different molecules that contain organic carbon	None	None	None	None	Some elemental carbon	Some elemental carbon and organic carbon	Elemental carbon and organic carbon as thermally based lump sums
Elements Aluminum, arsenic, bromine, cadmium, calcium, chlorine, chromium, copper, iron, lead, manganese, nickel, phosphorus, potassium, selenium, silicon, sodium, sulfur, titanium, uranium, vanadium, zinc	All	All	None	None	None	None	None
Extraction	Yes	Yes	Yes	No	No	No	No
Destructive	Yes	Yes	Yes	Yes	No	Yes	Yes

Table 1- 3 Methods used to analyze different species of fine particulate matter.

	GC/ HRGC & HRGC/ MS	MALDI	DRIFT	Supercritical Fluids	X-R Fluorescence	PIXE	FTIR
Inorganics ammonium, bromide, chloride, fluoride, nitrate, nitrite, phosphate, potassium, sodium, sulfate	None	None	None	None	None	None	All as functional groups (N-H, Br-C, Cl-C, N-O, P-O, K-O, Na-O, S-O)
Organics Carbonate Thousands of different molecules that contain elemental carbon (black carbon, graphitic carbon or soot) Thousands of different molecules that contain organic carbon	Some molecules (elemental carbon and organic carbon)	Some molecules (elemental and organic carbon)	Some molecules (elemental carbon and organic carbon)	Some molecules (elemental carbon and organic carbon)	None	None	All as functional groups (alkane, alkene, carbonyl, aromatic, alcohol, etc)
Elements Aluminum, arsenic, bromine, cadmium, calcium, chlorine, chromium, copper, iron, lead, manganese, nickel, phosphorus, potassium, selenium, silicon, sodium, sulfur, titanium, uranium, vanadium, zinc	None	None	None	None	All	All	Some
Extraction	Yes	Yes	No	Yes	No	Yes	No
Destructive	Yes	Yes	No	Yes	No	Yes	No

Table 1-3 Methods used to analyze different species of fine particulate matter.

For comparison purposes, this table also summarizes the strengths of Fourier Transform Infrared Spectroscopy (FTIR). In brief, FTIR directs infrared radiation through a sample and measures the absorbed light with a standard infrared detector. Functional groups are identified by the wavenumber at which they absorb light and the concentration of the functional group is proportional to the amount of light that is absorbed by the sample. When applied to fine particle analysis, this technique can be used to measure the functional groups present in all of the inorganic and organic species in the sample (Allen et al, 1994). This method does not require extraction, and it does not destroy the sample.

As seen in **Table 1-3**, all of the methods that could be used to measure $PM_{2.5}$ speciation are only able to measure a fraction of the species or are only able to measure them as lump sums. In order to measure the complete fine particle composition, samples must be analyzed by several different methods, compounding sample preparation and analysis errors. Further, many of the methods require extraction and destroy the sample during analysis. In comparison, FTIR is able to measure 100% of organic and inorganic species with chemical specificity and using a single approach, does not require extraction and does not destroy sample during analysis.

1.7. HOW FTIR WORKS

The FTIR spectrometer consists of an optical bench and a computer. The optical bench includes a light source, a sample compartment, a beamsplitter, a moving mirror and a fixed mirror, and a detector as shown in **Figure 1-7**.

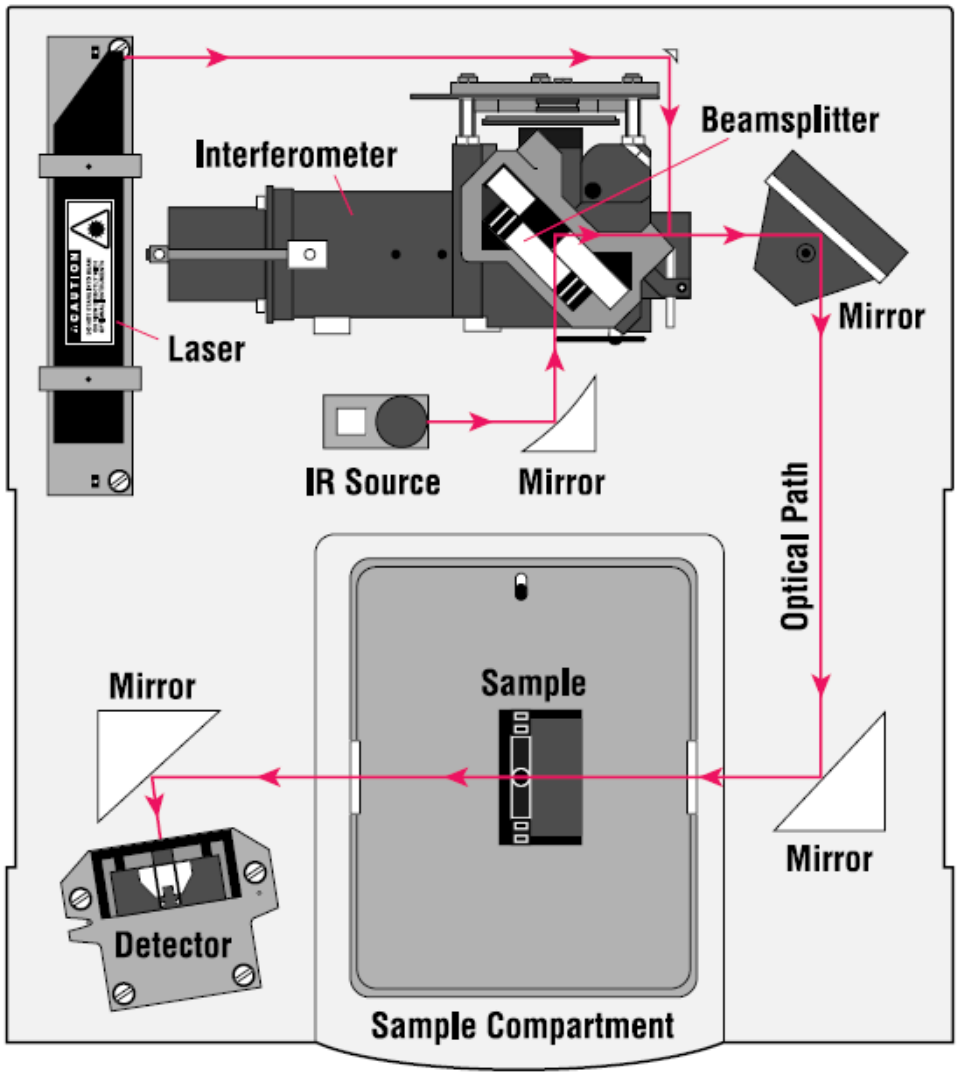

Figure 1- 7 IR spectrometer components (Thermo Nicolet, 2001)

The source is a ceramic material that, when heated, radiates light over the IR wavenumber range of 4000 cm^{-1} to 400 cm^{-1}, or wavelength range of 2.5 μm to 25 μm. This light is transmitted to the beamsplitter, a laminate of KBr that reflects and transmits light equally, and sends equal amounts of incident radiation into two directions at right angles to each other. One beam is sent to a fixed mirror and then redirected to the beamsplitter. The other beam is sent to a moving mirror which moves backwards and

forwards at a constant speed of 1.898 cm/s. The longer the path of the moving mirror, the higher the resolution of the measurement. Our FTIR is capable of resolutions of 0.1 to 0.5 cm^{-1}. The two beams are recombined at the beamsplitter, producing a light spectrum with constructive interference at times when the two path lengths are the same and destructive interference when they differ. The recombined beam then passes through the sample. The IR beam can pass through the sample in two different ways: transmission technique and attenuated total reflection (ATR). Transmission is the most popular; it passes the infrared beam directly through the sample. This technique has a high signal to noise ratio and can measure solids, liquids, gases and polymers. ATR uses reflectance to redirect the beam through a thin layer of the sample, instead of passing all the way through the sample. ATR is used to obtain spectra of solids, liquids and thin films.

The recombined beam is guided to the sample. Infrared light is absorbed by the sample if the radiation interacts with a functional group in the sample that can undergo a change in dipole and the incoming radiation has sufficient energy for a transition to the next allowed vibrational energy state. Provided these conditions are met, the sample absorbs portions of the recombined beam at wavelengths characteristic of the functional groups in the sample.

Non-absorbed light passes through the sample unchanged and is detected by an electrical transducer that measures the non-absorbed energy as a function of time for all wavelengths in the MIR spectrum simultaneously. Deuterated triglycine sulfate (DTGS) detectors are the most common means to detect energy in the MIR range. The resulting

distribution is an interferogram, a large number of sinusoidal signals added together, each of which contain information about the wavenumber of an infrared peak and its amplitude at that wavenumber. A computer uses Fourier transform to convert the interferogram in time to an absorbance spectrum in frequency as shown in **Equation 1-3**.

Equation 1- 3

$$S(t) = \int_{-\infty}^{\infty} I(\nu) e^{-i\nu 2\pi t}\, d\nu \quad \rightarrow \quad I(\nu) = 2Re \int_{-\infty}^{\infty} S(t) e^{2i\pi\nu t} dt$$

Where *t* represents time, *v* represents frequency, *S(t)* is the interferogram signal in the time domain and *I(v)* is spectrum or inverse transform of *S(t)*.

The resulting absorbance spectrum indicates the radiation absorbed by the sample as a function of frequency. Each individual functional group has a unique signature that contains one or more peaks in the MIR spectrum. An example of blank Teflon filter spectrum is shown in **Figure 1-8**.

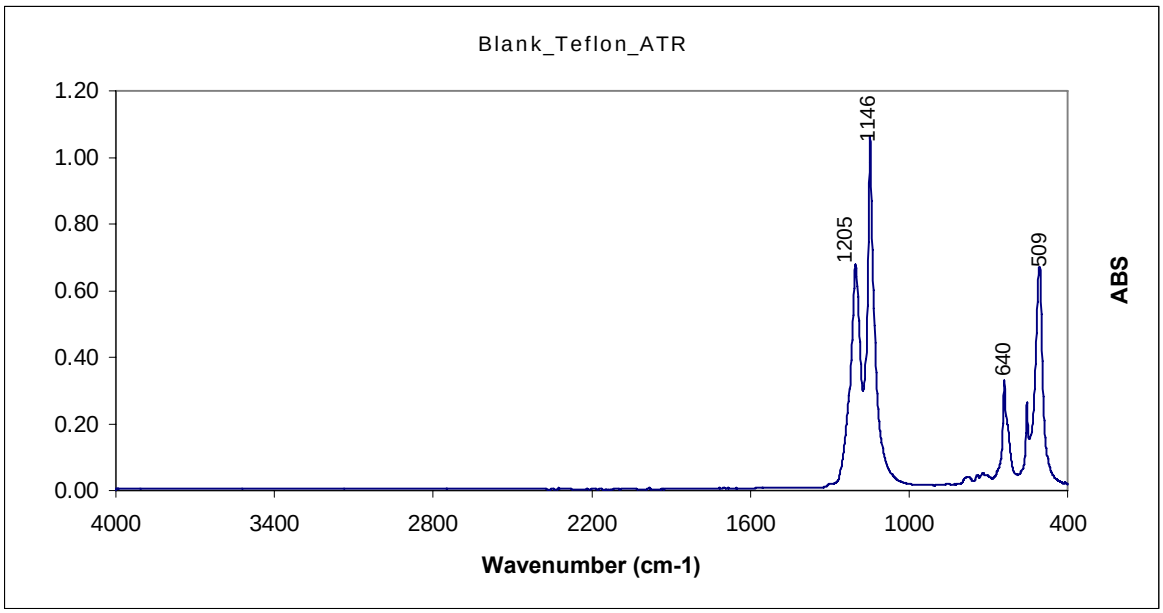

Figure 1- 8 FTIR spectra of blank Teflon. Teflon peaks at 1205, 1146, 640 and 509 cm^{-1}

The identity of the functional group is determined by the signature or by select peaks in the signature. The concentration of the functional group is determined by integrating absorbance over the wavenumber range of a peak in the signature, or sometimes, just by the height of a peak in the signature, and adjusting the value for the molar absorptivity of the functional group, as shown in **Equation 1-4**.

Equation 1- 4 $$C_x = \frac{ABS_x}{\varepsilon_x \, l_x}$$

where C_x is the molar concentration of functional group *x* in the IR beam through the sample in mol m^{-3}, ε_x is the molar absorptivity of functional group *x* at a specific wavelength in absorbance m^2 mol^{-1} that vary by functional group and by wavelength of

light for a single functional group, ABS_x is the integrated area of the absorbance peak of functional group *x* centered at the wavelength for which ε_x was measured in absorbance units, and l_x is the path length of the infrared beam through the sample containing functional group *x* in m.

1.8. USE OF FTIR BY OTHER RESEARCHERS

This method has been used to measure fine particle speciation, to some extent, despite the issues that may limit its accuracy.

FTIR has been used mostly qualitatively to identify functional groups in aerosol samples (Kellner, 1978; Allen et al., 1994, Coates, 2000, Reff et al., 2005); and has been used to provide data to support the study of atmospheric photochemistry (Palen et al., 1992, Holes et al, 1997, Dekermenjian et al, 1999); few studies have been made for quantitative purposes (Krost and McClenny, 1994). There is lack of information about the use of FTIR to compute relative molar absorptivities and there is not reported data about its accuracy (Palen et al., 1992, Holes et al., 1997, Dekermenjian et al., 1999), and no approaches to optimize the spectral interpretation have been reported, many studies have encountered issues with peak shifting or overlapping peaks but did not develop an approach to address these issues (Allen et al., 1994 and Dekermenjian et al., 1999)

Also, little documentation of molar absorptivities, baselines, infrared functional group peak ranges limits the ability to identify and determine right approaches to evaluate other

issues that are needed for quantitation purposes. There is no information about approaches to identify when functional group peak shifting occurs and to separate overlapping functional groups in the infrared spectrum. These are limitation on why FTIR studies have not been used yet to quantify the whole composition of ambient aerosol.

1.9 CHALLENGES TO USING FTIR TO MEASURE FINE PARTICLE SPECIATION

The accurate determination of concentration using FTIR requires an accurate measurement of the area under a species peak absorbance curve, and knowledge of the molar absorptivity of the species and the path length of light through the sample containing the species. For inhomogeneous mixtures of liquids and solids, these three quantities are difficult to determine and very little has been published in the literature on the subject.

Accurate measurements of absorbance area:

The absorbance area is the integrated area under the species signature absorbance peak. The challenges to this measurement are fine particle samples that are spatially inhomogeneous, the MIR signatures of interferents such as gases in the analysis chamber or the sampling substrate, the paucity of information in the literature on the signatures of functional groups or their appropriate baselines, and the fact that species signatures in complex mixtures will shift and overlap.

Knowledge of molar absorptivity:

The molar absorptivity is the specific absorbance per mole of the species. It indicates the sensitivity of the species to a particular range of MIR light. No information has been published in the literature on the molar absorptivity of fine particle species. And, while limited information is available for relative molar absorptivities (i.e., that compare the molar absorptivities of two species in the same sample), the reported values are inconsistent and without documentation of uncertainty or methodology.

Knowledge of path length:

The path length through a fine particle sample is the depth of the sample. Fine particle samples that are collected onto substrates penetrate only partially into the substrate and accumulate on the surface of the substrate. Samples collected by impaction have nonuniform depths by nature. While the path length through a liquid sample collected by extraction is easily defined, this type of sample will result in issues with accurately calculating absorbance area.

1.10 CONTRIBUTIONS OF THE RESEARCH TO THE FIELD

The research makes several significant contributions: it develops systematic methods to acquire molar absorptivity and method detection limit and reports values of both; it develops systematic methods to collect samples for, acquire spectra of, and analyze spectra of fine particles; and it develops algorithms to compute concentration that depend only on measurable quantities. When the work is published, it will address the incredible

lack of information in the literature on the FTIR analysis of fine particles or of any liquid or solid multicomponent mixture.

1.11. PROPOSED RESEARCH PLAN

The goal of this dissertation is to evaluate the feasibility of, and develop and optimize a method that uses FTIR to measure the detailed chemical composition of organics and inorganics in ambient $PM_{2.5}$. The use of FTIR will lead to the analysis of a $PM_{2.5}$ sample using a single technique, without the need for extraction, nondestructively and free of analysis artifacts.

This method has been used quantitatively despite issues that may limit its accuracy. Therefore for its optimal use, this research has developed and evaluated optimal approaches of the FTIR operation, spectra interpretation and data reduction. The main components of this research are identified below. Each component is addressed in a separate chapter of this dissertation, in terms of the challenges and issues, prior work to address the issue, the goal and proposed research to address the issue, and the results that have been obtained. The issues addressed in the present research are summarized below.

Chapter 2: Quantitation

An algorithm that does not depend on path length and uses all parameters calculated during the spectral analysis was developed in order to determine the concentrations of the functional groups present in the sample and in the actual ambient air. For accurate

quantitation results, all issues related with the spectral interpretation must be solved first before inserting them into the algorithms developed.

Experiment 1 Quantitation using an internal standard: two algorithms that uses Teflon and a chemical standard added onto the sample in substrate were develop in order to calculate the concentration of ambient aerosol samples.

Experiment 2 Quantitation using an external standard: one algorithm that uses an external measurements as external standard was developed in order to calculate the concentration of ambient aerosol samples without depending on the path length of sample and actual molar absorptivity.

These experiments will be explained in detail in the subsequent chapters, as well as the results of this research.

Chapter 3: Sample Collection/Preparation

These experiments were designed to optimize how samples are collected for FTIR analysis. FTIR is not easy adaptable to a sample collection system, therefore samples must be collected in a methodical fashion beforehand and introduced manually into the FTIR for analysis. Therefore, before FTIR analysis of $PM_{2.5}$, a minimum loading of fine particles must be collected onto a substrate that is transparent to MIR, without introducing sampling artifacts, and in a small and well defined area on the substrate so as to avoid analysis artifacts.

Experiment 3 Minimization of sampling artifacts: In this experiment the sampling system was configured to obtain a PM2.5 sample that is representative of a particle in the ambient air.

Experiment 4 Selection of sampling substrate: In this experiment, several common sampling substrates were evaluated to identify which are transparent to MIR light. The substrates to be analyzed are Teflon, quartz, nylon and cellulose fiber.

Experiment 5 Identification of minimum sample loading: In this experiment, several dilutions for different chemical compounds were prepared and evaluated to determine the minimum mass of $PM_{2.5}$ onto the substrate that would result in a quantifiable amount of particles.

Chapter 4: Sample Analysis

These experiments were designed to effectively handle the sample analysis in the FTIR spectrometer. These experiments will help to get sample spectra free of interferents that may obscure the sample interpretation. FTIR may use two different techniques for analyzing the sample that may affect the signal to noise ratio if light does not penetrate through the whole sample, therefore aerosol samples collected on the optimal substrates must be analyzed by both techniques. Two types of background spectra will be evaluated to determine if the aerosol spectra is improved when using an open path or blank in path background. Gases in the infrared chamber may affect the spectra interpretation;

therefore different approaches to remove the interfering gases are analyzed. Also changes in the baseline of the experiment will be determined by using an internal standard which absorbance will be compared over time.

Experiment 6 Use of transmission or reflectance spectroscopy: light path through sample: two types of IR techniques were used to collect samples spectra that were evaluated to determine which result in a better signal to noise ratio. The IR techniques to be evaluated are the transmission technique and the attenuated total reflection technique.

Experiment 7 Use of background spectra: two different ways of obtaining background spectra were evaluated in order to determine if the aerosol spectra are improved. The background spectra to be evaluated are collected by using a clean substrate in the light path or without it.

Experiment 8 Approach to minimize interference in the analysis chamber: four different gas removal approaches were evaluated in order to remove the interfering gases in the IR chamber and determine if the aerosol spectra are more accurate and easily to interpret. The removal options to be evaluated are the mathematical atmospheric suppression, the purge using cylinder, the purge using a pump, and the non removal option.

Experiment 9 Use of sampling substrate as an internal standard: changes in baseline and absorbance areas during spectral analysis will be evaluated by determining whether or not

the use of internal standards will help to identify them. The internal standard to be evaluated is the Teflon absorbance in the spectra of a blank substrate.

Chapter 5: Spectra Interpretation

These experiments were designed to select the best approach to interpret the IR spectra of aerosol samples. These spectra can be difficult to interpret since the samples contain billions of particles, each of which can contain millions of chemicals. Functional groups in the aerosol spectra has to be identified and their ABS areas accurately measured by defining the correct baselines and end points of the functional group peaks as well as the peak shifting. ABS measurements of targeted functional group at different concentrations were evaluated to determine the linearity of ABS and their relative molar absorptivities. This information will be used to identify, evaluate and determine the correct approaches to split overlapping functional group peaks.

Experiment 10 Assessment of absorbance linearity: Several standards were prepared with different compounds Octane, Octanoic Acid, 2-Dodecanol and 1-Decen-3-ol, and analyzed by using the FTIR. The spectra were analyzed by using a base case to measure the absorbances of the targeted functional groups. Different functional groups were targeted, hydroxyl, alkane-hydrogen, alkene-carbon in the spectra of each compound, and calibration curves were developed with the absorbances versus concentrations to determine the linearity of the absorbance areas.

Experiment 11 Measurement of relative molar absorptivity: same compound spectra were evaluated from the calibration curve developed in previous experiment. The targeted functional groups evaluated are same as previous experiment. The slope of the calibration curves were used to calculate the relative molar absorptivity of the functional groups relative to the alkane-hydrogen group.

Experiment 12 Approach to draw baselines: end points and baseline: Same compound spectra were evaluated to identify and define the wavenumber ranges of functional groups present in the aerosol sample. Peaks in aerosol and compound spectra obtained in the laboratory were compared with library spectra of different compounds and also compared with the data obtained from the literature review. Absorbance areas for different baseline cases were compared to determine which results in more reliable results.

Experiment 12 Approach to address peak shifting: same compounds were evaluated to determine if functional groups peak shifting occurs across compounds, and if they affect the absorbances or features of the peak. Best approach was selected and applied for following experiment.

Experiment 13 Approach to split overlapping peaks: same compound spectra were evaluated to identify the overlapping peaks and determine the best approach to split the peaks by using relative molar absorptivities.

1.12 REFERENCES

Allen, D., Palen, E., Haimov, M., Hering, S. and Young, J. (1994). Fourier Transform Infrared Spectroscopy of aerosol collected in a Low Pressure Impactor (LPI/FTIR): Method development and field calibration. Aerosol Science and Technology 21, 325-342.

Bolleter, W., Bushman, C., Tidwell, P. (1961). Spectrophotometric determination of ammonia as indophenol. Analytical Chemistry 33, 592-594.

Boudel, R., Fox, D., Turner, B. and Stern, A., 1994. Fundamentals of air pollution. Academic Press, 22-34.

Cahill, T. and Surovik, I. (1990). Visibility and Aerosols During the 1986 Carbonaceous Species Methods Comparison Study. Aerosol Science and Technology, 12(1): 149-160.

CAMNET, 2008. Real Time Air Pollution and Visibility Monitoring. http://www.hazecam.net/newark/gallery.htm

CCOHS, March 22 1999. How do particles enter the respiratory system? Canadian Center for Occupational Health and Safety. http://gala.ccohs.ca/oshanswers/chemicals/how_do.html

Dalluge, J., VanStee, L., Xu, X., Williams, J., Beens, J., Vreuls, R., Brinkman, U. (2002). Unraveling the composition of very complex samples by comprehensive gas chromatography coupled to time-of-flight mass spectrometry: Cigarette smoke. Journal of Chromatography A (974), 169-184.

Dekermenjian, M., Allen, D., Atkinson, R. and Arey, J. (1999). FTIR analysis of aerosol formed in the ozone oxidation of sesquiterpenes. Aerosol Science and Technology 30, 349-363.

Demerjian, K. (2004). EPA PM Supersite Final Report: $PM_{2.5}$ technology assessment and characterization study in New York state (PMTACS-NY).

Dzubay, T. and Stevens, R. (1975). Ambient Air Analysis with Dichotomus Sampler and X-Ray Fluorescence Spectrometer. Environmental Science and Technology 9, 663-667.

EPA. Particulate Matter ($PM_{2.5}$) Speciation Guidance Final Draft. October 7th, 1999.

EPA June 8th 2007. What is acid rain? www.epa.gov/acidrain/what/index.html

EPA March 6th 2008. Health and Environmental effects of Particulate Matter. http://www.epa.gov/ttn/oarpg/naaqsfin/pmhealth.html

EPA April 4th 2008. Module 3: Characteristcs of Particles-Particle size categories. www.epa.gov/air/oaqps/eog/bces/module3/category/category.htm

EPA, May 9th 2008. PM Standards. EPA. www.epa.gov/air/particlepollution/standards.html

EPA, June 19th, 2008. New York Designation Map. www.epa.gov/pmdesignations/1997standards/final/statemaps/New_York.htm

EPA, December 23 2009. NCore Networks and Site Information. http://www.epa.gov/ttn/amtic/ncore/networks.html

EPA, January 29th 2010. Air Pollution Control Orientation Course. http://www.epa.gov/apti/course422/ap7a.html

Gordon, R.J., Trivedi, N.J., Singh, B.P., Ellis, E.C. (1988). Characterization of aerosol organics by diffuse reflectance FTIR. Environmental Science and Technology 22, 672-677.

Hansen, A., Rosen, H., Novakov, T. (1984). The Aethalometer an instrument for the real-time measurement of optical absorption by aerosol particles. The Science of the Total Environment 36, 191-196.

Hildemann, L., Markowski, G., Cass, G. (1991). Chemical composition of emissions from urban sources of fine organic aerosol. Environmental Science and Technology 25, 744-759.

Holes, A., Eusebi, A., Grosjean, D. and Allen, D. (1997). FTIR analysis of aerosol formed in the photo-oxidation of 1,3,5-Trimethylbenzene. Aerosol Science and Technology 26, 516-526.

Kellner, R. (1978). Identification and determination of particulate compounds: infrared spectroscopy, extraction and chromatography. Analysis of Airborne Particles by Physical Methods (edited by Malissa H and Robinson JW). CRC Press, Boca Raton FL.

Krost, K. and McClenny, W. (1994). FTIR transmission spectroscopy for quantitation of ammonium bisulfate in fine particulate matter collected on Teflon filters. Applied Spectroscopy 48 (6), 702-705.

Lall, R., Kendall, M., Ito, K. and Thurston, G., 2004. Estimation of historical annual $PM_{2.5}$ exposures for health effects assessment. Atmospheric Environment 38, 5217-5226.

Lundanes, E., Greibrokk, T. (1985). Group separation of oil residues by supercritical fluid chromatography. Journal of Chromatography 349, 439-446.

Mansoori, B., Johnston, M., Wexler, A. (1996). Matrix assisted laser desorption/ionization (MALDI) size- and composition – selected aerosol particles. Analytical Chemistry 68, 3595-3601.

Mazurek, M., Simoneit, B., Cass, G., Gray, A. (1987). Quantitative high-resolution gas chromatography and high-resolution gas chromatography/mass spectrometry analyses of carbonaceous fine aerosol particles. International Journal of Environmental Analytical Chemistry 29, 119-139.

NYS Department of Environmental Conservation, 2008. Annual monitoring network plan: New York State ambient air monitoring program.

Paatero, P., 1997. Least squares formulation of robust non-negative factor analysis. Chemometrics and Intelligent Laboratory Systems 37, 23-35.

Palen, J., Allen, D., Pandis, S., Paulson, S., Seinfeld, J. and Flagan, R. (1992). Fourier Transform Infrared analysis of aerosol formed in the photo-oxidation of Isoprene and β-Pinene. Atmospheric Environment 26A (7), 1239-1251.

Schwab, J., Felton, H.D. and Demerjian, K., 2004. Aerosol chemical composition in New York State from integrated filter samples: urban/rural and seasonal contrasts. Journal of Geophysical Research 109, D16SO5 DOI: 1029/2003JDOO4078.

Seinfeld, J. and Pandis, S., 1998. Atmospheric Chemistry and Physics: From air pollution to climate change. US: John Wiley and Sons.

Solomon, P and Allen, D., 2004. Special Issue of Aerosol Science and Technology on findings from the fine particulate matter Supersites Programs. Aerosol Science and Technology 38 (S1), 1-4.

Stolzenburg, M. and Hering, S. (2000). Method for the automated measurement of fine particle nitrate in the atmosphere. Environmental Science and Technology 34, 907-914.

Thermo Nicolet, (2001). Introduction to Fourier transform infrared spectrometry. Thermo Nicolet Corporation. < http://mmrc.caltech.edu/FTIR/FTIRintro.pdf>

Wittig, A.E. and Allen, D., 2008. Improvement of the Chemical mass balance model for apportioning –sources of non-methane hydrocarbons using composite aged source profiles. Atmospheric Environment 42, 1319-1337.

CHAPTER 2 QUANTITATION

In this chapter, methods are developed to determine the molar concentration of fine particle species in the ambient air as a function of the integrated absorbance of the species measured using FTIR.

Absorbance is proportional to the concentration of the species in the light path, which in turn is proportional to the concentration in the air. However, there are a great many parameters specific to FTIR that are difficult to measure for nonhomogeneous solid samples which are likely the reason why this analytical approach has not been used extensively for fine particle speciation. One example includes the light path length through the fine particles collected on a substrate. Since the particles may not penetrate fully through the substrate and since particles will accumulate on the surface of the substrate, this quantity is difficult to determine without laborious cross-sectioning of samples and microscopes. Another example includes the absolute molar absorptivity of a functional group at the particular peak in its signature integrated to determine absorbance area. By Beer Lambert's Law, this is related to the absorbance of the functional group at the wavelength of the peak to be integrated, the concentration of the functional group in the light path, and the path length through the sample containing the functional group. Therefore, since the absolute molar absorptivity depends on path length, it is difficult to estimate experimentally.

In this chapter, these difficult to measure quantities are related to other more measurable quantities, thereby making the method quantitative.

2.1 EXPERIMENT 1: QUANTITATION USING AN INTERNAL STANDARD

2.1.1 Issue

An internal standard is a chemical of known concentration that is present in the sample and that can be measured using FTIR. The FTIR spectrum of a sample with an internal standard will show the signatures of the fine particle species as well as the signature of the internal standard. To be useful for fine particle speciation using FTIR, the internal standard must have a signature in the MIR spectrum and peaks in its MIR signature that are unique of those of the fine particle species, thereby allowing reliable quantitation of its integrated absorbance. Generally, when an internal standard is used, the additional knowns are measured absorbance area of the internal standard, concentration in the sample, and possibly the light path length through the internal standard.

Internal standards are difficult to add to ambient fine particle samples in a homogenous way. Since the FTIR measures fine particle speciation at a specific location on the sampling filter, it requires homogeneity in number of moles of the internal standard with location across the filter.

2.1.2 Goal

The goal of this experiment is to identify possible internal standards that complement the way fine particles are collected onto a substrate for analysis by FTIR and derive an

algorithm to calculate the concentration of a fine particle species in the ambient air as a result of the species absorbances measured by FTIR, the internal standard absorbance measured by FTIR, sampling quantities (e.g., flow rate), and other easily measured quantities (e.g., sample mass).

2.1.3 Literature Review

Fine particulate matter collected on substrates has been analyzed by FTIR to identify the functional groups present in the ambient aerosol. However, most of their studies took a qualitative approach and only identified the chemical composition of the particles or only computed the relative amount of species present in the sample. For example, Palen et al. (1993), Holes et al. (1997) and Dekermenjian et al. (1999) used FTIR to measure the relative abundance of fine particle species in samples collected in smog chambers. This quantity was calculated by:

Equation 2- 1 $$\frac{C_{xb}}{C_{yb}} = \frac{ABS_{xb} / \varepsilon_x l_b}{ABS_{yb} / \varepsilon_y l_b} = \frac{ABS_x}{ABS_y} \times \varepsilon_{y/x}$$

Where x and y are functional groups present in the sample, b indicates the portion of the sample that is in the beam of FTIR light and therefore measured, Cb is the concentration of x or y in the beam, ABS is the absorbance of the functional groups measured in the FTIR light beam (absorbance units), ε is the absolute molar absorbance of the functional group for the signature peak that is integrated to determine absorbance (absorbance m^2 mol^{-1}), and l_b the length of the FTIR light beam through the sample (m).

No studies have tried to use internal standards to make FTIR a quantitative method for fine particle speciation.

2.1.4 Experimental Approach

Identify internal standard candidates

Possible internal standards include a chemical applied to the sample after collection or the Teflon substrate itself. Ideal internal standards are those that:

- Can be uniformly deposited at a known concentration across the surface area of the substrate or are homogeneously distributed through the sample at a known concentration
- Adheres to the top of the sample or is homogeneously integrated into the sample
- Have a unique MIR signature with sharp strong peaks that do not overlap with the signatures of the fine particle species
- Does not degrade quality of sample

Spectral interpretation

All spectra were analyzed by using different approaches that were evaluated in Chapter 5. Approaches used include the shaving and horizontal baselines, shifting and non shifting of peaks respect to Octane and Methanol, and all overlapping peaks were quantified by splitting at the non shifted endpoint.

Derive algorithm for quantitation using an internal standard

Derive an algorithm for the concentration of fine particle species concentrations in the ambient air that:

- Depends on measurable FTIR properties for both the fine particle species and the internal standard, the known concentration of the internal standard on/in the sample, and measurable sample properties
- Does not depend on path length of the sample or absolute molar absorptivity

2.1.5 Results and Discussion

Identify internal standard candidates

Possible internal standards include a chemical applied to the sample after collection, and the Teflon substrate.

The Teflon in the substrate is a reasonable candidate for an internal standard. The filter manufacturers follow strict quality control practices to produce filters in "lots" that have a uniform number of fibers across the filter volume. Its signature, as discussed repeated in prior chapters is unique and possesses sharp strong and unique peaks at 1213 and 1152 cm^{-1} that do not overlap with the signatures of the fine particle species. Also, since the Teflon is the substrate, it does not have to be further integrated into the sample and therefore handling artifacts that could cause contamination are unnecessary. The porous nature of the filter makes the concentration of the Teflon in the FTIR light path only approximate, but the approximate concentration is straightforward to determine as shown at the end of the algorithm derivation.

Derive algorithm for quantitation using an internal standard

An algorithm was derived to determine the concentration of fine particle species in the ambient air based on measureable FTIR properties for both the fine particle species and the internal standard, the known concentration of the internal standard on/in the sample, and measurable sample properties. Path length through the sample and absolute molar absorptivity was eliminated from the algorithm by theoretical derivation. The derivation uses several subscripts consistently: x which is a functional group with an unknown concentration, y which is a functional group with a known concentration, which is the ambient air, b which is the MIR beam, s which is the sample collected on the filter, and f which is the filter that the sample is collected onto. These locations are illustrated in the following figure.

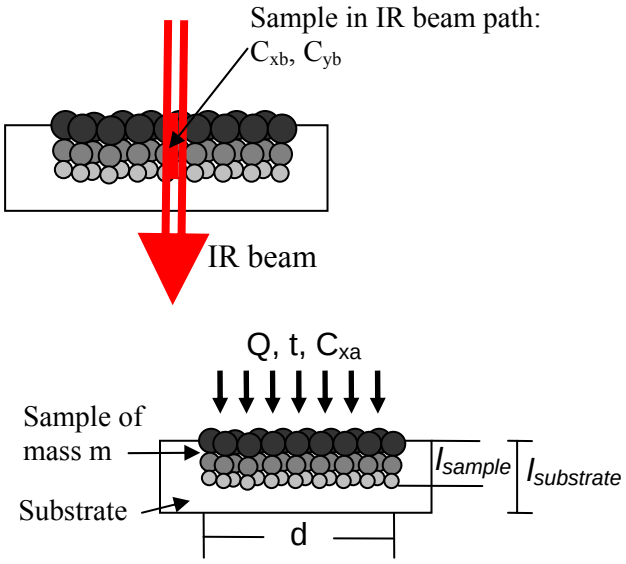

Figure 2- 1 Illustrate the substrate and sample with all variables used in the algorithms develop in this chapter

Other quantities of import include V which represents volume, ABS with represents integrated absorbance of a peak in the signature of a functional group, ε which represents molar absorptivity and l which indicates the length of the MIR beam through the sample or filter.

The derivation begins with Beer Lambert's Law which relates concentration to absorbance:

Equation 2- 2 $$C_{x\,in\,b} = \frac{ABS_{x\,in\,b}}{\varepsilon_x l_{x\,in\,b}}$$

Where the subscripts x and b represent the unknown functional group and the beam respectively, $C_{x\ in\ b}$ is the molar concentration of the unknown functional group in the beam (mol/L), $ABS_{x\ in\ b}$ is the integrated absorbance area of the unknown functional group in the beam (absorbance units), ε_x is the molar absorptivity of the integrated signature peak of the unknown functional group, and $l_{x\ in\ b}$ is the thickness of the sample with a uniform amount of the functional group that the beam passes through (m).

The concentration of the functional group in the ambient air is a function of the number of moles of the functional group in the beam scaled by the constant α and divided by the sampling volume, as shown below:

Equation 2- 3 $$C_{x\,in\,a} = \frac{C_{x\,in\,b} V_b\, \alpha}{Q\, t}$$

Where the subscripts x, a and b represent the functional group, the air and the beam respectively, $C_{x\ in\ a}$ is the concentration of the unknown functional group in the ambient air and $C_{x\ in\ b}$ is its concentration in the beam (mol/L), V_b is the volume of the beam that passes through the filter and sample, Q is the flowrate of ambient air drawn through the filter to collect the sample (L/min), t is the duration of sample collection (min), and α is a theoretical constant.

The value of α is determined by assuming that the concentration of the functional group in the beam is the same as its concentration in the entire sample (i.e., the sample is homogeneous with surface area), such that Cx in the beam equals that in the filter. When this is true:

Equation 2- 4 $C_{x\,in\,b} = \frac{n_{x\,in\,b}}{V_b} \equiv C_{x\,in\,s} = \frac{n_{x\,in\,s}}{V_s}$ **and so** $\alpha = \frac{n_{x\,in\,s}}{n_{x\,in\,b}} = \frac{V_s}{V_b}$

Where the new subscript f represents the filter and n is the number of moles (mole).

Combining the first two equations:

Equation 2- 5 $C_{xa} = \frac{\frac{ABS_{x\,in\,b}}{\varepsilon_x l_{x\,in\,b}} V_s\ \alpha}{Q\ t}$

The molar absorptivity of unknown functional group x can be related to molar absorptivity of the known functional group y using relative molar absorptivity as well as Beer Lambert's law written for the known functional group, as shown below:

$$\xi_{x/y} = \frac{\varepsilon_x}{\varepsilon_y} \quad \textbf{and so} \quad \varepsilon_x = \xi_{x/y}\ \varepsilon_y = \xi_{x/y}\ \frac{ABS_{y\ in\ b}}{C_{y\ in\ b}\ l_{y\ in\ b}}$$

Where $\xi_{x/y}$ is the relative molar absorptivity for the unknown and known functional groups.

Substituting this result into the prior expression yields:

Equation 2- 6 $$C_{x\ in\ a} = C_{y\ in\ b}\ \frac{ABS_{x\ in\ b}\ /\ l_{x\ in\ b}}{ABS_{y\ in\ b}\ /\ l_{y\ in\ b}\ \xi_{x/y}}\ \frac{V_s\ \alpha}{Q\ t}$$

This last equation is the general form of this algorithm that was further simplified for 3 cases: (a) internal standard is the Teflon substrate, (b) internal standard is a chemical coating the sample, and (c) the internal standard is a chemical that is uniformly distributed throughout the sample.

Case (a): $l_{x\ in\ b} = l_s$. since the functional group is part of the sample

$l_{y\ in\ b} = l_f$. since the light passes through the entire thickness of the filter

$V_s = \pi\ r_s^2\ l_s\ \left(1 - \eta_f\right)$ assuming that the sample fills the filter voids where r_s is the radius of the sample and η_f is the porosity of the filter

Using the case (a) simplifications, the final equation to determine the average concentration of the unknown functional group in the air $C_{x\ in\ a}$ when the internal standard is the Teflon substrate is:

Equation 2-6(a) $$C_{x\ in\ a} = C_{y\ in\ b}\frac{ABS_{x\ in\ b}\ l_f}{ABS_{y\ in\ b}\ \xi_{x/y}}\frac{\pi r_s^2\left(1-\eta_f\right)\alpha}{Q\ t}$$

Where $C_{y\ in\ b}$ is the concentration of Teflon in the beam which is equal to its concentration in the filter estimated from MW and η_f porosity of the filter provided by the manufacturer, $ABS_{y\ in\ b}$ and $ABS_{x\ in\ b}$ are the integrated absorbance areas of the known and unknown functional group signature peaks measured by FTIR, $\xi_{x/y}$ is the relative molar absorptivity of the two functional groups determined by calibration of the FTIR, l_f is the filter thickness measured using calipers or provided by the manufacturer, r_s is the radius of the sample measured using calipers or taken as the inside diameter of the filter pack, α is the ratio of the sample volume to the beam volume, Q is the sampling flow rate which is likely to be 16.67 LPM, and t is the sampling duration which is likely to be 4 to 24 hours.

Case (b): $l_{x\ in\ b} = l_s$. since the functional group is part of the sample

$l_{y\ in\ b} = l_c$. where c represents the coating

$V_s = \pi\ r_s^2\ l_s\left(1-\eta_f\right)$ assuming that the sample fills the filter voids where r_s is the radius of the sample and η_f is the porosity of the filter

Using the case (b) simplifications, the final equation to determine the average concentration of the unknown functional group in the air $C_{x\ in\ a}$ when the internal standard is a thin coating on the surface of the sample is:

Equation 2-6(b) $$C_{x\ in\ a} = C_{y\ in\ b}\frac{ABS_{x\ in\ b}\ l_c}{ABS_{y\ in\ b}\ \xi_{x/y}}\frac{\pi r_s^2\left(1-\eta_f\right)\alpha}{Q\ t}$$

Where $C_{y\ in\ b}$ is equal to its concentration across the entire sample and is determined based on the volume of coating applied and the density of the chemical provided by the manufacturer, $ABS_{y\ in\ b}$ and $ABS_{x\ in\ b}$ are the integrated absorbance areas of the known and unknown functional group signature peaks measured by FTIR, $\xi_{x/y}$ is the relative molar absorptivity of the two functional groups determined by calibration of the FTIR, l_c is thickness of the coating, r_s is the radius of the sample measured using calipers or taken as the inside diameter of the filter pack, η_f is the filter porosity provided by the manufacturer, α is the ratio of the sample volume to the beam volume, Q is the sampling flow rate which is likely to be 16.67 LPM, and t is the sampling duration which is likely to be 4 to 24 hours.

Case (c): $l_{x\ in\ b} = l_s$. since the functional group is part of the sample

$l_{y\ in\ b} = l_s$. since the internal standard is homogeneously distributed in the sample

$V_s = \frac{m_s}{\rho_s}$ where m and ρ are measurable quantities fine particle mass and density

Based on the case (c) simplifications, the final equation to determine the average concentration of the unknown functional group in the air $C_{x\ in\ a}$ when the internal standard is distributed uniformly through the sample during sample collection is:

Equation 2-6(c) $$C_{x\ in\ a} = C_{y\ in\ b} \frac{ABS_{x\ in\ b}}{ABS_{y\ in\ b}\ \xi_{x/y}} \frac{m_s\ \alpha}{\rho_s\ Q\ t}$$

Where $C_{y\ in\ b}$ is determined from the mass loading of the chemical into the sample stream during sampling, $ABS_{y\ in\ b}$ and $ABS_{x\ in\ b}$ are the integrated absorbance areas of the known and unknown functional group signature peaks measured by FTIR, $\xi_{x/y}$ is the relative molar absorptivity of the two functional groups determined by calibration of the FTIR, m_s is the mass of fine particles collected on the substrate, ρ_s is the density of fine particles reported in the literature to be 2000 Kg m^{-3}, α is the ratio of the sample volume to the beam volume, Q is the sampling flow rate which is likely to be 16.67 LPM, and t is the sampling duration which is likely to be 4 to 24 hours.

These algorithms are less sensitive to the measurements of the path length and sample diameter than to the relative molar absorptivity. The two absorbance terms will have similar magnitude and uncertainty. The dimensionless relative molar absorptivity will range in value from 10^{-2} to 10 and its uncertainty has yet to be assessed. The flow rate will be 16.67 LPM (0.96 $m^3\ h^{-1}$) and the sampling time will range from 4 to 24 hours. The concentration of the internal standard will be on the order of 10^{-4} mol m^{-3} and can be made with great precision and accuracy. The path length and sample diameter will each be on the order of 10^{-3} m and will have modest uncertainties based on the caliper.

2.2 EXPERIMENT 2: QUANTITATION USING AN EXTERNAL STANDARD

2.2.1 Issue

An external standard is an additional analytical method capable of measuring the concentration of one of the fine particle species in the fine particle sample that is analyzed by FTIR. Generally, when an external standard is used, the additional knowns include the number of moles of one of the fine particle species in the sample.

There are several reasonable candidates for external standards, as noted in Chapter 1. However, for the most part they are destructive or they require extraction which compromises the integrity of the sample, or they do not measure the complete mass of a species in the sample due to extraction inefficiency or the inability of the method to measure all of the molecules in the fine particle sample which contain the species.

2.2.2 Goal

The goal of this experiment is to identify possible external standards that are able to measure one of the components of fine particles to a high degree of accuracy (i.e., considering processing steps such as extraction that reduce accuracy), and derive an algorithm to calculate the concentration of a fine particle species in the ambient air as a result of the species absorbances measured by FTIR, the concentration of a species in the sample measured using an external method, sampling quantities (e.g., flow rate), and other easily measured quantities (e.g., sample mass).

2.2.3 Literature Review

As previously mentioned, most studies that use FTIR to characterize fine particle speciation only use a qualitative approach given the issues described above.

However, a couple studies have gone a step further to estimate the absolute concentration of functional groups in the fine particles. All of these methods have used external standards to do so. These studies assumed reasonably that $\frac{C_{x\,in\,b}}{C_{y\,in\,b}} = \frac{C_{x\,in\,a}}{C_{y\,in\,a}}$ and therefore:

Equation 2- 7 $$C_{x\,in\,a} = C_{y\,in\,a} \times \frac{ABS_{x\,in\,b} \big/ \varepsilon_x l_b}{ABS_{y\,in\,b} \big/ \varepsilon_y l_b} = C_{y\,in\,a} \times \frac{ABS_x}{ABS_y} \times \xi_{y/x}$$

Where C_a is the concentration of x or y in the ambient air. Carlton et al. (1999) collected fine particle samples on filters intended characterize personal aerosol exposure. They then analyzed the samples using FTIR for functional group identification and using GC/MS to measure the concentration of PAHs in the entire sample, C_{ya}. They could then use the prior equation to calculate the concentration of all of the rest of the species in the fine particle sample. Blando et al. (2001) generated and collected fine particle samples to evaluate the relationship between infrared absorption and functional group (carbonyl, ammonium and sulfate) loading. They produced KBr pellets containing the sampled fine

particles for analysis by FTIR, and then used IC as an external standard to approximate the concentration of sulfate in the ambient sample.

2.2.4 Experimental Approach

Identify external standard candidates

Review the methods described in Chapter 1 and identify reasonable candidates for external standards. Ideal methods are those that:

- Are adaptable to Teflon filters
- Are nondestructive
- Do not require extraction or are highly efficient for the extraction of the target species
- Have high accuracy in the measurement of the target species

Spectral interpretation

All spectra were analyzed by using different approaches that were evaluated in Chapter 5. Approaches used include the shaving and horizontal baselines, shifting and non shifting of peaks respect to Octane and Methanol, and all overlapping peaks were quantified by splitting at the non shifted endpoint.

Derive algorithm for quantitation using an external standard

Derive an algorithm for the concentration of fine particle species concentrations in the ambient air that:

- Depends on measurable FTIR properties, measurable external method properties and measurable sample properties
- Does not depend on path length of the sample or absolute molar absorptivity

2.2.5 Results and Discussion

Identify external standard candidates

The methods described in Chapter 1 were reviewed. Since most of the organic methods measure carbon as a lump sum, those methods that measure inorganics are considered to be more reasonable because of their chemical specificity. Examples include ion chromatography of any of the inorganic ions and flash volatilization of nitrate and sulfate.

Ion chromatography (IC) is adaptable to Teflon filters, and in fact samples intended for analysis by IC are typically collected onto Teflon filters. The method is destructive and requires extraction, which is not preferable, but the extraction is very efficient and the IC analysis is very accurate.

Flash volatilization is not adaptable to Teflon filters and requires that the sample be collected on a metal strip that a large charge can be applied to. Therefore, use of this approach will require simultaneous collocated sample collection onto a Teflon filter for the FTIR and onto a metal strip for the flash volatilization. The method is destructive, but since the analysis will be done on a collocated sample and not on the Teflon filter intended for FTIR analysis, this is less of an issue. Flash volatilization is a newer method

that has been less characterized than IC. However Wittig et al. (2001) demonstrated the linearity and accuracy of the method when rigorous quality control measures were also implemented.

Both of these methods provide a value of the concentration of the inorganic ion in the ambient air, which can be used in the algorithm to eliminate variables that are more difficult to measure.

Derive algorithm for quantitation using an external standard

This algorithm builds on the ones developed for an internal standard. Beginning from Equation 2-2:

Equation 2- 8 $$C_{x\,in\,a} = C_{y\,in\,b}\,\frac{ABS_{x\,in\,b}/l_{x\,in\,b}}{ABS_{y\,in\,b}/l_{y\,in\,b}\;\xi_{x/y}}\,\frac{V_s\;\alpha}{Q\;t}$$

The concentration of functional group y in the beam now depends on the number of moles of functional group in the sample measured using the external standard:

Equation 2- 9 $$C_{y\,in\,b} = \frac{n_{y\,in\,s}/\alpha}{V_b} = \frac{n_{y\,in\,s}}{V_s}$$

Where $n_{y\,in\,s}$ is the number of moles of the known functional group in the entire sample collected on the filter and measured using the external method, V_b is the volume of the sample in the beam that passes through the and the dimensionless scaling constant α.

Equation 2- 10 $$C_{x\,in\,a} = n_{y\,in\,s}\,\frac{ABS_{x\,in\,b}/l_{x\,in\,b}}{ABS_{y\,in\,b}/l_{y\,in\,b}\;\xi_{x/y}}\,\frac{\alpha}{Q\,t}$$

There is only one case to evaluate: (a) an external standard measures the concentration of one of the functional groups present in the sample, so that both FTIR and external measurements are available of the same functional group

Case (a) $l_{x\,in\,b} = l_s$. since the unknown functional group is part of the sample

$l_{y\,in\,b} = l_s$. since the known functional group is also part of the sample

Using these case (a) assumptions, the final expression for the concentration of an unknown functional group in the ambient air when using an external standard is:

Equation 2-10(a) $$C_{x\,in\,a} = n_{y\,in\,s}\,\frac{ABS_{x\,in\,b}}{ABS_{y\,in\,b}\;\xi_{x/y}}\,\frac{\alpha}{Q\,t}$$

Where $n_{y\ in\ b}$ is the number of moles of the known functional group in the sample measured using the external standard, $ABS_{y\ in\ b}$ and $ABS_{x\ in\ b}$ are the integrated absorbance areas of the known and unknown functional group signature peaks measured by FTIR, $\xi_{x/y}$ is the relative molar absorptivity of the two functional groups determined by calibration of the FTIR, α is the ratio of the sample volume to the beam volume, Q is the sampling flow rate which is likely to be 16.67 LPM, and t is the sampling duration which is likely to be 4 to 24 hours.

This algorithm is less sensitive to the external measurement of one of the functional groups in the sample than it is to the relative molar absorptivity, since the order of the moles of the functional group in the sample will be approximately 10^{-4}.

2.3 CONCLUSIONS

Three algorithms were derived that relate fine particle species concentration to FTIR absorbances of the fine particle species (ABS), general properties of ambient particles such as density (ρ) and relative molar absorptivity (ξ), quantities related to how the sample was collected such as sampling flow rate (Q) and sample duration (t), and known concentration of an internal standard in the sample measured by FTIR (C_y) or measured by an external analytical method (n_y).

The algorithms purposely do not depend on properties that are difficult to accurately measure, such as path length or absolute molar absorptivity.

2.4 REFERENCES

Blando, J., Procja, R. and Turpin, B., 2001. Issues in the quantitation of functional groups by FTIR spectroscopic analysis of impactor-collected aerosol samples. Aerosol Science and Technology 35, 899-908.

Carlton, A., Turpin, B., Johnson, W., Buckley, B., Simcik, M., Eisenreich, S. and Porcja, R., 1999. Microanalysis methods for characterization of personal aerosol exposures. Aerosol Science and Technology 31, 66-80.

Dekermenjian, M., Allen, D., Atkinson, R. and Arey, J., 1999. FTIR analysis of aerosol formed in the ozone oxidation of sesquiterpenes. Aerosol Science and Technology 30, 349-363.

Holes, A., Eusebi, A., Grosjean, D. and Allen, D., 1997. FTIR analysis of aerosol formed in the photooxidation of 1,3,5-Trimethylbenzene. Aerosol Science and Technology 26, 516-526.

Palen, E., Allen, D., Pandis, S., Paulson, S., Seinfeld, J. and Flagan, R., 1993. Fourier transform infrared analysis of aerosol formed in the photooxidation of 1-Octene. Atmospheric Environment 27A (9), 1471-1477.

CHAPTER 3 SAMPLE COLLECTION/PREPARATION

Recall that before the $PM_{2.5}$ can be analyzed by FTIR, it must be uniformly collected into a small area on a substrate that can be directly analyzed by FTIR without introducing artifacts. The experiments presented in this chapter develop methods to collect samples for FTIR analysis.

The research and development of a sampling approach will address the following issues:

- Experiment 3: Minimization of sampling artifacts
- Experiment 4: Selection of sampling substrate
- Experiment 5: Identification of minimum sample loading

3.1 EXPERIMENT 3: MINIMIZATION OF SAMPLING ARTIFACTS

In this experiment, the configuration of a sampler used to collect fine particle samples for FTIR analysis is determined, with the goal of minimizing sampling artifacts.

3.1.1 Issue

Fine particle samples can be collected by absorption into a liquid, by impaction onto a nonporous substrate, or by filtration through a porous substrate. Each of these methods has its own limitations.

Absorption is subject to many of the same issues as extraction, discussed in the prior chapter. Impaction onto a substrate causes spatial inhomogeneities in the sample due to

particle bounce, and is inefficient for small particle collection. Both of these issues limit its ability to collect a representative fine particle sample.

Filtration also has some issues. Positive sampling artifacts are the gain of gases by adsorption to the sampling substrate, which have a similar chemical form as components in the fine particles and therefore are indistinguishable from them during analysis. Examples include gaseous HNO_3g and particulate NO_3-s, and gaseous volatile organics and particulate organics.

Negative sampling artifacts are the loss of fine particle components by volatilization from a sampling substrate because of an excessive pressure drop across the substrate.

3.1.2 Goal

The goal of this experiment is to propose a sampler able to collect a PM2.5 sample that is representative of the particles in the ambient air, and in a way that complements the FTIR analysis.

3.1.3 Literature review

The inefficiencies of absorption and impaction have been well documented. In addition to these inefficiencies, both approaches result in samples that are spatially inhomogeneous. For the case of absorption, particles will be present in the solvent in

dissolved, suspended and settled form. In the case of impaction, the sample will be collected on a nonporous substrate in concentric rings due to particle bounce.

Filtration is also subject to some issues, but these issues can be addressed to a large extent through sampler design. Positive artifacts due to gases in the sample stream that adsorb to filters have been minimized by denuding the sample of these gases at a location upstream of the substrate. Denuders are not used in the nationwide sampling networks because of the assumption that the concentration of interfering gases is at least an order of magnitude smaller than the concentration of the same chemical compounds in the particle-phase (Turpin et al., 2000). Wittig et al. (2004) showed that nitric acid concentrations observed in Pittsburgh PA in 2000 were over ten times larger than the particle-bound nitrate during the daytime and at summer, and were non-existent during the winter. While removal of these interfering gases may imbalance the equilibrium of the particle-phase compounds, this is not expected to be an issue in the proposed work because of the planned short sample times. The selection of the denuder depends on the class of interferents to be removed. Takahama et al. (2004) evaluated the effectiveness of a denuder coated with magnesium oxide (MgO) and citric acid (CA) to remove nitric acid and ammonia gases and Subramanian et al. (2004) evaluated the effectiveness of an activated carbon monolith (AC) denuder for the removal of organic gases from ambient $PM_{2.5}$ samples collected in Pittsburgh PA in 2000. Their results showed that all the positive artifacts were eliminated (anywhere from 0% to 1100% of the ambient particulate species concentration) and the negative artifacts due to volatilization from the denuder were 6.3% on average of the ambient particulate organic carbon.

Negative artifacts can be minimized by keeping the velocity of the sampled air across the sample substrate, face velocity, low. Face velocity is defined as:

Equation 3- 1 $$\textit{Face Velocity} = \mathrm{Q(LPM)} \times \left[\pi \times \left(\frac{\mathrm{D(m)}}{2} \right)^2 \right]^{-1}$$

Where Q is the flow rate of the sample in L min^{-1}, D is the diameter of the filter in m.

In order to collect more time-resolved samples, larger flow rates of ambient air through the sampler are desirable. However, unless the filter size is also increased, face velocity will linearly increase which, by Bernoulli's principle, leads to larger pressure drops across the sampling substrate. If the pressure at the back of the substrate drops to below the vapor pressure of a particle-bound compound, the compound will volatilize from the particle and escape from the substrate to the gas phase.

The face velocity used in the STN nationwide monitoring network is approximately 16 cm/s, which allows these samplers to avoid losses of semi-volatile particle-bound compounds, such as nitrate or many organics. However, face velocities that are nearly 2.5 times higher have been used in special studies with equal success (Carlton et al., 1999).

3.1.4 Experimental Approach

From the literature review, propose a sampler design that allows representative fine particle samples to be collected onto filters:

- Identify a general configuration based on standard samplers
- Identify denuders that can be used to minimize positive sampling artifacts
- Identify minimum face velocity to minimize negative sampling artifacts

3.1.5 Results and Discussion

General sampler configuration

The configuration of a conventional sampler is illustrated in **Figure 3-1**.

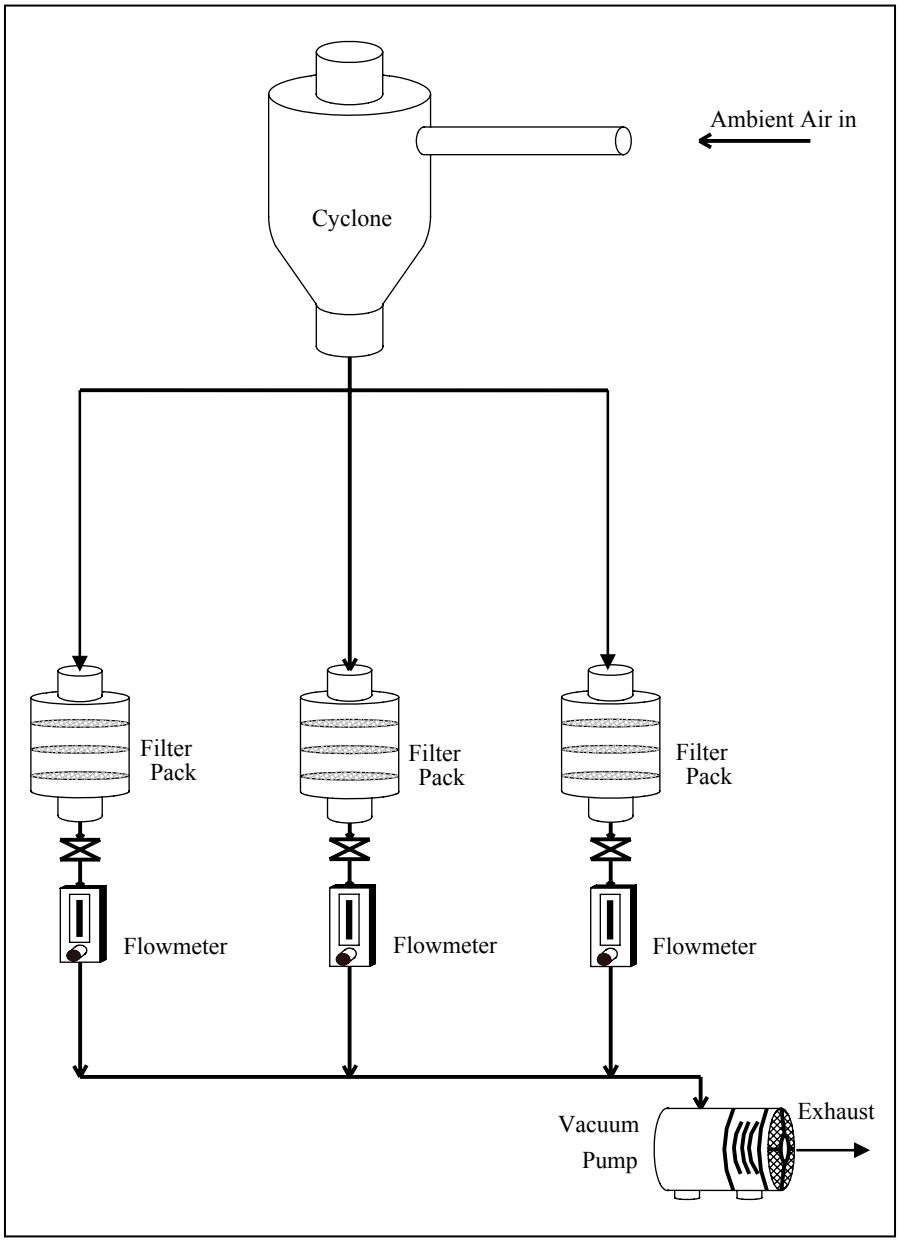

Figure 3- 1 Configuration of the conventional sampling system

Air is first drawn through a cyclone which removes particles larger than 2.5 um in aerodynamic diameter using centripetal force.

The sample air is next drawn through the substrate, which collects the sample by impaction, filtration and sieving. The substrate is typically mounted in filter packs which hold it in place by its edges to avoid sample contamination or loss. The filter packs are made of the inert material Teflon, but the substrate material depends on the class of compounds to be collected. The filter pack can hold a single substrate or multiple substrates in series to monitor negative sampling artifacts or for quality control purposes.

The filtered air then passes through a flow meter which regulates the flow through the entire system, through a vacuum pump which establishes the flow through the entire system, and then exits the system as exhaust. Sampling durations are typically 24 hours, generally from midnight to midnight.

Denuders to minimize positive sampling artifacts

Since the goal of this work is to measure the concentration of fine particle speciation, which includes inorganics such as nitrate NO_3- and semi-volatile organics, it is important for this work to minimize both positive and negative artifacts.

Our sample collection systems will be modified from the conventional design showed earlier, to accommodate denuders in the lines intended for collecting samples for organic speciation and inorganic speciation analysis. MgO, CA and AC denuders will be placed immediately upstream of the filter packs to remove nitric acid, ammonia and organic gases, respectively, prepared using the approaches described by Takahama et al. (2004) and Subramaniam et al. (2004).

Face velocity to minimize negative artifacts

The STN nationwide monitoring network collects fine particle samples at a flow rate of 16.67 LPM, onto filters of diameter 0.047 m. This results in a face velocity of 0.016 ms^{-1}. This value of face velocity will be used to avoid volatilization losses of semi-volatile particle-bound compounds, such as nitrate and many organics.

Sampling durations of 2-24 hours will be considered, where shorter times may be used when the ambient $PM_{2.5}$ concentration is high. The actual sampling time depends on the minimum loading, discussed at the end of this chapter.

3.2 EXPERIMENT 4: SELECTION OF SAMPLING SUBSTRATE

3.2.1 Issue

Substrates that are not transparent to MIR have the potential to obscure the MIR signature of organic and inorganic compounds in the $PM_{2.5}$ sample. From this perspective, the ideal substrate has a signature outside of the MIR region altogether.

3.2.2 Goal

Our goal is to identify a single substrate that is able to efficiently collect $PM_{2.5}$ containing both organic and inorganic compounds and that is transparent to MIR. The substrates that will be tested include Teflon, quartz fiber, nylon and cellulose fiber filters and ZnSe disks.

3.2.3 Literature Review

Teflon filters have been used extensively to collect PM2.5 samples for particle-bound and gas-phase inorganic speciation (Takahama et al., 2004; Wittig et al., 2004) because the way that this type of sample is typically analyzed: extraction followed by Ion Chromatography (IC) (Gordon et al., 1988). Their inert quality improves extraction efficiency, and extraction is necessary for IC analysis. Teflon is a generic name for a wide class of polymers. Reff et al., 2005 report that Teflon filters (Gelman Sciences) have a strong MIR signatures at 1213 and 1152 cm^{-1} which may overlap with fine particle species signatures (Allen et al., 1989; Krost et al., 1994; Maria et al., 2002). Since the chemical composition of Teflon can vary, the MIR signature of commercially available Teflon filters will have to be determined.

Quartz fiber filters have been used extensively to collect PM2.5 samples intended for particle-bound organic and elemental carbon speciation because of the way that this type of sample is typically analyzed: directly in a Gas Chromatograph (GC) which operates at high temperature. For this purpose, they are quite efficient (Turpin et al., 2000; Cabada et al., 2004a; Subramanian et al., 2004). Quartz fiber filters have a strong and broad signal in the MIR range at 1040 and 794 cm^{-1} (Carlton et al., 1999), which may interfere with the signatures of fine particle species. However, differences in the manufacture of the quartz filters can have a large impact on the signature and so the actual MIR signature of the Tissuequartz filters will have to be determined.

Nylon membranes are used to collect and analyze negative sampling artifacts for nitrate. Like Teflon filters, nylon filters are used for inorganic speciation (Takahama et al., 2004), but there is not information about the MIR signature of nylon filters.

Acid impregnated cellulose fiber filter are used to capture the volatilized ammonium that escape the denuder (Takahama et al., 2004). The MIR signature of this substrate type has not been published and will have to be determined.

Optically polished ZnSe disks have not been used extensively but offer promise. They are not filters, but impaction surfaces, so their collection efficiency is likely to be lower than that of the filter-based substrates already discussed. According to Palen et al. (1992) and Allen et al. (1994), these disks are transparent to MIR radiation allowing direct analysis by FTIR. Additionally, unlike any of the substrates already discussed, they are reusable when properly cleaned.

A synopsis of the results of prior work to evaluate the substrates considered in this work is presented in **Table 3-1**. **Table 3- 1** Typical use of substrates considered in this work.

Substrate	Typical use	Reported MIR interference
Generic Teflon filter	Efficient collection of fine particles for inorganic speciation	Sharp signatures at 1250, 1213, 1152, 1100 & 554 cm^{-1}
Generic quartz fiber filter	Efficient collection of fine particles for organic speciation	Strong and broad signature at 794 cm^{-1}
Generic nylon membrane	Efficient collection of fine particles for nitrate speciation	Unknown
Generic cellulose fiber filter	Efficient collection of fine particles for ammonium speciation	Unknown
Generic ZnSe polished disk	Unknown efficiency collection of fine particles for organic and inorganic speciation	None

Table 3- 1 Typical use of substrates considered in this work.

3.2.4 Experimental Approach

This experiment uses the FTIR to determine the MIR signatures of potential sampling substrates.

The following sampling substrates were evaluated in a blank state (i.e., unsampled): nylon membranes (Whatman, 7410-004), cellulose-fiber filters (Whatman, 1441-047), ZnSe disks (Reflex Analytical Corporation, 23-23014), Teflon filters (Savillex, #1145,or Pall Gelman Teflo, R2PJ047), and quartz fiber filters (Pall Gelman, Tissuequartz 2500 QAO-UP). The sampler described in the prior experiment, is not used because this experiment involves the FTIR analysis of blank substrates.

The FTIR was used in a conservative manner to avoid results confounded by variables to be evaluated in later experiments.

- FTIR scan rate is low so spectra resolution is high (i.e., 250 scans per spectrum)

- Spectroscopy approach - use transmission and reflectance; for transmission, load holders with blank substrates and use automated shuttle to move filters into and out of the FTIR light path; for reflectance, place filter directly on ATR accessory
- Background spectra - use open-path background approach to account for gases in the analysis chamber; acquire background spectra every 10 to 15 minutes
- Gas interferent minimization - do not use any settings in the software to mathematically suppress signatures of analysis chamber gases in spectrum

For each sample (i.e., each substrate), the FTIR was used to collect 3 each of the following spectra in immediate succession:

- Open-path background (OPBG) of chamber gases
- Blank substrate corrected using the most recent open-path background

These spectra were further processed using the FTIR instrument software to develop 3 replicate spectra of each of the blank substrates, resulting in 36 spectra (6 substrates, 2 spectroscopy approaches, 3 replicates):

- The background-corrected blank substrate and sample on substrate spectra were subtracted without using the correction factor

These FTIR settings are addressed in later chapters.

The spectra were then analyzed. Signatures in the MIR range were analyzed to identify potential interferences with the fine particle speciation signatures. The most ideal

substrates have no signature in the MIR region. The second-best substrates have sharp but weak signatures in MIR regions that do not overlap with targeted inorganic and organic species.

3.2.5 Results and Discussion

FTIR analyses of blank nylon membranes (Whatman, 7410-004) and cellulose-fiber filters (Whatman, 1441-047) indicate broad signatures across the MIR spectrum. Therefore, neither of these substrates are good candidates for fine particle speciation using FTIR.

FTIR analyses of blank ZnSe disks (Reflex Analytical Corporation) confirmed no signature in the MIR spectrum. Therefore, this substrate type is a good candidate for fine particle speciation.

Analyses of the Savillex and Pall blank Teflon filters, and quartz fiber filters (Tissuequartz 2500, QAO-UP) revealed that all have a MIR signature, but the signatures of some sampling substrates are sharper and smaller and therefore have less potential to interfere with the MIR spectra of fine particle species. This is illustrated in Error! Reference source not found..

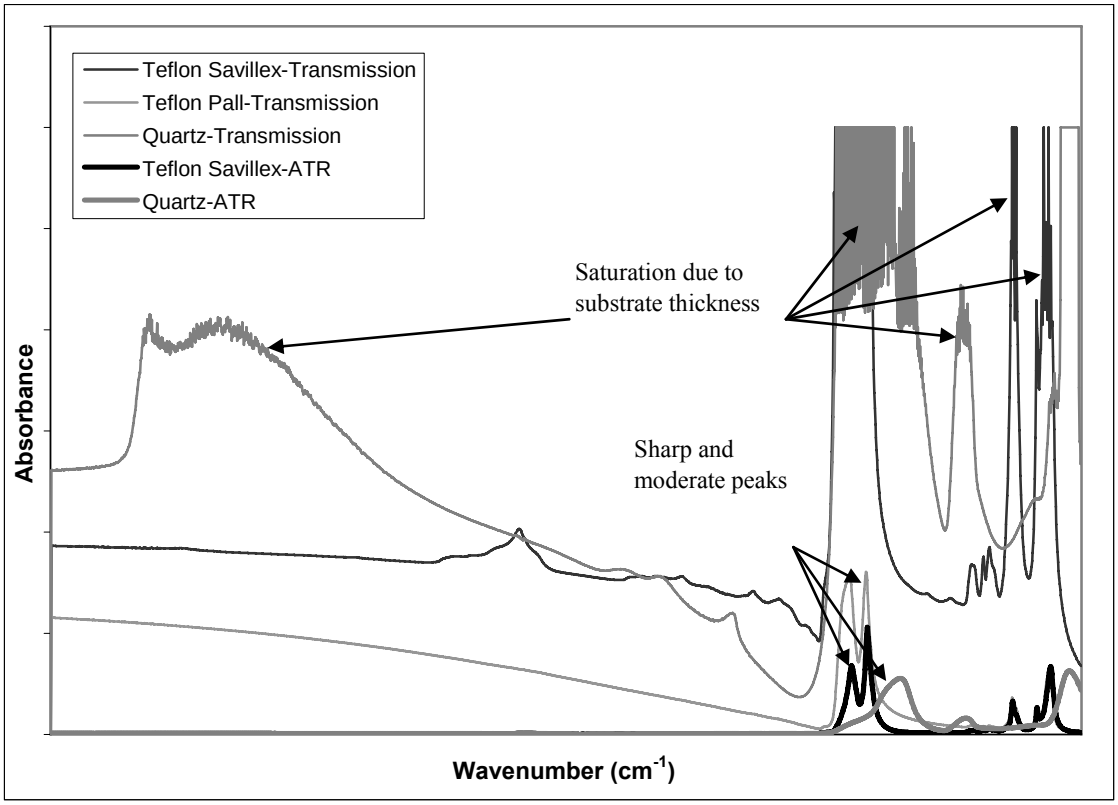

Figure 3- 2 Different blank spectra comparison obtained by the FTIR spectrometer.

This figure shows the signatures of blank Teflon and quartz fiber filters in the MIR spectrum. The transmission spectra of Savillex Teflon filters are saturated because of the filter's thickness but the attenuated total reflectance spectra of the same filter results in sharp moderate peaks which may obscure the sample signature. This can be explained by the fact that the MIR light passes all the way through the substrate to collect a transmission spectrum, but only passes through a portion of the substrate to collect a total reflectance attenuation spectrum. This distinction is discussed in great detail in **Experiment 4**. The transmission spectra of Teflon filters from Pall manufacturer result in a sharp moderate peaks at 1250-1100 cm^{-1} and at 560-490 which may interfere with some fine particle species signatures. However, since the ATR and transmission spectra of both

types of Teflon filters has MIR signatures that are sharp and moderate, these filters are still good candidates for PM2.5 speciation using FTIR.

Quartz filters have a broad signature in the MIR spectrum over a large portion of the MIR spectrum from 1350-400 cm^{-1}. Their transmission spectra are saturated in a large portion of the MIR range but their ATR spectra are not, because of the same distinction in the light path explained above. However, since the ATR spectrum of the quartz filter has MIR signatures that are sharp and moderate, this filters are still good candidates for PM2.5 speciation using FTIR.

Results from this experiment show that the best substrate to collect aerosol samples is the Teflon substrate from Pall manufacturer, because it does not saturate the sample spectra, and the sharp and moderate Teflon signatures can be subtracted from the sample spectrum, which is the sample and the substrate signatures, in order to get only the spectrum of the sample. Also there is a possibility the sharp signal of Teflon in the spectrum can be used as an internal standard to assure that the FTIR spectrometer is working properly, by checking the location and absorbance of its signature periodically (**Experiment 7**).

3.3 EXPERIMENT 5: IDENTIFICATION OF MINIMUM SAMPLE LOADING

3.3.1 Issue

Temporally resolved $PM_{2.5}$ measurements allow for valuable insight into the temporal variability of air quality issues. However, at low sample times, the mass of $PM_{2.5}$

collected on the substrate may be too small to quantify. To avoid this, some samplers increase the filter surface area (e.g., STN samplers use 22 cm^2 and High-Vol samplers use 1000 cm^2) as opposed to the sample duration so that more $PM_{2.5}$ can be collected in a given time period. This is a useful approach if the sample is then extracted, or if the analysis analyzes the complete sample and not just a small area of it. Therefore, this option is not available if FTIR is used to determine fine particle speciation.

Another approach is to increase the flow rate of ambient air that passes through the substrate. For reasons already explained, this approach will cause a negative sampling artifact, and therefore this option is not reasonable.

Therefore, the minimum sample loading is dictated by the fixed flowrate of ambient air through the sampling substrate and the sensitivity of the FTIR to the target chemical species present in fine particles.

3.3.2 Goal

The minimum sample loading is the minimum time integrated mass of $PM_{2.5}$ that must be collected onto a sampling substrate in order to be above the FTIR detection limits for the target chemical species present in fine particles. In this work, the minimum detection limit is defined as the mass which achieves a signal to noise ratio above 3 (Krost et al., 1994).

3.3.3 Literature Review

Since the NCore nationwide monitoring networks are used for compliance purposes, sample durations are always for 24-hours beginning at midnight and ending the following midnight, to be consistent with the regulation time period. Only in special studies are sampling times and durations varied.

For our purposes, it is desirable to have flexible sampling times, so that the FTIR approach developed in this work can be used to address a variety of different issues, including compliance.

The specific mass loading can be approximated as:

Equation 3- 2 $$M = \frac{C \times Q \times t}{A}$$

Where M is the specific mass loading in g cm^{-2}, C is the concentration of the fine particles in the ambient air in g m^{-3}, Q is the flow rate of the aerosol collected onto the filter in LPM, t is the time of sample collection in hours, and A is the sampling area on the filter in cm^2.

During the Pittsburgh Supersite campaign, organic and inorganic aerosol samples were collected at 16.67 LPM onto 47mm filters for periods as short as 4 hours (Cabada et al., 2004b). The specific mass loading of these samples, to be later analyzed by IC and GC/FID, were related with the mass concentration (C) and is approximately 0.74 times C.

However, the specific mass loadings observed in the literature for samples intended for FTIR analysis are much higher. For example, the specific mass loading for $PM_{2.5}$ samples collected by Reff et al. (2005) was 5.6 times C, corresponding to a sampling flow rate of 10 LPM, a collection period of 24-hours, and substrates of 37mm diameter. PM_{10} samples, which include the $PM_{2.5}$, collected by Carlton et al. (1999) had specific mass loadings of 4.9 times C, corresponding to a flow rate of 4 LPM, a collection period of 24-hours and substrate diameter of 25mm. The need for higher specific mass loadings is in part explained by the fact that FTIR measures aerosol composition for the small fraction of the aerosol in the light path, whereas IC and GC/FID require extraction and measure the total aerosol collected onto the substrate.

Since the minimum mass loading is an instrument specific quantity, and since Reff et al. (2005) and Carlton et al. (1999) did not use FTIR in a quantitative capacity, the next experiments evaluate the detection limits of FTIR for the target species in fine particles.

3.3.4 Experimental Approach

In these experiments, the sampling system is not used. Instead, samples were created by delivering precise volumes of model compounds onto a Pall Teflon filter using the Finnpipette micro-liter automatic pipette.

Experiments were conducted for one organic model compound. The organic model compound was octanoic acid which includes four functional groups: alkane hydrogen

-(C-H), carbonyl -(C=O), alcohol -(O-H), and alkane carbon –(C-C)-. Octanoic acid is stable at room temperature therefore volatilization was not an issue in this experiment.

The mass of functional groups in the model compound was varied by diluting the model compound in a solvent. Octanoic acid (MW=144.211 g/mol, density=0.91 g/ml) was diluted in acetone (MW=58.08 g/mol, density=0.79 g/ml) at four different octanoic acid:acetone volume ratios: 1:0, 1:1, 1:3 and 1:4.

Dilution #	**Solute:Solvent**
	Octanoic Acid (OA):Acetone (A)
1	1:0 (500µl:0µl)
2	1:1 (500µl:500µl)
3	1:3 (250µl:750µl
4	1:4 (200µl:800µl

Table 3- 2 Dilution volumes of solutions evaluated in this experiment.

For each dilution, a 0.5 µl volume of the solution was applied to the Pall Teflon filter. The samples were then evaluated by FTIR using the instrument in the same conservative configuration used and described in the last experiment, resulting in 12 octanoic acid spectra (1 model compound, 4 dilutions, 3 replicates of each dilution).

These spectra were evaluated to determine the absorbance of each functional group in the compound. in its signature was identified for analysis. The peak endpoint and baseline ranges used to determine absorbance of each target functional group are given in **Table 3-3**.

Functional Group	Peak endpoints, cm^{-1}	Baseline range, cm^{-1}
Carbonyl -(C=O)	1790-1625	1790-1625
Hydroxyl -(O-H)	956-900	956-900
Aliphatic hydrogen -(C-H)	734-703	734-703
Aliphatic carbon -(C-C)-	1300-700	1300-700
Carbon oxygen -(C-O)	1320-1000	1320-1100
Ammonia -(N-H)	1430-1390	1430-1390
Sulfate -(S-O)	660-610	660-610

Table 3- 3 Peak endpoint and baseline ranges of the targeted functional groups analyzed in this experiment

These particular peak endpoints and baselines will be investigated in later experiments. The area under each peak was determined by integration, and replicate analysis results were statistically evaluated to determine absorbance area means and standard deviations.

The minimum mass loading was then computed based on the dilution which resulted in a quantifiable FTIR response (i.e., above a 3:1 signal to noise ratio). By Beer's Law:

Equation 3- 3 $$C_{xb} = \frac{ABS_{xb}}{\varepsilon_{xb} l_{xb}}$$

Where C_{xb} is related to the absorbance area of the functional group in the beam ABS_{xb} (absorbance units), the molar absorptivity of the functional group in the beam ε_{xb} (absorbance m^2 mol^{-1}), and the path length of the functional group in the beam l_{xb} (m).

Since ε is constant for a functional group, the volume of sample is constant, and l is constant for a single experiment, and since the relationship between moles and absorbance is linear, the minimum mass loading can be computed as:

Equation 3- 4 $$n_{x,\min} = (n_{x \text{ in } j} + n_{x \text{ in } k}) \times \frac{ABS_{x \text{ in } j}}{ABS_{x \text{ in } j+k}}$$

Where x is the functional group, $n_{x,min}$ is the minimum detectable number of moles of the functional group x in the sample by using the FTIR, n_x is the number of moles ox in the solute j an in the solvent, $ABS_{x \text{ in } j}$ is the minimum absorbance detectable of x in the solute calculated, $ABS_{x \text{ in } j+k}$ is the total measured absorbance of x in the infrared spectra.

The minimum mass loading of the sample can be computed as:

Equation 3- 5 $$M_{x,\min} = n_{x,\min} \times MW_x$$

Where M is the minimum mass loading of x for a detectable FTIR response, n is the minimum detectable number of moles of the functional group x, and MW is the molecular weight of the functional group.

This mass can be adjusted for sampling parameters to determine concentration:

Equation 3- 6 $$C_{x,\min} = \frac{n_{x,\min} \times MW_x}{Qt}$$

Where C_{xmin} is the minimum detectable concentration of the functional group in ambient fine particles, MW is the molecular weight of the functional group, and Q and t are the sampling flowrate and duration.

The moles of a functional group in the solute j, or in the solvent k, $n_{x\ in\ j}$ or $n_{x\ in\ k}$, were calculated as shown for the solute:

Equation 3- 7 $$n_{x\ in\ j} = \frac{V_{j\ in\ solution}}{V_{solution}} \times \frac{\rho_j}{MW_j} \times V_{sample} \times y_{x\ in\ j}$$

Where x is the functional group, n_x is the moles of x in the solute j, or in the solvent k, V is the volume of the solute j or the solvent k in the solution, $V_{solution}$ is the volume of the solution, ρ is the density of the solute j or the solvent k, MW is the molecular weight of the solute j or the solvent k, V_{sample} is the volume of sample analyzed by using the FTIR, and y_x is the molar fraction of x in the solute or the solvent.

The absorbance areas due to the amount of a functional group in the solute, $ABS_{i\ in\ j}$, were determined using Beer Lambert's Law:

Equation 3- 8 $$ABS_{x\ in\ j} = \frac{ABS_{x\ in\ j+k}}{\left(n_{x\ in\ j} + n_{x\ in\ k}\right)} \times n_{x\ in\ j}$$

Where ABS_x is the computed absorbance of x in the solute, $ABS_{x \text{ in } j+k}$ is the absorbance of x in the solute and solvent, measured from the infrared spectrum, n_x is the moles of x in the solute and in the solvent.

The linearity of the instrument response to the various sample dilutions was then confirmed to validate the approach.

3.3.5 Results and discussion

For each dilution and experiment, several parameters had to be theoretically calculated based on the chemical structure of the compounds and the dilution.

The mole fraction of a functional group in each compound was determined from the chemical structure of each compound:

Octanoic Acid	CH_3-(C_6H_{12})-COOH
Acetone	CH_3-(CO)-CH_3

The mole fraction is the number of moles of the functional group per mole of compound, and the mole fraction of each functional group considered in this experiment are summarized in **Table 3-4** as a function of the compound they are in.

Functional Group	MW of functional group, g/mol	Mole fraction, y, of functional group in compound	
		Octanoic acid solute	Acetone solvent
Carbonyl -(C=O)	28	0.194	0.482
Hydroxyl -(O-H)	17	0.117	0.293
Aliphtic-hydrogen -(C-H)	13	0.090	0.224
Aliphatic-carbon -(C-C)	24	0.166	0.413

Table 3- 4 Molecular weight and mole fraction for each functional group targeted in this experiment.

Next the theoretical number moles of a functional group in a 0.5 ul volume of solution was calculated using **Equation 3-7**. An example is shown for the moles of alkane hydrocarbons -(C-H) from octanoic acid in a 0.5 ul sample of a 1:1 dilution of octanoic acid (OA) in acetone (A):

$$n_{\substack{-(C-H)\\ \text{in OA in}\\ \text{sample}}} = \frac{500\ \mu l\ OA\ in\ solution}{1000\ \mu l\ OA + A\ in\ solution} \times \frac{910\frac{\mu g}{\mu l}OA}{144.21\frac{\mu g}{\mu mol}OA} \times 0.5\mu.\ sample \times 15\frac{\mu mol\ C-H}{\mu mol\ OA} \times 10^{-6}\frac{mol}{\mu mol}$$

$$= 2.37 \times 10^{-5}\,mol$$

Similarly, the number of moles of alkane hydrocarbons -(C-H) from A in a 0.5 ul sample of a 1:1 dilution of OA in A:

$$n_{\substack{-(C-H)\\ \text{in A in}\\ \text{sample}}} = \frac{500\ \mu l\ A\ in\ solution}{1000\ ul\ OA + A\ in\ solution} \times \frac{790\frac{\mu g}{\mu l}OA}{58.08\frac{\mu g}{\mu mol}OA} \times 0.5\mu.\ sample \times 6\frac{\mu mol\ C-H}{\mu mol\ OA} \times 10^{-6}\frac{mol}{\mu mol}$$

$$= 2.04 \times 10^{-5}\,mol$$

Using a similar approach the moles of all of the functional groups were determined. These results are presented in **Table 3-5**.

Table 3-5 presents the different theoretical moles of the targeted functional groups in the solute and in the solvent. For each functional group the left column present the moles of the functional group in Octanoic acid (OA) and the right column present the moles of functional group in Acetone (A). The number of moles were calculated for the volume of sample analyzed, 0.5µl.

		Moles of functional group, mol							
Dilution #	**Octanoic acid: Acetone Solute:Solvent**	**Aliphatic carbon -(C-C)-**		**Carbonyl -(C=O)**		**Hydroxyl -(O-H)**		**Aliphatic hydrogen -(C-H)**	
		in OA	**in A**	**in OA**	**in A**	**in OA**	**in A**	**in OA**	**in A**
1	**1:0**	6.310×10^{-6}	0	3.155×10^{-6}	0	3.155×10^{-6}	0	4.733×10^{-5}	0
2	**1:1**	3.155×10^{-6}	6.801×10^{-6}	1.578×10^{-6}	3.400×10^{-6}	1.578×10^{-6}	0	2.366×10^{-5}	2.040×10^{-5}
3	**1:3**	1.578×10^{-6}	1.020×10^{-5}	7.888×10^{-7}	5.101×10^{-6}	7.888×10^{-6}	0	1.183×10^{-5}	3.060×10^{-5}
4	**1:4**	1.262×10^{-6}	1.088×10^{-5}	6.310×10^{-7}	5.441×10^{-6}	6.310×10^{-6}	0	9.465×10^{-6}	3.264×10^{-5}

Table 3- 5 Theoretical moles of functional groups in a mole of sample (i.e., moles of Octanoic Acid in 0.5µl of solution)

The integrated absorbance for each of the selected peaks for a functional group were determined for three replicate FTIR analyses and then averaged to determine average integrated absorbance. These absorbance values represent the combined absorbance of a functional group in both the solute and in the solvent. The minimum absorbance area that can be computed depends on the shape of the peak, however, an approximate threshold of 0.1 is reasonable. These results are shown in the following table.

	Absorbance area of functional group			
Dilution	**Aliphatic carbon -(C-C)-**	**Carbonyl -(C=O)**	**Hydroxyl -(O-H)**	**Aliphatic hydrogen -(C-H)**
1:0	44.11 ±0.48	83.95 ±3.44	47.75 ±2.04	138.46 ±3.37
1:1	5.52 ±0.04	10.04 ±0.07	4.11 ±0.04	5.93 ±0.28
1:3	2.48 ±0.11	3.93 ±0.17	1.88 ±0.10	5.71 ±0.42
1:4	1.43 ±0.11	2.4 ±0.24	1.12 ±0.11	4.61 ±0.36

Table 3- 6 Measured ABS of functional groups in solute and solvent at different dilutions

These absorbance areas were adjusted to determine the portion of the measured absorbance area that was due to the functional groups in the solute, using **Equation 3-9**, as shown for the alkane hydrogen functional group in a 1:1 dilution of octanoic acid in acetone:

Equation 3- 9 $$\mathrm{ABS}_{\mathrm{i\ in\ j}} = \frac{5.93}{\left(2.366 + 2.04\right)\times 10^{-5}} \times 2.366 \times 10^{-5} = 3.184$$

The adjusted absorbance areas that account only for the functional groups in the solute were computed for the remaining dilutions and functional groups and are presented in **Table 3-7**.

	Moles of functional group, mol			
Dilution	**Aliphatic carbon -(C-C)-**	**Carbonyl -(C=O)**	**Hydroxyl -(O-H)**	**Aliphatic Hydrogen -(C-H)**
1:0	44.110	83.950	47.750	138.460
1:1	1.749	3.183	4.110	3.184
1:3	0.332	0.526	1.880	1.592
1:4	0.149	0.249	1.120	1.036

Table 3- 7 Calculated ABS of functional groups present in Octanoic acid

The values of adjusted absorbance are all smaller than the measured values for all dilutions that involve acetone. In most cases, the adjustment is small and results in values that are still above detection limits of the instrument.

The minimum sample loading was determined by developing a relationship between moles and absorbance and then by extending the relationship to the minimum detectable absorbance, approximately 0.1 absorbance units. These relationships are shown in **Figure 3-3**.

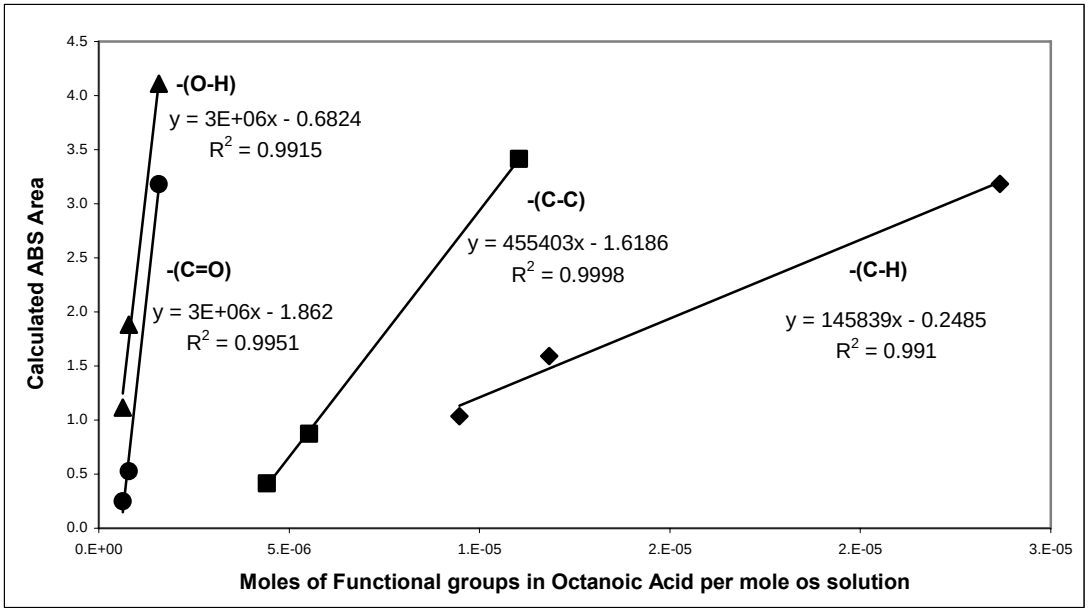

Figure 3- 3 Calibration curve plot for the functional groups in octanoic acid.

Figure 3-3 shows the relationship between the moles of different functional groups present in octanoic acid from **Table 3-4** and their adjusted ABS areas from **Table 3-10**. The relationship for each of the functional groups is linear, and the data fit each with a correlation coefficient close to one.

The minimum mass loading was determined by extending these relationships to the minimum detectable absorbance area. For the alkane hydrogen example -(C-H), the minimum mass loading is calculated for functional groups in the solution prepared at dilution of 1:1using Equation 3-5 to be:

$$n_{\text{-(C-H) min}} = (2.366\times10^{-5} + 2.04\times10^{-5}) \times \frac{3.184}{5.93} = 2.366\times10^{-5}\, moles$$

This calculation was repeated for all of the functional groups, and the results are shown in **Table 3-8**.

Functional Group	Minimum Loading onto filter (moles)	Minimum detectable concentration in ambient fine particles (µg/m3)
Aliphatic carbon -(C-C)-	3.155×10^{-6}	3.15
Carbonyl -(C=O)	1.578×10^{-6}	1.84
Hydroxyl-(O-H)	1.578×10^{-6}	1.12
Aliphatic hydrogen -(C-H)	2.366×10^{-5}	12.81

Table 3- 8 Minimum loading of different functional groups onto a substrate.

The minimum molar loading for all of the functional groups that can be detected using FTIR is on the order of 10^{-5} to 10^{-6} moles.

This table also shows the minimum concentration of a functional group in fine particles that can be measured using FTIR, determined using Equation 3-6, the molecular weight of each functional group in **Table 3-4**, and assuming a sampling duration of 24 hours at 16.67 LPM. For the alkane hydrogen -(C-H) functional group this quantity is calculated to be:

$$C_{\text{-(C-H),min}} = \frac{2.366 \times 10^{-5} \times 13}{16.67 LPM \times 24h} = 12.81 \mu g / m^3$$

Shorter sampling times are possible if the concentration of the functional group in the fine particle is larger than that shown in **Table 3-12**.

The methods employed in this experiment were validated mostly through **Figure 3-3**. This figure demonstrates that Beer's Law holds even for samples on Teflon substrates that are analyzed by FTIR since the relationship between moles and absorbance is linear within a reasonable amount of uncertainty. Therefore, the methods used in this experiment to determine minimum mass loading are valid. It also shows that the experimental methods are not overly sensitive to external factors which may cause volatilization or condensation.

Although the peak endpoints and baselines used in these experiments were not yet refined, this fact is not expected to affect the conclusions because the methods were applied consistently and because the conclusions were based on comparisons of absorbances and not absolute values of absorbance.

3.4 REFERENCES

Allen, D. and Palen, E., 1989. Recent advances in aerosol analysis by infrared spectroscopy. Journal of Aerosol Science 20 (4), 441-455.

Cabada, J., Pandis, S., Subramanian, R., Robinson, A., Polidori, A. and Turpin, B., 2004a. Estimating the secondary organic aerosol contribution to $PM_{2.5}$ using the EC tracer method. Aerosol Science and Technology 38 (S1), 140-155.

Cabada, J., Rees, S., Takahama, S., Khlystov, A., Pandis, S., Davidson, C. and Robinson, A., 2004b. Mass size distribution and size resolved chemical composition of fine particulate matter at the Pittsburgh supersite. Atmospheric Environment 38, 3127-3141.

Carlton, A., Turpin, B., Johnson, W., Buckley, B., Simcik, M., Eisenreich, S. and Porcja, R., 1999. Microanalysis methods for characterization of personal aerosol exposures. Aerosol Science and Technology 31, 66-80.

EPA, January 17, 2006. 40 CFR Part 50: National Ambient Air Quality Standards for Particulate Matter; Propose Rule.

Gordon, R., Trivedi, N. and Singh, B., 1988. Characterization of aerosol organics by diffuse reflectance Fourier transform infrared spectroscopy. Environmental Science and Technology 22, 672- 677.

Krost, K. and McClenny, W., 1994. FTIR transmission spectroscopy for quantitation of ammonium bisulfate in fine-particulate matter collected on Teflon filters. Applied Spectroscopy 48 (6), 702-705.

Maria, S., Russel, L., Turpin, B. and Porcja, R., 2002. FTIR measurements of functional groups and organic mass in aerosol samples over the Caribbean. Atmospheric Environment 36, 5185-5196.

Reff, A., Turpin, B., Porcja, R., Giovennetti, R., Cui, W., Weisel, C., Zhang, J., Kwon, J., Alimokhtari, S., Morandi, M., Stock, T., Maberti, S., Colome, S., Winer, A., Shendell, D., Jones, J. and Farrar, C., 2005. Functional group characterization of indoor, outdoor, and personal $PM_{2.5}$: results from RIOPA. Indoor Air 15, 53-61.

Solomon, P., 2004. Special issue of Atmospheric Environment on findings from EPA's particulate matter Supersites Program. Atmospheric Environment 38, 3101-3106.

Subramanian, R., Khlystov, A., Cabada, J. and Robinson, A., 2004. Evaluation of Measurement Methods: Positive and negative artifacts in particulate organic carbon measurements with denuded and undenuded sampler configurations. Aerosol Science and Technology 38 (S1), 27-48.

Takahama, S., Wittig, B., Vayenas, D., Davidson, C. and Pandis, S., 2004. Modeling the diurnal variation of nitrate during the Pittsburgh air quality study. Journal of Geophysical Research 109, D16S06, doi: 10.1029/2003JD004149.

Turpin, B., Saxena, P. and Andrews, E., 2000. Measuring and simulating particulate organics in the atmosphere: problems and prospects. Atmospheric Environment 34, 2983-3013.

Wittig, B., Takahama, S., Khlystov, A., Pandis, S., Hering, S., Kirby, B. and Davidson, C., 2004. Semi-continuous $PM_{2.5}$ inorganic composition measurements during the Pittsburgh air quality study.

CHAPTER 4 SAMPLE ANALYSIS

This chapter discusses the development and optimization of the method to acquire FTIR spectra of ambient $PM_{2.5}$ samples collected using the collection system discussed in the previous chapter. The conservative FTIR settings used in the prior chapter will now be varied to optimize the analysis. Some challenges to these experiments are the inhomogeneity of a fine particle sample collected onto a filter, water present in the $PM_{2.5}$ sample, the sensitivity of the spectrum to the analysis environment, and the infrared signature of the different substrates.

The research and development of the analysis approach will address these challenges through several experiments:

- Experiment 6: Use of transmission or reflectance spectroscopy
- Experiment 7: Use of background spectra
- Experiment 8: Approach to minimize interference in the analysis chamber
- Experiment 9: Use of sampling substrate as an internal standard

4.1 EXPERIMENT 6: USE OF TRANSMISSION OR REFLECTANCE SPECTROSCOPY

There are two ways to collect a FTIR spectrum: transmission spectroscopy and reflection spectroscopy. There are also several substrate types that fine particles can be collected on: Teflon and quartz by various manufacturers. Since the fine particle samples will be

measured while on the substrate, in this experiment we identify the spectroscopy-substrate pair which is best suited for the speciation of ambient fine particles.

4.1.1 Issue

The primary difference between transmission and reflectance spectroscopy is the path of the light through a sample. **Figure 4-1** illustrates this primary difference.

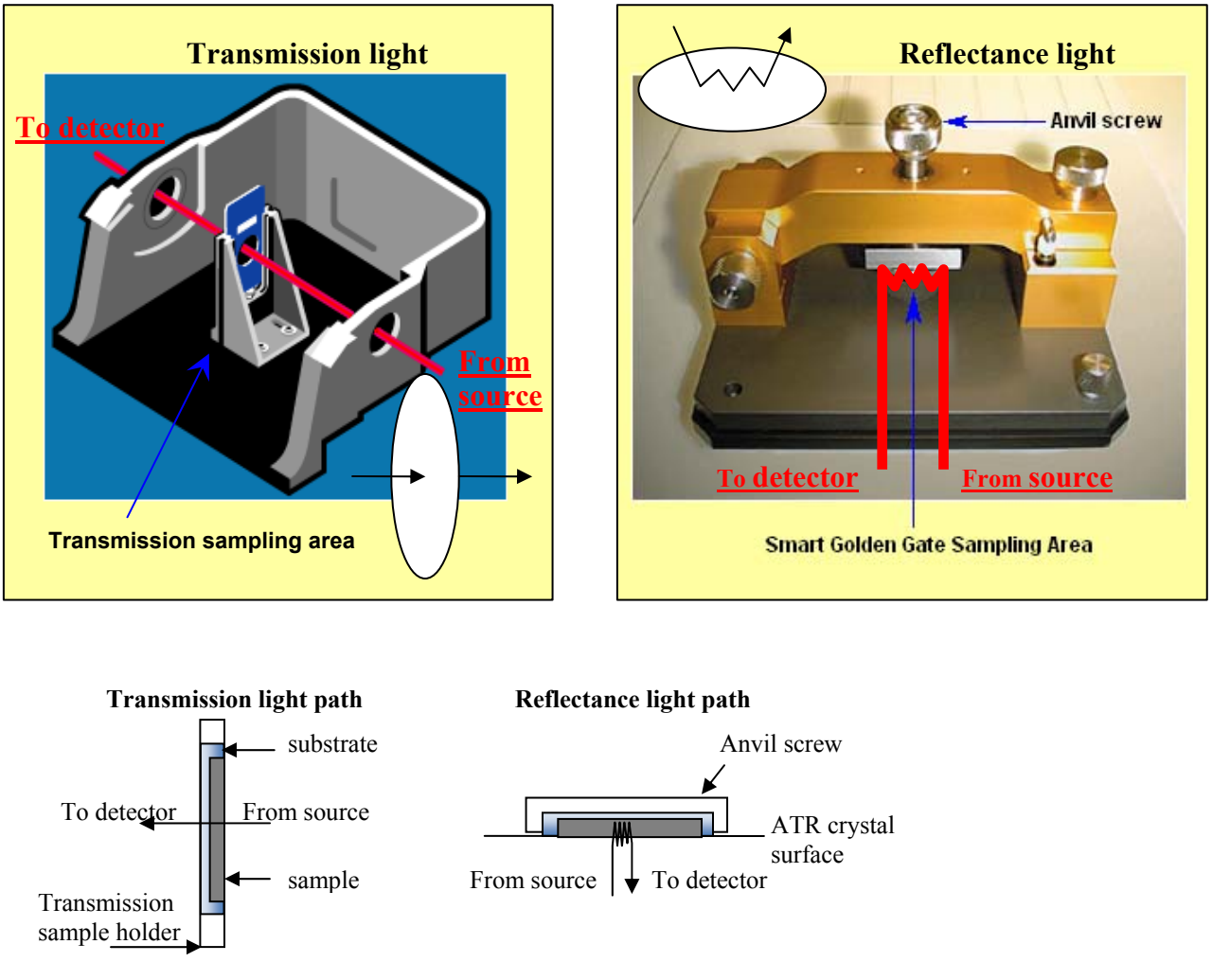

Figure 4- 1 Difference between transmission and reflectance light paths.

As shown in the figure, in transmission spectroscopy, the sample and a blank are placed side by side in vertical holders which holds them by their edges, and are shuttled in and out of the light path automatically, eliminating the need to handle either blank or sample. Typically, one of the holders holds the blank and the other holds a sample. The MIR light passes from the source, into the analysis chamber, through the sample in the holder, across the rest of the analysis chamber, and out to the detector. The light path length through the sample in transmission spectroscopy is between 1 and 20 μm, which include the thickness of the substrate plus some incremental thickness above the portion of fine particles embedded in the substrate.

In reflectance spectroscopy, the sample is placed face down onto a crystal that is transparent to infrared light and that has a high refractive index, and held firmly against the crystal by tightening an anvil screw. The MIR light passes from the source, into the crystal which redirects the light into the topmost 1 to 5 μm of the sample and then out of the sample multiple times across a short stretch of the sample. After several passes, the crystal directs the light beam to the detector. As a result, in reflectance spectroscopy the MIR light passes through only a small portion of the sample instead of passing all the way through it. The tightening of the anvil screw may break the sample and/or compromise its integrity. Only one sample can be placed onto the crystal at a time, and therefore the prior blank or sample must be removed from the crystal and the crystal cleaned before a new sample can be analyzed.

The choice between reflectance and transmittance is usually based on the physical state of the sample (e.g., liquid, powder, solid, film, etc.). Liquid and powder samples must be held horizontally in the analysis chamber so that they maintain their integrity and do not move out of the light path during analysis. Solid samples and films can be held vertically or horizontally, provided that they are supported in the analysis chamber at their edges. The crystal used in reflectance spectroscopy is typically horizontal, and therefore can be used for liquid or powder samples, as well as solid and film samples. Transmission spectroscopy, on the other hand, typically holds the sample vertically and so only solid or film samples can be analyzed by this approach.

However, there are other consequences to the decision of transmission versus reflectance spectroscopy that are important when developing a method for acquiring FTIR spectra of ambient $PM_{2.5}$ samples on substrates: the signal to noise ratio of the substrate and of the sample, the portion of the sample that is analyzed, and the risk of handling artifacts during analysis.

The first issue relates to the signal to noise ratio, which should be at least 3, and is the ratio of signal in a spectrum, between the intensity of an absorbance band and the noise at a nearby point in the baseline. When the light path passes through a larger volume of the sample, the MIR absorbance is larger and the signal to noise ratio is improved. As a result, better signal to noise ratios are obtained for transmission spectroscopy versus for reflectance spectroscopy of the same sample, but saturation can occur, especially of the substrate signature since the substrate is present in the sample in much higher

concentration than the fine particles. Conversely, saturation can be avoided when a sample is analyzed using reflectance spectroscopy versus using transmission spectroscopy, but then the signal to noise ratio is also lowered. Neither approach is clearly optimum for fine particle speciation.

The next issue pertains to the portion of the sample that is analyzed (i.e., that is in the light path). Typically, fine particles will be collected onto a substrate over an extended period of time, by filtration and sieving. Even if the sampler distributes the fine particles evenly across the filter surface, the resulting sample will not be uniform with depth because of changes in the ambient particle composition over the time of sampling and because smaller particles will migrate further into the substrate until sieving becomes the dominant mechanism of collection. When using transmission spectroscopy to analyze this sample, the spectra reflects the average $PM_{2.5}$ composition over the thickness of the sample and therefore the sample collection period. When using reflectance spectroscopy, the spectra reflects the average $PM_{2.5}$ composition over the depth of penetration of the light which may only account for the largest and possibly most recent ambient particles. If the sample is thicker than 5μm the reflectance light beam the spectra will not reflect the average $PM_{2.5}$ composition over the thickness of the sample and the sample collection period.

Another issue is artifacts introduced during the analysis. Since the transmission sample holders contact the sample at its edges, the integrity of the sample is maintained during loading and analysis. Since transmission analysis chambers can hold a blank and a

sample side by side, their two spectra can be obtained without needing to manually move the holder into place in the analysis chamber. Also, the analysis chamber can be closed to the environment for the back to back analysis of the blank and the sample. All of these features minimize analysis artifacts due to handling. On the other hand, samples analyzed by reflectance must be manually placed on the crystal and the anvil screw tightened to hold the sample against the crystal surface. This level of handling damages the sample and is more likely to result in contamination. Further, blanks and sample spectra can only be obtained by manually switching the sample and cleaning the crystal in between analyses. Finally, since reflectance spectroscopy does not occur in a chamber, the samples may be subjected to different environmental conditions between sample and blank analysis. These features cause analysis artifacts that do not occur when using transmission spectroscopy.

A final issue relates to the determination of the path length through the sample and substrate. This will be discussed further in **Chapter 4.**

4.1.2 Goal

The goal of this experiment is to evaluate which of the FTIR spectroscopy approaches best lends itself to the analysis of fine particles collected onto a substrate: transmission or reflectance.

4.1.3 Literature Review

While several researchers confirmed the issues described above through their research, very little has been done to explore how to address these issues for fine particle speciation. Smith (1996) found that the transmission spectroscopy of samples 20 microns thick results in saturated MIR signatures and of samples 1 micron results in signatures that are below detection limits. McClenny et al., (1985) used transmission spectroscopy to determine concentration of ammonium and sulfate collected onto Teflon filters reporting that measurements by transmission spectroscopy were precise and repetitive. However, Pollar and Jaklevic (1988) report that Teflon in filters interfere with the signature of sample when using transmission spectroscopy. Krost and McClenny (1994) found that manipulation, storage and removal of the Teflon filter during processing affect measurements when using transmission spectroscopy. Farinas et al. (1994) found that one source of error when using the reflectance spectroscopy is related to the precision used to measure and prepare films of uniform thickness.

For the purposes of this research, it is desirable to identify which of the spectroscopy approaches (i.e., transmission or reflection) result in larger absorbances that are above detection limits. Also two Teflon filters by different manufacturers were analyzed by both spectroscopy approaches, to evaluate if the type of filter may affect the absorbances of the Teflon in the spectra. Manipulation of the filter sampling is minimized when using both spectroscopy approaches, to have results that are not biased by this manipulation.

4.1.4 Experimental Approach

In this experiment, three unsampled filters and two ambient samples of fine particles were analyzed by both transmission spectroscopy and by reflectance spectroscopy, and at multiple locations on the filters. The resulting spectra were analyzed and compared to identify the spectroscopy approach which is better suited to fine particle speciation.

The blank substrates included two Teflon substrates (Pall and Savillex) and one blank quartz fiber filter.

Two samples were collected onto Teflon substrates (Pall and Savillex) using the sampling system described in Chapter 2. The sampler was set up in this configuration:

- Organic and inorganic gas denuders described in Chapter 2 were used upstream of all sampling legs to remove potentially interfering gases
- The sample rate in each leg was 16.67 LPM, to avoid volatilization of particle-bound semi-volatile compounds due to high face velocity
- The sampling duration was 48 hours, to assure that minimum sample loadings on the substrate are obtained

Samples were collected on October 8, 2008 starting at 2 p.m. for 48 hours at the CCNY site, and October 14 starting at 2 p.m. for 48 hours at the CCNY site. The CCNY site is located on the roof of the Administration Building at City College of New York. On these days, the average $PM_{2.5}$ mass concentration was high/low at 16.3 and 8.4 μg m^3, respectively.

After collection, all samples were desiccated in a Fisher Scientific desiccator with porcelain plate (Fisher #08-615 series) for 4 hours. Then samples were placed in sterile disposable dishes (Fisher S33580) with a diameter of 100 and depth of 15 mm using clean tweezers, and stored in a refrigerator (Danby #DCR412W) at -20 ^{o}C until the time of analysis. Samples were allowed to equilibrate at room temperature just prior to analysis.

The transmission spectroscopy analyses used the sample shuttle (Thermo Nicolet #840-058-200) to move the sampled substrate into and out of the light path so that background spectra could be collected without handling the sample or opening the analysis chamber. One of the holders held the sample to collect its spectrum and the other was empty to collect the background.

The reflectance spectroscopy analyses used a cap (Thermo #GS10503) over the sample to minimize volatilization of semi-volatile components in the fine particles.

The transmission and reflectance spectra were acquired using the most conservative approaches parameters that were investigated later in this chapter:

- Use of background spectra: A background is a spectrum of the gases and any other materials in the analysis chamber that interfere with the blank or sample spectrum. The background spectrum is automatically subtracted from the blank or sample spectrum, resulting in a final spectrum that is free of the interferents. In

this experiment a background of just the gases in the chamber was collected every 10 to 15 minutes to account for changes in the gas composition in the analysis chamber. Blank and sample spectra were corrected using the most recent background spectrum.

- Approach to minimize interference in the analysis chamber: In addition to acquiring frequent background spectra, there are also methods to remove the gases from the analysis chamber which include purging the chamber and mathematically suppressing the signatures of the gas interferents. In these experiments, no additional removal was done.
- Use of sampling substrate as an internal standard: Later experiments will investigate the use of the Teflon substrate as an internal standard for quality assurance and conversion of the fine particle speciation absorbance into concentration. In these experiments, no internal standards were used.

Many transmission and reflectance spectra were obtained of the three blank substrates (Teflon from Pall Gelman Teflo #R2PJ047 and Savillex, #1145, and Quartz from Tissuequartz #2500 QAO-UP); and of the two sampled substrates. For each sample, three replicate spectra were obtained at each of the four locations on the sample illustrated in **Figure 4-2**.

Figure 4- 2 Location where spectra were obtained.

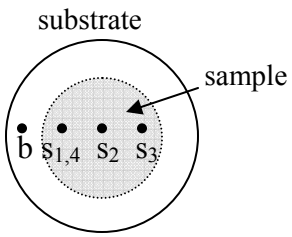

Figure 4- 2 Location where spectra were obtained.

In **Figure 4-2**, b is the location on the substrate that is unsampled which was analyzed to acquire a blank spectrum. The $s_{1,}$ s_2 and s_3 locations are in the sampled region of the substrate are where sample spectra were obtained. While s_1 and s_4 are at the same location, the spectrum at s_1 was collected first and the spectrum at s_4 was collected last.

A total of 12 blank spectra were collected for the two Teflon and the quartz substrates (i.e., 2 samples, 2 spectroscopy approaches, 1 location per sample, and 3 spectra per location), and 48 blank corrected sample spectra (i.e., 2 samples, 2 spectroscopy approaches, 4 locations per sample, and 3 spectra per location) were obtained and analyzed for this experiment. These spectra are summarized in **Table 4-1**.

Spectra number	Sample date and time	Substrate type	Spectroscopy approach	Substrate location	Spectra that were compared			
					Signal to noise ratio	Sample inhomogeneity across	Sample inhomogeneity with depth	Handling artifacts
$\#1_{1,2,3}$	10/08/08 from 2pm for 48hr	2 blank Teflon 1 blank Quartz Sample in Teflon	Transmission	B	x			
$\#2_{1,2,3}$				S1		x	x	x
$\#3_{1,2,3}$				S2		x		
$\#4_{1,2,3}$				S3		x		
$\#5_{1,2,3}$				S4				x
$\#6_{1,2,3}$			Reflectance	B	x			
$\#7_{1,2,3}$				S1		x	x	x
$\#8_{1,2,3}$				S2		x		
$\#9_{1,2,3}$				S3		x		
$\#10_{1,2,3}$				S4				x
$\#11_{1,2,3}$	14/08/08 from 2pm for 48hr	2 blank Teflon 1 blank Quartz Sample in Teflon	Transmission	B	x			
$\#12_{1,2,3}$				S1		x	x	x
$\#13_{1,2,3}$				S2		x		
$\#14_{1,2,3}$				S3		x		
$\#15_{1,2,3}$				S4				x
$\#16_{1,2,3}$			Reflectance	B	x			
$\#17_{1,2,3}$				S1		x	x	x
$\#18_{1,2,3}$				S2		x		
$\#19_{1,2,3}$				S3		x		
$\#20_{1,2,3}$				S4				x

Table 4- 1 Shows the date and time of sample collection, the substrate type, the FTIR analysis approach, and the location on the substrate where the spectrum was collected.

Each of the sample spectra were then blank corrected by subtracting the blank spectrum from the sample plus substrate spectrum, resulting in spectrum of only the ambient fine particles.

Each of these spectra was then analyzed to determine the integrated absorbance area of two target functional groups, alcohol -(O-H) at 3502-2393 cm^{-1}, 1388-1363 cm^{-1} and 981-852 cm^{-1}, and alkane hydrogen -(C-H) at 3037-2769 cm^{-1}, 1382-1371 cm^{-1}, and 734-703 cm^{-1}. Baseline, peak shifting, and peak splitting approaches for PM speciation will be presented in the next chapter. For the current experiment, a set of consistent approaches were used for all of the blank and sample spectra.

- Baseline: baselines for the functional group peaks were traced horizontally from the most defined endpoint of the peaks to the nearest point that make the baseline horizontal
- Shifting: shifting was not accounted, however the baselines and endpoints were traced based in the location of the peak in the infrared spectrum
- Splitting: splitting was not addressed, however to measured the absorbance areas of peaks whose signatures are close to each other, a vertical line was traced in order to define the overlapping endpoint of the peaks

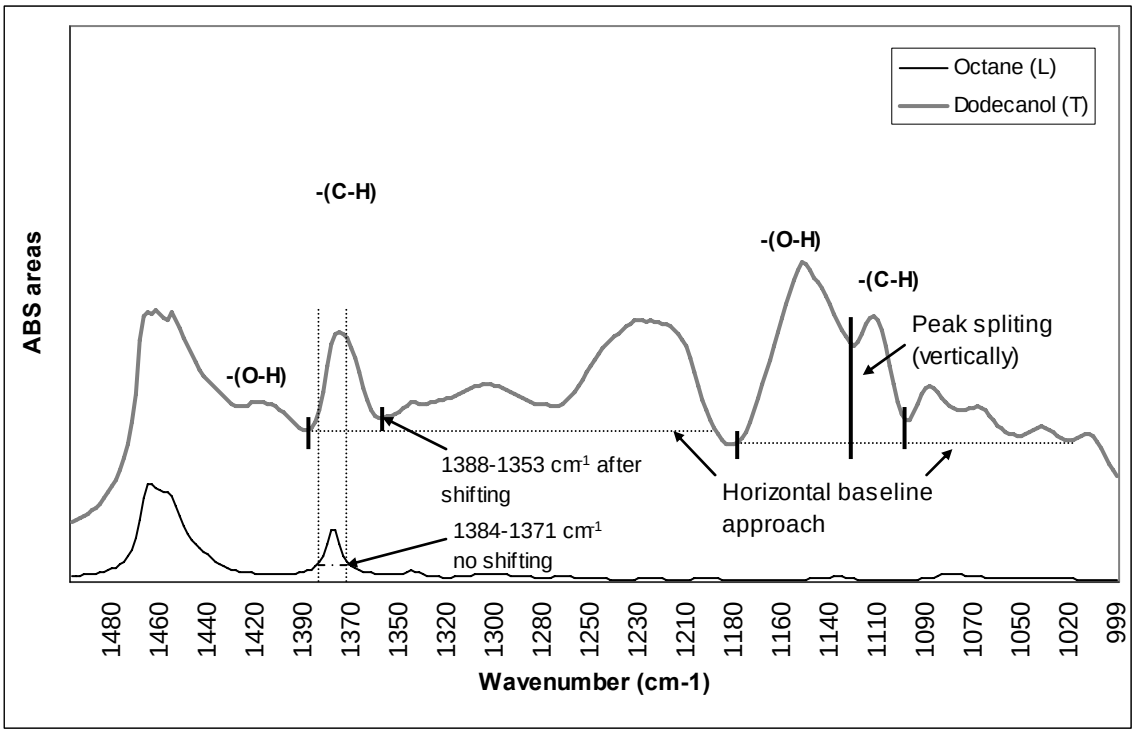

Figure 4- 3 exemplifies the baseline, shifting and splitting approaches used to determine the integrated absorbance area of the six target functional group signature peaks.

Figure 4-3 presents, the approaches used in this experiment to determine the baselines, the shifting and the splitting of functional group peaks. These issues were explained more in detail in Chapter 5. In this experiment horizontal baselines were traced from one of the most defined endpoints of the peak to the nearest point in the spectrum that makes de baseline horizontal, as seen for the –(C-H) peak in the figure. For peak shifting, as in figure, the –(C-H) peak in upper spectrum was compared with the –(C-H) peak in the lower library spectrum, however shifting was not accounted in this experiment. To split overlapping peaks in this experiment, a vertical line was traced between the overlapping point, as seen for the –(O-H) and –(C-H) peaks in the figure, where it was assumed that the overlapping points was one of the endpoints of the overlapping peaks.

The integrated absorbance areas were then averaged and their percent uncertainty determined as shown below.

Equation 4- 1 $$ABS_{x,AVG} = \frac{\sum^{j} ABS_{x,j}}{j}$$

Where x is the targeted functional group, j is the number of data available; ABS_x is the absorbance of the functional group for the different replicates.

Equation 4- 2 $$Uncertainty(\%) = \frac{ABS_{x,AVG}}{ABS_{x,STDEV}} \times 100$$

Where $ABS_{x,AVG}$ is the average of the replicates measured absorbance areas for a functional group x, and $ABS_{x,STDEV}$ is the standard deviation of the replicates measured absorbance areas for the same functional group x.

The results were then analyzed. Selected spectra identified in **Table 4-1** were analyzed and/or their functional group absorbances compared to address each of these following issues:

- Signal to noise ratio: Evaluate the resolution and strength of spectra collected at the b (blank) location of different samples using different spectroscopy approaches. Estimate the minimum detection limit assuming a 3 to 1 signal to

noise ratio by calculating the absorbance of the spectra noise in a wavenumber region where no signature was present, and then multiplying the value by 3. Evaluate the resolution and strength of spectra collected at the b location of different blank substrate using different spectroscopy approaches. Identify optimal blank-spectroscopy pairs that result in substrate spectra that are not saturated or noisy and that have the lowest detection limit.

- Sample inhomogeneity with depth into substrate: Analyze spectra collected at the s_1 location of a substrate using different spectroscopy approaches. Compare the ratios of absorbances by spectroscopy method for each fine particle species. If the sample is homogenous with depth or if the reflectance light path passes through the entire fine particle sample, the ratios will be close to 1 and the ABS areas will be consistent across functional. The optimal spectroscopy approach is able to account for the full fine particle composition of samples collected over an average time of 24 hours.
- Sample inhomogeneity across substrate: Analyze spectra of fine particles at different s_1, s_2 and s_3 locations on the sample collected using the same spectroscopy approach. Compare the ratio of absorbances by location for each fine particle species. If the sample is homogeneous or the spectroscopy method is insensitive to small differences in homogeneity, the ratios will be close to 1. The optimal spectroscopy approach results in fine particle absorbances that do not depend on the location at which the measurement was made.
- Handling artifacts: Analyze spectra collected at the s_1 and s_4 locations (i.e., at the same location but with the s_2 and s_3 spectra collected in between) using the same

spectroscopy approach. Compare the sample peak heights and peak areas for the different spectra. Differences in the s_1 and s_4 spectra indicate a loss of sample integrity during subsequent analyses which involved repositioning the sample. The optimal spectroscopy approach allows a sample to be repositioned and analyzed multiple times.

4.1.5 Results and Discussion

Signal to noise ratio

The spectra of blanks that were compared for this analysis are shown in **Figure 4-4**.

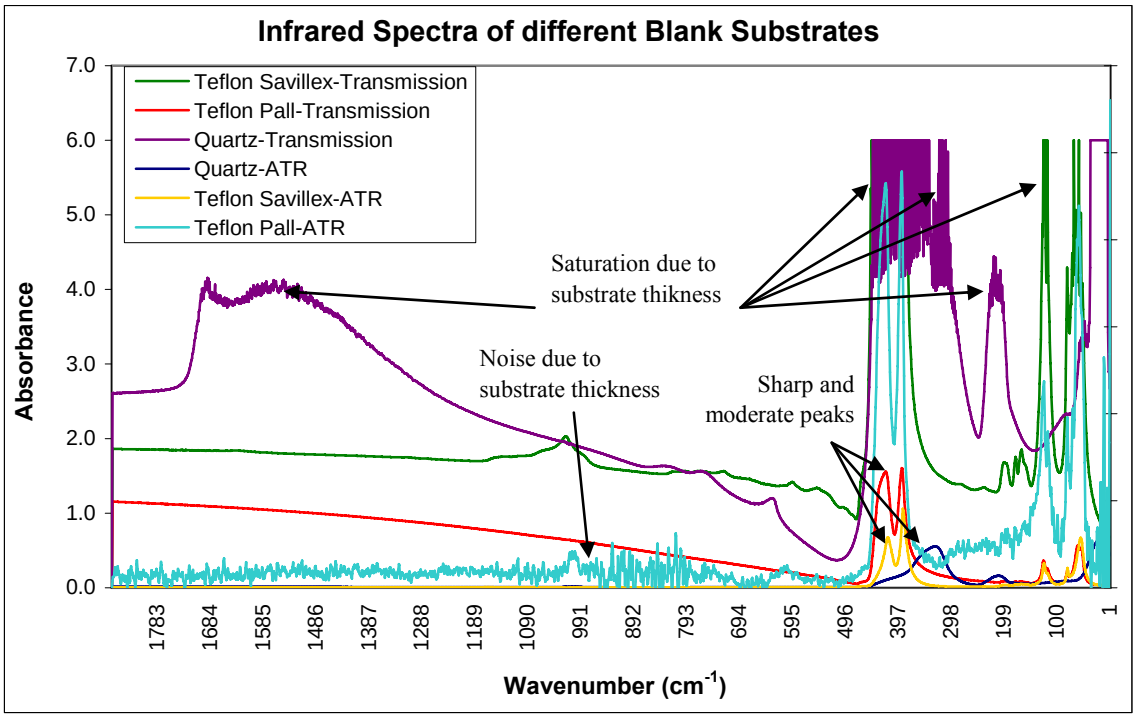

Figure 4- 4 Comparison of different blank spectra obtained by FTIR spectrometry.

Figure 4-4 presents the six spectra of the two Teflon and one quartz blank substrates collected using transmission and reflectance spectroscopy. As expected, the spectral signature of the substrate is stronger when transmission spectroscopy is used versus when reflectance spectroscopy is used. The transmission spectra of Teflon Savillex filters and the quartz filters have saturated signatures with some noise, while that of Teflon Pall filter has a signature that is resolved and free of noise. The reflectance spectra of Teflon Savillex filters and the quartz filter are resolved and free of noise, however the Teflon Pall filter is resolved but quite noisy. This may be because the Pall filter is thinner than the other filters and possibly broke upon tightening sample in place with the anvil screw.

For a 3 to 1 signal to noise ratio, the minimum detectable absorbance for the filter types that have resolved signatures are given in the table below. These values were determined by calculating the absorbance of the spectra noise in a wavenumber region where no signature was present, and then multiplying the value by 3.

	Wavenumber range over which noise absorbance was determined	**Minimum detectable absorbance based on a 3:1 signal:noise ratio**
Teflon Pall filters analyzed by transmission spectroscopy	3500-3000 cm^{-1}	0.711
Teflon Savillex filters analyzed by reflectance spectroscopy	3870-3300 cm^{-1}	2.097
Quartz Tissuequartz filters analyzed by reflectance spectroscopy	3645-3160 cm^{-1}	1.465

Table 4- 2 Shows the wavenumber ranges where water absorbs and minimum detectable absorbance of sample in all of the three substrates evaluated.

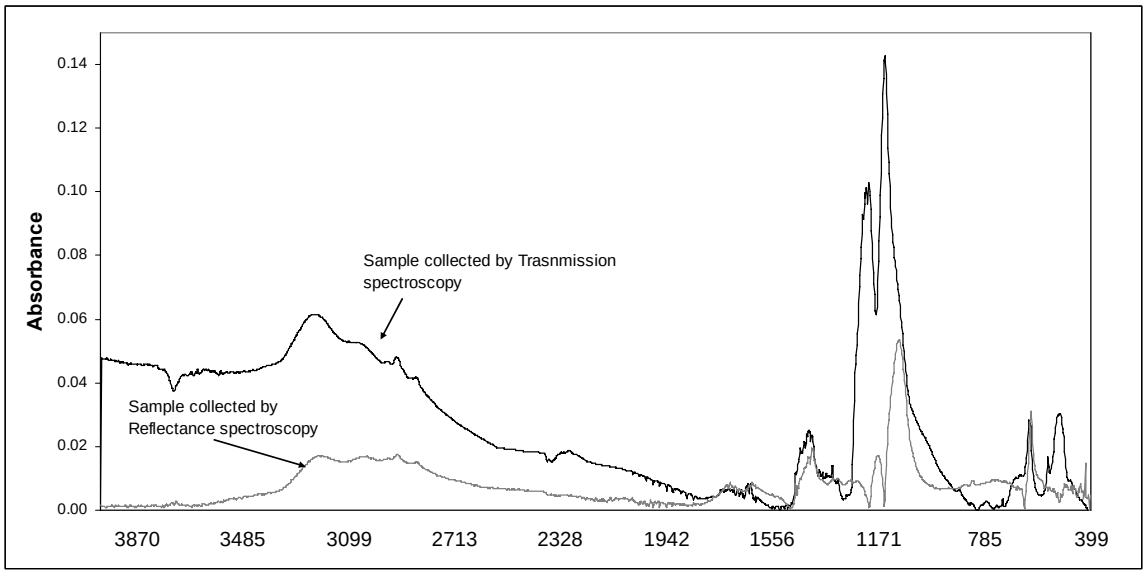

Figure 4- 5 presents the blank corrected spectra of fine particles acquired at different locations on the substrate and using the two different spectroscopy techniques that were compared for this analysis.

Figure 4-5 shows the blank corrected spectra of fine particles collected onto Teflon substrate (Pall Corporation) and analyzed by the two different spectroscopy techniques. As expected, the spectral signature of the fine particles is also stronger when transmission spectroscopy is used versus when reflectance spectroscopy is used. In all of the spectra, the fine particle signatures are well resolved and with minimal noise. However, the fine particle signatures are stronger in the transmission spectra than they are in the reflectance spectra.

Based on the these analyses, optimal substrate-spectroscopy pairs include Teflon Pall filters analyzed by transmission spectroscopy, and the Teflon Savillex and quartz filters analyzed by reflectance spectroscopy.

Sample inhomogeneity with depth into substrate

Figure 4-6 compares the integrated absorbance area of each of the targeted functional groups in the spectra of the fine particles measured at the same location on a sample but using the two different spectroscopy approaches: transmission and reflectance.

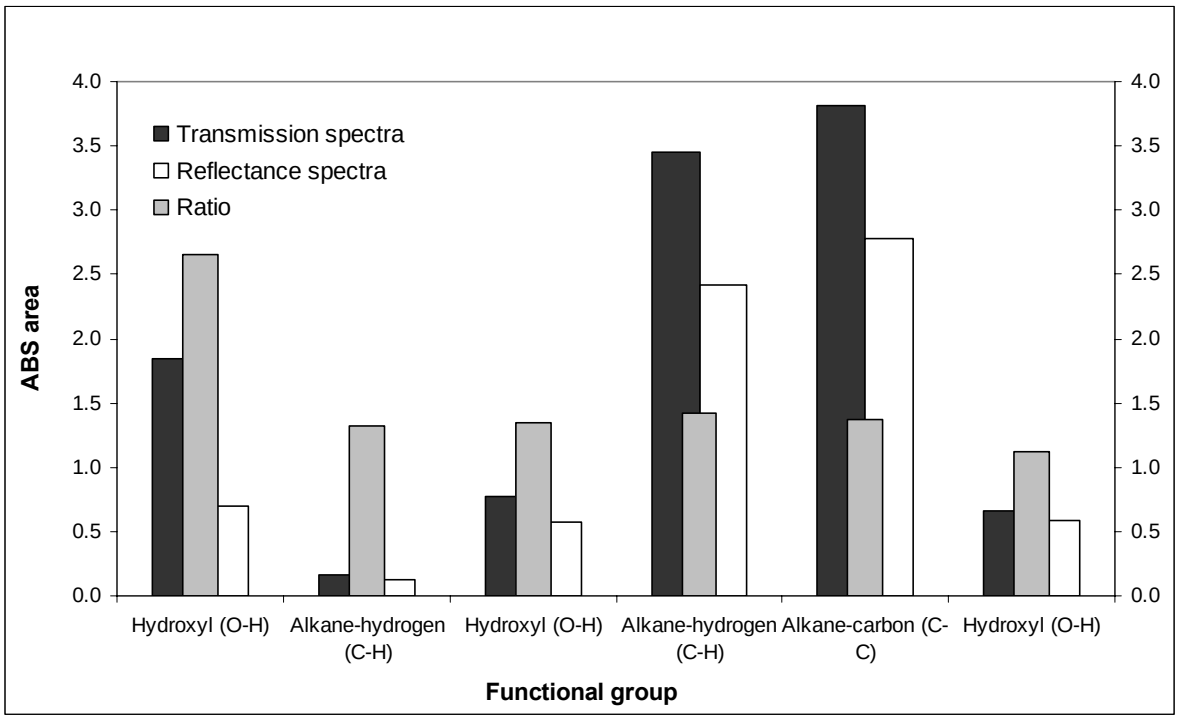

Figure 4- 6 Measured ABS area of sample collected on Teflon substrate using both transmission and reflectance approaches.

The absorbances measured with transmission are consistently higher than those measured using reflectance, consistent with the findings already discussed in the prior section. However, the ratio of the two method absorbances by functional group is inconsistent. If the samples were homogeneous with depth, the ratio would less than one but consistent

across functional groups. Since it is not consistent, we conclude that from the reflectance spectroscopy light path does not penetrate into the full fine particle sample and therefore cannot measure the speciation of the full sample.

Sample inhomogeneity across substrate

Comparison of the integrated absorbance area of each of the targeted functional groups by location in the sample and by spectroscopy method are shown in **Figure 4-7.**

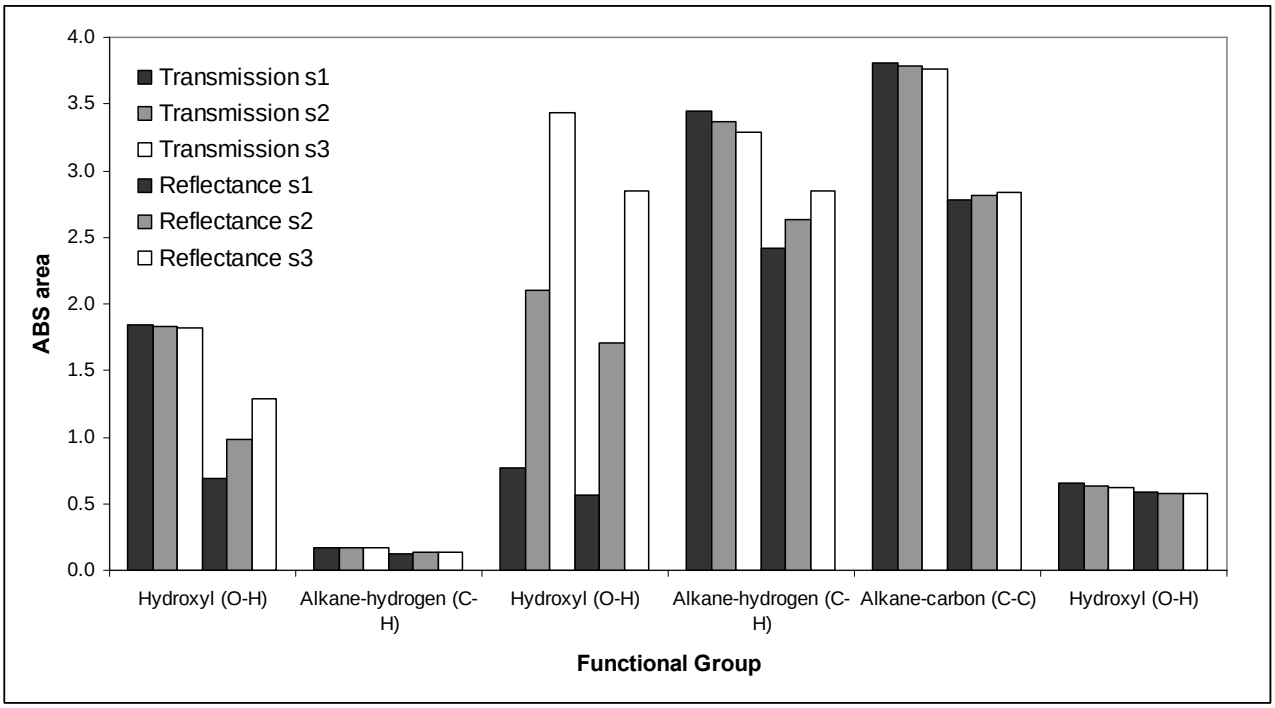

Figure 4- 7 ABS areas of different functional groups measured by using transmission and reflectance technique at two different locations in the spectra.

Figure 4-7 shows that the absolute absorbance of a particular functional group varies by location and spectroscopy method. The absorbances measured with transmission are consistently higher than those measured using reflectance, consistent with the findings

already discussed in the prior section. The differences by location with transmission spectroscopy indicate that the samples do have small spatial inhomogeneities, since the automatic shuttle allowed the s_1, s_2 and s_3 spectra to be collected without handling. These differences are much pronounced in the reflectance spectra because of spatial differences in the top 5 um of fine particles collected on the substrate and because of sample manipulation during the s_1, s_2 and s_3 spectra collection. This last point is discussed in greater detail next.

This analysis suggests that transmittance spectra are minimally sensitive to the location on the sample where the spectra are acquired and that repeat spectra at different locations are possible without compromising the integrity of the sample.

Handling artifacts

The integrated absorbances of each targeted functional groups at the s_1 and s_4 locations measured by transmission and reflectance approaches are shown in **Table 4-8.**

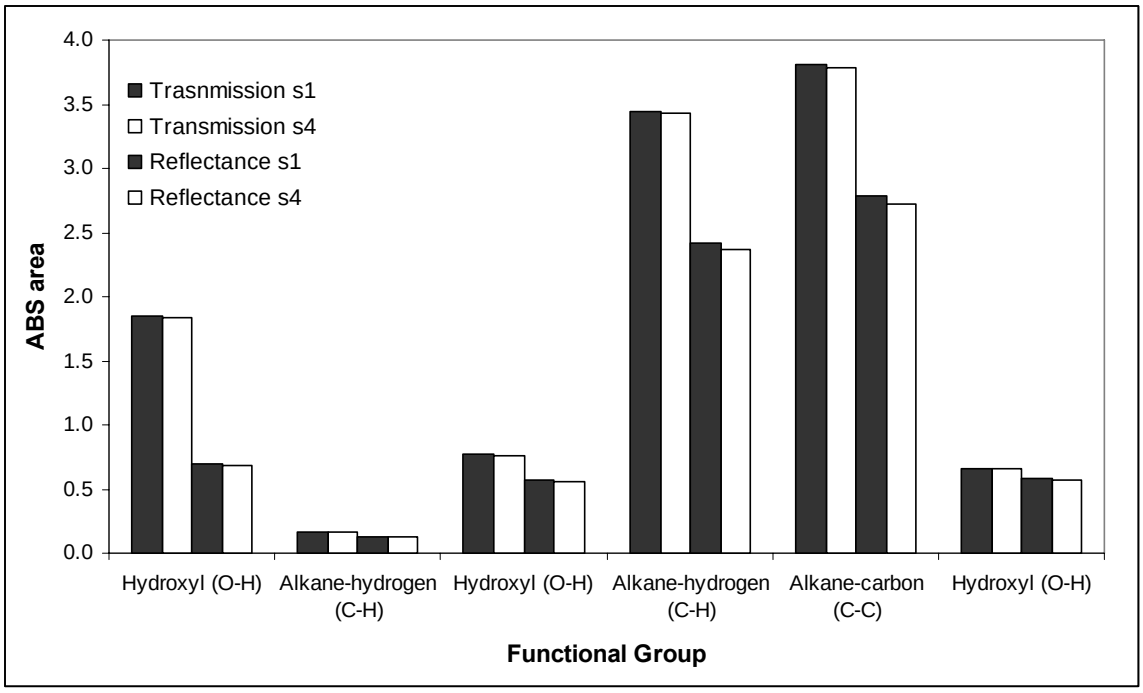

Figure 4- 8 compares the integrated absorbance area of each of the targeted functional groups at the s1 and s4 locations on the sample by spectroscopy method.

Figure 4-8 present the spectra of the sample collected at the same location but collecting the spectra at different times by using both infrared spectroscopy approaches in order to compare spectral futures. Spectra are identified as s_1 and s_4. The first two bars in the chart represent the average ABS of fine particle species collected by transmission spectroscopy. The last two bars in the chart represent the average ABS of the fine particle species collected by reflectance spectroscopy. The absorbances measured with transmission are consistently higher than those measured using reflectance, consistent with the findings already discussed in the prior section. Spectral futures are similar when using both approaches, similar peak areas measured by the transmission spectroscopy and by the reflectance spectroscopy confirm that handling artifacts have not been introduced during sample analysis in any of the spectroscopy approaches.

Conclusion

The optimal substrate-spectroscopy pair for fine particle speciation is transmission spectroscopy of samples collected onto Pall Teflon filters. Transmission spectroscopy results in strong but resolved fine particle signatures that are not sensitive to location on the substrate, that are repeatable even when the sample must be repositioned, and that account for the full fine particle sample since the light penetrates the whole depth of the sample. The transmission spectra signatures of Pall Teflon filters are also resolved and free of excessive noise.

4.2 EXPERIMENT 7: USE OF BACKGROUND SPECTRA

A background is a spectrum of the gases and any other materials in the analysis chamber that interfere with the blank or sample spectrum. The background spectrum is automatically subtracted from the blank or sample spectrum, resulting in a final spectrum that is free of the interferents.

Through this experiment, the optimal background approach for fine particle speciation is identified.

4.2.1 Issue

In the prior experiment, a background spectrum was collected immediately before each blank (i.e., unsampled) or sample spectrum. This background spectrum is automatically subtracted from the blank or sample spectrum by the OMNIC software.

Background spectra are typically collected of an empty analysis chamber (i.e., with no blank or sample in the beam path), and therefore only account for gases present in the volume of the MIR light beam as it passes through the analysis chamber. However, if a clean substrate is placed in the beam path, the background spectrum can be used to remove the spectral signal of a substrate from the sample spectrum leaving only the fine particle signatures.

The main issue associated with how the background is collected is the compounding of mathematical error. A fine particle spectrum can be produced by subtracting a spectrum of the substrate which is background-corrected for the chamber gas from a spectrum of the sample and substrate which is background-corrected for the chamber gas, or simply by collecting a single spectrum of the substrate and sample which is background-corrected for the chamber gas and substrate. The first approach requires 3 subtraction steps and the second approach requires only 1 subtraction step.

The FTIR OMNIC software used in this research provides another option: a correction factor which minimizes the negative subtraction artifacts caused by using the first approach.

4.2.2 Goal

The goal of this experiment is to determine the background-correction approach which results in the most consistent fine particle spectra that is also free of negative subtraction artifacts.

4.2.3 Literature Review

In previous studies, the background spectrum was collected in different ways. Krost and McClenny (1994), Carlton et al. (1999) and Reff et al. (2005) collected an open path background spectra to account for the instrument conditions, then a blank substrate and sample spectra, thus the blank was subtracted from the sample spectra. Allen et al. (1994) and Blando et al. (2001) collected a background spectrum of a clean substrate in the beam path to account for the instrument conditions and the clean substrate.

In these previous studies there was no analysis of the effects of the background approach on the fine particle speciation. Therefore, in this experiment these approaches were systematically evaluated and compared in order to identify the approach that is best for fine particle speciation.

4.2.4. Experimental Approach

This experiment builds on the prior one: all samples in this experiment are collected onto Pall Teflon substrates and analyzed by transmission spectroscopy.

In this experiment, fine particle samples were generated in the laboratory using model compounds. A solution of concentrated ammonium sulfate (Sigma Aldrich #09980) in deionized water was prepared at a concentration of 1 g L^{-1}, nebulized using the system shown below, and then collected at 16.67 LPM onto a Pall Teflon substrate using the CCNY sampler. Ammonium sulfate was selected for this experiment because is a stable compound which does not volatilize at room temperature and because its MIR signature is known, sharp and strong.

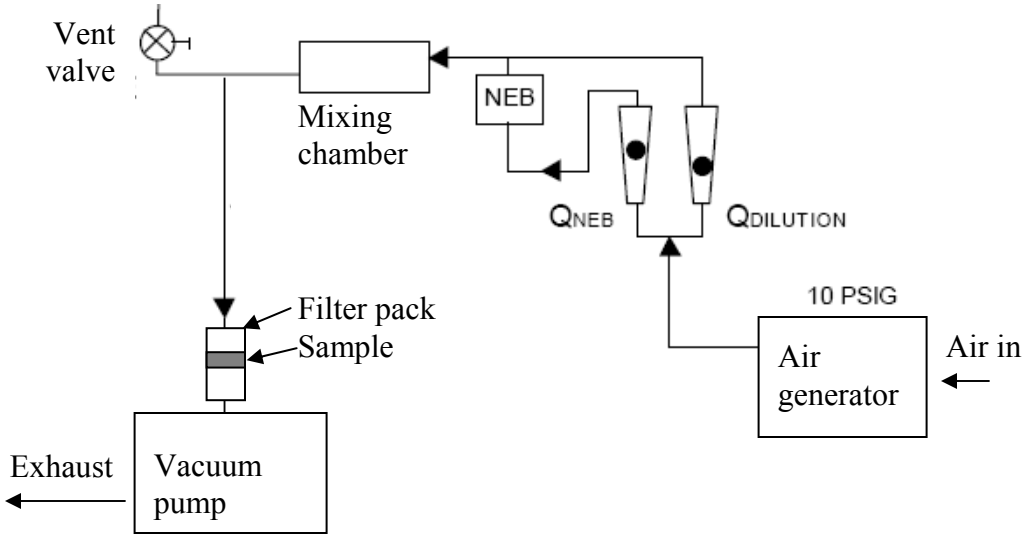

Figure 4- 9 Nebulization system used to collect sample onto the Teflon substrates.

Figure 4-9 shows the nebulization system used to collect ammonium aerosol sample onto a Pall Teflon substrate. The flow of the generated air is controlled by two flowmeters, one for nebulizing the ammonium solution and the other for the dilution between air and the nebulized ammonium solution. The nebulized solution and the air will be mixed in

the mixing chamber and then by using a vacuum pump the sample was drawn to the filter pack where it was collected onto the substrate.

After collection, the sample was desiccated in a desiccator (Fisher #08595C) with a desiccator plate (Fisher #08636C) for approximately 4 hours and then frozen in a compact refrigerator (Danby #DCR412W) at -20^{o}C until analysis.

Samples were analyzed by transmission spectroscopy only. The two holders were loaded with the sampled substrate and a blank substrate and the automated shuttle was used to move the substrate and blank into and out of the FTIR light path without handling.

The FTIR was operated in a slightly different configuration than described in the last experiment, integrating the recommendations of the last experiment into its operation and allowing a different variable to be investigated. In this experiment, the background approach was varied:

- Use of background spectra: Several different background approaches were used
  - Open path background (OPBG): same as prior (a background of the analysis chamber gases was used to develop fine particle spectra)
  - Blank in path background (BPBG): a background of the analysis chamber gases and a blank substrate was used to develop fine particle spectra
- Approach to minimize interference in the analysis chamber: same as prior experiment (no removal by purge or atmospheric suppression)
- Use of sampling substrate as an internal standard: same as prior experiment (not used)

Selection of background approach

These experiments compared the effects of differences in background approach on the fine particle spectra: blank in path versus open path with and without the OMNIC correction factor.

The analysis chamber was closed to minimize the flow of laboratory room air into the chamber, and then 3 replicates of the following 5 spectra were collected:

- Background of clean substrate at location b resulting in the blank-in-path background
- Spectrum of sample at location s_1 corrected using the blank-in-path background
- Background of chamber gases resulting in the open-path background
- Spectrum of clean substrate at location b corrected using the open-path background
- Spectrum of sample on clean substrate at location s1 corrected using the open-path background

These spectra were processed to develop 3 replicates of 3 fine particle spectra:

(1) Spectrum of sample at location s1 corrected using the blank-in-path background
(2) Spectrum of sample on clean substrate at location s1 corrected using the open-path background *minus the* spectrum of clean substrate at location b corrected using the open-path background

(3) Spectrum of sample on clean substrate at location s1 corrected using the open-path background *minus the* spectrum of clean substrate at location b corrected using the open-path background, computed by the FTIR OMNIC software using a subtraction factor to minimize negative subtraction artifacts

These three fine particle spectra were compared to qualitatively identify subtraction artifacts. The optimal background approach does not result in subtraction artifacts.

The three fine particle spectra were then analyzed using the same approach employed in the last experiment to determine the integrated absorbance area of each of the target functional groups.

The absorbances of the fine particle functional groups were statistically evaluated using the same approach employed in the last experiment to determine their means and standard deviations. Ideally, the mean absorbance areas of a functional group should not vary with background type within a reasonable amount of uncertainty. However, we expect the standard deviation of the absorbance area for each functional group to be highest when using an open-path background approach because of the multiple levels of subtraction needed to produce the fine particle spectrum. We also expect the use of the blank in path background with OMNIC factor correction to result in the lowest absorbance areas for species with signatures near the CO_2 and H_2O signatures since this approach mathematically manipulates and then subtracts the sample and blank spectra to minimize CO_2 and H_2O signatures. The optimal background approach is the one that

results in the largest fine particle species absorbances, and with the smallest standard deviation.

Selection of background frequency

For the optimal background approach, an additional experiment was conducted to evaluate the frequency at which background spectra should be obtained to achieve accurate fine particle spectra.

The analysis chamber was closed to minimize the flow of laboratory room air into the chamber, and then 3 replicates of the following 5 spectra were collected:

- At time 0, the optimal background and blank spectra were collected, followed immediately by a spectrum of the sample at location s_1 corrected using the background and blank
- After 10 minutes, an additional spectrum of the sample at location s_1 was collected and corrected using the background and blank from time 0
- After 20 minutes, an additional spectrum of the sample at location s_1 was collected and corrected using the background and blank from time 0
- After 30 minutes, an additional spectrum of the sample at location s_1 was collected and corrected using the background and blank from time 0

The resulting 4 spectra (with replicates) were compared. The change in absorbance with wavenumber and as a function of time was determined by subtracting the time zero spectrum from the 10 minute, 20 minute or 30 minute spectra. The oldest spectrum that

resulted in a change in the spectrum that was within the noise estimated in **Experiment 5**, at 20 min, was identified. The time at which this spectrum was collected relative to time zero was taken as the frequency with which backgrounds should be collected.

4.2.5 Results and Discussion

Selection of background approach

The three fine particle spectra compared in this experiment, illustrating qualitative differences in the background approaches are shown in **Figure 4-10**.

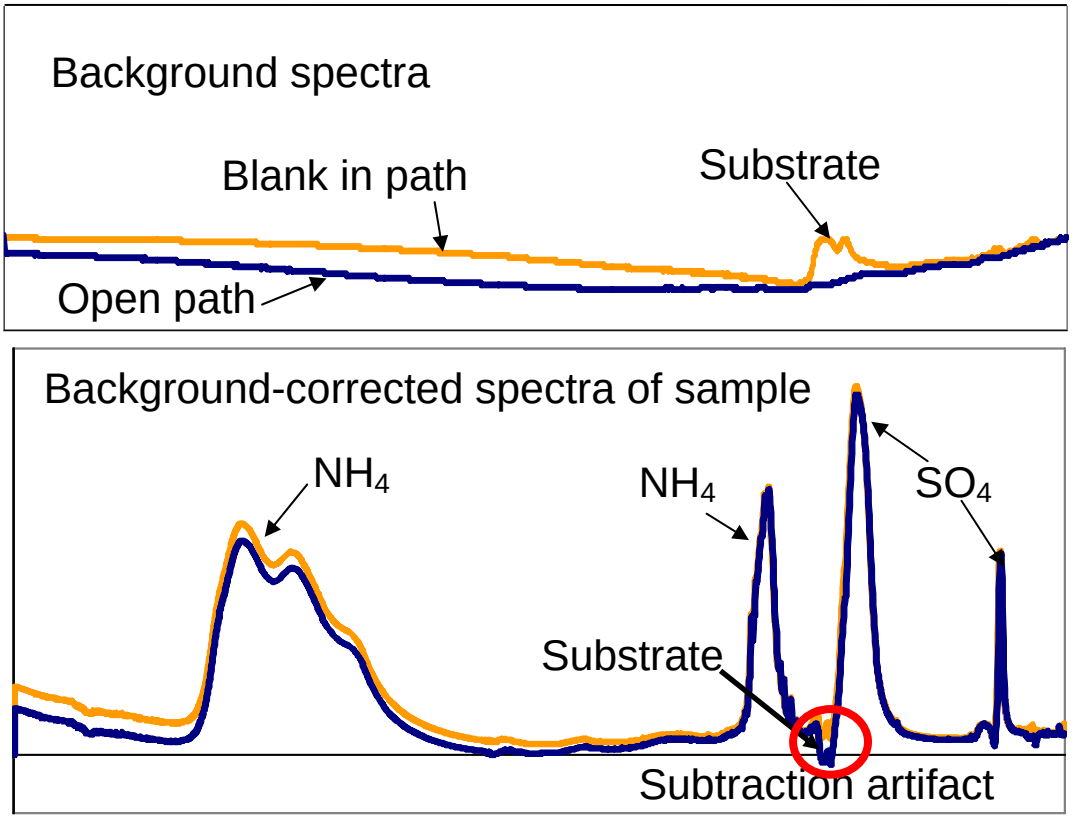

Figure 4- 10 Spectra of the three different background types and background corrected spectra of fine particles analyzed in this experiment.

The top cell illustrates differences in an open-path versus a blank-in-path spectrum. The bottom cell shows the three background corrected spectra of the same fine particle sample. The signatures of Teflon, ammonium and sulfate are identified in the spectra, as well as the subtraction artifact peak which occurs when two background-corrected spectra are subtracted from each other and the OMNIC software does not use a factor to minimize the subtraction artifact.

The average and standard deviation of the integrated absorbance area of the fine particle speciation at several peaks in the species signatures are presented in **Table 4-3**, as a function of the three different background approaches.

Functional Group	**Peak Wavenumber**	**Absorbance area ± percent uncertainty for various background-correction approach**		
		(1) Blank in path	**(2) Open path with factor**	**(3) Open path without factor**
SO_4	1141-1103 cm^{-1}	26.6 ± 4.2%)	22.8 ±4.4%)	22.8 ±3.6%)
SO_4	684-612 cm^{-1}	5.1 ±7.2%)	4.6 ±6.2%)	4.6 ±4.9%)
NH_4	1573-1410 cm^{-1}	24.3 ±1.8%)	24.2 ±3.4%)	24.2 ±3.4%)
NH_4	3480-3170 cm^{-1}	60.0 ±2.6%)	58.8 ±4.5%)	58.8 ±4.3%)

Table 4- 3 Uncertainties calculated for the ABS areas of SO_4 and NH_4 in the fine particle spectra collected using the three different background-correction approaches

Results in **Table 4-3** shows that the mean absorbance areas vary across the signature of a single species because of differences in molar absorptivity across the signature. Subtraction would affect the ABS of peaks. Teflon overlaps with SO_4 and NH_4 at two different regions, 684-612 cm^{-1} and 1573-1410 cm^{-1} respectively.

The mean absorbance areas for a single species signature peak are similar for all three background approaches within the uncertainty also presented. The areas resulting from the blank-in-path background correction are the largest although only by a small amount, due to fewer subtraction steps. The open-path background approach with and without the correction factor are similar, indicating that the factor correction does not actually affect the signatures of either ammonium or sulfate peaks in the vicinity of the CO_2 and H_2O signatures. For the most part, the uncertainties follow a similar trend as the means just discussed. The exception is the uncertainties of the sulfate signature at 684-612 cm-1 which are largest overall due to the interference of Teflon signature at 560-490 cm^{-1}.

The optimal background approach is the open path approach without the correction factor since it results similar absorbances as the other approaches when uncertainty is also considered and consistently low uncertainty in the absorbance areas of the target functional groups. As a result, in all future experiments, this approach will be used to collect spectra of the fine particles.

Selection of background frequency

Since the optimal background approach was determined to be the open path background, the additional experiments to determine background frequency used this background approach.

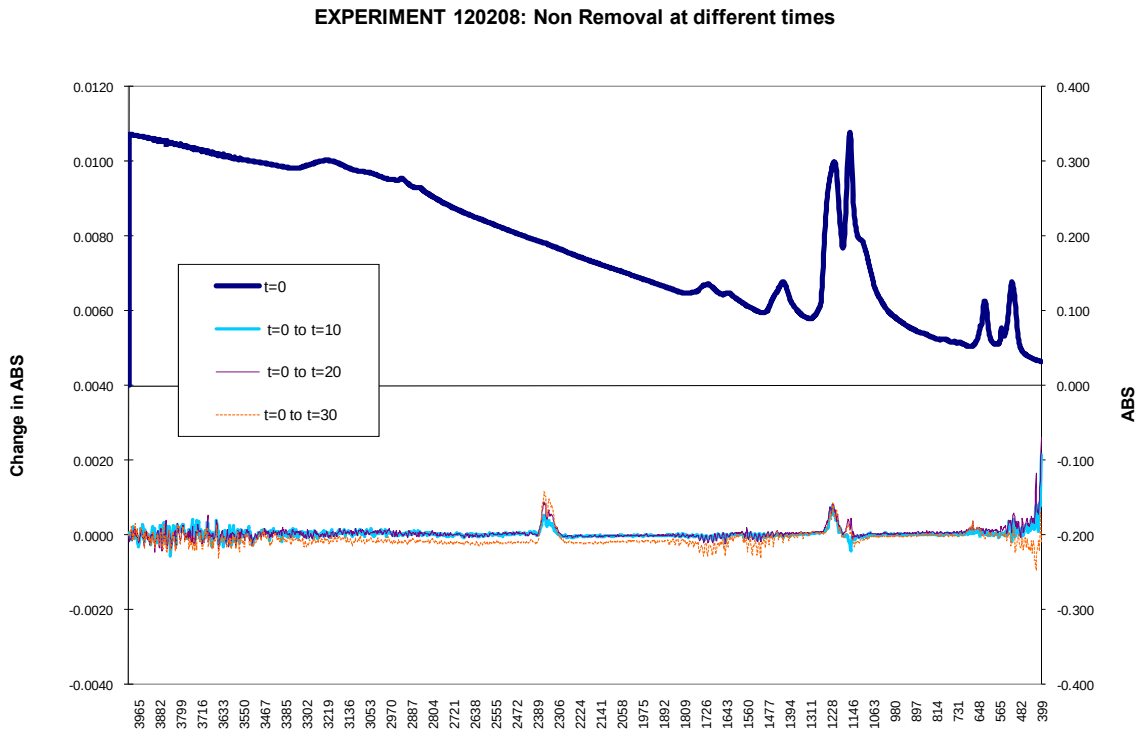

Figure 4- 11 Presents the fine particle spectrum at time zero and the difference in fine particle spectra after 10 minutes, 20 minutes and 30 minutes.

The upper cell shows an example of a fine particle spectrum at time zero, which is one of the three replicate spectra measured in the prior experiment using the open path background approach. The lower cell shows examples of the absolute difference in absorbance for the 3 subsequent spectra collected at the same location on the substrate but at different times. As expected, the differences in absorbance after 30 minutes are larger and noisier than the differences in absorbance after 20 minutes or 10 minutes, since the analysis chamber gas concentration gradually changes with time.

Noise becomes apparent in the spectra collected after 10 minutes, as does a small CO_2 peak. The noise across the spectrum is similar in magnitude after 20 minutes, but then becomes significantly larger at 30 minutes. Since the absorbance differences across the spectrum at 20 minutes are still on the order of the noise estimate of 3, 20 minutes is considered to be the maximum time in between background spectra.

4.3 EXPERIMENT 8: APPROACH TO MINIMIZE THE EFFECTS OF INTERFERENTS ON FINE PARTICLE SPECTRA

Interferents are gases present in the FTIR analysis chamber which have signatures in the MIR range and may be confused with the signatures of fine particle species. There are several approaches that can be used to minimize the presence of these interferents in the fine particle spectra. This experiment examines two of these approaches and identifies the one that is best suited for fine particle speciation.

4.3.1 Issue

The common gases that have MIR signatures that interfere with the signatures of fine particle species are water vapor and CO_2. CO_2 has a signature at 2350 and 667 cm^{-1}, which may overlap with peaks in the signatures of alkane-hydrogens –(C-H), ammonium -(N-H), and sulfur-oxides or sulfates -(S-O). Water vapor has a signature at 3900-3400 cm^{-1} and 1850-1350 cm^{-1}, which may overlap with peaks in the signatures of alcohols –(O-H), alkane-hydrogens -(C-H), carbonyls -(C=O), alkenes -(C=C), amines or ammonium-(N-H) and nitrogen-oxides or nitrates –(N-O). It is also easily confused with the signature of water present in the fine particles.

Ideally, the background spectrum measures the concentration of interferents in the analysis chamber and therefore the background-correction of a sample spectrum should eliminate them from the fine particle spectrum. However, this is not the case as shown in the prior experiment. An explanation for this is that the concentration of gases in the analysis chamber differs in the background and the sample spectra because the analysis chamber is fed by room air and the background and sample spectra are not collected simultaneously.

Another approach is to remove the interferents from the chamber or from the sample spectrum. Two possible ways to do this are:

- Do nothing
- Use atmospheric suppression, a setting in the OMNIC software, to suppress the signatures of CO_2 and water vapor

Atmospheric suppression is performed by the OMNIC software. It involves a minimization of the signature of CO_2 and water vapor in a spectrum. Since there is actually water in fine particles, it is unclear whether it will also falsely minimize the signature of water in the fine particle spectrum. It is also unclear whether it will affect the signatures of other fine particle species. Finally, even background spectrum that are recollected every 20 minutes reflect small changes in the concentration of gases in the analysis chamber. As a result, this OMNIC setting will perform different amounts of

correction for background and sample spectra, which may result in subtraction artifacts such as negative CO_2 and water signatures.

4.3.2 Goal

The goal of this experiment is to investigate approaches to remove gas phase interferents from fine particle spectra and identify the approach that results in the most accurate fine particle spectrum.

4.3.3 Literature Review

The EPA FTIR Protocol (1995) suggests a post analysis calculation to determine errors caused by CO_2 and water vapor in the analysis of gas phase samples using FTIR. Signorell et al. (2000) studied non-volatile molecular nanoparticles using FTIR and found during the experimental analysis that the infrared signal of CO_2 gas at 2349 cm^{-1} and water vapor at 1595 cm^{-1} interfere with the signal of the aerosols samples in that region, however they do not provide information on how to avoid the interference of these gases.

In this research the interference of CO_2 and water vapor was addressed in order to have spectra free of these interfering gases. The atmospheric suppression option from the OMNIC settings against the non removal option were evaluated and compared in order to select the option that results in a spectrum free of interfering gases from the analysis chamber. Also the optimal option will not suppress the signature of the water or other

functional groups present in the sample that appeared at the same wavenumber regions of the interfering gases.

4.3.4 Experimental Approach

This experiment used a blank Pall Teflon substrate as well as the sample on the Pall Teflon substrate from the last experiment. Recall that the sample from the last experiment was generated in the lab by nebulizing a solution of concentrated ammonium sulfate in deionized water, sampling the particles onto the substrate using the CCNY sampler, desiccating the samples, and then freezing them. In between experiments these samples were kept in the freezer.

As with the last experiment, the blank substrate and sample were analyzed by transmission spectroscopy and the two holders were loaded with the blank and sampled substrates and automatically shuttled into and out of the FTIR light path without handling.

The FTIR was operated in a slightly different configuration than described in the last experiment, integrating the recommendations of the last experiment into its operation and allowing a different variable to be investigated. In this experiment, the approach to minimize interference is varied:

- Use of background spectra: Open path backgrounds (OPBG) were collected
- Approach to minimize interference in the analysis chamber:
    - No removal

- Atmospheric suppression

- Use of sampling substrate as an internal standard: same as prior experiment (not used)

Atmospheric suppression was achieved simply by selecting this setting in the OMNIC software.

For both approaches to minimize interference in the analysis chamber, the analysis chamber was closed and the approach implemented, and then 10 minutes later, several spectra were obtained one after the other.

Blank experiments: For both approaches to minimize interference in the analysis chamber, 3 replicates each of an open path background of the analysis chamber gases and a spectrum of the unsampled substrate at position s1 were collected. These experiments resulted in 6 blank spectra (2 removal approaches, 3 replicates of each).

Each of the blank spectra were quantitatively compared to identify differences in the spectra as a result of interferent removal approach. The absorbance areas of peaks in the Teflon and water signatures were determined, statistically evaluated and compared to identify the effectiveness of the removal method as well as whether the removal method had an indirect effect on other species in the spectra (i.e., the Teflon). The approaches to determine peak absorbance area and mean and standard deviations of the area were identical to those in the prior experiment. Since the blank substrates do not contain any

fine particles, there is no water present in the substrate and any water observed is the result of water vapor in the analysis chamber. Ideally, since there is no water on the blank substrate, the 2 removal approaches should result in identical Teflon absorbance areas. Since all blank spectra are obtained immediately after the background, the two removal approaches should also result in identical CO_2 and water absorbance areas.

Sample experiments: For both approaches to minimize interference in the analysis chamber, 3 replicates each of an open path background of the analysis chamber gases, a spectrum of the substrate at position b on the sampled substrate, and a spectrum of the sample and substrate at position s_1 on the sampled substrate. All spectra were background-corrected, and then the background-corrected blank spectra were subtracted from the background-corrected sample spectra. These experiments resulted in 6 fine particle spectra (2 removal approaches, 3 replicates of each).

Each of the fine particle spectra were quantitatively compared. The absorbance areas of peaks in the ammonium, sulfate and water signatures were determined and statistically evaluated and then compared. Since the fine particle samples contain water, the spectra should also contain water. Ideally, the 3 removal approaches should result in identical ammonium, sulfate and water absorbance areas since the fine particle sample contains all three of these functional groups. However, if the atmospheric suppression approach results in lower ammonium, sulfate or water absorbance areas, or if the ratio of the absorbance areas of the two water peaks differ when atmospheric suppression is used

versus when it is not, then atmospheric suppression cannot be used for fine particle speciation.

The optimal interferent minimization approach results in the largest and most consistent functional group absorbance areas and a ratio of water signature peak absorbance areas that are consistent with the no removal approach.

4.3.5 Results and Discussion

Blank experiments

The absorbances of Teflon and water in the blank spectra are presented in **Table 4-4.**

Removal Option	Absorbance area: Average ± Uncertainty (± %Uncertainty)			
	Teflon 1178-1120 cm^{-1}	**Teflon 580-547 cm^{-1}**	**Water 3450-3350 cm^{-1}**	**Water 1766-1594 cm^{-1}**
No Removal	46.9±0.005 (±0.01%)	1.940±0.005 (±0.25%)	0.013±0.008 (±60.2%)	0.112±0.057 (±51.3%)
Atmospheric suppression	45.8±0.004 (±0.01%)	1.871±0.016 (±0.85%)	0.005±0.001 (±10.8%)	0.014±0.001 (±4.0%)

Table 4- 4 Average ABS areas and uncertainty of Teflon in the spectra collected with the different removal options.

Table 4-4 presents the absorbances of Teflon and water in the blank spectra collected under the non-removal and atmospheric suppression options. Two different signatures for Teflon and water were evaluated. The absorbances for the Teflon peaks are consistent across the removal options and result in low standard deviation and low uncertainty indicating that the removal approaches do not affect the Teflon signatures. The presence

of water was not expected in the spectra, since the blank Teflon substrate does not contain water on it, however the absorbance of water presented in table are the result of the water in the analysis chamber. The absorbance of water in the spectra varies across the removal options, ideally both spectra should have identical water absorbance since both were taken under the same conditions, immediately after the background spectra, however both spectra presented water absorbance at relative small amounts. Spectra collected under the non-removal option presented a slightly bigger amount of water absorbance and higher uncertainty than the atmospheric suppression option,

In order to decide which removal option will be used the sample spectra was analyzed.

Sample experiments

Figure 4-12 provides an example of fine particle spectra collected with each of the interferent removal approaches.

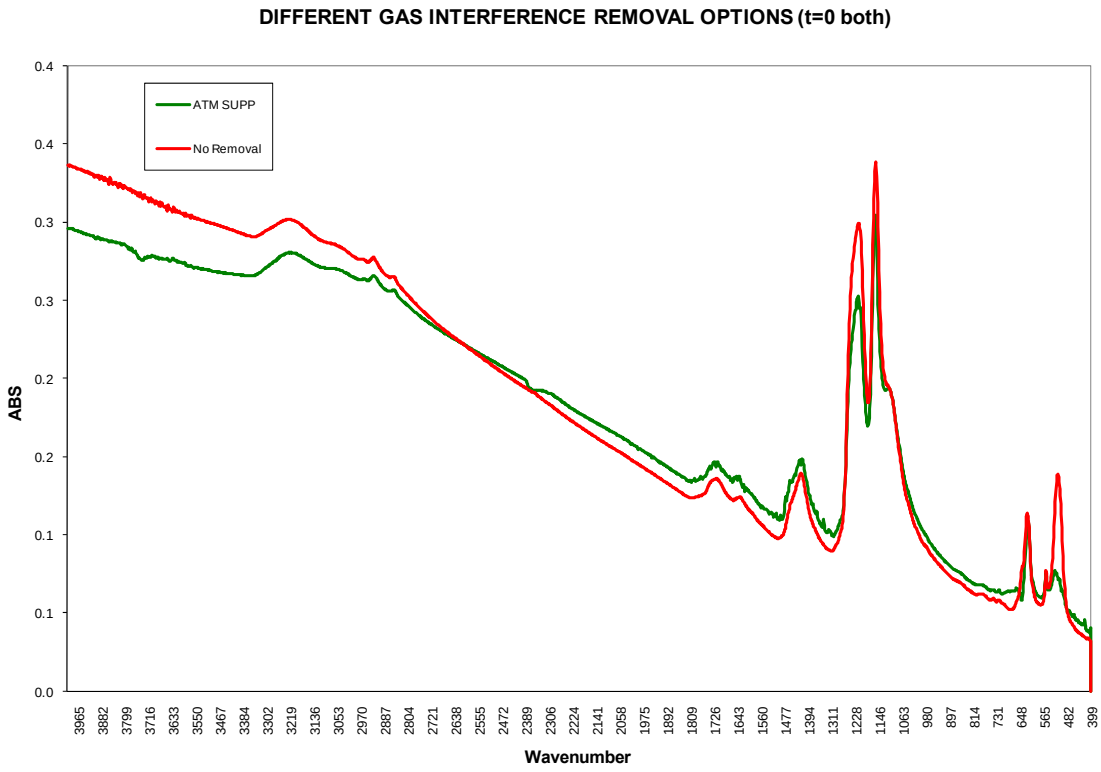

Figure 4- 12 Spectra of sample collected by using the different gas removal options.

There are notable differences in the intensity of fine particle species peaks and noise level as a function of interferent removal method. The atmospheric removal option results in more noise than the other approaches and the sulfate and ammonium peak intensities are differently shaped. The physical purge option also results in some noise, but the sulfate and ammonium peak intensities are similar to those of the no removal option and some water is observed in the sample.

Comparison of the integrated area of the ammonium, sulfate, and water signature peaks in the fine particle spectra as a result of interferent removal approach is presented in **Table 4-5**.

Removal Option	Absorbance area: Average ± STDEV (±%Uncertainty)			
	Ammonium 3480-3097 cm^{-1}	Ammonium 1573-1319 cm^{-1}	Sulfate 684-580 cm^{-1}	Water 1766-1594 cm^{-1}
No removal	4.735±0.010 (±0.21%)	3.471±0.003 (±0.09%)	1.725±0.007 (±0.38%)	1.19±0.05 (±5.4%)
Atmospheric suppression	5.302±0.026 (±0.50%)	3.293±0.012 (±0.35%)	1.277±0.002 (±0.15%)	1.09±0.02 (±2.2%)

Table 4- 5 Presents the absorbances for the ammonium, sulfate and water peaks in the samples spectra.

With a single exception, the absorbance areas of the fine particle species are higher when the analysis chamber gases are not removed than when they are removed mathematically using the atmospheric suppression setting. The standard deviation of the absorbance areas are small, so the absolute values of absorbance are representative of the mean values presented in the table. The single exception is the ammonium peak at 3480 cm^{-1}, which has a larger absorbance area when atmospheric suppression is used versus when it is not. This may be explained by the fact that this ammonium peak overlaps with water. When atmospheric suppression is used, its signature at this wavenumber range is distorted relative to the one with no removal.

As a result of these experiments, the atmospheric suppression setting should not be used for fine particle speciation. Instead, the analysis chamber will be loaded with the blank and substrate, closed, and background spectra will be recollected every 20 minutes.

4.4 EXPERIMENT 9: USE OF SAMPLING SUBSTRATE AS INTERNAL STANDARD

Internal standards are unique chemicals present at known concentrations in an otherwise unknown sample.

In this experiment, the consistency of the Teflon signature is investigated to determine if this unique chemical could be used as an internal standard and quality control measure in the FTIR analyses of fine particle samples.

4.4.1 Issue

Any experimental method is strengthened by the use of an internal standard. In the case of fine particle speciation using FTIR, the most ready internal standard is the substrate itself, since the fine particles are unlikely to contain Teflon and since the substrates are manufactured in lots intended to be identical. Therefore, the signature of Teflon should be the same from sample to sample, despite changes in the fine particle composition.

Provided that Teflon is a reasonable internal standard, its signature in a fine particle sample may serve multiple purposes. It can be used to indicate issues with the FTIR, since malfunctions with the instrument are likely to affect the entire sample spectrum including the Teflon signature. However, it may also be used to facilitate the calculation of concentration from absorbance. This virtue of an internal standard is explored in Chapter 5.

4.4.2 Goal

In this experiment, the consistency of the Teflon signature at different locations on a substrate and across lots of the filters is explored to determine whether the sampling substrate itself can be used as an internal standard.

4.4.3 Literature Review

Carlton et al. (1999) used FTIR transmission spectroscopy to identify functional groups and bonds in ambient $PM_{2.5}$ samples, by using NIST standard solutions they observed variations in the instrument response. This required the periodic collection of a background spectrum periodically to account for the atmospheric changes and instrument response. They collected background spectra every half hour to identify any changes during the spectral analysis. Blando et al. (2001) used aerosol standards to verify the spectral accuracy during the analysis.

In this research, the Teflon signature was evaluated to determine if it can be used as internal standard. Teflon signature may be used to decided when a new background spectrum must be taking or as an indicator of instrument response.

4.4.4 Experimental Approach

In this experiment, blank Pall Teflon filters were analyzed.

As with the last experiment, these blank substrates were analyzed by transmission spectroscopy. The two holders were loaded with different blank substrates and automatically shuttled into and out of the FTIR light path without handling.

The FTIR was operated in a slightly different configuration than described in the last experiment, integrating the recommendations of the last experiment into its operation. Now the approach to minimize interference is varied:

- Use of background spectra: Open path backgrounds (OPBG) were collected
- Approach to minimize interference in the analysis chamber: No removal was used
- Use of sampling substrate as an internal standard: investigated in this experiment

Since the sampling substrate is already a part of the sample, the viability of the sampling substrate as an internal standard was investigated simply by analyzing the blank spectra of multiple blank Pall Teflon filters at multiple locations on each filter, as described below.

For each filter, the analysis chamber was closed and then 3 replicates each of the following spectra were obtained:

- an open path background of the analysis chamber gases
- a spectrum of the unsampled substrate at position s1
- a spectrum of the unsampled substrate at position s2
- a spectrum of the unsampled substrate at position s3

Open path backgrounds were recollected every 20 minutes. Each of the blank spectra were background-corrected using the most recent open path background, resulting in 27 replicate blank substrate spectra (3 filters, 3 positions on each filter, 3 replicates of each).

Each of the blank spectra were quantitatively compared. The absorbance areas of the Teflon signature peaks at 1178 and 554 cm^{-1} were determined and statistically evaluated to compute mean absorbance area and standard deviation using the methods described in Experiment 4. Since a single substrate is intended to uniformly filter material and since the substrates are produced in lots intended to be identical, ideally, the absorbance areas will not vary by location or lot. However, the 1178 cm^{-1} signature peak does overlap to some extent with a peak in the signature of sulfate, and therefore the absorbance area of this peak may be more uncertain.

4.4.5 Results and Discussion

The absorbance areas of the two Teflon signatures as a function of filter and filter location are shown in **Figure 4-13**.

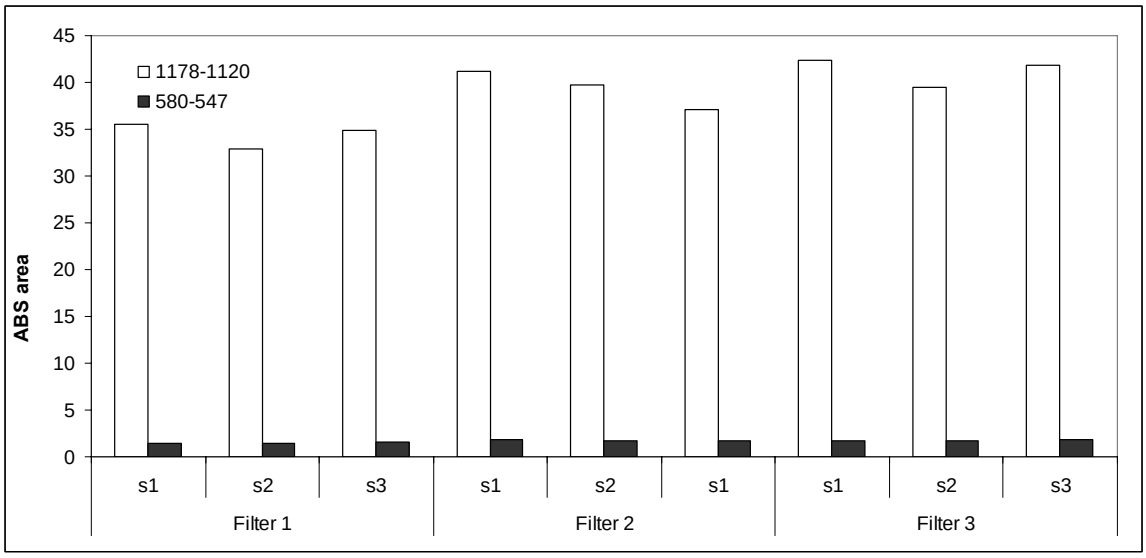

Figure 4- 13 Represent the absorbance areas for the Teflon peaks in each unsampled substrate at different positions in the filter.

From figure it is shown that ABS areas for the peak at 1178-1120 cm^{-1} are bigger than ABS areas at 580-547 cm^{-1}. Data use to generate this figure are presented in **Table 4-6**.

		AVERAGE ±STDEV (±Uncertainty)	
Filter ID	**Position**	**Teflon 1178cm^{-1}**	**Teflon 554cm^{-1}**
Filter 1	S1	35.54±0.009(±0.03%)	1.49±0.017(±1.2%)
	S2	32.92±0.006(±0.02%)	1.42±0.019(±1.3%)
	S3	34.85±0.012(±0.03%)	1.52±0.003(±0.2%)
Filter 2	S1	41.19±0.017(±0.04%)	1.81±0.019(±1.05%)
	S2	39.69±0.01(±0.03%)	1.77±0.018(±0.99%)
	S3	37.12±0.002(±0.004%)	1.67±0.018(±1.09%)
Filter 3	S1	42.32±0.006(±0.01%)	1.72±0.021(±1.23%)
	S2	39.50±0.006(±0.01%)	1.72±0.031(±1.80%)
	S3	41.88±0.009(±0.02%)	1.79±0.010(±0.51%)

Table 4- 6 Absorbance areas and uncertainties for two Teflon peaks in the spectra of three different unsampled substrate at different sampling positions.

The absorbance areas of the 1178 cm^{-1} peak in the Teflon signature are larger than those of the 554 cm^{-1} peak. Uncertainties are low for both Teflon signatures, however the one at 1178 cm^{-1} is slightly higher. Differences by filter indicate that the ABS varies from one filter to another; therefore not all filters from one lot have the same absorbances. Differences by position indicate that also the Teflon in filter is not uniform through the whole substrate.

When the substrate actually has a fine particle sample, it will be more difficult to accurate quantify the absorbance area of the 1178cm^{-1} Teflon peak. So, the uncertainty already observed will be compounded. The 554 cm^{-1} peak is more suited to the purpose of an internal standard because differences in absorbance with location on a single filter are low and because it only interferes with the signature of carbon-iodine CI, a species that is uncommon in ambient fine particles. However, since differences in the absolute absorbance of Teflon at the 554 cm^{-1} peak by filter are high, this peak cannot be used as a quality control measure.

These results suggest that Teflon can be used as an internal standard, but not as a quality control measure. The absorbance area of the 554 cm^{-1} peak in the blank spectrum at position b can be used as the internal standard absorbance area.

4.5 CONCLUSIONS

The experiments in this chapter identified an optimal configuration of the FTIR instrument when being used to speciate fine particle samples. The main results of these experiments are:

- Experiment 4: transmission spectroscopy is favored over reflectance spectroscopy
- Experiment 5: open path backgrounds are favored over blank in path backgrounds, and open path backgrounds should be collected at a frequency of every 20 minutes
- Experiment 6: no removal is favored over atmospheric suppression
- Experiment 7: the Teflon signature at 580-547 cm^{-1} can be used as an internal standard but not as an indicator of instrument performance

These optimal configurations were used in the experiments presented in Chapter 4.

4.6 REFERENCES

Allen, D. and Palen, E., 1989. Recent advances in aerosol analysis by infrared spectroscopy. Journal of Aerosol Science 20 (4), 441-455.

Allen, D., Palen, E., Haimov, M., Hering, S. and Young, J., 1994. Fourier transform infrared spectroscopy of aerosol collected in a low pressure impactor (LPI/FTIR): Method development and field calibration. Aerosol Science and Technology 21, 325-342.

Blando, J., Procja, R. and Turpin, B., 2001. Issues in the quantitation of functional groups by FTIR spectroscopic analysis of impactor-collected aerosol samples. Aerosol Science and Technology 35, 899-908.

Carlton, A., Turpin, B., Johnson, W., Buckley, B., Simcik, M., Eisenreich, S. and Porcja, R., 1999. Microanalysis methods for characterization of personal aerosol exposures. Aerosol Science and Technology 31, 66-80.

EPA, February 3, 1995. Protocol for the use of Fourier transform infrared (FTIR) spectrometry for the analysis of gaseous emissions from stationary sources.

Farinas, K., Doh, L., Venkatraman, S. and Potts, R., 1994. Characterization of solute diffusion in a polymer using ATR-FTIR spectroscopy and bulk transport techniques.

Krost, K. and McClenny, W., 1994. FTIR transmission spectroscopy for quantitation of ammonium bisulfate in fine-particulate matter collected on Teflon filters. Applied Spectroscopy 48 (6), 702-705.

Reff, A., Turpin, B., Porcja, R., Giovennetti, R., Cui, W., Weisel, C., Zhang, J., Kwon, J., Alimokhtari, S., Morandi, M., Stock, T., Maberti, S., Colome, S., Winer, A., Shendell, D., Jones, J. and Farrar, C., 2005. Functional group characterization of indoor, outdoor, and personal $PM_{2.5}$: results from RIOPA. Indoor Air 15, 53-61.

Signorell, R., Kunzmann, M. and Suhm, M., 2000. FTIR investigation of non-volatile molecular nanoparticles. Chemical Physics Letters 329, 52-60.

Smith, B., 1996. Fundamentals of Fourier transform infrared spectroscopy. CRC Press, Inc. 1996 Corporate Blvd., N.W., Boca Raton, Florida.

CHAPTER 5 SPECTRA INTERPRETATION

The main goal of this chapter is to investigate develop, optimize and use methods to interpret the FTIR spectra of fine particles, including methods to determine peak range and baseline, to determine relative molar absorptivities, to account for peak shifting, and to split peaks where multiple functional group signatures overlap.

The major challenge to these experiments is the need for an iterative solution.

The research and development of the analysis approach will involve several experiments:

- Experiment 10: Assessment of absorbance linearity
- Experiment 11: Measurement of molar absorptivity
- Experiment 12: Alternate peak baseline approach
- Experiment 13: Alternate peak shifting approach
- Experiment 14: Alternate peak splitting approach

In Chapter 3, methods were developed to collect samples for fine particle speciation using FTIR, and in Chapter 4 methods were developed to collect FTIR spectra of the fine particle samples. Both of these prior chapters used a set of consistent methods to interpret the fine particle spectra and determine functional group absorbances in the spectra. These methods were not yet refined, but this fact is not expected to affect the conclusions drawn in the prior chapters for two reasons: 1) the methods were applied consistently and 2) the conclusions in prior chapters were based on comparisons of absorbances and not absolute

values of absorbance. As a result, through the experiments in these prior chapters, a set of methods were proposed, most of which were carried forth into the experiments presented in this chapter.

In this chapter, the spectra interpretation methods are refined so that the resulting fine particle speciation absorbances are accurate. However, since the spectra interpretation methods are interrelated, the experiments described in this chapter had to be performed iteratively. To determine the concentration of a fine particle species, the species signature peak must be integrated over the appropriate baseline and endpoints that accounts for shifting and overlapping, and then converted to concentration using an accurate value of molar absorptivity. The values of molar absorptivity depend on the accurate integration of signature peaks, but the determination of accurate methods to integrate signature peaks are based on molar absorptivity. Hence an iterative solution is needed. The experiments are presented one at a time for clarity, but at the end of this chapter, the iterative solutions are presented and the best set of methods is identified and the values of the relative molar absorptivity are finalized.

5.1. EXPERIMENT 10: ASSESSMENT OF ABSORBANCE LINEARITY

By Beer Lambert's Law, absorbance and concentration of a functional group are linearly proportional to the molar absorptivity of the functional group and the length of the light path through the sample.

5.1.1. Issues

A single functional group peak has a unique IR signature in the IR spectrum, which may contain one or more different peaks. The intensity of the different peaks in a functional group spectrum depends on the molar absorptivity of the particular bond or its response to a particular IR wavelength of light (Harris and Bertolucci, 1978). As a result, while each peak in a functional group signature represents the same concentration of the functional group, the peak intensities may vary because of the sensitivity of the functional group bond to a particular wavelength of light.

While the relationship between concentration and absorbance should be linear, non-linearity may be observed because of several factors. It may be due to volatilization of semi-volatile components of the sample. This is expected to result in a decrease of absorbance as the experiment progresses. This is an experimental artifact since volatilization from ambient aerosols occurs at much lower rate due to the matrix effect of the aerosol. Different ratios of acetone and alcohol were tested to minimize volatilization. It may also be due to shifting or overlapping of neighboring functional groups. These issues are explored in later experiments. Finally, it may be due to the spread of the sample on the substrate. This is an experimental artifact which occurs because the samples in this experiment are liquids and not solid ambient particles. This artifact was avoided by applying a uniform and small volume of model compound onto a substrate, which does not penetrate the substrate fully.

5.1.2. Goal

The goal of this experiment is to assess the linearity of the concentration-absorbance relationship for liquid or solid samples.

5.1.3. Literature Review

There is no reported information on the linearity of absorbance for liquid or solid samples, likely because of the challenges in accurately delivering a known concentration into the FTIR light path and in accurately computing absorbance.

However, there is some guidance on the methodology selection of compounds to study. Palen, et al. (1992), Holes et al. (1997), and Dekermenjian et al. (1999) analyzed pure model compounds containing their target functional groups to determine values of relative molar absorptivity that were quite variable. Their methods were not documented well, so it is possible that their experiments were affected by volatilization or other unknown variables. The chemical standards that were used to determine the value of relative molar absorptivity are listed in **Table 5-1**.

Functional group	Palen, et al. 1992	Palen, et al. 1993	EPA Method 8410, 1994	Dekermenjian, et al. 1999	Blando, et al. 2001
Oxygenated aliphatic groups					
Organonitrate (RNO_2)	butyl nitrate	octyl nitrate			
Aldehyde (RC=OH)	3,5-dimethyl-4-hydroxy benzaldehyde	octyl aldehyde	bis(2-chloroethoxy) methane	2,4-nonadiene-2-carbox aldehyde	
Ketone (RC=OR')	2-ethyl cyclohexanone	3-octanone		2,7-dimethyl-6-hydroxy-2-octen-4-one; 5,7-dimethyl-3,5,9-decatrien-2-one	
Ether (ROR')			butyl benzyl phthalate		
Carboxylic acid (RC=OOH)	benzoic acid	1-octanol; octanoic acid	butyl benzyl phthalate	retinoic acid	glutaric acid; oxalic acid, palmitic acid; adipic acid
Peroxide (RC=OOR')			butyl benzyl phthalate; bis(2-chloro ethoxy) methane		
Alcohol (ROH)		1-octanol			
Aromatic groups					
Aromatic ring (Φ)	2,4,6-trimethyl phenol		phenol; 2-chlorophenol; 2,4-dichlorophenol; terphenyl; 1-fluoronaphthalene; anthracene; phenanthrene; butyl benzyl phthalate	4-(3-methyl crotyl)-phenol	
Nitro-aromatic (Φ-NO_2)	2,6-dimethyl-4-nitrophenol				

Table 5- 1 Model compounds used for calibration purposes in previous studies.

The compounds were selected to complement the chemical structure of the chemicals they were studying using FTIR. For example, Palen et al. (1993) used butyl nitrate to determine relative molar absorptivities of organonitrates (6.5), and Palen et al. (1992 and 1993) used 1-octanol to determine relative molar absorptivities of alcohols, and Dekermenjian used carboxaldehyde to determine the relative molar absorptivities of alcohols. They were also selected to account for differences in FTIR spectra with additional functional groups.

Schwarzenbach (2003) also provided some guidance on how standards might be prepared. He indicated that volatilization of organic semi-volatile compounds can be minimized by dilution of the compound in a like solvent to reduce the Henry's Law constant.

The experiment that follow similarly selected model compounds that are permutations of each other, and developed standards by diluting the pure model compounds in like solvents to minimize volatilization.

5.1.4. Experimental Approach

This experiment focused on organic compounds over inorganic compounds, since their functional group signatures are more difficult to quantify in the infrared spectra due to shifting and overlapping.

The experiment used library spectra as well as laboratory spectra.

The compounds chosen for these experiments include: methanol, octane, octanoic acid, 2-dodecanol, 1-decen-3-ol. Methanol and octane were used to establish a baseline from which octanoic acid, 2-dodecanol and 1-decen-3-ol were expected to vary because of their more complicated functionality. These compounds were selected because they have unique and common functional group in their molecular structure, and because they are stable since they do not volatilize at room temperature. They were also selected because they are slight permutations on each other, structurally; allowing differences in their spectra as a result of functional groups physically next to each other which cause "neighboring" effects on the spectra, and functional groups with signature peaks that occur in similar wavenumber ranges and cause "overlapping" effects in the spectra. Octane is the simplest compound since it contains only alkane carbon -(C-C)- and alkane hydrogen -(C-H) functional groups. Its spectrum was considered to be the basis that the other spectra were compared to. Octanoic Acid, 2-Dodecanol, 1-Decen-3-ol are more complex than octane and both "neighboring" effects that shift peak location and "overlapping" effects that make it difficult to resolve peaks are expected.

These differences in molecular structure and functional group breakdown are illustrated in **Table 5-2**.

Model Compound	Molecular Structure	Functional Group	Moles of functional group per molecule
Methanol	 CH_3OH	Aliphatic carbon -(C-H)	3
		Alcohol -(O-H)	1
Octane	 $CH_3(CH_2)_6CH_3$	Aliphatic carbon -(C-H)	18
		Aliphatic carbon -(C-C)-	7
Octanoic Acid	 $CH_3(CH_2)_6COOH$	Aliphatic carbon -(C-H)	15
		Aliphatic carbon -(C-C)-	7
		Carbonyl -(C=O)	1
		Alcohol -(O-H)	1
2-Dodecanol	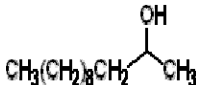 $CH_3(CH_2)_9CH(OH)CH_3$	Alkane hydrogen -(C-H)	24
		Alkane carbon –(C-C)-	11
		Alcohol -(C-O)-	1
		Alcohols -(O-H)	1
1-Decen-3-ol	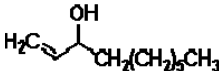 $CH_3(CH_2)_6CH(OH)CH=CH_2$	Alkane hydrogen -(C-H)	19
		Alkene hydrogen =(C-H)	3
		Alkane carbon –(C-C)-	9
		Alkene carbon-(C=C)-	1
		Alcohol -(O-H)	1

Table 5- 2 Structure, functional groups, and number of moles of functional group per molecule for the chemical standards used in this experiment.

The first two columns show chemical formula and molecular structure. The third and fourth columns show how the molecule is broken down into functional groups. The specific bond in the functional group that is actually observed by FTIR is indicated by the parentheses. For these organic functional groups, the unidentified element attached to the hanging bond is carbon. For example the notation -(O-H) indicates that this functional group is observed by the bond between an H and O, which is singly bonded to a carbon (i.e., not an OH- ion).

Absorbance calculation

The library spectra of pure methanol and pure octane were obtained to identify the –(O-H) and –(C-H) functional group signature endpoints, respectively.

Laboratory spectra of dilutions of octanoic acid, 2-dodecanol and 1-decen-3-ol were obtained to assess linearity. Octane was not evaluated because spectra of its dilutions were not reproducible for this experiment.

Substrates containing these model compounds were prepared with accuracy since this experiment developed a calibration curve between concentration and absorbance. Volatilization of organic semi-volatile compounds was avoided by dilution of the compound in a like solvent. Spreading of the liquid standard rate was avoided by delivering the same volume, 0.5 ul, of each standard onto a substrate to obtain a <1 cm diameter sample that did not penetrate the substrate. Substrates were prepared through these steps:

- Develop standards of each of the model compounds diluted in acetone or ethanol
    - Using the digital pipette, deliver the volumes of the chemical compounds given in **Table 5-2** into a precleaned 10 ml glass bottle with gas tight seal, seal and mix
    - Refrigerate standards in between experiments at -20 degrees

Standard	Solute (i.e., Model compound)	Solvent	Solute:Solvent (Vol:Vol)
1	Octanoic Acid	Acetone	1:0 (100µl:0µl)
2			1:1 (100µl:100µl)
3			1:3 (100µl:300µl)
4			1:4 (100µl:400µl)
5	2-Dodecanol	Ethanol	1:0 (100µl:0µl)
6			1:1 (100µl:100µl)
7			1:3 (100µl:300µl)
8			1:4 (100µl:400µl)
9	1-Decen-3-ol	Ethanol	1:0 (100µl:0µl)
10			1:0.25 (100µl:25µl)
11			1:0.5 (100µl:50µl)
12			1:1 (100µl:100µl)

Table 5- 3 Standard dilutions prepared for the three model compounds used in this experiment (solute) and the solvents.

- Deliver 0.5 µl of standard onto a clean Pall Teflon filter using the automatic pipette
- Place sample in the sample holder in the FTIR analysis chamber and analyze immediately

The FTIR was used in its optimal configuration for fine particle speciation, identified in **Chapter 4**:

- Spectroscopy approach - use direct transmission; load two holders with sampled substrate and blank substrate; use automated shuttle to move filters into and out of the FTIR light path
- Background spectra - use open-path background approach; acquire background spectra every 20 minutes
- Gas interferent minimization - do not use atmospheric suppression

For each sample (i.e., each standard on a substrate), the FTIR was used to collect 3 each of the following spectra in immediate succession:

- Open-path background (OPBG) of chamber gases
- Blank substrate at location b corrected using the most recent open-path background
- Sample and substrate corrected using the most recent open-path background

These spectra were further processed using the FTIR instrument software to develop spectra (of just the model compound:

- The background-corrected blank substrate and sample on substrate spectra were subtracted without using the correction factor

The resulting 27 spectra (3 model compounds, 3 dilutions of each model compound, 3 replicates) were evaluated to determine the integrated absorbance areas of these targeted functional groups: alkane-hydrogen -(C-H) because the group is present in all organic compounds in general, hydroxyl -(O-H) because the group is present in three of the compounds analyzed in this experiment, and alkene –(C=C)- because it is present in one of the compounds analyzed in this experiment. These functional group signatures were integrated using a basic spectral interpretation, which from this point forward is referred to as the "Base case". All later experiments vary this approach.

The base case spectral analysis included:

- Baseline: shaving baseline which draws a baseline by connecting the two endpoints of the peak
- Shifting: not accounted for, so actual (shifted) endpoints of the peak are ignored and instead the peak endpoints are considered to be the endpoints of octane and methanol functional group peaks
- Splitting: done simply using the endpoints for octane and methanol

The absorbance areas for each of the targeted functional groups in each spectrum were determined and statistically evaluated the replicate experiments to determine average and standard deviation measured absorbance area.

Concentration calculation

Compute the concentration of the moles of a functional group present in the standard, including the moles in the model compound as well as the moles in the solvent.

Equation 5- 1 $$n_{x \text{ in } j} = \frac{V_{j \text{ in solution}}}{V_{solution}} \times \frac{\rho_j}{MW_j} \times V_{sample} \times y_{x \text{ in } j}$$

Equation 5- 2 $$n_{Total} = n_{x \text{ in } j} + n_{x \text{ in } k}$$

Where x is the functional group, n_x is the moles of x in the solute j, or in the solvent k, V is the volume of the solute j or the solvent k in the solution, $V_{solution}$ is the volume of the solution, ρ is the density of the solute j or the solvent k, MW is the molecular weight of

the solute j or the solvent k, V_{sample} is the volume of sample analyzed by using the FTIR, and y_x is the molar fraction of x in the solute or the solvent; n_{total} is the total moles of x in the solution.

Develop a calibration curve of concentration versus absorbance determined using the shaved baseline, for each functional group, and statistically evaluate the linearity of the calibration by determining using least squares, the equation of the line, and the value of the correlation factor R^2.

5.1.5. Results and Discussion

An analysis of the pure compound octane and methanol spectra revealed these base case signature peak endpoints, where the "#"indicates the peak number in the signature:

- From octane:
    - -(C-H)#1 endpoints are 3037-2769 cm^{-1}
    - -(C-H)#2 endpoints are 1384-1371 cm^{-1}
    - -(C-H)#3 endpoints are 734-703 cm^{-1}
- From methanol:
    - -(O-H)#1 endpoints are 3592-3108 cm^{-1}

The base case approaches were used to determine the area of each of these peaks. The resulting areas and standard deviations are shown below.

Standard	Solute:Solvent ul:ul	Absorbances of functional group using the shaved baseline approach in 0.5 µl of standard	
		-(O-H)	-(C-H)
1	Octanoic Acid: Acetone 100:100	55.37±1.39	1.70±0.01
2	Octanoic Acid: Acetone 100:300	16.96±0.62	0.34±0.002
3	Octanoic Acid: Acetone 100:400	8.36±0.25	0.15±0.001
4	2-Dodecanol:Ethanol 100:100	26.04±0.26	30.65±0.64
5	2-Dodecanol:Ethanol 100:300	4.30±0.01	6.10±0.08
6	2-Dodecanol:Ethanol 100:400	0.91±0.02	1.68±0.04
7	1-Decen-3-ol:Ethanol 100:25	72.46±1.25	35.53±0.25
8	1-Decen-3-ol:Ethanol 100:50	28.33±0.51	19.83±0.16
9	1-Decen-3-ol:Ethanol 100:100	8.51±0.31	10.26±0.15

Table 5- 4 Average and standard deviations for the ABS areas of the targeted functional groups in the solute at the different standard prepared

Ideally the concentrations of each functional group in each dilution were calculated. Only the moles of functional groups in solute were used to calculate the concentration. An example of the calculation (**Equation 5-1**) for the concentration of –(C-H) at 1:1 dilution is given below:

$$n_{\text{-(C-H) in Octanoic Acid}} = \frac{100\mu l}{200\mu l} \times \frac{910\mu g/\mu l}{144.21 g/mol} \times 0.5\mu l \times 15 \times \frac{1g}{10^{-6}} = 2.37 \times 10^{-5} \text{ moles}$$

However, a volatilization occurs during the time of the FTIR analysis, and it was probed that the sample amount used for the analysis decreases with time due to volatilization. A volatilization experiment was conduct in order to calculate the rate of volatilization for each dilution.

Same dilutions were prepared, and the same volume used for the FTIR analysis was weighed using an analytical balance. The volume (0.5ul) was delivered into the same filter used for the FTIR analysis (Pall Teflon), previously weighed. Using a chronometer the weight of the volume delivered was recorded at different intervals of time during five minutes. Initially, between zero and two minutes, the weight was unstable, then the weight was recorded every five seconds until approximately one minute when the weigh started to become stable, then the weigh was recorded every thirty seconds until five minutes, which is the duration time of the FTIR analysis.

The data showed that the mass decreases with time, therefore volatilization is occurring during the time of the analysis. The mass recorded for each dilution was converted to moles of the respective solute, and a linearity plot was developed in order to determine the volatilization rate for each dilution.

The linearity plot for the 1-Decen-3-ol and Ethanol dilutions are shown in Figure 5-1. The X axis represents the time in minutes and the Y axis represents the concentration in moles. The plots were done for the 1:0, 100:100, 100:50 and 100:25 dilutions. As it is observed in the plots the concentration decreases with time, due to volatilization. The

volatilization rate is faster during the first 40 seconds (0.67 minutes) of the experiment, and then it started to become stable.

The initial concentration was unknown due to different factors, such as volatilization, the small volume used, and the instability of the weigh in the two first seconds. Since the volatilization rate is faster at the beginning of the experiment and then becomes stable, the data was break in three different sections in order to determine its linearity. The initial concentrations, from 2 to 40 seconds, were used to determine the concentration at time zero, needed for the FTIR analysis.

All R^2 values were in an acceptable range (>0.6), therefore the linearity equation was used to calculate the initial concentration for each dilution.

Similar analysis was made for the 2-Dodecanol/Ethanol and Octanoic Acid/Acetone dilutions.

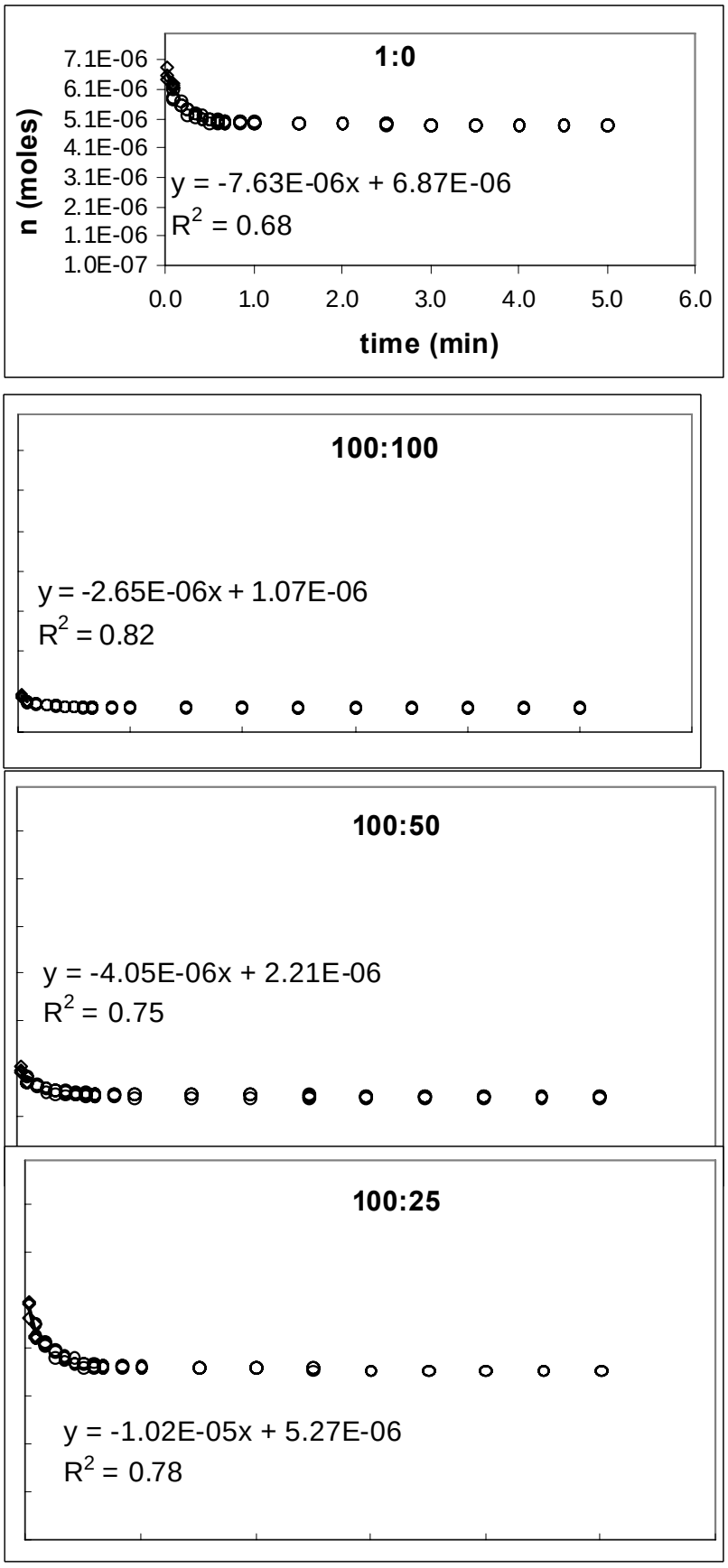

Figure 5- 1 Volatilization rate for 1-Decen-3-ol and Ethanol dilutions

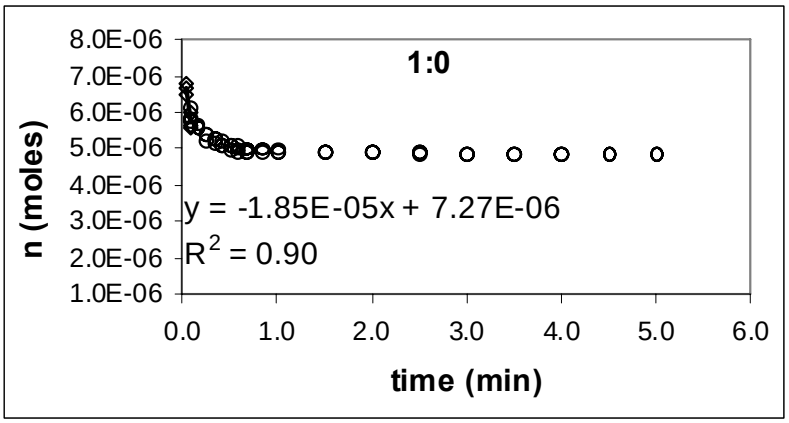

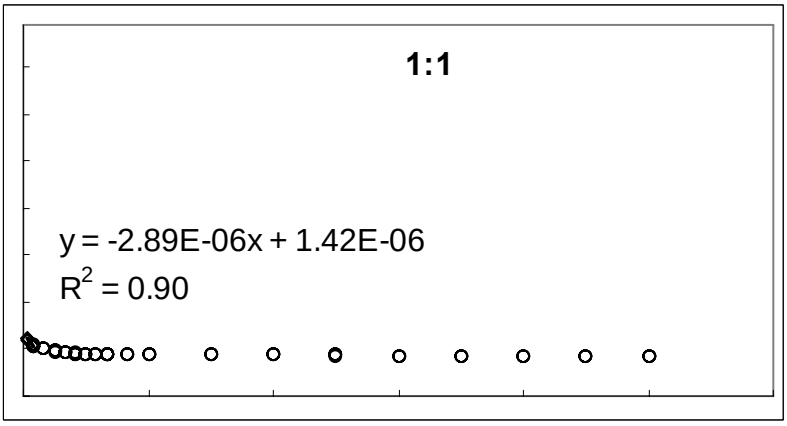

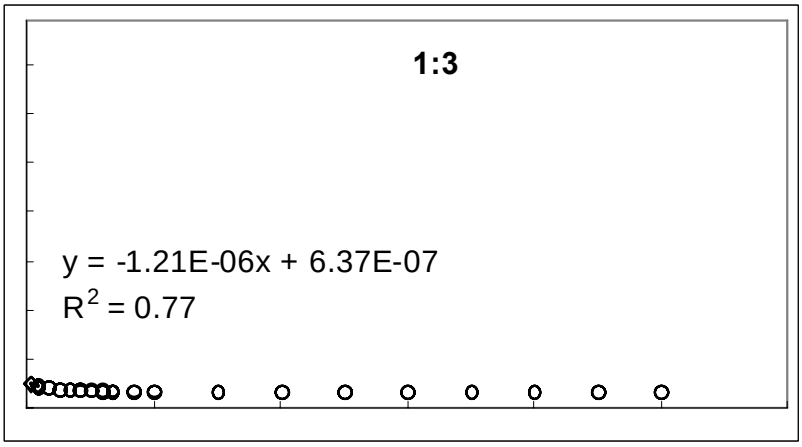

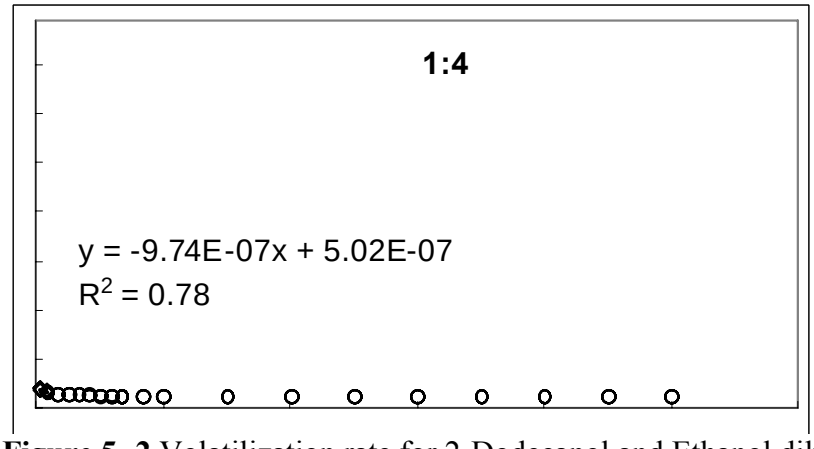

Figure 5- 2 Volatilization rate for 2-Dodecanol and Ethanol dilutions

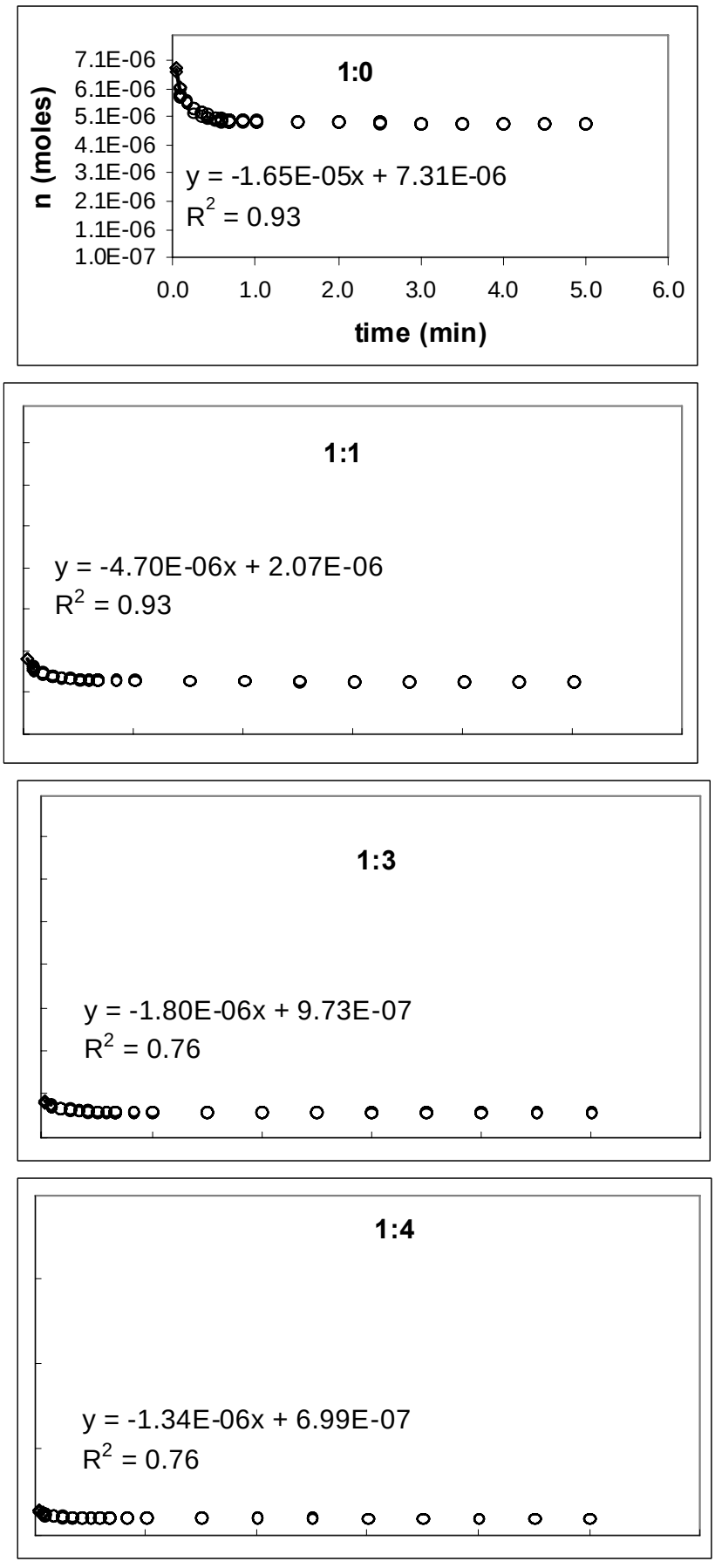

Figure 5- 3 Volatilization rate for Octanoic Acid and Acetone dilutions

Different factors were calculated by relating the initial and final concentration determined in this experiment. These factors were used to calculate the actual number of moles corresponding to the ABS areas measured during the FTIR analysis. An example of the calculation for the 1-Decen-3-ol/Ethanol 1:0 dilution is given below:

$$\text{Volatilization factor} = \frac{n_5}{n_0} = \frac{5.72\text{x}10^{-6}}{6.87\text{x}10^{-6}} = 0.832$$

These factors are listed in the following **Table 5-5 (a,b,c)** for each of the different dilutions.

Decenol/Ethanol	Time (min)	Slope	intercept	n	Factor
1:0	0	7.63E-06	6.87E-06	6.87E-06	
	5			5.72E-06	**0.832**
1:1	0	2.65E-06	1.07E-06	1.07E-06	
	5			6.96E-07	**0.650**
100:25	0	1.02E-05	5.27E-06	5.27E-06	
	5			3.63E-06	**0.689**
100:50	0	4.05E-06	2.21E-06	2.21E-06	
	5			1.55E-06	**0.702**

Table 5- 5 a

Dodecanol/Ethanol	Time (min)	Slope	intercept	n	Factor
1:0	0	1.85E-05	7.27E-06	7.27E-06	
	5			4.72E-06	**0.650**
1:1	0	2.89E-06	1.42E-06	1.42E-06	
	5			9.65E-07	**0.680**
1:4	0	9.74E-07	5.02E-07	5.02E-07	
	5			3.46E-07	**0.689**
1:3	0	1.21E-06	6.37E-07	6.37E-07	
	5			4.43E-07	**0.695**

Table 5-5 b

Octanoic Acid/Acetone	Time (min)	Slope	intercept	n	Factor
1:0	0	1.65E-05	7.31E-06	7.31E-06	
	5			4.88E-06	**0.667**
1:1	0	4.7E-06	2.07E-06	2.07E-06	
	5			1.38E-06	**0.667**
1:4	0	1.34E-06	6.99E-07	6.99E-07	
	5			4.83E-07	**0.690**
1:3	0	1.8E-06	9.73E-07	9.73E-07	
	5			6.82E-07	**0.701**

Table 5-5 c

Factors were used to calculate the actual concentration of the different dilutions analyzed with the FTIR, by multiplying the factor to the theoretical concentration ($C_{theoretical)}$). An example of the calculation of the actual concentration ($C_{(actual)}$) for the Octanoic Acid and acetone 1:0 dilution is shown below:

$$C_{actual} = C_{theoretical} \times \text{Factor} = 1.58 \times 10^{-6} \text{ moles} \times 0.67 = 1.05 \times 10^{-6} \text{ moles}$$

Standard	Solute:Solvent ul:ul	Concentration of functional group in solute in 5ul of standard	
		-(O-H)	-(C-H)
1	Octanoic Acid: Acetone 100:100	$1.05x10^{-6}$	$1.58\ x10^{-5}$
2	Octanoic Acid: Acetone 100:300	$5.53x10^{-7}$	$8.29\ x10^{-6}$
3	Octanoic Acid: Acetone 100:400	$4.35x10^{-7}$	$6.53x10^{-6}$
4	2-Dodecanol:Ethanol 100:100	$7.56x10^{-7}$	$1.89x10^{-5}$
5	2-Dodecanol:Ethanol 100:300	$3.87x10^{-7}$	$9.66x10^{-6}$
6	2-Dodecanol:Ethanol 100:400	$3.07x10^{-7}$	$7.66x10^{-6}$
7	1-Decen-3-ol:Ethanol 100:25	$1.48x10^{-6}$	$2.51x10^{-5}$
8	1-Decen-3-ol:Ethanol 100:50	$1.25x10^{-6}$	$2.13x10^{-5}$
9	1-Decen-3-ol:Ethanol 100:100	$8.70x10^{-7}$	$1.48x10^{-5}$

Table 5- 6 Corrected concentration of each functional group in the solute in 0.5 µl of the standards prepared for analysis

The linearity of concentration and absorbance was determined by evaluating the correlation coefficient of a linear fit to the data, as shown below.

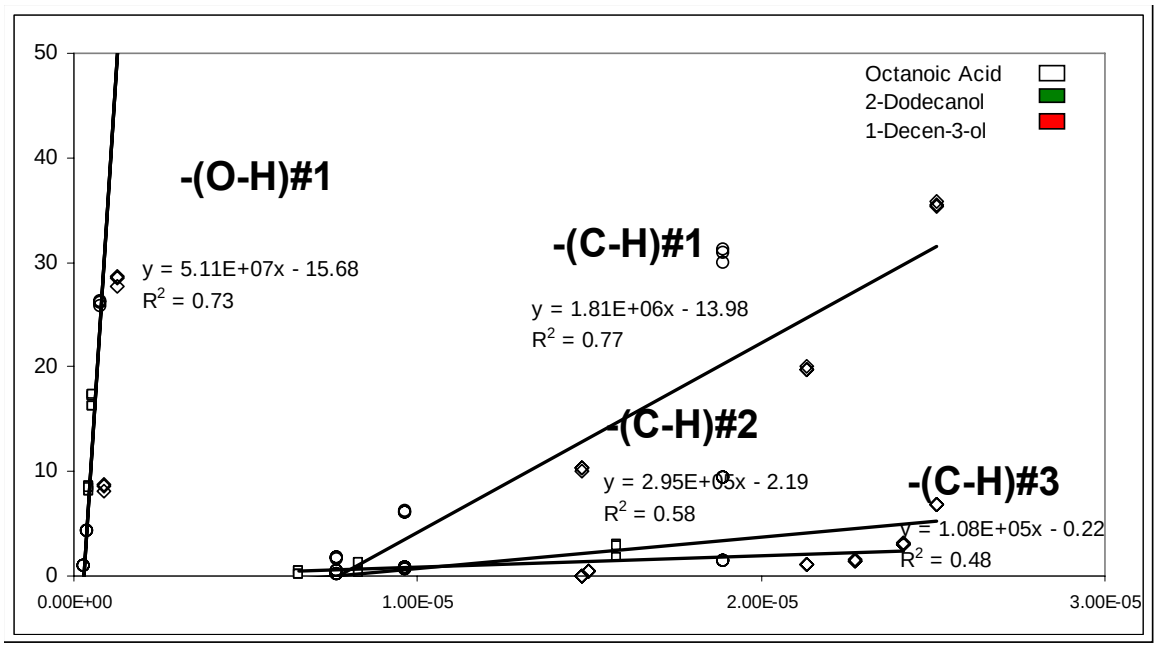

Figure 5- 4 Linearity of ABS area for select –(C-H), and –(O-H)- functional groups.

This figure presents all of the data acquired in this experiment. The symbols for a single model compound-solvent pair are the same color, but their shape varies depending upon the functional group studied. The –(O-H)#2 peak was not included in this plot because in the spectra of the standard dilutions this peak was not resolved enough to get reliable absorbance areas that lead to the development of a good calibration curve.

While the data points are scattered, they are approximately linear. This is true for all four functional groups. The lines for –(C-H)#1 and –(O-H)#1 have more scatter or uncertainty than the lines for –(C-H)#2, or –(C-H)#3.

Scattering may be due to several possible factors such as electronic or chemical, shifting and overlapping of the peaks. Therefore if the peak shifts or if the peaks are not split correctly a high uncertainty value is expected. It is very important to determine whether shifting or overlapping peaks are the reason for the scattering obtained in this calibration curve. This issue will be addressed in the next experiments, and these calibration lines will be recomputed in response to improvements in the methodology developed through these later experiments

5.2. EXPERIMENT 11: MEASUREMENT OF MOLAR ABSORPTIVITY

Molar absorptivity is a functional group signature peak-specific quantity that accounts for the amount of MIR light that is absorbed by the functional group bond per mole of functional group per unit area.

5.2.1. Issues

Even if the approaches to measure the absorbance of fine particle species are accurate, the methods to measure molar absorptivity and path length are not. In the case of path length, the thickness of the fine particle sample is very difficult to estimate since the fine particles do not breakthrough the substrate during sampling and since they accumulate somewhat on its surface. And since path length cannot be measured accurately, molar absorptivity cannot be measured accurately.

One solution to this problem is to instead measure relative molar absorptivity, which is the ratio of the molar absorptivity of two different peaks in a MIR spectrum. Since the path length through a sample is constant, mathematically, the value of $\xi_{x/y}$ is:

Equation 5- 3 $\xi_{x/y} = \frac{\varepsilon_x}{\varepsilon_y} = \frac{ABS_x}{ABS_y}\frac{[C_y]}{[C_x]}$

Where x and y represent different peaks in the MIR spectrum, ξ is the dimensionless relative molar absorptivity of the two peaks, ABS is the absorbance area of the two peaks in absorbance units, ε is the molar absorptivity of the same two peaks in abs m^2 mol^{-1}, and C is the corresponding molar concentration of the functional groups corresponding to x and y in mol m^{-3}. The relative molar absorptivity is simply the slope of a calibration curve relating known concentrations to observed absorbances of the same functional groups.

When x and y are two peaks in the same functional group signature, $[C_x] = [C_y]$ and:

Equation 5- 4 $\xi_{x/y} = \frac{\varepsilon_x}{\varepsilon_y} = \frac{ABS_x}{ABS_y}$

Where now x and y represent the different peaks in the MIR spectrum of the same functional group. The relative molar absorptivity is now simply the ratio of observed absorbances at different peaks in a functional group signature (i.e., at one concentration).

Despite this simplification of the problem, the development of calibration curves of liquid or solid samples is nontrivial since liquids may volatilize or spread across a substrate, thereby changing the intended concentration actually in the light path, and resulting in absorbance calibration curves that are nonlinear.

5.2.2. Goal

The goal of this experiment is to develop methods to measure the relative molar absorptivity of multiple peaks in a single functional group signature which result in linear calibration curves.

5.2.3. Literature Review

Prior research of fine particle speciation favor the use of relative molar absorptivities over absolute molar absorptivities for the reasons described above.

The resulting relative molar absorptivities with respect to aliphatic carbon (C-H) at 2800-3000 cm^{-1} present in the same compound are presented below.

Functional Group	**Peak endpoints (cm^{-1})**	**Relative molar absorptivity**		
		Palen et al. (1992)	**Palen et al. (1993)**	**Dekermenjian et al. (1999)**
Aliphatic carbon -(C-H)	2800-3000	1	1	1
Organonitrates -(-ONO_2)	1276	-	6.5	-
Carboxylic Acid –CO(-O-H)	2400-3200	43.2	38.9	98
Ketones -(-C=O)-	1675-1800	6.3	4.8	8.5
Alcohols -(-O-H)	3100-3600	23.5	21.6	33
Carbonyl in aldehydes -(C=O)	1720-1727	3.8	-	7.3

Table 5- 7 Relative molar absorptivities of functional groups with respect to aliphatic carbon (C-H) as identified in previous studies

The relative molar absorptivities for aliphatic carbon equal 1 because this same functional group signature peak is used as the basis. In the case of organonitrates, only the

wavenumber of the peak maximum was reported. The values for a single functional group vary by study. Since their experimental methods were not detailed, some of these deviations may be due to methodological issues with how the peak endpoints and baselines were determined and the effect of volatilization on replicate analyses.

Cliff and Lorimer (1972) developed a technique to quantify the amount of a thin film observed in a conventional microscope that used a ratio based on the intensity of the band and the thickness. Their idea is related to the idea of relative molar absorptivity, and in fact, Blando et al. (2001) built on it to calculate relative molar absorptivities. They used the approach to quantify the concentration of sulfate and carbonyls in ambient aerosol, but they were unable to complete their analyses for other functional groups because they were not sure how to address the nonhorizontal spectrum baseline typical of FTIR analyses.

This research drew on these prior works by using similar approaches to select a series of related model compounds with functional groups that are also present in ambient aerosol. However, since specific experimental methods to determine relative molar absorptivity of liquid standards was not documented and the uncertainties were not reported, the results of this prior work were only used to emphasize the need for compounds that are not volatile and the need for systematic approaches of calculating absorbance area.

5.2.4. Experimental Approach

Spectra from Experiment 10 were reanalyzed in this experiment by using the same "base case" approach. The relative molar absorptivity was determined using the slopes for each functional group from the calibration linearity plots obtained in Experiment 10.

Spectra were evaluated the same "base case" way as in the last experiment to determine absorbance:

- Baseline: shaving baseline which draws a baseline by connecting the two endpoints of the peak
- Shifting: not accounted for, so actual (shifted) endpoints of the peak are ignored and instead the peak endpoints are considered to be the endpoints of octane and methanol functional group peaks
- Splitting: done simply using the endpoints for octane and methanol

The relative molar absorptivity was determined by:

- ξ as the ratio of the slopes of the calibration lines presented in the prior experiment using **Equation 5-3**

5.2.5. Results and Discussion

The approach to determining relative molar absorptivity was developed and tested for the –(C-H) functional group, using the -(C-H)#3 peak at 734-703 cm^{-1} and the -(C-H)#2 peak at 1384-1371 cm^{-1} in the –(C-H) signature. This functional group was selected because it

is common to all organic compounds. The -(C-H)#2 peak was selected because it is strong, sharp and unique.

Relative molar absorptivities were calculated using the slopes of the calibration linearity plots developed in **Experiment 10**.

For example, the relative molar absorptivity of -(C-H)#2 at 1384-1371 cm^{-1} relative to -(C-H)#3 at 734-703 cm^{-1} in octane based on the calibration lines is:

$$\xi_{(CH)\#3/(CH)\#2} = \frac{m_{(CH)\#3}}{m_{(CH)\#2}} = \frac{1.08\times10^{5}}{2.95\times10^{5}} = 0.37$$

Where m is the slope from the calibration curve developed for each targeted functional group.

A similar computation was performed to obtain the other values.

Functional Group	**Base case**		
	Slope	$\xi_{y/x}$	R^2
-(C-H)#1	1.81E+06	0.060	0.77
-(C-H)#2	2.95E+05	0.366	0.58
-(C-H)#3	1.08E+05	1.000	0.48
-(O-H)#1	5.11E+07	0.002	0.73

Table 5- 8 Relative molar absorptivities of the –(C-H), and -(O-H) functional group based on ratios of the slopes from calibration curves for each functional group.

This table presents the relative molar absorptivities of the targeted functional groups respect to the –(C-H)#3. Since the calibration lines represent multiple species, there is only one value for each functional group peak combination.

The values of relative molar absorptivity are variable but far less so than values reported in the literature. One explanation for the observed variability is overlapping of the -(C-H)#2 peak at 1384-1371 cm^{-1} with the –(O-H) peak at 1388-1363 cm^{-1}. In future experiments a method was developed to address this issue.

As the approaches to analyze spectra considering peak shifting and peak splitting are developed and their efficacy assessed, different approaches to interpret fine particle spectra may be recommended over those used in the "base case". Changes in the spectral analysis will affect computed absorbance and therefore relative molar absorptivity computed from absorbance ratios or from ratios of calibration line slopes. If the linearity of the functional groups is confirmed and the uncertainty is reduced, then the values of relative molar absorptivity for targeted functional groups can be determined for compounds in general, and not for a single compound and therefore applied to other compounds not considered in these experiments.

5.3. EXPERIMENT 12: ALTERNATE PEAK BASELINE APPROACH

The peak baseline is the bottom of the species signature peak used to determine integrated absorbance area.

The prior experiments used a baseline that was simply a line drawn between the two inflection points on either side of the peak. In this experiment, an alternate baseline approach is investigated.

5.3.1. Issues

Baselines are not reported in the literature but they are clearly important if one is to integrate across a peak to determine its absorbance.

If this method is to be used to measure fine particle speciation, a consistent approach is needed to determine the endpoints and baseline of a single functional group in the fine particle that accounts for complex mixtures of changing composition.

5.3.2. Goal

As shown in **Figure 5-2**, the baseline may not be a horizontal line, and it is possible that an inflection denoting the start or end of the peak may not extend all the way to the baseline.

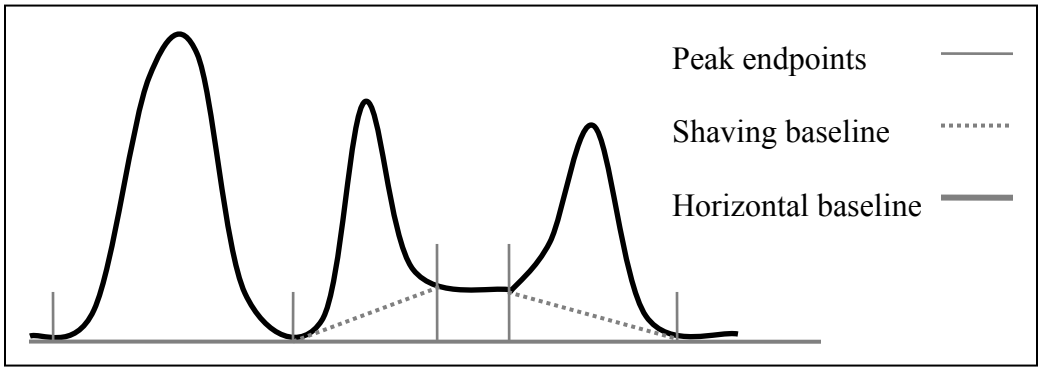

Figure 5- 5 Examples of peak endpoints and baselines

The peak endpoints are based simply on inflection and so remain the same regardless of the baseline approach. The shaving baseline approach connects the two endpoints of the peak with a straight line. The horizontal baseline approach connects two points on the spectrum with a horizontal line. The two points will not be the infection points of the peak if the inflection points are not at the same absorbance. Clearly, the selection of the peak range and baseline will have a dramatic impact on the value of the absorbance area of the peak.

The goal of this experiment is to determine the effects of varying the baseline approach from a simple shaving approach (peak endpoint to peak endpoint) to a horizontal approach on the absorbance of functional groups in fine particles.

5.3.3. Literature Review

While spectra of pure compounds have been reported in the literature, the baselines used to determine absorbance are far less documented. Holes et al. (1997) and Dekermenjian

et al. (1999) illustrated the baselines they used to compute absorbance area. However, the methodology for doing so was not documented and their baselines were inconsistent for a single functional group signature peak from compound to compound. Other quantities computed in their work were also inconsistent, suggesting that their approach for determining baselines was perhaps not optimum.

Since there is little reported information regarding methods to develop baselines, this experiment developed a methodology to identify baselines and identified the baselines to be used for the target functional group peaks focused on in this work.

5.3.4. Experimental Approach

In this experiment, the same 12 pure compound spectra evaluated in the previous experiment were re-evaluated using an alternate baseline approach.

Peak-specific shaving and horizontal baseline approaches were proposed and used to determine the integrated absorbance areas of these targeted functional groups: 3 alkane-hydrogen -(C-H) signature peaks near 734, 1382 and 3037 cm^{-1} targeted because the group is present in all organic compounds, and 2 hydroxyl -(O-H) signature peaks near 3502 and 998 cm^{-1} targeted because the group is present in many of the compounds analyzed in this experiment.

The following spectral interpretation varied the “base case” approach of drawing baselines from a shaving approach to a horizontal approach (alternate baseline). The

other “base case” approaches were kept the same as in the “base case” allowing for comparison:

- Shifting: no shifting, so actual (shifted) endpoints of the peak are ignored and instead the peak is integrated using the endpoints of octane and methanol functional group peaks
- Splitting: no splitting, so overlapping peaks were just split at the endpoints for octane and methanol and then integrated

The horizontal baseline approach was implemented through these steps:

- Identify if the peak is part of a broader peak or not
- Establish the horizontal straight baseline
    - If the peak is part of a broader one, the baseline is of the broader peak, drawn between the two wavenumber locations of equal absorbance on the spectrum
    - If the peak is not part of a broader one, the baseline is drawn between the lower inflection point of the peak and any other region on the spectrum of equal absorbance

5.3.5. Results and Discussion

Spectra were first compared to those from the literature to map observed peaks to specific functional group signatures. Example spectra are presented in Figure 5-3.

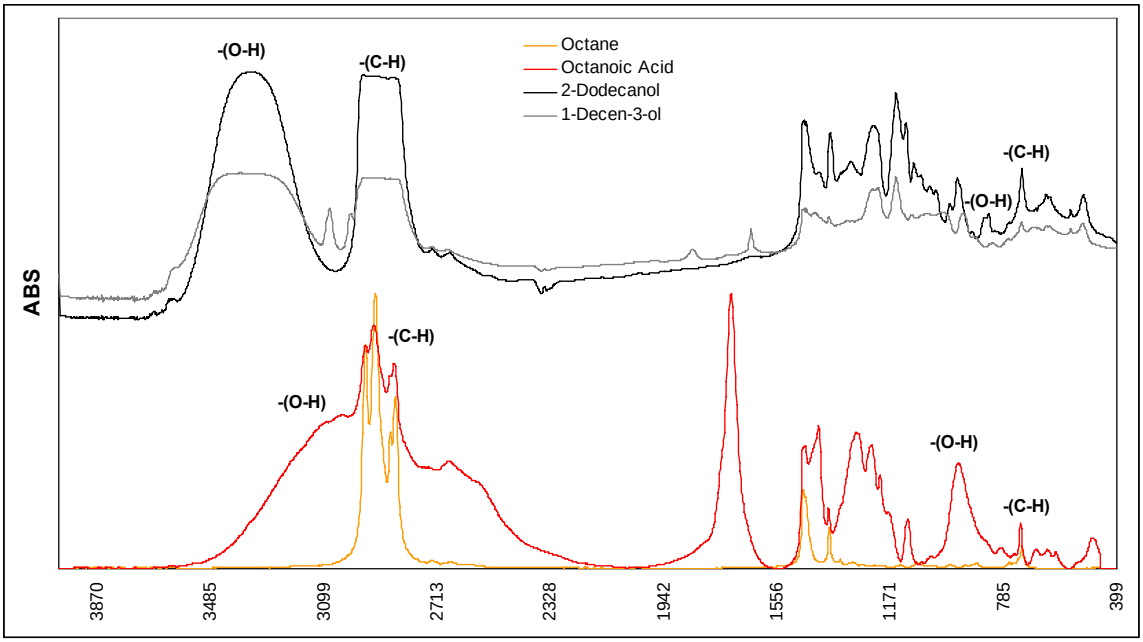

Figure 5- 6 Targeted functional groups, hydroxyl –(O-H) and aliphatic carbon –(C-H) at different regions in the IR spectra of the four pure model compounds

The -(C-H) peak near 734 cm^{-1} is sharp, strong and unique. The -(C-H) peak near 3037 cm^{-1} appears to be affected by other functional groups that absorb in the same infrared region. The hydroxyl -(O-H) peak near 3502 cm^{-1} is broad and strong, and overlaps with functional groups that absorb in the same infrared region. The -(O-H) peak near 998 cm^{-1} is unique and sharp.

Figure 5-4 illustrates the base case baselines (i.e., shaving) and the alternate case baseline (i.e., horizontal) for the target functional groups.

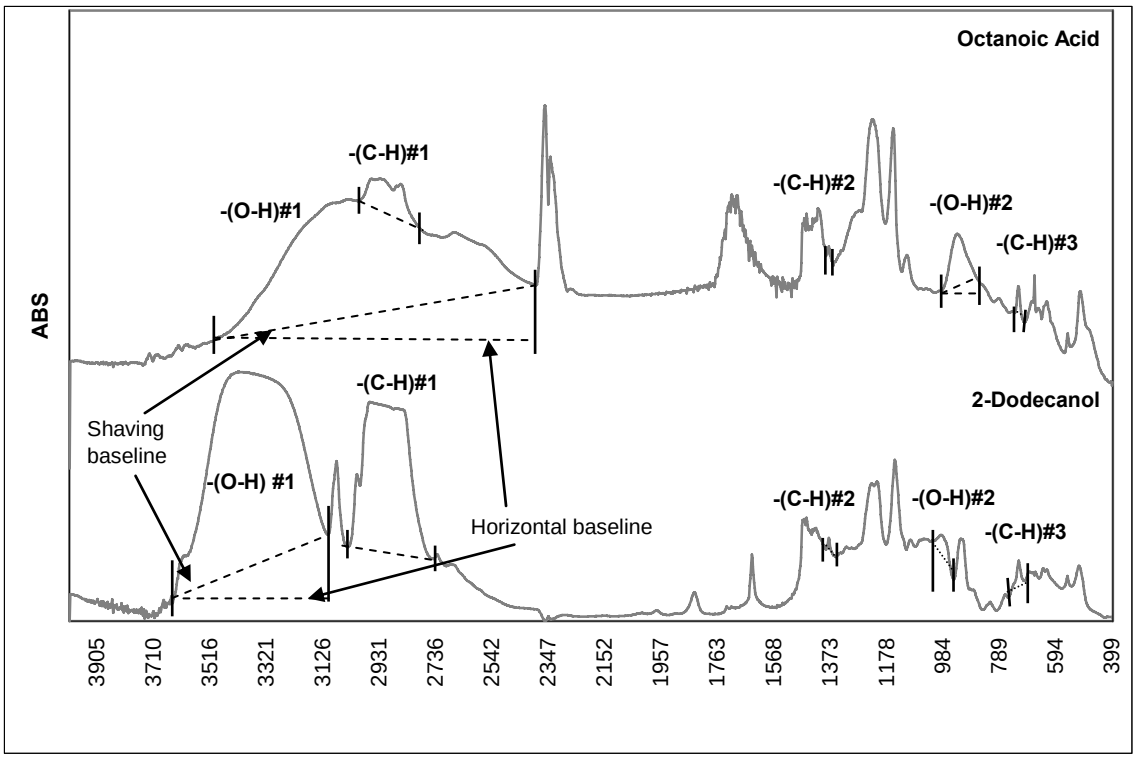

Figure 5- 7 Examples of baseline approaches used to compute area of targeted signature peaks of the functional groups in the four pure model compounds

The horizontal baselines fall below the shaving ones, but the endpoints are the same and are simply those of –(C-H) in octane and –(O-H) in methanol. In the next experiment, these endpoints are varied.

Results for the baseline ranges of the targeted functional groups in the IR spectra of each compound analyzed are presented in **Table 5-9**.

The peak baseline ranges define the left and right starting points of the baseline and are simply those of –(C-H) in octane and –(O-H) in methanol in this experiment. Ranges for horizontal baselines extend beyond the peak endpoints in order to capture the larger

background onto which the peak is superimposed. As did the peak endpoint ranges, the baseline ranges also depend on the compound since neighboring functional groups can shift the location of the peak. This is certainly the case for the –(O-H) peaks since the -(O-H) functional groups are neighbors to the -(C-H) ones. This phenomenon will be discussed and explored in great detail in a later experiment, as will the concern that peaks may be difficult to identify when their signatures exhibit shifting and overlap.

		Peak endpoints/ Baseline endpoints						
OVERALL		Octane (L)	Octanoic Acid (L)	Octanoic Acid (T)	2-Dodecanol (L)	2-Dodecanol (T)	1-Decen-3-ol (T)	Methanol
-(C-H) #1	Base case	3037-2769/ 3037-2769	3037-2769/ 3037-2769	3037-2769/ 3037-2769	3037-2769/ 3037-2769	3037-2769/ 3037-2769	3037-2769/ 3037-2769	3037-2769/ 3037-2769
	Alternate baseline (horizontal)	3037-2769/ 3100-2638	3037-2769/ 3064-2842	3037-2769/ 3064-2842	3037-2769/ 3544-2769	3037-2769/ 3058-2584	3037-2769/ 3043-2719	3037-2769/ 3037-2769
-(C-H) #2	Base case	1382-1371/ 1382-1371	1382-1371/ 1382-1371	1382-1371/ 1382-1371	1382-1371/ 1382-1371	1382-1371/ 1382-1371	1382-1371/ 1382-1371	1382-1371/ 1382-1371
	Alternate baseline (horizontal)	1382-1371/ 1396-1359	1382-1371/ 1479-1365	1382-1371/ 1473-1363	1382-1371/ 1388-1357	1382-1371/ 1390-1193	1382-1371/ 1384-1371	1382-1371/ 1382-1371
-(C-H) #3	Base case	734-703/ 734-703	734-703/ 734-703	734-703/ 734-703	734-703/ 734-703	734-703/ 734-703	734-703/ 734-703	734-703/ 734-703
	Alternate baseline (horizontal)	734-703/ 755-705	734-703/ 738-715	734-703/ 757-713	734-703/ 738-705	734-703/ 738-701	734-703/ 738-592	734-703/ 734-703
-(O-H) #1	Base case	-	3592-3108/ 3592-3108	3592-3108/ 3592-3108	3592-3108/ 3592-3108	3592-3108/ 3592-3108	3592-3108/ 3592-3108	3592-3108/ 3592-3108
	Alternate baseline (horizontal)	-	3592-3108/ 3592-2159	3592-3108/ 3592-468	3592-3108/ 3592-2603	3592-3108/ 3581-2360	3592-3108/ 3588-2516	3592-3108/ 3592-3108
-(O-H) #2	Base case	-	956-900/ 956-900	956-900/ 956-900	956-900/ 956-900	956-900/ 956-900	956-900/ 956-900	956-900/ 956-900
	Alternate baseline (horizontal)	-	956-900/ 964-900	956-900/ 958-900	956-900/ 1562-914	956-900/ 1492-902	956-900/ 1483-894	956-900/ 956-900

Table 5- 9 Peak endpoint and baseline ranges of the targeted functional groups as a function of model compound

The effects of these two baseline approaches on absorbance area are compared in the following table.

		ABS areas					
OVERALL		Octane (L)	Octanoic Acid (L)	Octanoic Acid (T)	2-Dodecanol (L)	2-Dodecanol (T)	1-Decen-3-ol (T)
-(C-H) #1	Base case	79.498	41.247	3.381	82.001	158.534	65.446
	Alternate baseline (horizontal)	83.230	20.382	0.406	82.762	175.865	65.582
-(C-H) #2	Base case	1.025	0.477	0.089	0.801	3.036	0.324
	Alternate baseline (horizontal)	1.241	0.789	0.136	0.752	4.622	0.2
-(C-H) #3	Base case	0.599	1.194	0.234	0.884	2.495	0.626
	Alternate baseline (horizontal)	0.853	1.206	0.208	1.001	2.887	0.771
-(O-H) #1	Base case	-	-29.49	-4.377	102.397	312.396	167.025
	Alternate baseline (horizontal)	-	94.473	17.669	114.707	333.378	154.431
-(O-H) #2	Base case	-	3.597	5.432	0.216	5.291	2.07
	Alternate baseline (horizontal)	-	5.432	0.529	0.491	8.514	4.053

Table 5- 10 Measured ABS areas of the targeted functional groups as a function of model compound

This table compares the absorbances calculated using the base case and the alternate baseline approaches when the same endpoints are used, so differences in the absorbances are only due to how the baseline was drawn and not shifting or how overlapping peaks are split. The base case values are identical to those already reported in the prior experiment.

Absorbance areas are typically largest when using the horizontal baseline approach since the horizontal baseline typically falls below the shaving baseline. An exception to this is the absorbances for the –(C-H)#1 peak in the Octanoic Acid (L) and Octanoic acid (T), the –(C-H)#2 peak in the Dodecanol (L), 1-decen-3-ol (T), the –(C-H)#3 peak in the Octanoic acid (T), the –(O-H)#1 peak in the Octanoic acid (L), in the Octanoic acid (T) and in the 1-decen-3-ol (T), and the –(O-H)#2 peak in the Octanoic Acid (T). Also the negative values for the –(O-H)#1 peaks in the Octanoic acid, are the results of this, the –(O-H)#1 peak in the Octanoic acid spectra are totally off from the referenced endpoints, leading to negative values. This approach works for some functional groups but not for all of them. These results depend on the peak endpoints, and so they may change in the next experiment.

The best baseline approach may vary by functional group peak, and the best approach for any functional group peak is the one that results in the most linear and least scattered calibration line between concentration and absorbance. Since the baseline approach and the shifting approach both affect absorbance calculation, the calibration lines were re-

calculated at the end of the next experiment after the combination of approaches to interpret fine particle spectra was recommended over those used in the "base case".

The effect of this experiment on relative molar absorptivity

This approach leads to substantially different absorbance area, but the effects are inconsistent by functional group signature peak. Therefore, the effect on relative molar absorptivity will also be inconsistent.

5.4. EXPERIMENT 13: ALTERNATE PEAK SHIFTING APPROACH

The peak endpoints are the specific wavenumbers over which a particular species signature peak occurs. Peak shifting is a phenomenon where the wavenumber location of a peak in the signature of a particular functional group actually moves from its expected location due to neighboring functional groups in the molecule that change how the initial bond absorbs MIR light.

The prior experiments computed absorbance area assuming that the –(O-H) and –(C-H) peak endpoints in all compounds were the same as those for methanol and octane, respectively. This experiment re-analyzes the 12 pure compound spectra used in previous experiments, but now varies the way that peak endpoints are determined.

5.4.1. Issues

Species signatures are seldom reported in the literature (i.e., which includes spectral libraries), and if they are, generally the signatures are of full compounds and not single species in a compound. One of the reasons for this is that although each functional group

in a compound has a unique signature in the IR spectrum, neighboring functional groups can make the unique IR signatures to shift in wavenumber. So, the spectra of compounds containing different functional groups may be slightly shifted. Fine particles contain mixtures of simple and complex molecules and so a range of shifting is expected to occur in the signatures of functional groups present in the fine particles, reflective of the distribution of functional groups in the molecules in the particles. It is unclear how shifting is further complicated by the nonhomogeneous mixtures of chemicals found fine particles.

Consider the structures of the four model compounds:

Octane	Octanoic Acid	2-Dodecanol	1-Decen-3-ol
$CH_3(CH_2)_6CH_3$	$CH_3(CH_2)_6COOH$	$CH_3(CH_2)_9CH(OH)CH_3$	$CH_3(CH_2)_6CH(OH)CH=CH_2$
	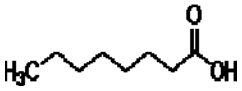	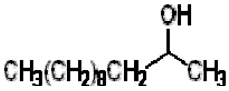	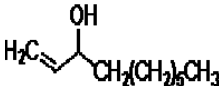

Octane has 18 –(C-H) bonds. Octanoic acid has 15 –(C-H) bonds, 2 of which are closely neighbored by other functional groups. 2-dodecanol has 24 –(C-H) bonds, 5 of which are closely neighbored by an –(O-H) group. 1-decen-3-ol has 19 –(C-H) bonds, 2 of which are closely neighbored by an –(O-H) group and 2 of which are closely neighbored an alkene -(C=C)- group. Therefore, there is no expectation that the absorbances of the –(C-H) peak should be the same or the peak endpoints. The question is, how extreme is the shifting and can it be accounted for?

It is unclear to what extent shifting will occur. If a peak shifts substantially, the functional group may not be identifiable. It is also unclear if peak shifting will occur at both ends of a peak or only at one end of a peak, and if it will change the shape of the peak. Differences in the shape of a peak may result in differences in integrated absorbance.

5.4.2. Goal

The goal of this experiment is to determine whether or not peak shifting is significant in the spectra of ambient aerosol, if it can be predicted and the extent to which it affects the absorbance areas of functional group signature peaks.

5.4.3. Literature Review

The spectra of fine particle species have been reported in the literature. For example, Palen et al. (1993) identified functional groups and their wavenumber ranges formed in the formation of fine particles as a result of the photooxidation of 1-Octene. Building on Palen's research, other researchers such as Holes et al. (1997), Dekermenjian et al. (1999) and Reff et al. (2005) also identified other functional groups in the MIR range. Coates (2000) published a practical approach to interpret infrared spectra and identify the peak ranges of several functional groups. A summary of the findings of these and other scientists is presented below.

Functional Group	Bond		Peak Range cm^{-1}			Maximum range cm^{-1}
		Allen et al., 1994	Dekermenjian et al., 1999	Coates, 2000	Reff et al., 2005	
Alcohol (ROH)	-(O-H)	3750-3500	3600-3100	3645-3600	3645-3600	3750-3500
				3570-3200	3570-3200	3592-3108
				1410-1310		1388-1363
						956-900
	-(C-O)					1260-1050
Carboxylic Acid (RC(=O)OH)	-(O-H)				1640	3502-2393
						1388-1363
						981-852
	-(C=O)					1790-1625
	-(C-O)					1320-1000
Alkene (HC=CH)	-(C=C)			1680-1620		1680-1620
	=(C-H)					
	-(C-H)			3095-3075		3106-3041
Alkane (HC-CH)	-(C-C)			1300-700		1300-700
	-(C-H)	3000-2800	3000-2800	2900-2880	3000-2800	3037-2769
		1455-1452		1350-1330		1480-1450
						1382-1371
						734-703
Amide $RC(=O)NR_2$	-(N-H)					1580-1510
Ammonium - (NH_4^+)	-(N-H)	3200-3170		3300-3030	3230	3300-3000
		1435-1410		1430-1400	1418	1430-1390
						910-665
Bisulfate (HSO_4^-)	-(S-O)	1180				1200-1160
		1029				1050-1000
		867				880-840
		590-580				590-580

Sulfate (SO_4^{-2})	-(S-O)	1135-1103		1130-1080	1110	1170-1050
		615-612		680-610	618	660-610
Nitrate (NO_3^-)	-(N-O)	1335-1318		1380-1350		1360-1290
		835-825		840-815		850-810
Carbonate (CO_3^{-2})	-(C-O)			1500-1410		1490-1410
				880-860		880-860
Silicate (SiO_4^{-4})	-(Si-O)	812-772			500	510-470
Teflon						1178-1120, 560-490
Water (H_2O)	-(O-H)	3450-3350				3900-3400
		1623			1620	1850-1350
Carbon Monoxide (CO_2)	-(C-O)					2400-2290

Table 5- 11 Functional groups identified and their respective wavenumber ranges

This table shows the different peak endpoints used in various studies. Missing values were not reported. The Teflon, water and CO_2 peak wavenumber ranges are included since they are possible interferents. Single values indicate that the researcher only identified the peak by its mode and not its endpoints. Missing values were not reported.

The literature review of functional group endpoints demonstrated some difference in the location of signature peaks in many functional groups relevant for fine particle speciation. Allen et al. (1994) found that intermolecular and intramolecular interactions shifted the carbonyl peaks in the infrared spectrum. Dekermenjian et al. (1999), used standards to determine the location of the peak endpoints for the targeted functional groups (C-H, COOH, C=O and O-H) collected in smog aerosol chamber, and calculated

the absorbance areas of the functional groups present in the aerosol. While Dekermenjian's methods to identify peak endpoints were not presented, it is likely that the differences in peak endpoints reported in 1999 and in 1999(a) are due to peak shifting.

While shifting has been observed in the literature, the consistency of shifting or its affects on peak shape have not been documented. Therefore, one of the goals of this experiment is to develop methods to characterize shifting.

5.4.4. Experimental Approach

The peak endpoints for a particular functional group peak differ if the functional group is experiencing neighboring effects. These results are presented along with the baseline results for direct comparison.

This experiment analyzed the same 12 spectra analyzed in the prior experiment: the same 3 library spectra of octane, octanoic acid and 2-dodecanol and the same 3 replicate spectra each of pure octanoic acid, 2-dodecanol and 1-decen-3-ol measured in the laboratory determined in the prior experiment.

These 4 model compounds have gradually increasing complexity in molecular structure that allow shifting to be systematically assessed by comparison: octane only has –(C-C)- and –(C-H) groups, octanoic acid also has a –C=O(O-H) group, 2-dodecanol also has an

–(O-H) group, and 1-decen-3-ol has an -(O-H) and a –(C=C)- group. The –(C-H) and –(O-H) functional groups were targeted for this experiment.

Each of the 12 model compound spectra were evaluated for the targeted functional group peaks in the following way:

- Identify each of the peak endpoints and baseline ranges using shaving baseline approach and repeat for the horizontal baseline approach, and compute the absorbances
- Compare functional group wavenumber ranges in complex model compounds to those for the simple model compound (octane) to determine if shifting occurs at both endpoints and the mode of the peak
- Evaluate the wavenumber shift magnitude and assess whether is large enough to cause peak to overlap with adjacent peaks

5.4.5. Results and Discussion

Shifting of the –(C-H)#3 peak

A comparison of the endpoints of the target peaks observed in the complex model compounds relative to the simple model compound revealed that the shifting does not necessarily occur across the entire peak. This is illustrated below for the –(C-H)#3 peak observed in the model compound spectra.

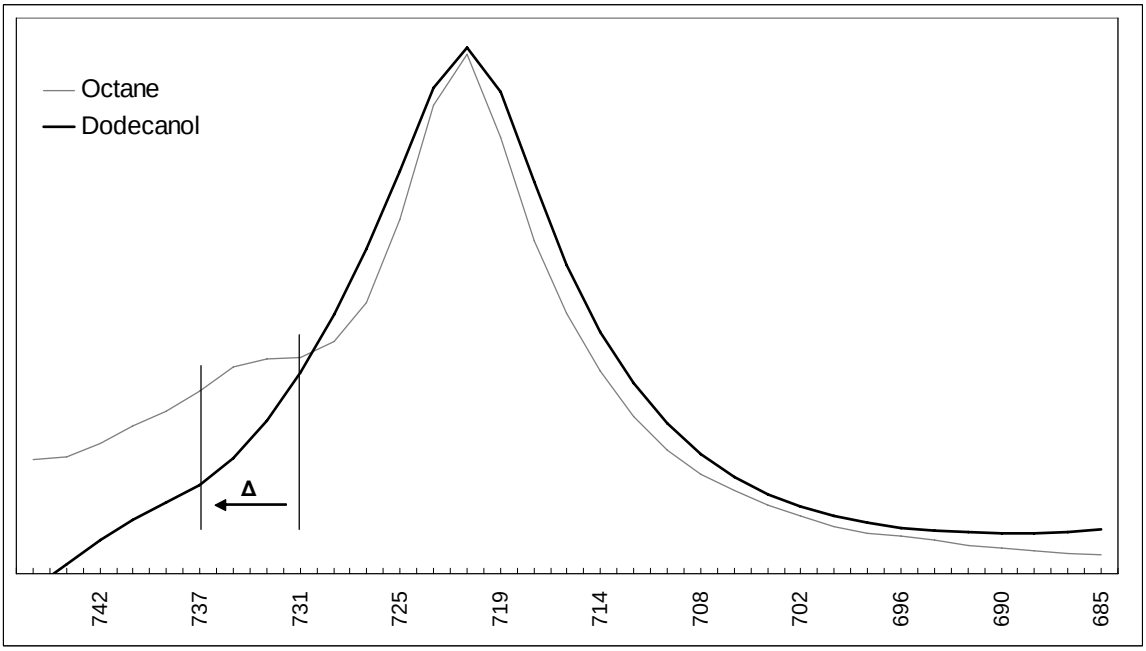

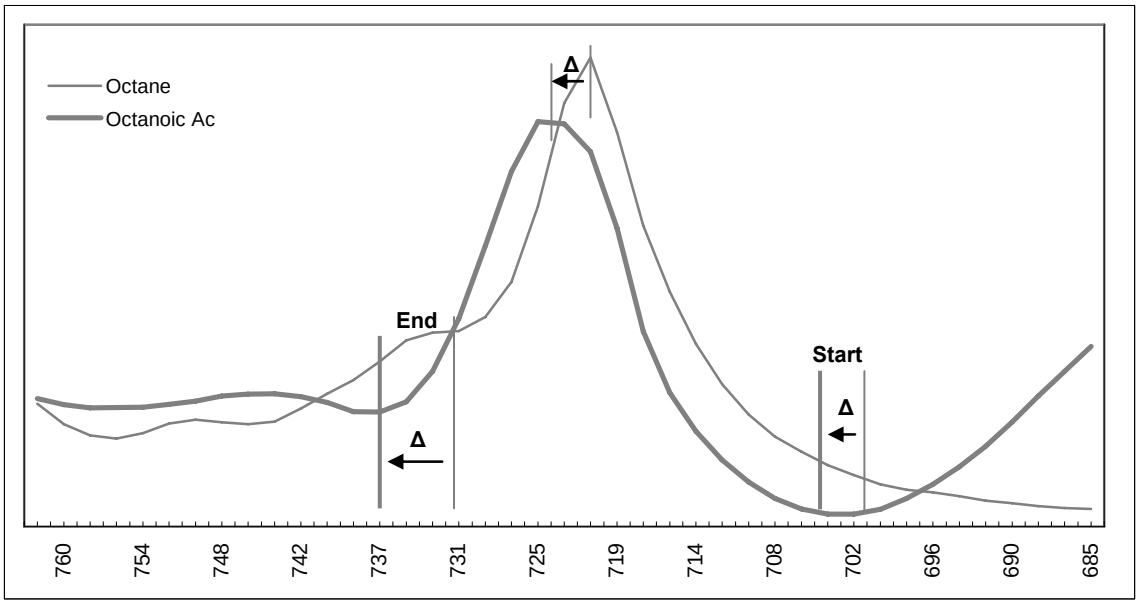

Figure 5- 8 Close up of differences in shifting of the –(C-H)#3 peak relative to octane

These figures show only the –(C-H) #3 peak. The 2-dodecanol peak shows shifting only to the left and only by 4 cm^{-1}. The maximum or leftmost points of the peak are not shifted. The octanoic acid peak, however, shows shifting of the maximum and left

endpoints of the peak. The peak maximum shifted by 3.1 cm^{-1}, the left endpoint shifted by 4. The peak shape is also affected by shifting.

This shifting is not excessive and therefore there is not much concern that the shifting causes the functional group peak to overlaps with signature peaks of other functional groups present in nearby spectral regions of the complex compounds.

Although the shifting is slight, the potential error in computed area may be large if shifting is not accounted for. This is illustrated in the following figures which highlight the impact that shifting can have on absorbance area, as a function of the baseline approach. The quantitative difference in computed absorbance is presented in **Table 5-12.**

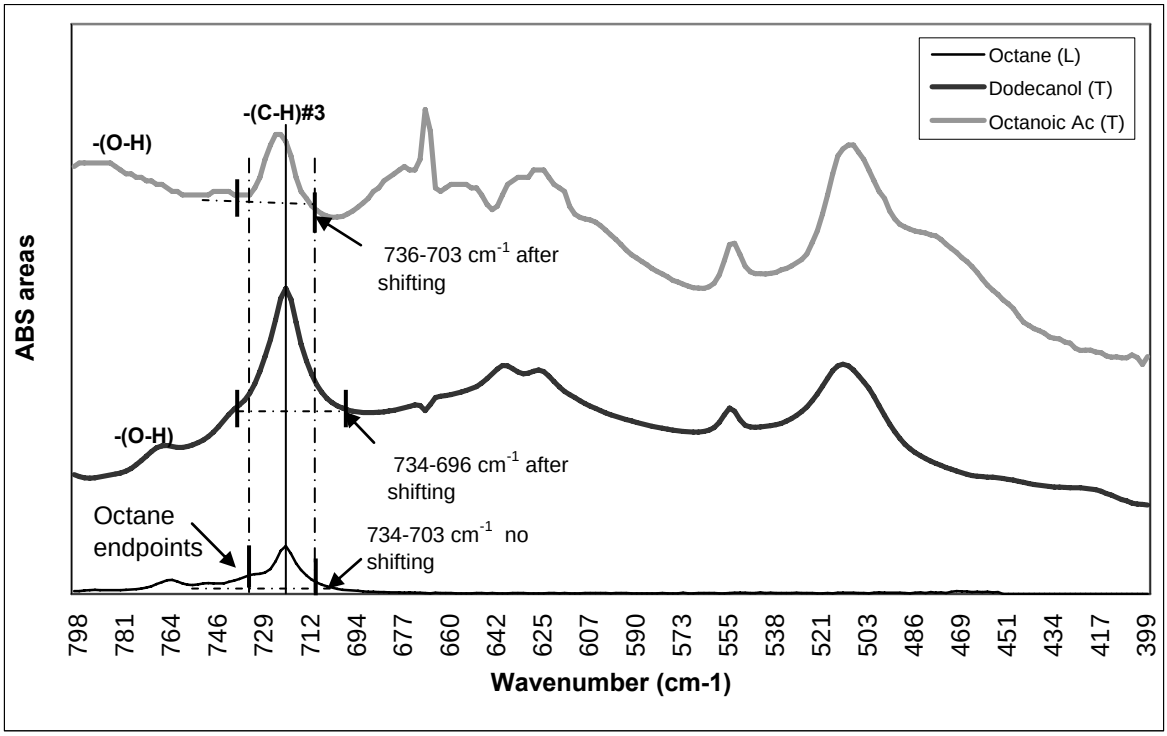

Figure 5- 9 Differences in the amount of shifting of the –(C-H)#3 peak relative to octane when shaving versus horizontal baseline approaches are used

		ABS areas					
OVERALL		Octane (L)	Octanoic Acid (L)	Octanoic Acid (T)	2-Dodecanol (L)	2-Dodecanol (T)	1-Decen-3-ol (T)
-(C-H) #3	Alternate shifting	0.599	1.197	0.232	0.882	2.488	0.623
	Alternate baseline and shifting	0.853	1.146	0.206	0.999	2.447	0.757

Table 5- 12 Shifting of the –(C-H)#3 721.7 cm^{-1} peak mode and 734-703 cm^{-1} peak endpoints for octane in more complex compounds.

The shifted peak mode and shifted peak endpoints are the observed wavenumbers of the mode and endpoints for the model compound. The absorbance with no shift is determined using the octane endpoints and the absorbance with shift is determined using the observed shifted endpoints. The percent difference is computed relative to the shifted absorbance since it is more accurate.

The peak modes show a slight shift relative to the values for octane. Shifting also affects the end point locations, which tend to shift to the left. However, when the shaving baseline approach is used, the shifting is small enough that the impact on calculated absorbance is minimal. The impacts of shifting are more pronounced when the horizontal baseline approach is used, which suggests that the shaving approach for this peak provides a more robust value of absorbance.

From this table it is concluded that the 734-703 cm^{-1} peak of the -(C-H) functional group is likely to experience shifting, and the magnitude of shifting will depend on the actual neighboring functional groups and numbers of –(C-H) they neighbor. However, the effects of shifting on absorbance are minimized when the shaving baseline approach is used to compute ABS areas, allowing fixed endpoints to be used in spectral interpretation with little consequence.

Shifting of the –(C-H)#2 peak

A similar analysis was conducted for the –(C-H) #2 signature peak. Again, shifting is evaluated relative to the location of the –(C-H)#3 peak in the spectra of octane at 1384-1371 cm-1. The following figures illustrate that the -(C-H)#3 peaks in 2-dodecanol and octanoic acid shift slightly with respect to the –(C-H)#3 peak in octane and that the shapes of the peaks are also affected by the presence of other functional groups. This is especially pronounced for octanoic acid.

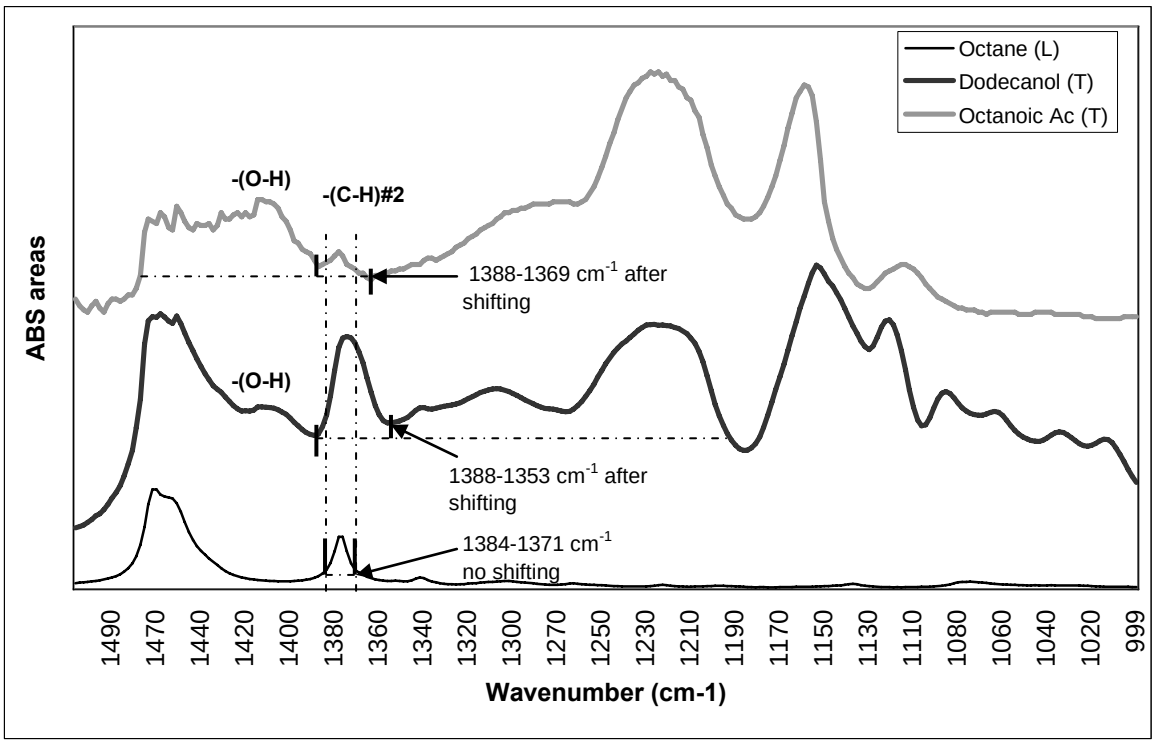

Figure 5- 10 Differences in the amount of shifting of the –(C-H) peak at 1384-1371 cm-1 relative to octane when shaving versus horizontal baseline approaches are used

A visual inspection of the spectra of this peak reveals a substantial difference in the breadth and shape of this peak depending on the compound. The spectra also show that this peak is close to the peak of another functional group, and therefore, the correct

absorbance determination will also depend on how the overlap between the peaks is accounted for.

		ABS areas					
OVERALL		Octane (L)	Octanoic Acid (L)	Octanoic Acid (T)	2-Dodecanol (L)	2-Dodecanol (T)	1-Decen-3-ol (T)
-(C-H)#2	Alternate shifting	1.025	0.531	0.089	0.796	2.842	0.322
	Alternate baseline and shifting	1.241	0.728	0.124	0.701	4.514	0.221

Table 5- 13 Shows the effect of shifting of the –(C-H)#2 peak at 1384-1371 cm^{-1} and its computed absorbance area in the spectra of all four compounds analyzed.

This table contains the same type of information as the last one did. The effects of neighboring functional groups are more inconsistent for this peak in the –(C-H) signature, since the percent difference is more variable and in some cases quite large. It is unclear why the two spectra of the same compound, octanoic acid, result in different percent differences. Since the spectral library does not report whether spectra are adjusted in any way, and since the laboratory spectrum was obtained using an approach refined specifically for fine particles, the library spectrum will not carry significant weight in the conclusions. As with the case of –(C-H)#3, the effect of shifting of –(C-H)#2 is more pronounced when the horizontal baseline approach is used to determine the peak area.

This suggests that if this peak is used as the basis to compute concentration, shifting should be accounted for so the absorbance of this peak is to be accurately determined.

Shifting of the –(C-H)#1 peak

This analysis was also conducted for the –(C-H)#1 peak at 3037-2769 cm^{-1}. In the following figure, the spectra of the model compounds in the region of this peak are shown.

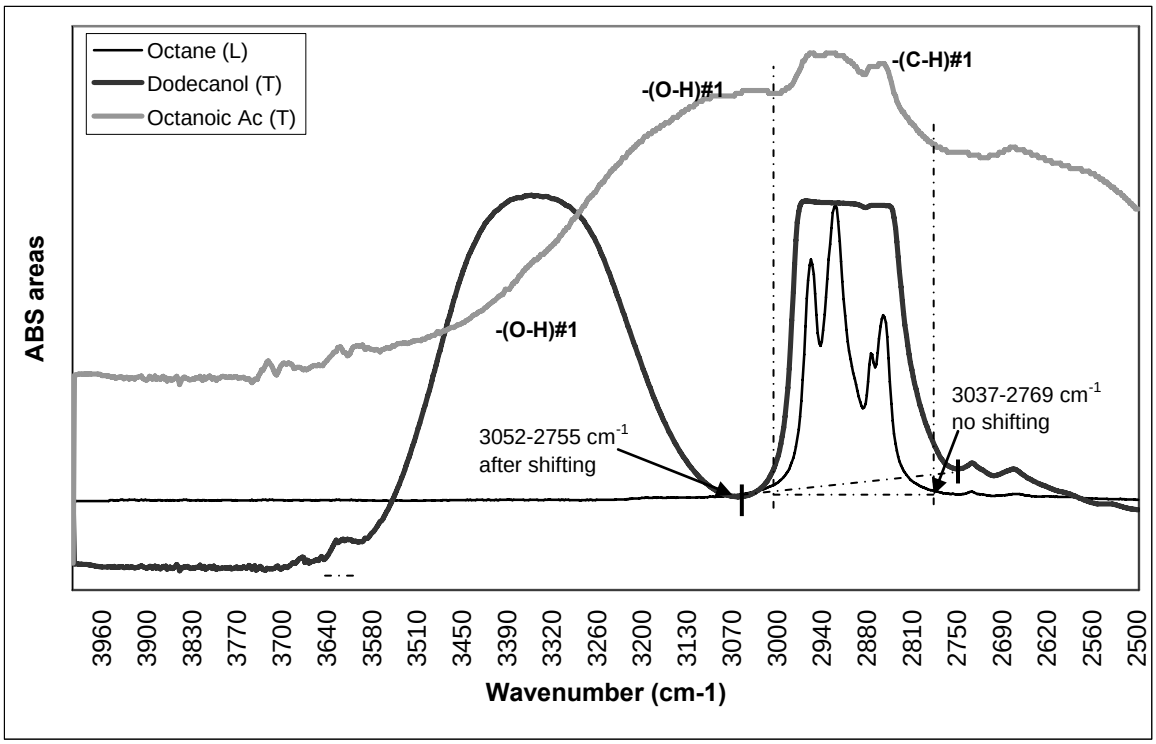

Figure 5- 11 Differences in the amount of shifting of the –(C-H) peak at 3037-2769 cm^{-1} relative to octane when shaving versus horizontal baseline approaches are used

By visual inspection, this peak is affected by neighboring functional groups as well as overlapping functional groups. In both compounds, the -(C-H)#1 peak is shifted slightly when compared to the endpoints of the same peak in octane. However, it is also clear that it overlaps with –(O-H). It is also clear that the –(O-H) group is affected by shifting due to the carbonyl group in carboxylic acids. As a result the –(C-H)#3 peak spectrum is superimposed on a very broad –(O-H) spectrum. The correct approach for quantifying this peak is unclear and will be explored further in the next experiment. The quantitative consequences of shifting on computed absorbance are presented in **Table 5-14**.

		ABS areas					
OVERALL		Octane (L)	Octanoic Acid (L)	Octanoic Acid (T)	2-Dodecanol (L)	2-Dodecanol (T)	1-Decen-3-ol (T)
-(C-H)#1	Alternate shifting	79.498	?	?	82.29	189.43	66.05
	Alternate baseline and shifting	83.230	?	?	82.792	117.567	68.820

Table 5- 14 Shows the effect of shifting of the –(C-H)#1 peak at 3037-2769 cm^{-1} on computed absorbance area for several compounds with additional neighboring functional groups relative to octane.

The effects of shifting are small, with the exception of the library spectrum of dodecanol. Again, it is unclear why the library and laboratory spectra of dodecanol result in such

different percent differences, and for the same reasons as given before, the library spectrum will not be heavily considered in the conclusions.

The amount of shifting is small in compounds containing –(O-H) groups and although the –(O-H) signature is close by, there is little issue with overlap. When the compounds contain carboxylic acids, the shifting does not appear to be any more significant, but the overlap with the shifted –(O-H) peak is significant and therefore the absorbance of the (C-H)#3 peak is difficult to determine. This seeming problem is investigated in the next experiment.

Shifting of the –(O-H)#1 peak

This analysis involved a final peak: the –(O-H)#1 peak at 3592-3108 cm^{-1}. Since octane does not include this functional group, the effect of shifting was evaluated relative to methanol. Methanol was selected because it does not contain any functional groups besides –(C-H) and –(O-H) to cause shifting in the target peak.

Again, a review of chemical structure:

Methanol	Octanoic Acid	2-Dodecanol	1-Decen-3-ol
CH_3OH	$CH_3(CH_2)_6COOH$	$CH_3(CH_2)_9CH(OH)CH_3$	$CH_3(CH_2)_6CH(OH)CH{=}CH_2$

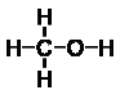
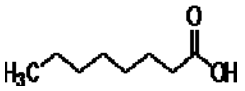
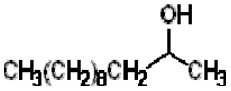
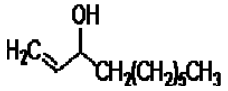

Differences in the number of different functional groups neighboring the –(O-H) group are expected to result in different amounts of shifting. The effects of the carbonyl in octanoic acid on the –(O-H)#1 peak is expected to be large, and the last analysis confirmed this. Shifting in 1-decen-3-ol is expected to also be significant because of the neighboring alkene double bond, but the one carbon of separation will likely help to diminish this effect. The –(O-H)#1 peak in the spectrum of 2-dodecanol is not expected to experience significant shifting relative to methanol because the –(O-H) group in both are neighbored by –(C-H) groups.

Shifting due to neighboring functional groups is illustrated in the following spectra.

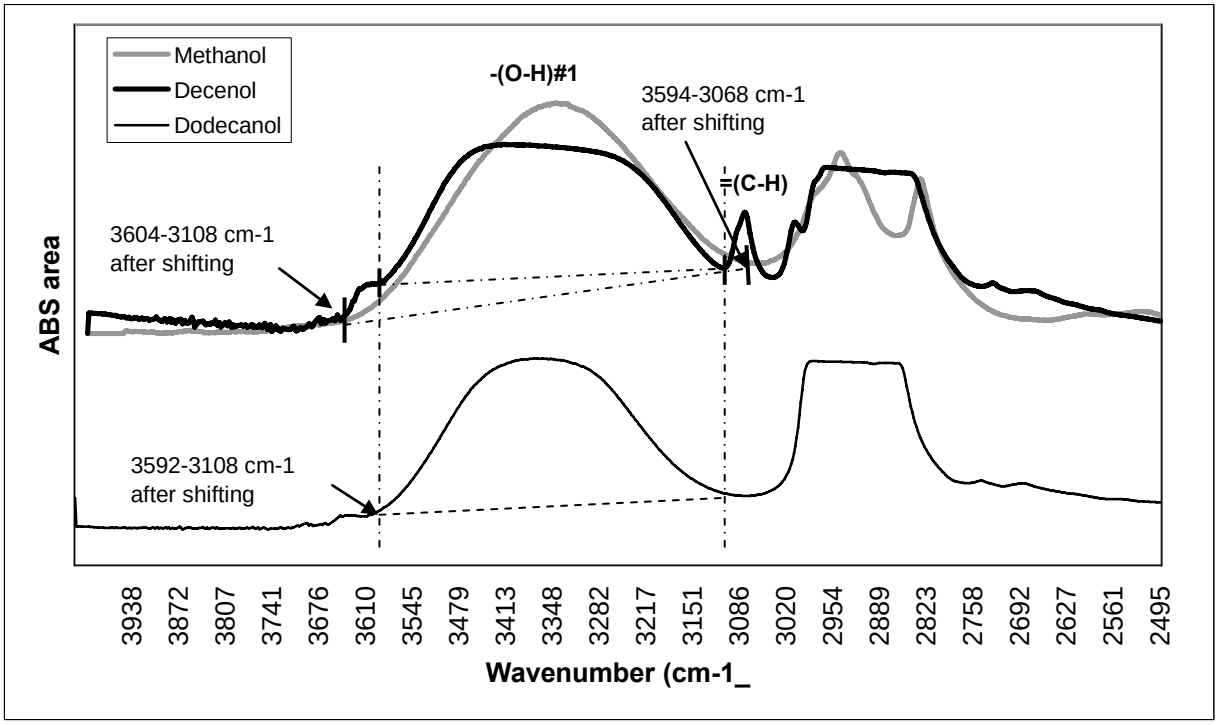

Figure 5- 12 Differences in the amount of shifting of the –(O-H) peak at 3592-3108 cm^{-1} relative to methanol when shaving versus horizontal baseline approaches are used

As expected, shifting is more pronounced in 1-decen-3-ol than in 2-dodecanol. The quantitative consequences of shifting on computed absorbance are presented in **Table 5-13**.

		ABS areas					
OVERALL		Octane (L)	Octanoic Acid (L)	Octanoic Acid (T)	2-Dodecanol (L)	2-Dodecanol (T)	1-Decen-3-ol (T)
-(O-H) #1	Alternate shifting	-	344.340	50.132	92.559	297.204	140.061
	Alternate baseline and shifting	-	?	?	116.523	348.695	157.881

Table 5- 15 Effect of shifting of the –(O-H) peak at 3536-2387 cm^{-1} on computed absorbance area for several compounds with additional neighboring functional groups relative to methanol.

The notation "-" means that the functional group is not present in a particular compound, and the notation "?" means that the absorbance can not be calculated because it is an overlapping peak. The peak mode for all of the compounds showed a significant shift relative to the values for methane, but the values of peak mode are only approximate since the –(O-H) peak is so broad. Shifting also slightly affects the end point locations of the functional group peak, which tend to shift to the left end in 2-dodecanol (L) and in 1-decen-3-ol (T) relative to those of octane, and to the right as well in 2-dodecanol (T) due to the presence of the alkene hydrogen =(C-H) functional group.

The resulting absorbances as shown for using the shaving baseline approach are significantly different when shifting is accounted for versus if it is not. As a result, it is clear that the -(O-H) functional group at 3592-3108 cm^{-1} in methanol is affected by shifting due to the presence of the –(C-H) and =(C-H) functional groups, and most

significantly the –(C=O)- carbonyl group. Overlap is also an issue for this peak, which will be evaluated in the next experiment.

In order to select a "potential best case" to be used in the splitting experiment, the correct ABS areas of the functional groups are calculated from the calibration curves in Experiment 10. The correct ABS area is the ABS area of the functional groups in the pure compound, therefore the ABS areas calculated in Experiment 12 and 13 must be close to the corrected one. The potential base case is used to calculate the ABS areas of the overlapping peaks in the next experiment.

		ABS areas					
OVERALL		Octane (L)	Octanoic Acid (L)	Octanoic Acid (T)	2-Dodecanol (L)	2-Dodecanol (T)	1-Decen-3-ol (T)
	Correct ABS			20.3		179.5	57.9
-(C-H)#1	Base case	79.498	41.247	3.381	82.001	158.534	65.446
	Alternate baseline	83.230	20.382	0.406	82.762	175.865	65.582
	Alternate shifting	79.498	?	?	82.29	189.43	66.05
	Alternate baseline and shifting	83.230	?	?	82.792	117.567	68.820
	Correct ABS			0.4		2.7	0.7
-(C-H)#2	Base case	1.025	0.477	0.089	0.801	3.036	0.324
	Alternate baseline	1.241	0.789	0.136	0.752	4.622	0.2
	Alternate shifting	1.025	0.531	0.089	0.796	2.842	0.322
	Alternate baseline and shifting	1.241	0.728	0.124	0.701	4.514	0.221

Table 5-16 Correct ABS areas and the effects of the different baseline approaches on the absorbance areas of targeted functional groups in all four compound spectra.

	Correct ABS			0.35		2.59	0.65
-(C-H)#3	Base case	0.599	1.194	0.234	0.884	2.495	0.626
	Alternate baseline	0.853	1.206	0.208	1.001	2.887	0.771
	Alternate shifting	0.599	1.197	0.232	0.882	2.488	0.623
	Alternate baseline and shifting	0.853	1.146	0.206	0.999	2.447	0.757
	Correct ABS			70.8		352.9	159.4
-(OH)#1	Base case	-	-29.49	-4.377	102.397	312.396	167.025
	Alternate baseline	-	94.473	17.669	114.707	333.378	154.431
	Alternate shifting	-	344.340	50.132	92.559	297.204	140.061
	Alternate baseline and shifting	-	?	?	116.523	348.695	157.881
-(OH)#2	Base case	-	3.597	5.432	0.216	5.291	2.07
	Alternate baseline	-	5.432	0.529	0.491	8.514	4.053
	Alternate shifting	-	16.967	2.227	0.238	5.269	3.266
	Alternate baseline and shifting	-	17.189	2.312	0.422	8.602	3.805

Table 5- 16 Correct ABS areas and the effects of the different baseline approaches on the absorbance areas of targeted functional groups in all four compound spectra.

Table 5-16 presents a summary of four baseline approaches address in these experiments. The calculated absorbance areas for the four different baseline approaches, where differences between absorbances for shaving and horizontal, shifting and no shifting can be observed. The notation "-" means that the functional group is not present in a particular compound, and the notation "?" means that the absorbance cannot be calculated because it is an overlapping peak.

There is no baseline experiment for octane, because it has only –(C-H) and –(C-C) peaks that do not interfere with each other, therefore it is a good spectra to be taken as a reference. Also, the –(C-H) targeted has a smooth baseline, sharp and strong peak, and the inflections points or endpoints are well defined.

In conclusion, shifting was both expected and observed. The absorbance of the –(C-H)#3 peak is relatively immune to shifting, but the –(C-H)#2 and –(C-H)#1 peaks are more significantly affected by neighboring functional groups. The –(C-H)#1 peak is also considerably affected by overlap with the –(O-H) group. Until overlap is also addressed, it is unclear how sensitive the other peaks are to shifting. This issue is explored next. Notably, the results from the shifting analysis will be used to develop approaches to address overlap.

The correct ABS areas of the functional groups in the spectra of the pure compounds were calculated from the calibration curves. Comparing the calculated ABS areas for each functional group to the corrected ABS areas, the alternate baseline approach was overall selected as the "potential best case".

The horizontal baseline was considered to be the potential best case, in prior experiment, because it accounts the most area under the peak, then by comparing the ABS areas in the table with the correct ABS area, it is clear that shifting does not affected the absorbances, except the ones which peaks are in an overlapping regions.

The measured ABS areas under the potential best case (alternate baseline, no shifting) were used to plot a new calibration curve and then recompute the relative molar absorptivities, in order to calculate ABS areas of the overlapping peaks. In order to confirm that this approach works to split peaks, the relative molar absorptivities obtained from the base case and the potential best case were evaluated in the next experiment.

5.5. EXPERIMENT 14: ALTERNATE PEAK SPLITTING APPROACH

Overlapping peaks are peaks in two different functional group signatures that occupy a similar MIR wavenumber range. Peak splitting is the division of overlapping peaks from different functional group signatures for the purpose of determining the absorbance area of each.

This experiment re-evaluates the same spectra of pure compounds evaluated in the previous experiments, but now splits overlapping peaks using first principles as opposed to using the endpoints of octane and methanol.

5.5.1. Issues

A single ambient aerosol can contain hundreds of thousands of molecules with different functional groups. Overlapping occurs when two different functional group signatures have a peak that occupies a similar MIR wavenumber range. Since the peak now accounts for both functional groups, it is unclear how to define endpoints to assign absorbance areas to each group.

Although each functional group has a unique MIR signature, particular peaks in the signature may overlap with peaks from other functional group's signatures. When this occurs, it is difficult to distribute the absorbance area to the two functional groups. The effect of shifting further complicates the issue of overlap.

For example, the –(C-H) functional group has a unique signature which includes three peaks (i.e., -(C-H) #1, #2 and #3). Peak #3 in the region of 734-703 cm^{-1} is unique in the larger sense since no other functional group signature has a peak in that region. However, peak #1 in the region of 3536-2387 cm^{-1} is not unique since it overlaps with a peak in the signature of the –(O-H) group in a carboxylic acid. This overlap is illustrated in the following figure.

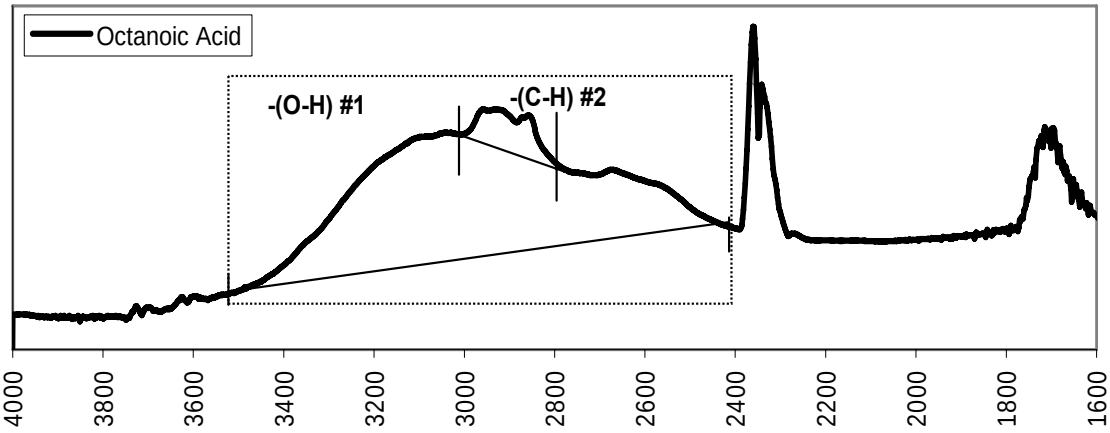

Figure 5- 13 Region of overlap between –(O-H) and –(C-H) functional group peaks in the Octanoic Acid IR spectrum.

Since many of the fine particle species overlap in the MIR spectrum, an approach to split these peaks is necessary in order to be able to determine the absorbance of the two

different functional groups. This is especially true when an overlapping peak is the only peak in a functional group signature.

5.5.2. Goal

The goal of this experiment is to develop and test an approach for splitting overlapping peaks to obtain accurate estimates of the absorbance.

5.5.3. Literature Review

Overlapping peaks have been identified in previous studies but not much research has been done to separate the peaks. Palen et al. (1992) found it difficult to interpret the peaks absorbance due to the overlap between aldehyde, ketone and carboxylic acid absorbances. Allen et al. (1994) found it difficult to determine the peak absorbances of sulfate and silicate due to overlapping. To split overlapping peaks they define the peak endpoints from the overlapping endpoint inflection to the non-overlapping inflection point.

Before overlapping peaks can be separated, the contributing species must be identified. The peak endpoint analysis completed in **Experiment 10** began this process by compiling regions where peaks are expected to overlap.

A review of the peak endpoints identified the literature (Allen et al. 1994, Carlton el al. 1999, Coates 2000, Reff et al. 2005) revealed that several fine particle species experience

some degree of overlap, limiting the utility of FTIR for fine particle speciation unless these peaks can be accurately split. The following table identifies peaks that are considered unique versus peaks that overlap. A more complete table with all functional groups that may overlap in the MIR spectra is presented in the Appendix.

Functional group	**Unique peak, cm^{-1}**	**Overlapping region, cm^{-1}**	**Functional group it overlaps with**
Hydroxyl-(O-H)	956-900	3592-3108	Ammonium -(N-H)
			Aliphatic carbon -(C-H)
			Alkene hydrogen =(C-H)
Alkene hydrogen =(C-H)		3106-3041	Hydroxyl -(O-H)
			Ammonium -(N-H)
		1000-890	Nitrate –(N-O)
Alkene carbon –(C=C)		1680-1620	Carbonyl -(C=O)
Aliphatic hydrogen –(C-H)	738-703	3037-2769	Hydroxyl -(O-H)
		1382-1371	Carbon oxygen -(C-O)
			Hydroxyl -(O-H)
			Nitrate –(N-O)
Carbonyl –(C=O)		1790-1625	Alkene carbon -(C=C)
			Hydroxyl -(O-H) (water)
Ammonium –(N-H)		3300-300	Hydroxyl -(O-H)
		1430-1390	Nitrate –(N-O)
			Carbonate -(C-O)
		910-655	Bisulfate –(S-O)
			Nitrate –(N-O)
Carbon oxygen -(C-O)		1260-1050	Teflon
Bisulfate –(S-O)		1200-1160	Teflon
		1050-1000	Phosphate –(P-O)
		880-840	Carbonate –(C-O)
Sulfate –(S-O)		1170-1050	Teflon
Nitrate –(N-O)		1240-1220	Teflon
		850-810	Alkene hydrogen =(C-H)
Carbonate –(C-O)		1490-1410	Ammonium –(N-H)
		880-860	Bisulfate –(S-O)
Teflon		1250-1100	Carbonate –(C-O)
			Sulfate –(S-O)
		560-490	Silicate -(Si-O)

Table 5- 17 Show functional groups unique peaks and overlapping peaks in the infrared spectra.

Water –(O-H)		3900-3400	Hydroxyl –(O-H)
Water –(O-H)		1850-1350	Carbonyl –(C=O)
			Hydroxyl –(O-H)
Carbon dioxide –(C-O)		2400-2290	

Table 5- 17 Show functional groups unique peaks and overlapping peaks in the infrared spectra.

Given the lack of guidance on the subject, a method was developed from first principles.

5.5.4. Experimental Approach

This experiment reanalyzed the same 12 spectra analyzed in the prior experiment: the same 3 library spectra of octane, octanoic acid and 2-dodecanol and the same 3 replicate spectra each of pure octanoic acid, 2-dodecanol and 1-decen-3-ol measured in the laboratory determined in the prior experiment.

The approach to split overlapping peaks is derived from Beer Lambert's law. The approach relates the known absorbance of one peak in a functional group signature to the unknown absorbance of a second peak in the sample signature, using the relative molar absorptivity of the two peaks determined for molecules that do not experience the overlap.

Equation 5- 5 $ABS_x = \frac{ABS_y}{\xi_{y/x}}$

Where x is the unknown peak in the signature and y is the known peak in the signature, ABS is the absorbance of the peak and $\xi_{y/x}$ is the relative molar absorptivity of the 2 peaks. The known peak may be unique in the composite fine particle spectrum, or it may simply be another overlapped peak whose absorbance was determined in the prior step using the approach just described.

The reanalysis involved these steps:

- Evaluate the peak characteristics for each targeted functional group studied in **Experiments 12** to identify whether they are sharp or broad, or strong or weak, or symmetric or asymmetric and overlapping with other functional groups
    - -(C-H)#1 at 3037-2769 cm^{-1}
    - -(C-H)#3 at 734-703 cm^{-1}
    - -(O-H)#1 at 3592-3108 cm^{-1}
    - -(O-H)#2 at 998-846 cm^{-1}
- Split the overlapping –(C-H)#1 and –(O-H)#1 peaks in the 3536-2387 cm^{-1} region of the spectra for different cases
    - Overlapping –(C-H) and alcohol –(O-H) in the 3592-2769 cm^{-1} region
    - Overlapping –(C-H) and carboxylic acid –(O-H) in the 3592-2769 cm^{-1} region
    - Overlapping –(C-H) in the 1388-1363 cm^{-1} region

The absorbances that results in potential best case from previous experiments were used to develop a new calibration curve in order to determine a strong relative molar

absorptivity that is used to effectively split overlapping peaks. Relative molar absorptivities are the ratios of the slope in the calibration curved between the unique and most common functional group peak and other functional group peaks.

The approach uses the potential best relative molar absorptivity value obtained from the calibration curve that use absorbances determined under the base case approach (**Experiment 10**), and the best relative molar absorptivity value obtained from calibration curve that uses the most reliable absorbances after comparing the base case and the alternate baseline approaches, that is a relative molar absorptivity from a calibration curve that uses absorbances measured under the alternate shifting baseline approach (**Experiment 12**). The relative molar absorptivity for the potential best case results are shown in the overall section of this chapter.

Absorbance calculated were compared with the correct ABS areas in order to determine which present more reliable results.

- Evaluation of the absorbance areas of overlapping peaks:

- ABS areas of overlapping peaks were calculated by using the relative molar absorptivities calculated from the potential best case linearity plot
- Calculated ABS areas will be compared to the correct ABS in order to determine the right approach to split the peaks.

Each of the 12 model compound spectra were evaluated for the targeted functional group peaks in the following way:

- Identify base case and potential best case relative molar absorptivities and compute the absorbance areas for the overlapping peaks

- Compute percent difference in absorbance as:

Equation 5- 6

$$\%Diff = \frac{ABS_{x,correct} - ABS_{x,calculated}}{ABS_{x,correct}} \times 100\%$$

Where $ABS_{x,calculated}$ is the absorbance of the peak based on the relative molar absorptivity obtained from a calibration curve or directly from the spectra, $ABS_{x,correct}$ is the absorbance of the peak determined from the calibration curve for each functional group at the concentration for the pure compound.

5.5.5. Results and Discussion

Absorbances of overlapping peaks were calculated by using the base case and potential best case relative molar absorptivities from the calibration curves. The base case relative molar absorptivities were calculated in Experiment 11, and the potential best case relative molar absorptivities were calculated from the new calibration curve presented in **Figure 5-11**.

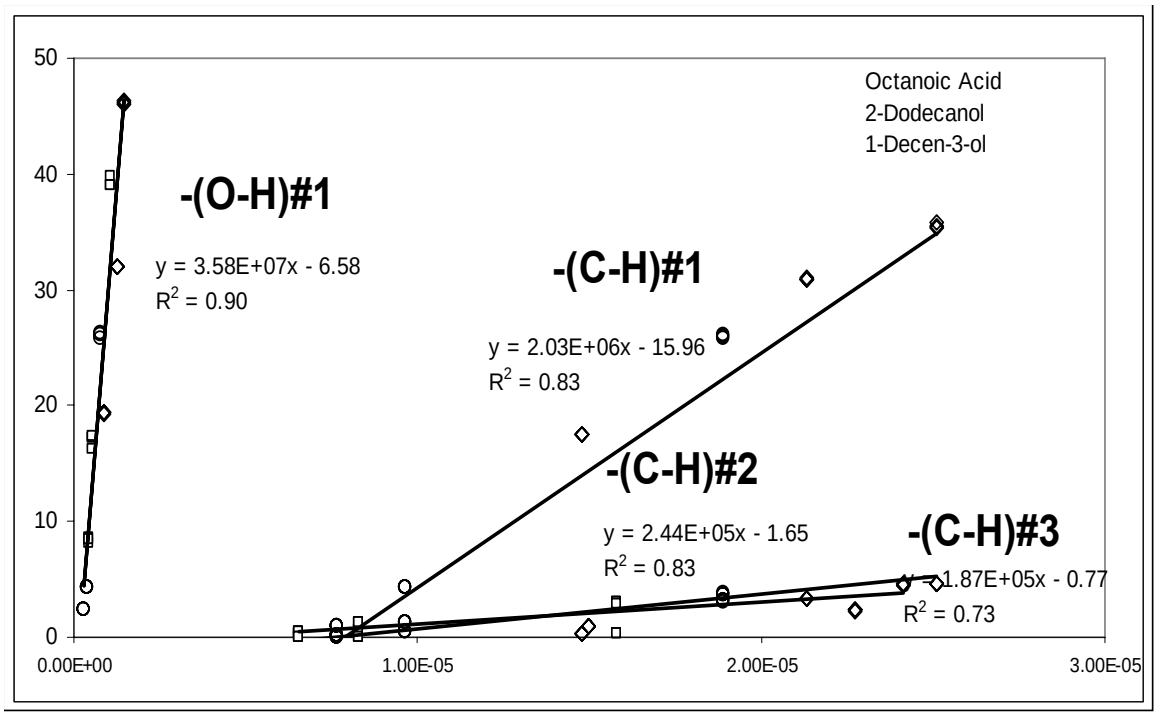

Figure 5- 14 Calibration curve developed when ABS areas were measured using the alternate baseline approaches (potential base case).

The relative molar absorptivities calculated are shown in the following table:

	Potential Best case	
	slope (ABS/Concentration)	$\xi_{y/x}$
-(C-H)#1	2.03 x 10^{+6}	0.092
-(C-H)#2	2.44 x 10^{+5}	0.766
-(C-H)#3	1.87 x 10^{+5}	1.000
-(O-H)#1	3.58 x 10^{+7}	0.005

Table 5- 18 Relative molar absorptivities computed by using the slope obtained from the potential best case calibration curve

Table 5-17 present the slopes and relative molar absorptivities computed by rationing the slopes of the targeted functional groups respect to the slope of the –(C-H)#3 functional group. The relative molar absorptivities were used to calculate the ABS areas of the overlapping peaks targeted in the spectra of the different compounds evaluated in this research.

Splitting of –(C-H) and –(O-H) in the 3592-2769 cm^{-1} of alcohols

By using all the information obtained in previous experiments, the relative molar absorptivities for the base case and potential best case, some of the overlapping peaks identified were split and their ABS areas calculated. Based in all variables discussed in this chapter, statistical analysis was made in order to decide the best approach to split overlapping peaks.

The –(C-H) peak at 3037-2769 cm^{-1} and –(O-H) peak at 3592-3108 cm^{-1} in **Figure 5-12** partially overlap at one of their endpoints in the IR spectra of the alcohols, 2-Dodecanol and 1-Decen-3-ol. The ABS areas of the –(C-H) peaks and –(O-H) peaks were determined by using the relative molar absorptivities obtained from the base case and best case approaches. Absorbances resulting from splitting are presented later in this chapter.

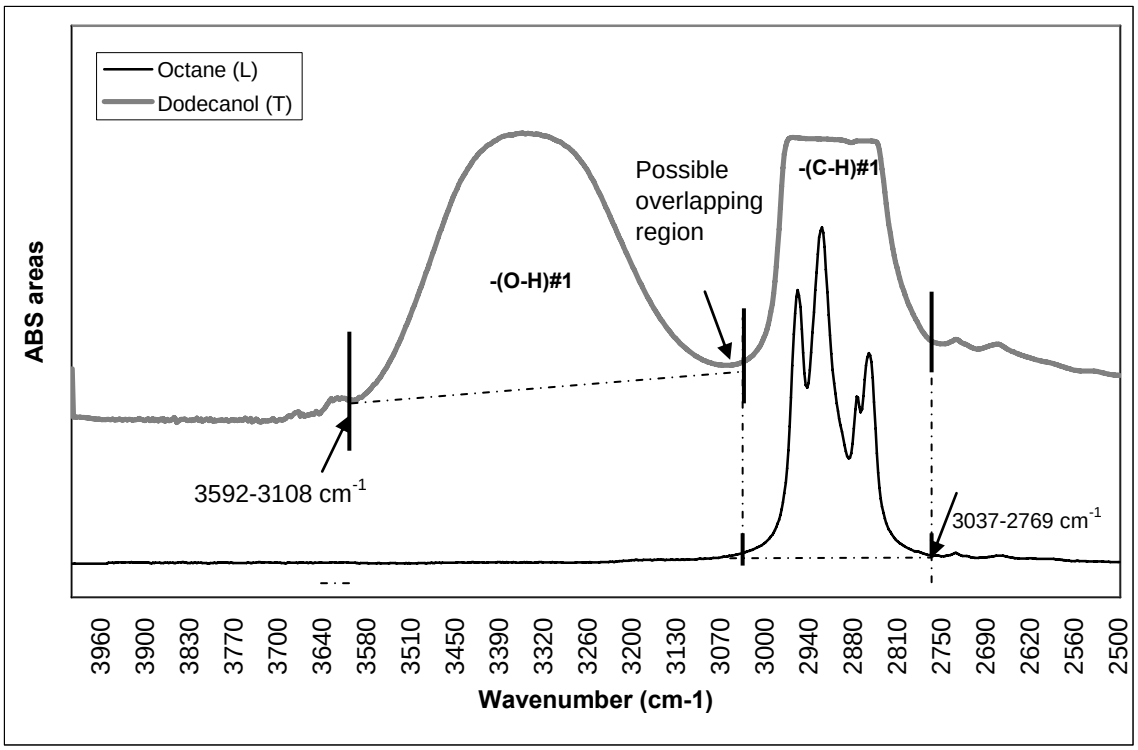

Figure 5- 15 Spectra of Dodecanol where appear peaks –(C-H) and –(O-H) in the region of 3502-2393 cm^{-1}

Splitting of –(C-H) and –(O-H) in the 3592-2769 cm^{-1} region of carboxylic acids

Octane has only –(C-H) functional group peaks that appear at different locations in the IR spectrum, therefore their wavenumber ranges and ABS areas can be determined directly from the spectrum. However same –(C-H) functional group peaks in the IR spectra of carboxylic acid and alcohol compounds may overlap with other functional groups present in these compounds. For example, in **Figure 5-12**, the signature of the –(C-H) peaks and the signature of the –(O-H) peaks overlap at 3037-2769 cm^{-1} in the spectra of Octanoic Acid. Absorbances were also computed by using the relative molar absorptivities obtained from the base case and best case approaches. Results are presented later in this chapter.

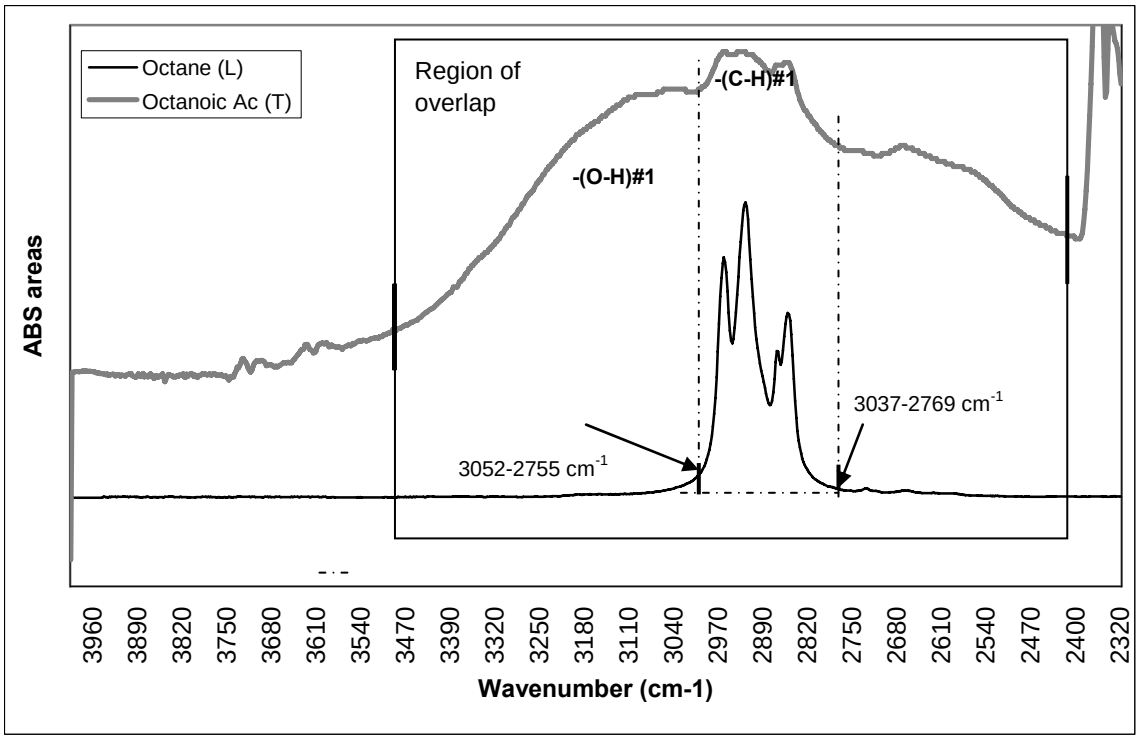

Figure 5- 16 Spectra of Dodecanol where appear peaks –(C-H) and –(O-H) in the region of 3502-2393 cm^{-1}

The ξ were calculated using **Equation 1**, between the slopes for –(C-H) peaks at 734-703 cm^{-1} and 3037-2769 cm^{-1} in the calibration plot from the base case and best case results:

The relative molar absorptivities determined relative to –(C-H) at 738-703 cm^{-1} are:

-(C-H)#3/-(C-H)#1

- Base case: $\xi = 0.060$
- Potential Best case: $\xi = 0.092$

-(C-H)#3/-(C-H)#2

- Base case: $\xi = 0.366$

- Potential Best case: $\xi = 0.766$

-(C-H)#3/-(O-H)#1

- Base case: $\xi = 0.002$
- Potential Best case: $\xi = 0.005$

An example of the computation of the calculate absorbance area for –(C-H)#1, by using the absorbance of –(C-H)#3 from the base case and the relative molar absorptivity obtained from the potential best case (0.14) for the –(C-H)#3 and –(C-H)#1. The other results are presented in table.

$$ABS_{-(CH)1calc} = \frac{0.230}{0.092} = 2.5$$

$$\%Diff = \frac{20.3 - 2.5}{20.3} \times 100 = 87\%$$

ABS areas calculated using the relative molar absorptivities are presented in the next section.

Splitting of –(C-H)#2 in the 1388-1363 cm^{-1} region

Figure 5-13 show spectral regions of octane, octanoic acid and 2-dodecanol where the -(C-H) peaks appear in an overlapping region.

Relative molar absorptivities computed from the base case and best case approaches were used to calculate the absorbance areas of the –(C-H) peak in the overlapping region.

Absorbances computed will be compared with the measured absorbances in order to determine the best relative molar absorptivity to be used.

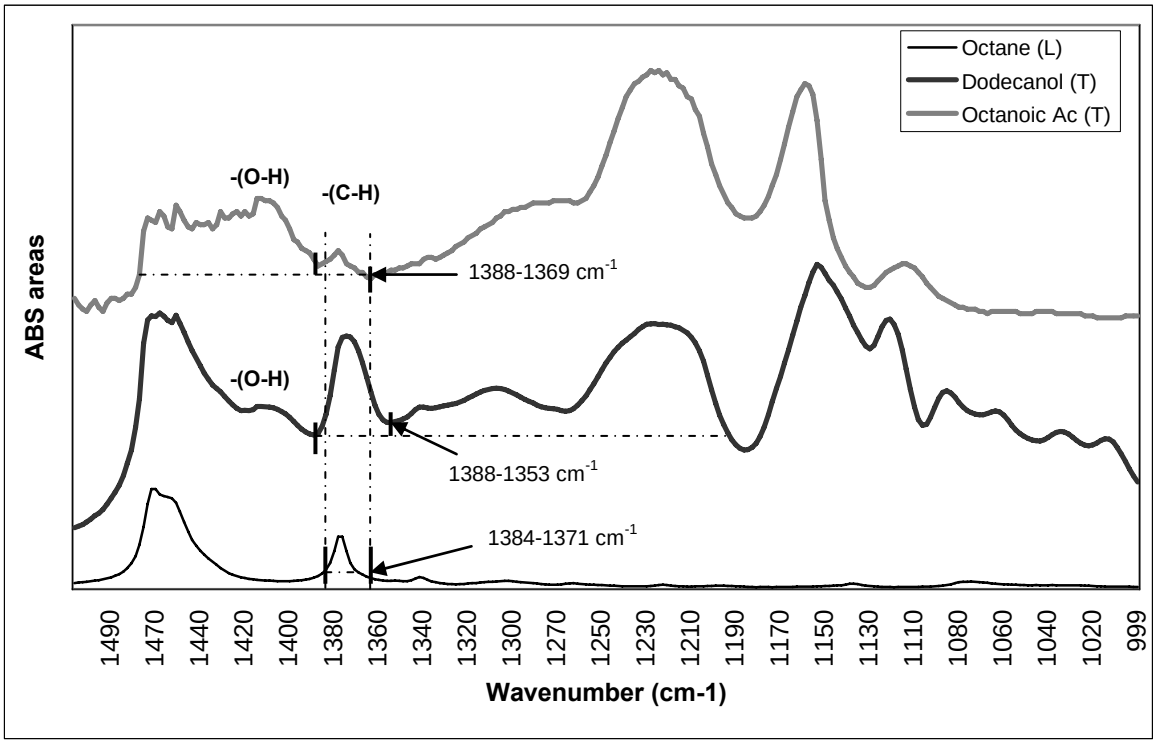

Figure 5- 17 Spectra of Octane, 2-Dodecanol and Octanoic acid where appear peaks –(C-H) at 1384-1371 cm^{-1} and –(O-H) at 1388-1363 cm^{-1}.

Calculated absorbance areas for the –(C-H)#2 peaks are presented in the next section.

5.6. OVERALL RESULTS AND DISCUSSION

Previous results were used iteratively in order to get ABS values more close to the correct ABS of the overlapping peaks. ABS resulting from the base case approach were used to develop a calibration curve from which relative molar absorptivities were used to

calculate ABS of the overlapping peaks. However when comparing their ABS to the correct ABS, the percentage difference was higher than when comparing ABS calculated for the potential base case to the correct ABS. Also ABS calculated for the potential best case, result in lower correlation coefficient R^2, respect to the best case results.

A summary of all the results from the Chapter 5 experiments is presented **Table 5-19**:

OVERALL		Octanoic Acid (T)	2-Dodecanol (T)	1-Decen-3-ol (T)
-(C-H)#1	Base case	3.4	158.5	65.4
	Alternate baseline	0.4	175.8	65.5
	Alternate shifting	?	189.4	66.1
	Alternate baseline and shifting	?	117.6	68.8
	Alternate shifting and splitting $\xi_{base\ case}= 0.060$ $\xi_{potencailbest\ case} = 0.092$	3.83	41.67	10.5
		2.28	31.41	8.37
	Alternate baseline, shifting and splitting $\xi_{base\ case}= 0.060$ $\xi_{potencailbest\ case}= 0.092$	3.83	41.67	10.5
		2.28	31.41	8.37
-(C-H)#2	Base case	0.08	3.0	0.32
	Alternate baseline	0.14	4.6	0.20
	Alternate shifting	0.09	2.8	0.32
	Alternate baseline and shifting	0.12	4.5	0.22
	Alternate shifting and splitting $\xi_{base\ case}= 0.366$ $\xi_{potencial\ best\ case}= 0.766$	0.63	6.83	1.72
		0.27	3.77	1.01
	Alternate baseline, shifting and splitting $\xi_{base\ case}= 0.366$ $\xi_{potencial\ best\ case} = 0.766$	0.63	6.80	1.69
		0.27	3.20	0.99

Table 5-19 Summary of all the absorbances measured and calculated using the different baseline approaches used in this experiment.

-(C-H)#3	Base case	0.23	2.50	0.63
	Alternate baseline	0.21	2.89	0.77
	Alternate shifting	0.23	2.49	0.62
	Alternate baseline and shifting	0.21	2.45	0.76
-(OH)#1	Base case	-4.4	312.4	167.0
	Alternate baseline	17.7	333.4	154.4
	Alternate shifting	50.1	297.2	140.1
	Alternate baseline and shifting	74.7	348.7	157.8
	Alternate shifting and splitting $\xi_{base\ case}= 0.002$ $\xi_{potencial\ best\ case} = 0.005$	115.00	1250.00	310.00
		42.00	578.00	154.00
	Alternate baseline, shifting and splitting $\xi_{base\ case}= 0.002$ $\xi_{potencial\ best\ case} = 0.005$	115.00	1245.00	310.00
		42.00	490.00	152.00

Table 5- 19 Summary of all the absorbances measured and calculated using the different baseline approaches used in this experiment.

Table 5-19 shows that the absorbances calculated for the potential best case for the pure compounds, and all the other absorbances for the different cases. However in order to select the best case, the calibration curve has to be plotted in order to decide the "best case", based on the R^2 value.

New calibration lines were computed using the all absorbances measured and calculated. The new calibration curves for each of the functional groups targeted were still linear and had far better correlation. The calibration curve for the ABS areas of each functional group for all the different cases analyzed is presented in **Figure 5-18, Figure 5-19, Figure 5-20, Figure 5-21.**

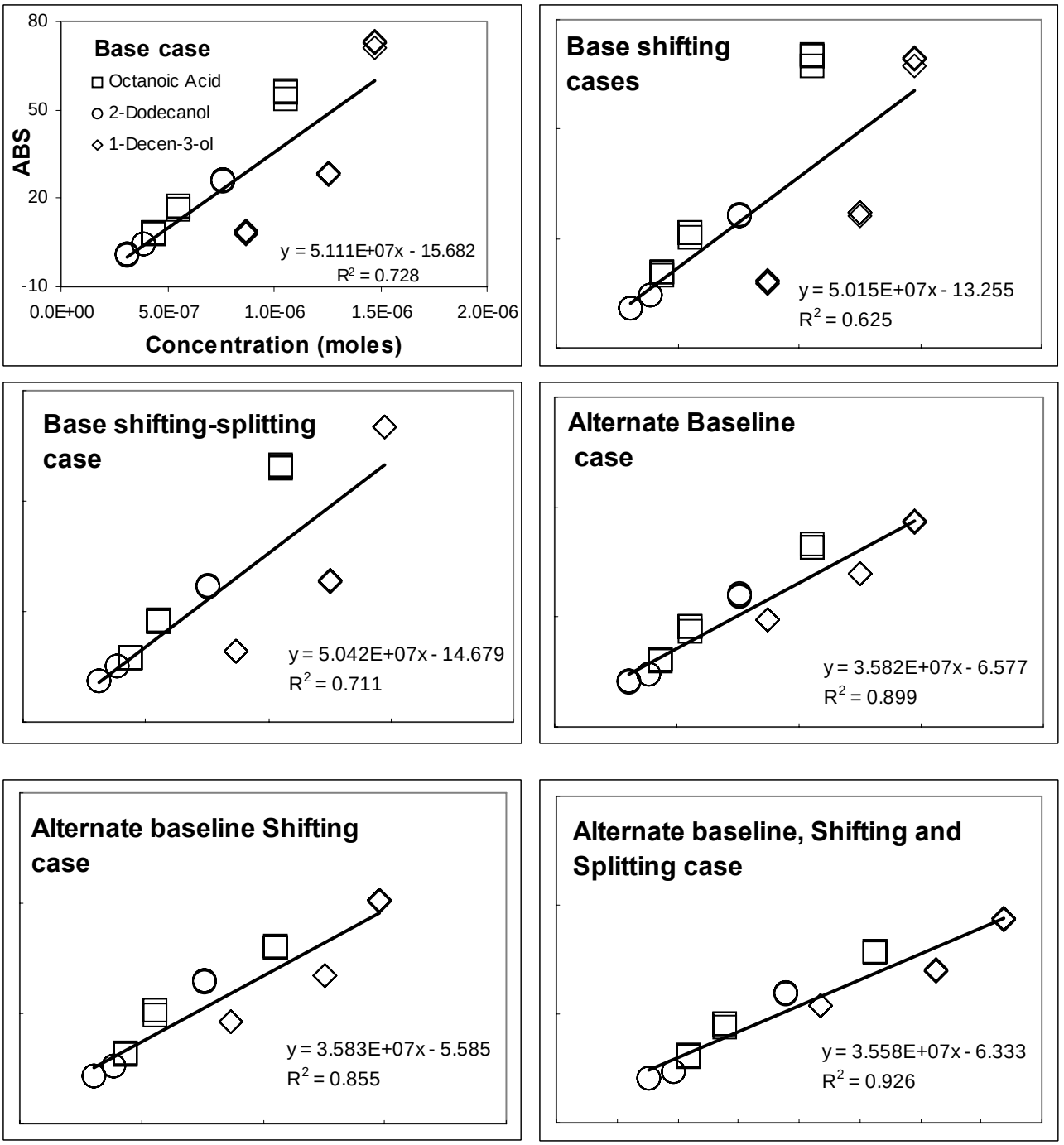

Figure 5- 18 –(O-H)#1 calibration curves for all cases analyzed in this experiment**.**

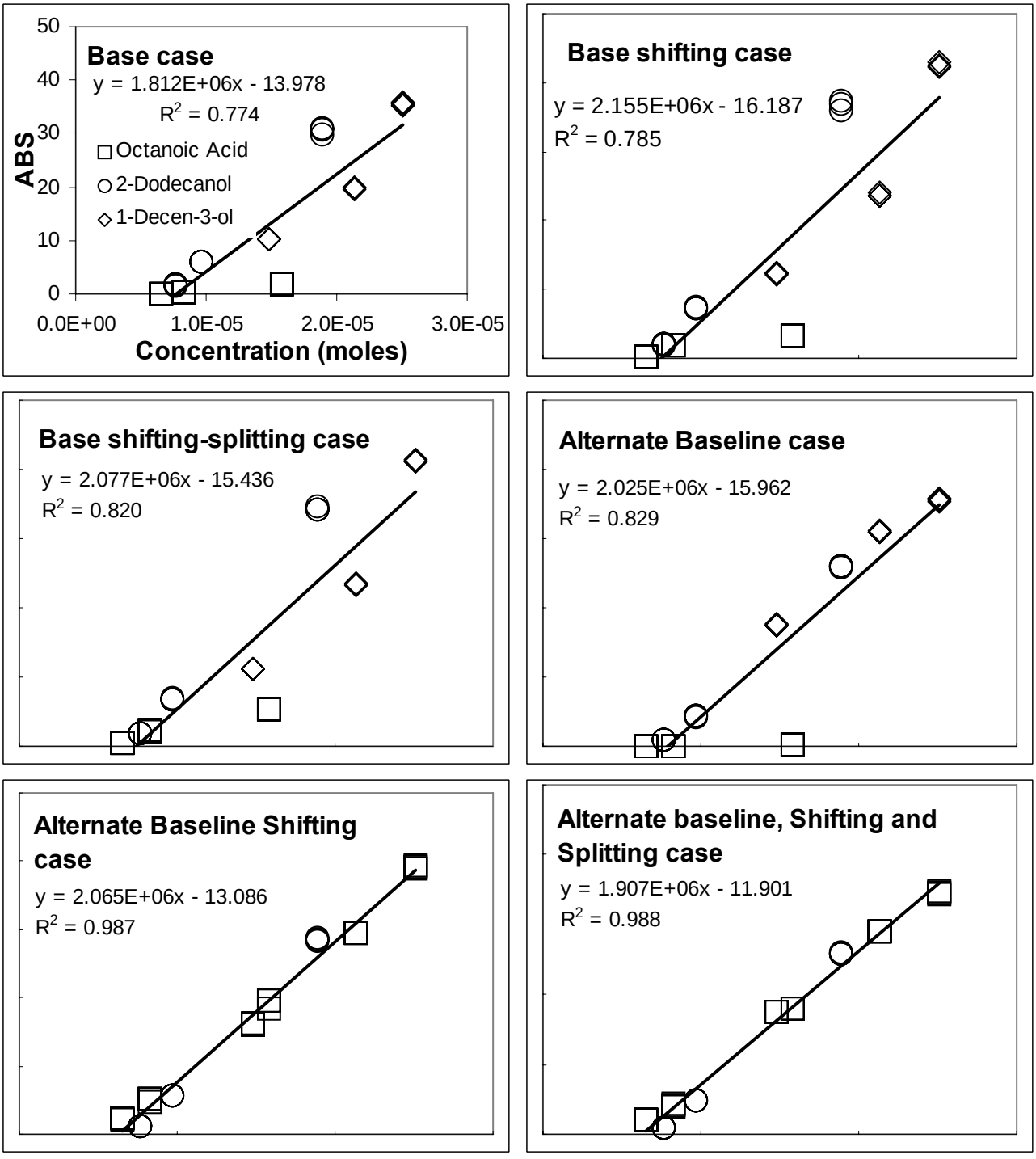

Figure 5- 19 –(C-H)#1 calibration curves for all cases analyzed in this experiment.

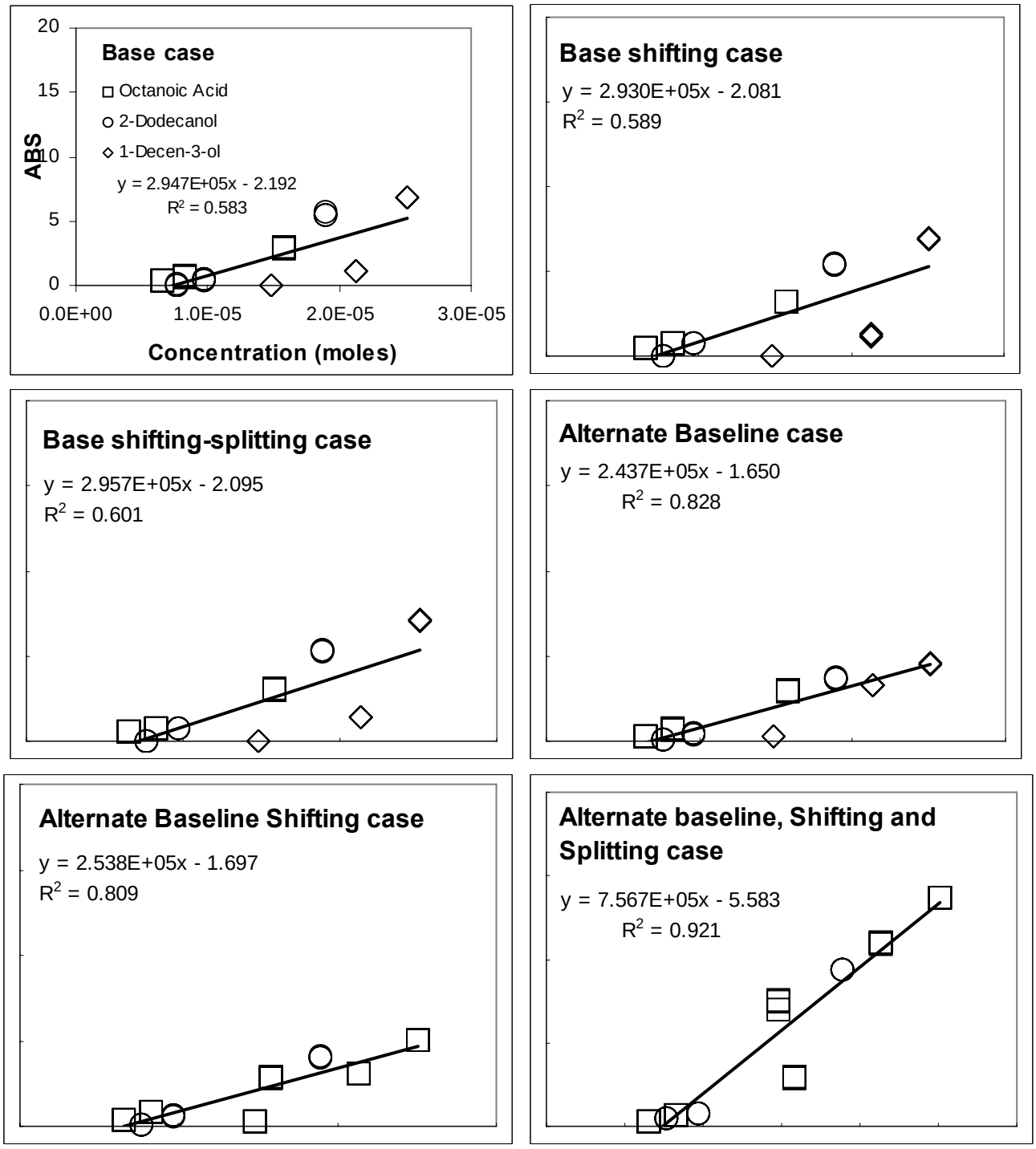

Figure 5- 20 –(C-H)#2 calibration curves for all cases analyzed in this experiment.

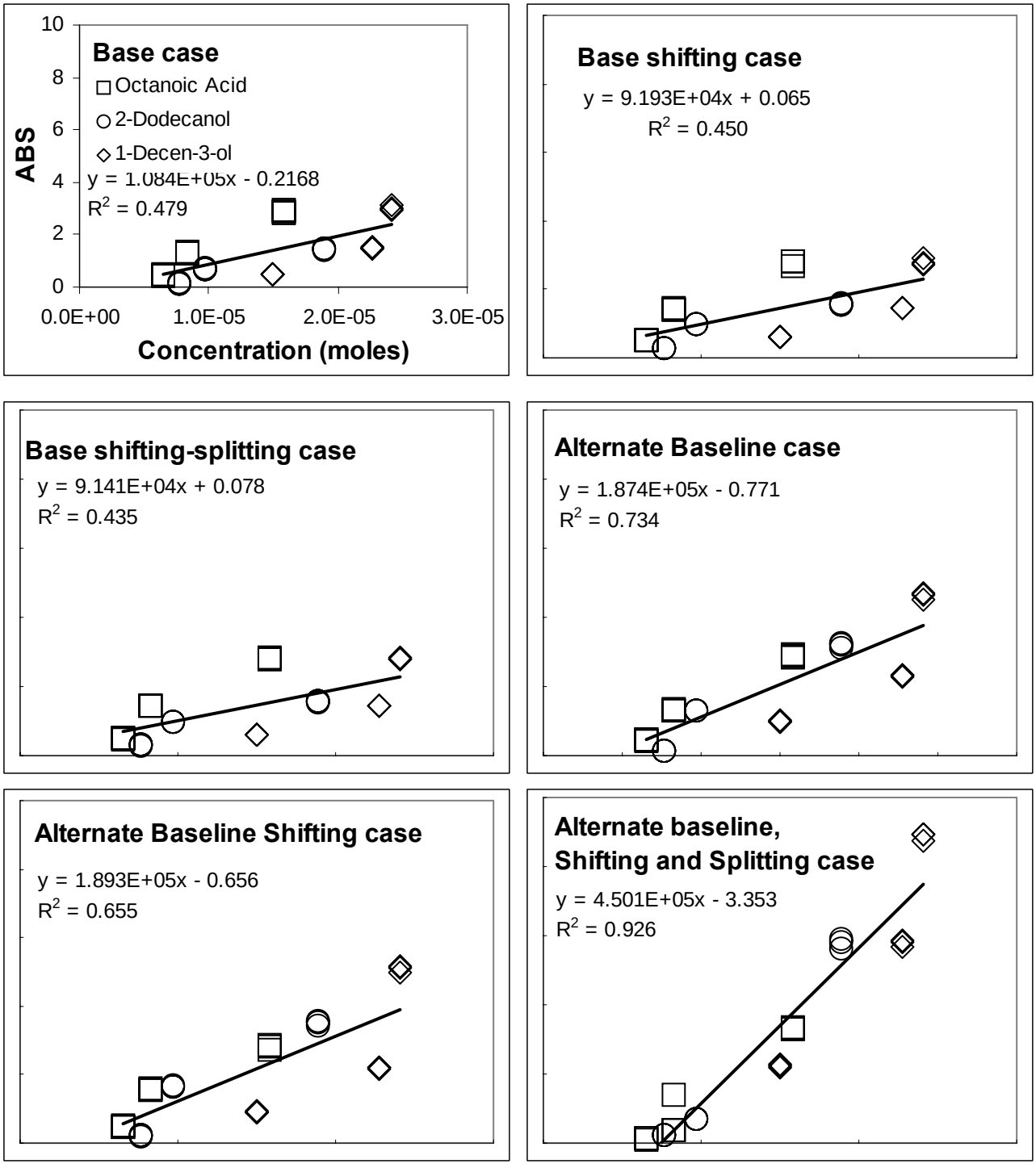

Figure 5- 21 –(C-H)#3 calibration curves for all cases analyzed in this experiment.

Figure 5-18, 5-19, 5-20, and 5-21 shows the linear plots for the targeted functional groups of –(C-H), -(O-H) developed when using all the cases approaches for each functional group. From the plot is observed that all cases present scatter however there is less scatter in the alternate baseline, shifting and splitting approach therefore data points also fit in the line. Also all the cases show a reasonable R^2, the case that have an improvement in the correlation coefficient, R^2, which values are closer to 1 is the alternate baseline, shifting and splitting approach, Also the correlation coefficient has improved compared with the values obtained in previous experiments; however the uncertainty has not decreased. Assuming a 95% confidence interval, statistics show a high uncertainty of 19.4 for –(C-H)#1 peak and of 21.6 for –(O-H)#1 peak, and a low uncertainty of 1.6 for –(C-H)#3 peak and 0.7 for –(C=C)#1 peak.

Uncertainty characterizes the dispersion of values that could be attributed to the concentration, absorbance, or sampling interferences. Low values of uncertainty validate the approaches used in this work and the results obtained using them.

The relative molar absorptivity based on the ratio of the slopes of the line was re-calculated. These new relative molar absorptivities are presented below, together with the correlation coefficient and relative molar absorptivities for the base and potential best case:

	Base case		**Potential Best case**		**Best case**	
	slope (ABS/Concentration)	R^2	slope (ABS/Concentration)	R^2	slope (ABS/Concentration)	R^2
-(C-H)#1	$1.81 \times 10^{+6}$	0.77	$2.03 \times 10^{+6}$	0.83	$1.91 \times 10^{+6}$	0.99
-(C-H)#2	$2.95 \times 10^{+5}$	0.58	$2.44 \times 10^{+5}$	0.83	$7.57 \times 10^{+5}$	0.92
-(C-H)#3	$1.08 \times 10^{+5}$	0.48	$1.87 \times 10^{+5}$	0.73	$4.50 \times 10^{+5}$	0.93
-(O-H)#1	$5.11 \times 10^{+7}$	0.73	$3.58 \times 10^{+7}$	0.90	$3.56 \times 10^{+7}$	0.93

Table 5- 20 New relative molar absorptivities from the new calibration curve obtained using best case approach.

Table 5-20 shows an improvement in the relative coefficient R^2 respect to the previous cases. Therefore, doing this analysis iterative analysis, it is probed that the linearity of the absorbances improves when the right approach to interpret the functional groups peaks is selected.

These relative molar absorptivities were used to calculate the absorbance areas for the best case approach, and worked well for the splitting –(C-H)#1 and –(O-H)#1. Therefore the approach to split overlapping peaks is successful and in future work will be applied to other functional group peaks that overlap.

5.7 CONCLUSIONS

The conclusion from these experiments is that these values obtained confirm that using the correct approach to split overlapping peaks is very important for a good spectral interpretation in order to measure the correct ABS areas of the functional groups in the complex aerosol spectra. The correct ABS areas will lead to construct a calibration curve where data points will fit to the line and with a correlation coefficient close to one. For calculation of the relative molar absorptivities of targeted functional groups and others as well, the uncertainty calculated will be used to provide an interval within which the value of the ABS areas and concentrations are believed to lie with a high level of confidence.

5.8 REFERENCES

Allen, D., Palen, E., Haimov, M., Hering, S. and Young, J., 1994. Fourier transform infrared spectroscopy of aerosol collected in a low pressure impactor (LPI/FTIR): Method development and field calibration. Aerosol Science and Technology 21, 325-342.

Blando, J., Procja, R. and Turpin, B., 2001. Issues in the quantitation of functional groups by FTIR spectroscopic analysis of impactor-collected aerosol samples. Aerosol Science and Technology 35, 899-908.

Carlton, A., Turpin, B., Johnson, W., Buckley, B., Simcik, M., Eisenreich, S. and Porcja, R., 1999. Microanalysis methods for characterization of personal aerosol exposures. Aerosol Science and Technology 31, 66-80.

Coates, J., 2000. Interpretation of infrared spectra, a practical approach. Encyclopedia of Analysis Chemistry (Meyers, R., ed.), 10815- 10837. John Wiley & Sons Ltd, Chichester.

Dekermenjian, M., Allen, D., Atkinson, R. and Arey, J., 1999. FTIR analysis of aerosol formed in the ozone oxidation of sesquiterpenes. Aerosol Science and Technology 30, 349-363.

Dekermenjian, M., Allen, D., Atkinson, R. and Arey, J., 1999(a). FTIR analysis of aerosol formed in the photooxidation of napthtalene. Aerosol Science and Technology 30, 273-279.

Schwarzenbach, R., Gschwend, P., Imboden, D., 2003. Environmental Organic Chemistry, Second Edition. John Willey and Sons Inc., Hoboken, New Jersey.

Harris, D. and Bertolucci, M. (1978). Symmetry and Spectroscopy: An Introduction to Vibrational and Electronic Spectroscopy. Dover Publications, INC., New York.

Holes, A., Eusebi, A., Grosjean, D. and Allen, D., 1997. FTIR analysis of aerosol formed in the photooxidation of 1,3,5-Trimethylbenzene. Aerosol Science and Technology 26, 516-526.

Kellner, R. (1978). Identification and determination of particulate compounds: infrared spectroscopy, extraction and chromatography. Analysis of Airborne Particles by Physical Methods (edited by Malissa H and Robinson JW). CRC Press, Boca Raton FL.

Palen, E., Allen, D., Pandis, S., Paulson, S., Seinfeld, J. and Flagan, R., 1992. Fourier transform infrared analysis of aerosol formed in the photooxidation of Isoprene and β-Pinene. Atmospheric Environment 26A (7), 1239-1251.

Palen, E., Allen, D., Pandis, S., Paulson, S., Seinfeld, J. and Flagan, R., 1993. Fourier transform infrared analysis of aerosol formed in the photooxidation of 1-Octene. Atmospheric Environment 27A (9), 1471-1477.

Reff, A., Turpin, B., Porcja, R., Giovennetti, R., Cui, W., Weisel, C., Zhang, J., Kwon, J., Alimokhtari, S., Morandi, M., Stock, T., Maberti, S., Colome, S., Winer, A., Shendell, D., Jones, J. and Farrar, C., 2005. Functional group characterization of indoor, outdoor, and personal $PM_{2.5}$: results from RIOPA. Indoor Air 15, 53-61.

CHAPTER 6 CONCLUSIONS AND RECOMMENDATIONS

6.1 CONCLUSIONS

This research focused on the development of an analytical method using FTIR to measure fine particle speciation in more detail and at a higher level of completeness than currently achieved by conventional or state of the art methods.

This method is a reliable approach for gas phase speciation. However, it has been used only minimally for liquid and solid phase speciation for several reasons. In order to determine concentration, spectra must be acquired and absorbance areas integrated. However there is little information in the literature to support these activities. Few MIR signatures are available and they are seldom of individual functional groups. Molar absorptivity data is not reported and the relative molar absorptivity data that is reported is uncompelling since the values are wildly variable and presented without uncertainty or any explanation as to how they were produced. Finally, very little information about functional group signature peak baselines or peak ranges that also account for shifting and overlapping is reported and what is reported is unfounded and inconsistent. In short, there is very little information available to support the use of FTIR for inhomogeneous multicomponent liquid or solid sample speciation.

Despite the fact that there is little research to support the use of this method for inhomogeneous multicomponent liquid or solid sample speciation, this method has been used to measure fine particle speciation because of the immense increase in the quality of

information that can be gained by it over other analytical methods used to measure fine particle speciation.

The goal of this research was to develop and optimize a systematic approach to use FTIR for fine particle speciation, to do what no researchers have done before: document these methods and system limitations in the literature, and to identify in the process whether it can actually be used for the purpose of fine particle speciation.

6.1.1 Chapter 1: Introduction

In this chapter, the need for an improvement in the detail and completeness of fine particle speciation was motivated, to support health studies, air pollution receptor and transport model refinement, and the development of more effective implementation plans to improve air quality. An exhaustive review of methods to measure components in fine particles was performed and FTIR was identified as the most promising approach because it is theoretically able to measure the speciation of the full organic and inorganic components of fine particles with detail without extraction, and it is nondestructive.

6.1.2 Chapter 2: Quantitation

Three algorithms were derived that relate fine particle species concentration to FTIR absorbances of the fine particle species (ABS), general properties of ambient particles such as density (ρ) and relative molar absorptivity (ξ), quantities related to how the sample was collected such as sampling flow rate (Q) and sample duration (t), and known

concentration of an internal standard in the sample measured by FTIR (C_y) or measured by an external analytical method (n_y).

- Experiment 1: Concentration using internal standard

  When the internal standard is the Teflon substrate

Equation 6-1 $$C_{x\,in\,a} = C_{y\,in\,b}\frac{ABS_{x\,in\,b}\;l_f}{ABS_{y\,in\,b}\;\varepsilon_{x/y}}\frac{\pi r_s^2\left(1-\eta_f\right)\alpha}{Q\;t}$$

  When the internal standard is a coating on the surface of the sample

Equation 6-2 $$C_{x\,in\,a} = C_{y\,in\,b}\frac{ABS_{x\,in\,b}\;l_c}{ABS_{y\,in\,b}\;\varepsilon_{x/y}}\frac{\pi r_s^2\left(1-\eta_f\right)\alpha}{Q\;t}$$

- Experiment 2: Concentration using external standard

Equation 6-3 $$C_{x\,in\,a} = n_{y\,in\,s}\frac{ABS_{x\,in\,b}}{ABS_{y\,in\,b}\;\varepsilon_{x/y}}\frac{\alpha}{Q\;t}$$

The algorithms purposely do not depend on properties that are difficult to accurately measure, such as path length or absolute molar absorptivity.

6.1.3 Chapter 3: Sample collection

A sampling approach was developed to produce fine particle samples that can be analyzed using a FTIR (Nicolet Series #6700) with a DTGS-KBr detector (Thermo-scientific #840-0698) for fine particle speciation. This approach included:

- Experiment 3: Sampling substrate – 47mm Pall Teflon filters (Gelman Teflo #R2PJ047) are used for sample collection since their MIR signatures are resolved, not saturated, and contain peaks that are unique or only minimally overlapping with fine particle signatures.

- Experiment 4: Sampler configuration – The sampler draws ambient air at 16.67 LPM to minimize volatilization of semi-volatiles in fine particle samples through a standard $PM_{2.5}$ cyclone (URG-2000-3ENB) to remove particles larger than 2.5 μm, through activated carbon monolith (MAST #4012) organic and magnesium oxide and citric acid (URG-2000-3CSS) inorganic denuders to remove interferent gases from the sample stream prior to particle collection, through a 47 mm filter to collect the fine particles, and then exhausts the filtered air.

- Experiment 5: Fine particle mass loading – A minimum sample collected onto substrate with fine particle mass loading of about 0.01 absorbance units equivalent to 3 times the baseline noise is required to exceed the FTIR detection limits. This can be achieved by sampling ambient air for 24 to 48 hours when the

average ambient fine particle mass concentrations range between 8.3 to 14.5 μg m^{-3} in NYC.

6.1.4 Chapter 4: Spectra acquisition

In **Chapter 4**, spectra acquisition methods were developed, to produce FTIR spectra that could be analyzed for fine particle speciation. These methods are summarized below.

- Experiment 6: Spectroscopy approach – Transmission spectroscopy is used to collect spectra since it accounts for the full fine PM sample, results in stronger fine particle signature peaks and is not prone to contamination, all issues observed in the reflectance spectroscopy approach. An automated sample shuttle (Thermo Nicolet #840-058-200) is used to avoid handling artifacts while repositioning the substrate for transmission spectroscopy analysis at multiple locations on the substrate and while moving the substrate into and out of the FTIR light path.

- Experiment 7: Background spectra – Open-path backgrounds are collected to account for gases in the analysis chamber that may interfere with the fine particle spectrum, and are selected over blank-in-path backgrounds which require less processing but which result in more uncertain peak absorbance areas. Open-path background spectra are collected at least every 20 minutes to minimize the impacts of changes in the analysis chamber gas composition during analysis on the fine particle spectrum. Both blank substrate spectra and sample on substrate

spectra are collected, and corrected using the most recent background, and then subtracted from each other to result in a fine particle spectra with minimal uncertainty and subtraction artifacts. Substrates are marked on the edge to facilitate consistent alignment in the holder which minimizes uncertainty.

- Experiment 8: Gas interferent minimization – The FTIR software (Thermo Scientific, OMNIC 7.3) "atmospheric suppression" setting is not used. While it mathematically reduces the signatures of water and CO_2 in a spectrum, it also affects the accuracy of absorbances of fine particle species including water.

- Experiment 9: Use of substrate as internal standard – The substrate can be used as an internal standard for quantification purposes since it has a signature peak that is unique and occurs over a predictable wavenumber range. However, the value of the blank absorbance used in the algorithm developed in **Chapter 2** to determine fine particle species concentration, must be determined for each filter since the Teflon density varies by filter lot.

6.1.5 Chapter 5: Spectra interpretation

In this chapter, methods to consistently process FTIR spectra for fine particle speciation were developed and evaluated. These methods are summarized below.

- Experiment 10: Assessment of absorbance linearity – The linearity of absorbance areas for four functional groups, alkane-hydrogen -(C-H) at 3037-2769 cm^{-1} and

734-703 cm^{-1}, hydroxyl -(O-H) at 3592-3108 cm^{-1} and alkene –(C=C) at 1680-1620 cm^{-1} was assessed by analyzing dilutions of several model compounds in a like solvent. Samples were prepared by delivering a 0.5 ul volume of each dilution standard onto a Pall Teflon filter and then analyzing the spectrum of the diluted compound. The resulting spectra were analyzed using a set of "base case" approaches that included shaved baselines, no accounting for shifting from octane of methanol peak endpoints, and a simple division of overlapping peaks based on octane and methanol endpoints. Since it was shown that compounds volatilize with time, a volatilization rate factor was calculated in order to determine the actual molar concentration in each dilution standard analyzed by the FTIR. The absorbance and molar concentrations were statistically evaluated and calibration lines for each functional group were developed which accounted for multiple compounds and multiple concentrations. Their correlation factors confirm that the relationship is linear, but also confirm the need for improved spectral interpretation. Experiments 12-14 refined these interpretations to reduce the uncertainty in the calibration lines.

- Experiment 11: Measurement of molar absorptivity – Relative molar absorptivities to be used in the algorithms derived in **Chapter 2** were computed using two different approaches: 1) a ratio of calibration line slopes from the prior experiment and 2) a ratio of functional group absorbances measured a similar way as in the last experiment but using pure model compounds instead of dilutions of them. The molar absorptivities compared to values in the literature and were less

variable than values reported in the literature, however, there was still much deviation in the values computed using the second approach by compound. This was explained by the fact that the relative molar absorptivities were based on the "base case" spectral interpretation approaches which only used shaved baselines, did not accounting for peak shifting, and divided overlapping peaks very simply.

Experiment 12: Alternate baseline approach - In this experiment, the same pure model compound spectra obtained for the prior experiment were re-analyzed by varying the "base case" approach to drawing a baseline. In the base case, all of the baselines were shaved, connecting the inflection points on either side of the peak. In this approach, a horizontal line was drawn originating at the lower inflection point or even possibly below it. This alternate baseline approach resulted in larger absorbance areas for particular target functional group signature peaks. The shaving approach was better for the –(C-H)#1and –(O-H)#2 peaks in octanoic acids and the horizontal one was better for the –(C-H)#1 peaks in all alcohols,-(C-H)#2, -(C-H)#3, and -(O-H)#1 in all compounds.

- Experiment 13: Alternate peak shifting approach - In this experiment, the same pure model compound spectra were re-analyzed. However, this time the "base case" approach to addressing peak shifting was varied. In the base case, the endpoints for each of the target functional groups in any compound were equal to the ones measured in the octane and methanol spectra. In this alternate peak shifting case, new endpoints were identified on a peak by peak basis, accounting for shifting of peaks due to neighboring effects. For overlapping peaks, shifting

could not be accounted for. In the final experiment, methods to split overlapping peaks that also accounted for shifting were addressed. The approach selected demonstrated that shifting of particular peaks for the alkane and alcohol functional groups cannot be neglected if absorbance measurements are to be accurate. Shifting did not need to be accounted for in the –(C-H)#3 peaks, but it did need to be accounted for in the –(C-H)#1, -(C-H)#2 and –(O-H) peaks.

- Experiment 14: Alternate peak splitting approach – In this final experiment, methods to split overlapping peaks were developed and tested. In the "base case" overlapping peaks were split at the endpoints identified in the octane and methanol spectra. This alternate approach was derived from Beer Lambert's law and used the relative molar absorptivity of a nonoverlapping and overlapping peak in the same functional group signature. The relative molar absorptivity values were recomputed first, by implementing the "best case" approaches identified in the earlier experiments. It also accounted for the shifting of overlapping peaks. The resulting calibration lines were linear and had very little scatter, demonstrating the benefits of the alternate spectra interpretation approaches for particular functional group signature peaks. The method was tested for the alkane hydrogen -(C-H) functional group for multiple compounds. Using the approach, more accurate measurements of the alkane and alcohol functional group peak absorption at the spectral region of 3037-2769 cm^{-1} were obtained than were possible through the "base case".

6.2 RECOMMENDATIONS FOR FUTURE EXPERIMENTS

6.2.1 Evaluate collection efficiency of CCNY sampler for different types of aerosol samples

The sampler design employs demonstrated practices for gas phase interferent removal, and common approaches for collecting ambient particles using filtration. However, the particle collection efficiency on the Pall Teflon filter is not reported in the literature and has not been characterized in the CCNY laboratory. Since the CCNY AQRL has a particle sizing instrument, it is possible to generate and direct laboratory aerosol to the sampler inlet, and measure its size distribution before and after sampling to assess particle collection efficiency.

6.2.3 Test the algorithms

The algorithms developed in Chapter 2 show that the concentration of functional groups in ambient aerosol samples can be calculated without depending on the path length of the sample and the relative molar absorptivity. However the algorithms were not validated. Since the CCNY AQRL has a gas chromatography instrument and chemical standards, it is possible to validate the algorithms and calculate the concentration of fine particles species in the ambient aerosol samples.

6.2.2 Extend Chapter 5 experiments to include other functional groups, and other model compounds and combinations of model compounds

The experiments in Chapter 5 were intended to develop methodologies. They were tested for multiple complex compounds and multiple functional groups to demonstrate the possible improvements to accuracy that could be made by implementing a scientific approach to spectra interpretation. However, fine particles contain many additional functional groups that were not evaluated, and mixtures of complex compounds. Since the CCNY AQRL has all the instrumentation and chemicals needed to investigate more functional groups, and prepare more mixtures with a wide variety of functional groups, it is possible to conduct the same experiments in order to compute relative molar absorptivities that involve more functional groups others than alkanes, alcohols and alkenes. The knowledge of more relative molar absorptivities will allow to address other overlapping functional groups across the entire ambient aerosol composition.

6.2.3 Further explore the use of Teflon as a quality control indicator

While it is clear that Teflon can be used as an internal standard, it would also be helpful if it could be used as a quality control measure. To be used for this purpose, the Teflon absorbance area should be identical regardless of where on the substrate the FTIR spectra was collected or what lot the filter was produced in. Different lots of the Pall Teflon filters have different densities, resulting in a large variability in integrated absorbance area at the Teflon signature peak at 560 cm^{-1}. It is possible that other filter manufacturers may produce filters with more consistent fiber densities.

6.2.3 Apply approach to wide range of ambient samples

The "best case" approaches identified for each functional group peak were identified. When additional "best case" approaches are developed through future work, real ambient fine particle samples can be analyzed. These analyses will serve two purposes: 1) They will be used to validate the algorithms derived in **Chapter 2**, and 2) they will allow us to use the method to obtain improved fine particle speciation measurements for all of the purposes that were identified in **Chapter 1**.

APPENDIX

LIST OF MATERIAL AND PART NUMBERS

A. Chemicals

ACS grade Ammonium sulfate (Fluka, # 09980)

GC grade 1-octane (mfg, #)

GC grade octanoic acid (Fluka, # 21639)

GC grade 2-dodecanol (Aldrich, # D221503)

GC grade 1-decen-3-ol (SAFC, # W382418)

Spectrophotometric grade Acetone (Mallinckrodt, # 243808)

Spectrophotometric grade Ethanol (Aldrich, # 459828)

B. Items were used in the sampler or for sample preparation:

47mm, 2.0 µm Teflon filter (Pall Gelman Teflo, R2PJ047)

47mm, 2.0 um Teflon filter (Savillex, # 1131)

47mm, 2.5 um quartz filter (Pallflex, Tissuequartz 2500QAO-UP)

0.1 to 10 µl Finnpipette (Labsystems, # 4500010)

10 to 100 ul Finnpipette (Fisherbrand, # 21377819)

100 to 1000 ul Finnpipette (Fisherbrand, # 1438674)

20 ml EPA vial and PTFE cap (National Scientific, # B7800-20)

1L Class A volumetric flask (Wildmad Labglass, # 50807170)

C. These items were used in FTIR operation:

- NICOLET 6700 FTIR (Thermo Electro Corporation)
- OMNIC Macro/Basic 7.3 software (Thermo Electro Corporation)
- Smart Golden Gate ATR accessory (Thermo Electro Corporation)
- Sample shuttle (Thermo Electro Corporation, #840-058200)

RAW DATA TABLES

Base Case Data

		-(O-H)#1		-(C-H)#1		-(C-H)#2		(C-H)#3	
	Dilutions	ABS	Concentration	ABS	Concentration	ABS	Concentration	ABS	Concentration
Octnaoic Acid/Acetone	100:100	53.7730	1.052E-06	1.6905	1.578E-05	2.8971	1.578E-05	2.9503	1.578E-05
		56.0900	1.052E-06	1.7108	1.578E-05	2.9921	1.578E-05	2.9050	1.578E-05
		56.2600	1.052E-06	1.7057	1.578E-05	2.9991	1.578E-05	2.8151	1.578E-05
	100:300	16.2490	5.529E-07	0.3381	8.294E-06	0.6566	8.294E-06	1.3300	8.294E-06
		17.2620	5.529E-07	0.3422	8.294E-06	0.7065	8.294E-06	1.3100	8.294E-06
		17.3710	5.529E-07	0.3411	8.294E-06	0.7124	8.294E-06	1.3100	8.294E-06
	100:400	8.0710	4.354E-07	0.1470	6.531E-06	0.3122	6.531E-06	0.4607	6.531E-06
		8.5360	4.354E-07	0.1488	6.531E-06	0.3270	6.531E-06	0.4468	6.531E-06
		8.4640	4.354E-07	0.1483	6.531E-06	0.3264	6.531E-06	0.4190	6.531E-06
Dodecanol/Ethanol	100:100	25.7461	7.563E-07	29.9355	1.891E-05	5.6565	1.891E-05	1.4752	1.891E-05
		26.1392	7.563E-07	30.8350	1.891E-05	5.5256	1.891E-05	1.4525	1.891E-05
		26.2411	7.563E-07	31.1673	1.891E-05	5.5128	1.891E-05	1.4076	1.891E-05
	100:300	4.3047	3.865E-07	6.0143	9.663E-06	0.4854	9.663E-06	0.7150	9.663E-06
		4.2993	3.865E-07	6.1092	9.663E-06	0.4954	9.663E-06	0.7050	9.663E-06
		4.3074	3.865E-07	6.1690	9.663E-06	0.4012	9.663E-06	0.7050	9.663E-06
	100:400	0.8928	3.065E-07	1.6247	7.664E-06	0.0547	7.664E-06	0.1536	7.664E-06
		0.9209	3.065E-07	1.6946	7.664E-06	0.0652	7.664E-06	0.1489	7.664E-06
		0.9280	3.065E-07	1.7198	7.664E-06	0.0599	7.664E-06	0.1397	7.664E-06
Decenol/Ethanol	100:25	73.4634	1.476E-06	35.5255	2.509E-05	6.8338	2.509E-05	3.0153	2.413E-05
		72.8621	1.476E-06	35.7834	2.509E-05	6.8271	2.509E-05	3.1201	2.413E-05
		71.0553	1.476E-06	35.2858	2.509E-05	6.8191	2.509E-05	2.9701	2.413E-05
	100:50	28.6927	1.253E-06	19.7506	2.131E-05	1.0905	2.131E-05	1.5460	2.271E-05
		28.5549	1.253E-06	20.0083	2.131E-05	1.0893	2.131E-05	1.4952	2.271E-05
		27.7392	1.253E-06	19.7250	2.131E-05	1.0885	2.131E-05	1.5015	2.271E-05
	100:100	8.7641	8.704E-07	10.3124	1.480E-05	0.0278	1.480E-05	0.5090	1.499E-05
		8.6001	8.704E-07	10.3814	1.480E-05	0.0273	1.480E-05	0.4925	1.499E-05
		8.1625	8.704E-07	10.0910	1.480E-05	0.0273	1.480E-05	0.4862	1.499E-05

Base Case Shifting Data

		-(O-H)#1		-(C-H)#1		-(C-H)#2		(C-H)#3	
	Dilutions	ABS	Concentration	ABS	Concentration	ABS	Concentration	ABS	Concentration
Octnaoic Acid/Acetone	100:100	67.2163	1.052E-06	3.2890	1.578E-05	3.2190	1.578E-05	2.8230	1.578E-05
		70.1125	1.052E-06	3.2680	1.578E-05	3.2040	1.578E-05	2.7980	1.578E-05
		70.3250	1.052E-06	3.2520	1.578E-05	3.1980	1.578E-05	2.6540	1.578E-05
	100:300	20.3113	5.529E-07	1.8590	8.294E-06	0.7340	8.294E-06	1.4670	8.294E-06
		21.5775	5.529E-07	1.8270	8.294E-06	0.7230	8.294E-06	1.4290	8.294E-06
		21.7138	5.529E-07	1.8320	8.294E-06	0.7120	8.294E-06	1.4090	8.294E-06
	100:400	10.0888	4.354E-07	0.2560	6.531E-06	0.4980	6.531E-06	0.5120	6.531E-06
		10.6700	4.354E-07	0.2210	6.531E-06	0.4760	6.531E-06	0.5230	6.531E-06
		10.5800	4.354E-07	0.2280	6.531E-06	0.4730	6.531E-06	0.5310	6.531E-06
Dodecanol/Ethanol	100:100	26.0036	7.563E-07	35.9227	1.891E-05	5.4250	1.891E-05	1.5490	1.891E-05
		26.4006	7.563E-07	37.0021	1.891E-05	5.4120	1.891E-05	1.5780	1.891E-05
		26.5035	7.563E-07	37.4007	1.891E-05	5.3820	1.891E-05	1.5590	1.891E-05
	100:300	4.3477	3.865E-07	7.2172	9.663E-06	0.7230	9.663E-06	0.9760	9.663E-06
		4.3423	3.865E-07	7.3310	9.663E-06	0.7260	9.663E-06	0.9650	9.663E-06
		4.3505	3.865E-07	7.4028	9.663E-06	0.7310	9.663E-06	0.9700	9.663E-06
	100:400	0.9018	3.065E-07	1.9497	7.664E-06	0.0367	7.664E-06	0.2780	7.664E-06
		0.9301	3.065E-07	2.0335	7.664E-06	0.0326	7.664E-06	0.2980	7.664E-06
		0.9372	3.065E-07	2.0638	7.664E-06	0.0316	7.664E-06	0.2870	7.664E-06
Decenol/Ethanol	100:25	69.7902	1.476E-06	42.6306	2.509E-05	6.9670	2.509E-05	2.8910	2.413E-05
		69.2190	1.476E-06	42.9401	2.509E-05	6.9320	2.509E-05	2.7530	2.413E-05
		67.5026	1.476E-06	42.3430	2.509E-05	6.9120	2.509E-05	2.7450	2.413E-05
	100:50	27.2581	1.253E-06	23.7007	2.131E-05	1.1230	2.131E-05	1.4720	2.271E-05
		27.1272	1.253E-06	24.0100	2.131E-05	1.3420	2.131E-05	1.4630	2.271E-05
		26.3522	1.253E-06	23.6700	2.131E-05	1.2380	2.131E-05	1.4580	2.271E-05
	100:100	8.3258	8.704E-07	12.3748	1.480E-05	0.0352	1.480E-05	0.6230	1.499E-05
		8.1701	8.704E-07	12.4577	1.480E-05	0.0361	1.480E-05	0.6180	1.499E-05
		7.7544	8.704E-07	12.1092	1.480E-05	0.0371	1.480E-05	0.6150	1.499E-05

Base Shifting and Splitting Case Data

		-(O-H)#1		-(C-H)#1		-(C-H)#2		(C-H)#3	
	Dilutions	ABS	Concentration	ABS	Concentration	ABS	Concentration	ABS	Concentration
Octnaoic Acid/Acetone	100:100	59.654	1.052E-06	5.462	1.578E-05	3.026	1.578E-05	2.815	1.578E-05
		59.354	1.052E-06	5.354	1.578E-05	3.125	1.578E-05	2.806	1.578E-05
		59.156	1.052E-06	5.421	1.578E-05	3.014	1.578E-05	2.795	1.578E-05
	100:300	17.546	5.529E-07	2.314	8.294E-06	0.745	8.294E-06	1.462	8.294E-06
		17.425	5.529E-07	2.245	8.294E-06	0.756	8.294E-06	1.453	8.294E-06
		17.405	5.529E-07	2.203	8.294E-06	0.761	8.294E-06	1.45	8.294E-06
	100:400	7.546	4.354E-07	0.451	6.531E-06	0.595	6.531E-06	0.501	6.531E-06
		7.426	4.354E-07	0.439	6.531E-06	0.587	6.531E-06	0.498	6.531E-06
		7.413	4.354E-07	0.427	6.531E-06	0.576	6.531E-06	0.487	6.531E-06
Dodecanol/Ethanol	100:100	26.985	7.563E-07	34.578	1.891E-05	5.314	1.891E-05	1.587	1.891E-05
		26.895	7.563E-07	34.298	1.891E-05	5.305	1.891E-05	1.548	1.891E-05
		26.546	7.563E-07	34.254	1.891E-05	5.312	1.891E-05	1.559	1.891E-05
	100:300	5.427	3.865E-07	6.987	9.663E-06	0.759	9.663E-06	0.997	9.663E-06
		5.312	3.865E-07	6.856	9.663E-06	0.768	9.663E-06	0.986	9.663E-06
		5.214	3.865E-07	6.754	9.663E-06	0.724	9.663E-06	0.973	9.663E-06
	100:400	1.245	3.065E-07	1.845	7.664E-06	0.0389	7.664E-06	0.301	7.664E-06
		1.325	3.065E-07	1.845	7.664E-06	0.0372	7.664E-06	0.311	7.664E-06
		1.346	3.065E-07	1.754	7.664E-06	0.0364	7.664E-06	0.314	7.664E-06
Decenol/Ethanol	100:25	70.123	1.476E-06	41.245	2.509E-05	7.105	2.509E-05	2.814	2.413E-05
		70.098	1.476E-06	41.345	2.509E-05	7.094	2.509E-05	2.806	2.413E-05
		70.025	1.476E-06	41.125	2.509E-05	7.086	2.509E-05	2.795	2.413E-05
	100:50	28.213	1.253E-06	23.547	2.131E-05	1.384	2.131E-05	1.452	2.271E-05
		28.465	1.253E-06	23.412	2.131E-05	1.379	2.131E-05	1.437	2.271E-05
		28.354	1.253E-06	23.148	2.131E-05	1.368	2.131E-05	1.425	2.271E-05
	100:100	9.217	8.704E-07	11.248	1.480E-05	0.0405	1.480E-05	0.619	1.499E-05
		9.145	8.704E-07	11.189	1.480E-05	0.0412	1.480E-05	0.607	1.499E-05
		9.134	8.704E-07	11.156	1.480E-05	0.0417	1.480E-05	0.601	1.499E-05

Alternate Baseline Case Data

		-(O-H)#1		-(C-H)#1		-(C-H)#2		(C-H)#3	
	Dilutions	ABS	Concentration	ABS	Concentration	ABS	Concentration	ABS	Concentration
Octnaoic Acid/Acetone	100:100	39.7700	1.052E-06	0.3383	1.578E-05	2.8971	1.578E-05	2.9503	1.578E-05
		39.0100	1.052E-06	0.3215	1.578E-05	2.9921	1.578E-05	2.9050	1.578E-05
		38.9500	1.052E-06	0.3254	1.578E-05	2.9991	1.578E-05	2.8151	1.578E-05
	100:300	16.2500	5.529E-07	0.0677	8.294E-06	0.6966	8.294E-06	1.3300	8.294E-06
		17.2600	5.529E-07	0.0651	8.294E-06	0.7165	8.294E-06	1.3100	8.294E-06
		17.3700	5.529E-07	0.0651	8.294E-06	0.7124	8.294E-06	1.3100	8.294E-06
	100:400	8.0700	4.354E-07	0.0294	6.531E-06	0.3122	6.531E-06	0.4607	6.531E-06
		8.5400	4.354E-07	0.0283	6.531E-06	0.3270	6.531E-06	0.4468	6.531E-06
		8.4600	4.354E-07	0.0283	6.531E-06	0.3264	6.531E-06	0.4190	6.531E-06
Dodecanol/Ethanol	100:100	25.7500	7.563E-07	25.7800	1.891E-05	3.7710	1.891E-05	3.2454	1.891E-05
		26.1400	7.563E-07	26.1500	1.891E-05	3.6838	1.891E-05	3.1955	1.891E-05
		26.2400	7.563E-07	25.9900	1.891E-05	3.6752	1.891E-05	3.0966	1.891E-05
	100:300	4.3000	3.865E-07	4.2967	9.663E-06	0.4854	9.663E-06	1.3000	9.663E-06
		4.3000	3.865E-07	4.3583	9.663E-06	0.4954	9.663E-06	1.2818	9.663E-06
		4.3100	3.865E-07	4.3317	9.663E-06	0.4012	9.663E-06	1.2818	9.663E-06
	100:400	2.3700	3.065E-07	0.8911	7.664E-06	0.0547	7.664E-06	0.1536	7.664E-06
		2.4000	3.065E-07	0.9039	7.664E-06	0.0652	7.664E-06	0.1489	7.664E-06
		2.3900	3.065E-07	0.8984	7.664E-06	0.0599	7.664E-06	0.1397	7.664E-06
Decenol/Ethanol	4.184028	46.2700	1.476E-06	35.5200	2.509E-05	4.5559	2.509E-05	4.5229	2.413E-05
		46.1500	1.476E-06	35.7800	2.509E-05	4.5514	2.509E-05	4.6801	2.413E-05
		45.9800	1.476E-06	35.2900	2.509E-05	4.5461	2.509E-05	4.6500	2.413E-05
	4.201389	32.0700	1.253E-06	31.0500	2.131E-05	3.2715	2.131E-05	2.3280	2.271E-05
		31.9500	1.253E-06	30.9700	2.131E-05	3.2679	2.131E-05	2.2680	2.271E-05
		31.9400	1.253E-06	30.9600	2.131E-05	3.2656	2.131E-05	2.3400	2.271E-05
	100:100	19.3800	8.704E-07	17.5900	1.480E-05	0.3062	1.480E-05	1.0179	1.499E-05
		19.2300	8.704E-07	17.5500	1.480E-05	0.3002	1.480E-05	0.9850	1.499E-05
		19.3900	8.704E-07	17.4900	1.480E-05	0.3003	1.480E-05	0.9725	1.499E-05

Alternate Baseline and Shifting Case Data

		-(O-H)#1		-(C-H)#1		-(C-H)#2		(C-H)#3	
	Dilutions	ABS	Concentration	ABS	Concentration	ABS	Concentration	ABS	Concentration
Octnaoic Acid/Acetone	100:100	38.5769	1.052E-06	18.5076	1.578E-05	2.8102	1.578E-05	2.8618	1.578E-05
		37.8397	1.052E-06	19.5067	1.578E-05	2.9024	1.578E-05	2.8179	1.578E-05
		37.7815	1.052E-06	19.6619	1.578E-05	2.9091	1.578E-05	2.7307	1.578E-05
	100:300	19.5000	5.529E-07	5.2800	8.294E-06	0.8359	8.294E-06	1.5960	8.294E-06
		20.7120	5.529E-07	5.1960	8.294E-06	0.8598	8.294E-06	1.5720	8.294E-06
		20.8440	5.529E-07	4.8000	8.294E-06	0.8548	8.294E-06	1.5720	8.294E-06
	100:400	8.8770	4.354E-07	2.1780	6.531E-06	0.3434	6.531E-06	0.5068	6.531E-06
		9.3940	4.354E-07	2.3430	6.531E-06	0.3598	6.531E-06	0.4915	6.531E-06
		9.3060	4.354E-07	2.3540	6.531E-06	0.3590	6.531E-06	0.4609	6.531E-06
Dodecanol/Ethanol	100:100	28.3250	7.563E-07	28.3580	1.891E-05	4.1481	1.891E-05	3.5699	1.891E-05
		28.7540	7.563E-07	28.7650	1.891E-05	4.0521	1.891E-05	3.5151	1.891E-05
		28.8640	7.563E-07	28.5890	1.891E-05	4.0427	1.891E-05	3.4063	1.891E-05
	100:300	5.5900	3.865E-07	5.5857	9.663E-06	0.6310	9.663E-06	1.6900	9.663E-06
		5.5900	3.865E-07	5.6658	9.663E-06	0.6440	9.663E-06	1.6664	9.663E-06
		5.6030	3.865E-07	5.6312	9.663E-06	0.5216	9.663E-06	1.6664	9.663E-06
	100:400	2.9625	3.065E-07	1.1139	7.664E-06	0.0684	7.664E-06	0.2304	7.664E-06
		3.0000	3.065E-07	1.1299	7.664E-06	0.0815	7.664E-06	0.2234	7.664E-06
		2.9875	3.065E-07	1.1230	7.664E-06	0.0748	7.664E-06	0.2095	7.664E-06
Decenol/Ethanol	4.184028	50.8970	1.476E-06	39.0720	2.509E-05	5.0115	2.509E-05	4.9752	2.413E-05
		50.7650	1.476E-06	39.3580	2.509E-05	5.0066	2.509E-05	5.1481	2.413E-05
		50.5780	1.476E-06	38.8190	2.509E-05	5.0007	2.509E-05	5.1150	2.413E-05
	4.201389	30.4665	1.253E-06	29.4975	2.131E-05	3.1079	2.131E-05	2.2116	2.271E-05
		30.3525	1.253E-06	29.4215	2.131E-05	3.1045	2.131E-05	2.1546	2.271E-05
		30.3430	1.253E-06	29.4120	2.131E-05	3.1023	2.131E-05	2.2230	2.271E-05
	100:100	17.8296	8.704E-07	16.1828	1.480E-05	0.2817	1.480E-05	0.9365	1.499E-05
		17.6916	8.704E-07	16.1460	1.480E-05	0.2762	1.480E-05	0.9062	1.499E-05
		17.8388	8.704E-07	16.0908	1.480E-05	0.2763	1.480E-05	0.8947	1.499E-05

Alternate Baseline, Shifting and Splitting Case Data

		-(O-H)#1		-(C-H)#1		-(C-H)#2		(C-H)#3	
	Dilutions	ABS	Concentration	ABS	Concentration	ABS	Concentration	ABS	Concentration
Octnaoic Acid/Acetone	100:100	37.1700	1.052E-06	18.0140	1.578E-05	2.8971	1.578E-05	3.3568	1.578E-05
		37.0100	1.052E-06	18.0160	1.578E-05	2.9921	1.578E-05	3.3184	1.578E-05
		37.0500	1.052E-06	18.0200	1.578E-05	2.9991	1.578E-05	3.3109	1.578E-05
	100:300	16.2500	5.529E-07	4.2300	8.294E-06	0.6966	8.294E-06	1.3900	8.294E-06
		17.2600	5.529E-07	4.3500	8.294E-06	0.7165	8.294E-06	0.3686	8.294E-06
		17.3700	5.529E-07	4.0200	8.294E-06	0.7124	8.294E-06	0.3663	8.294E-06
	100:400	8.0700	4.354E-07	2.1200	6.531E-06	0.3122	6.531E-06	0.1299	6.531E-06
		8.5400	4.354E-07	2.1300	6.531E-06	0.3270	6.531E-06	0.1185	6.531E-06
		8.4600	4.354E-07	2.1400	6.531E-06	0.3264	6.531E-06	0.1122	6.531E-06
Dodecanol/Ethanol	100:100	25.7500	7.563E-07	25.7800	1.891E-05	9.3565	1.891E-05	5.9007	1.891E-05
		25.6400	7.563E-07	25.8800	1.891E-05	9.4256	1.891E-05	5.8100	1.891E-05
		25.8400	7.563E-07	25.9900	1.891E-05	9.4128	1.891E-05	5.6303	1.891E-05
	100:300	4.3000	3.865E-07	4.9500	9.663E-06	0.7854	9.663E-06	0.7150	9.663E-06
		4.3000	3.865E-07	4.9100	9.663E-06	0.7954	9.663E-06	0.7050	9.663E-06
		4.3100	3.865E-07	4.9300	9.663E-06	0.8012	9.663E-06	0.7050	9.663E-06
	100:400	2.3700	3.065E-07	0.8911	7.664E-06	0.4547	7.664E-06	0.2304	7.664E-06
		2.4000	3.065E-07	0.8946	7.664E-06	0.4752	7.664E-06	0.2234	7.664E-06
		2.3900	3.065E-07	0.8984	7.664E-06	0.4799	7.664E-06	0.2095	7.664E-06
Decenol/Ethanol	4.184028	46.2700	1.476E-06	34.5200	2.509E-05	13.6521	2.509E-05	8.7458	2.413E-05
		46.1500	1.476E-06	34.7800	2.509E-05	13.6985	2.509E-05	8.9102	2.413E-05
		45.9800	1.476E-06	34.2900	2.509E-05	13.7125	2.509E-05	8.9400	2.413E-05
	4.201389	32.0700	1.253E-06	28.9700	2.131E-05	10.9521	2.131E-05	5.8200	2.271E-05
		31.9500	1.253E-06	28.9700	2.131E-05	10.9621	2.131E-05	5.6700	2.271E-05
		31.9400	1.253E-06	28.9600	2.131E-05	10.9742	2.131E-05	5.8500	2.271E-05
	100:100	22.3800	8.704E-07	17.5900	1.480E-05	7.5124	1.480E-05	2.2903	1.499E-05
		22.2300	8.704E-07	17.5500	1.480E-05	7.5090	1.480E-05	2.2162	1.499E-05
		22.3900	8.704E-07	17.4900	1.480E-05	6.9865	1.480E-05	2.1880	1.499E-05

FUNCTIONAL GROUPS PRESENT IN AMBIEN AIR FINE PARTULATE ($PM_{2.5}$)

IR location of functional groups present in ambient fine particulate matter. Graphic represent peaks that are considered unique (no overlapping) and peaks that overlap.

Wavenumber range: 4000-3000 cm^{-1}

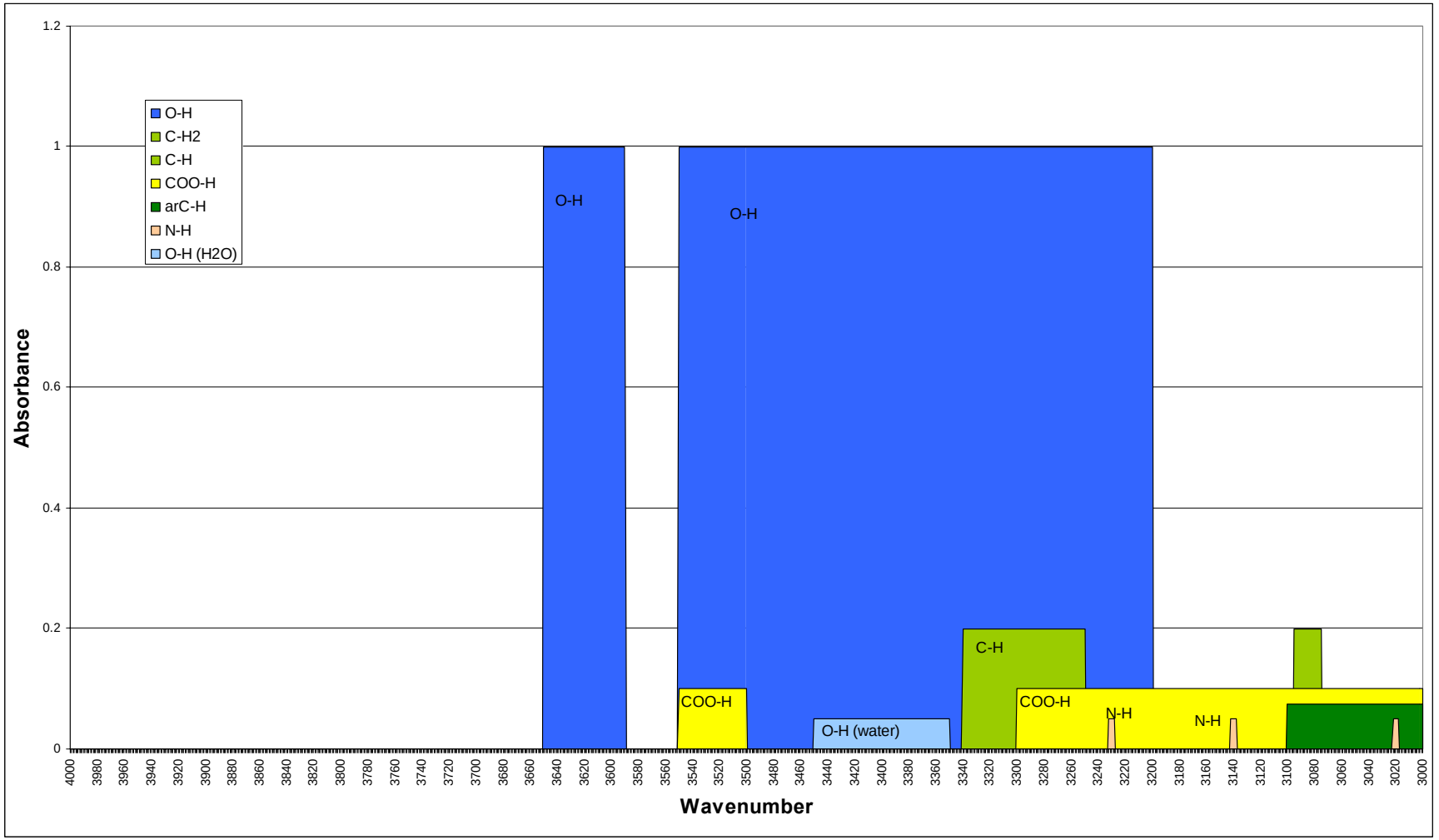

Wavenumber range: 3000-2000 cm^{-1}

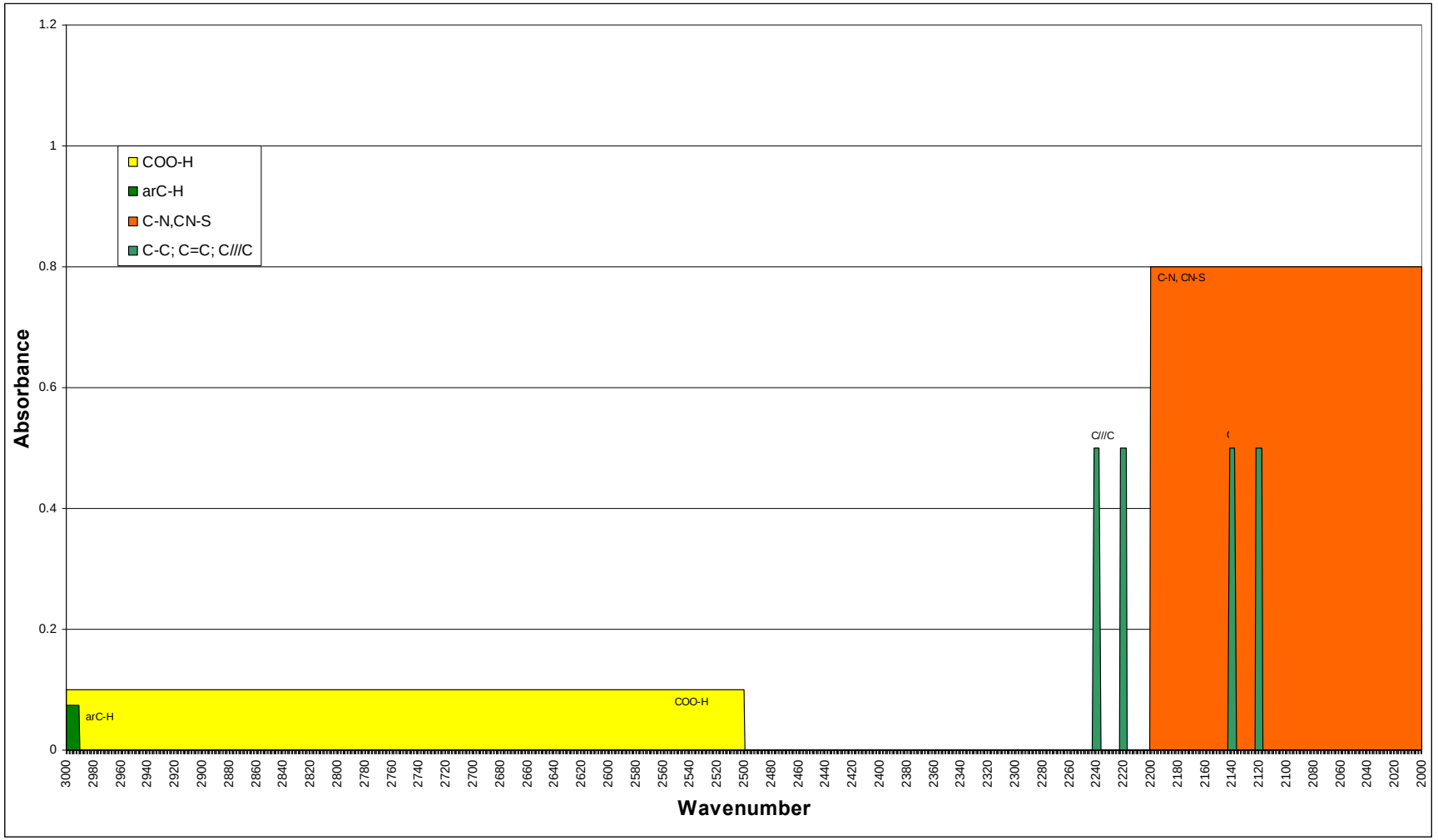

Wavenumber range: 2000-1000 cm^{-1}

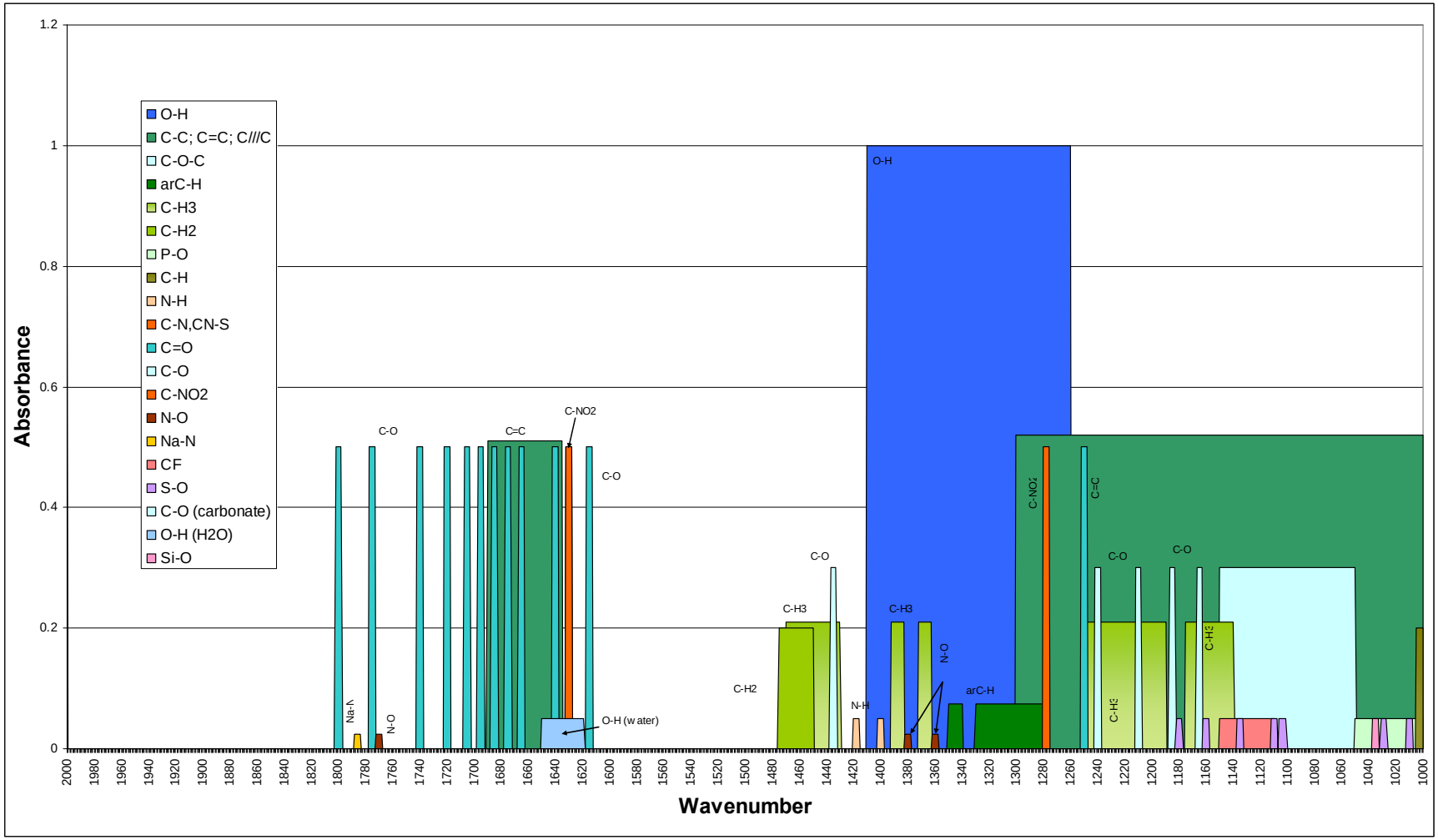

Wavenumber range: 1000-400 cm^{-1}

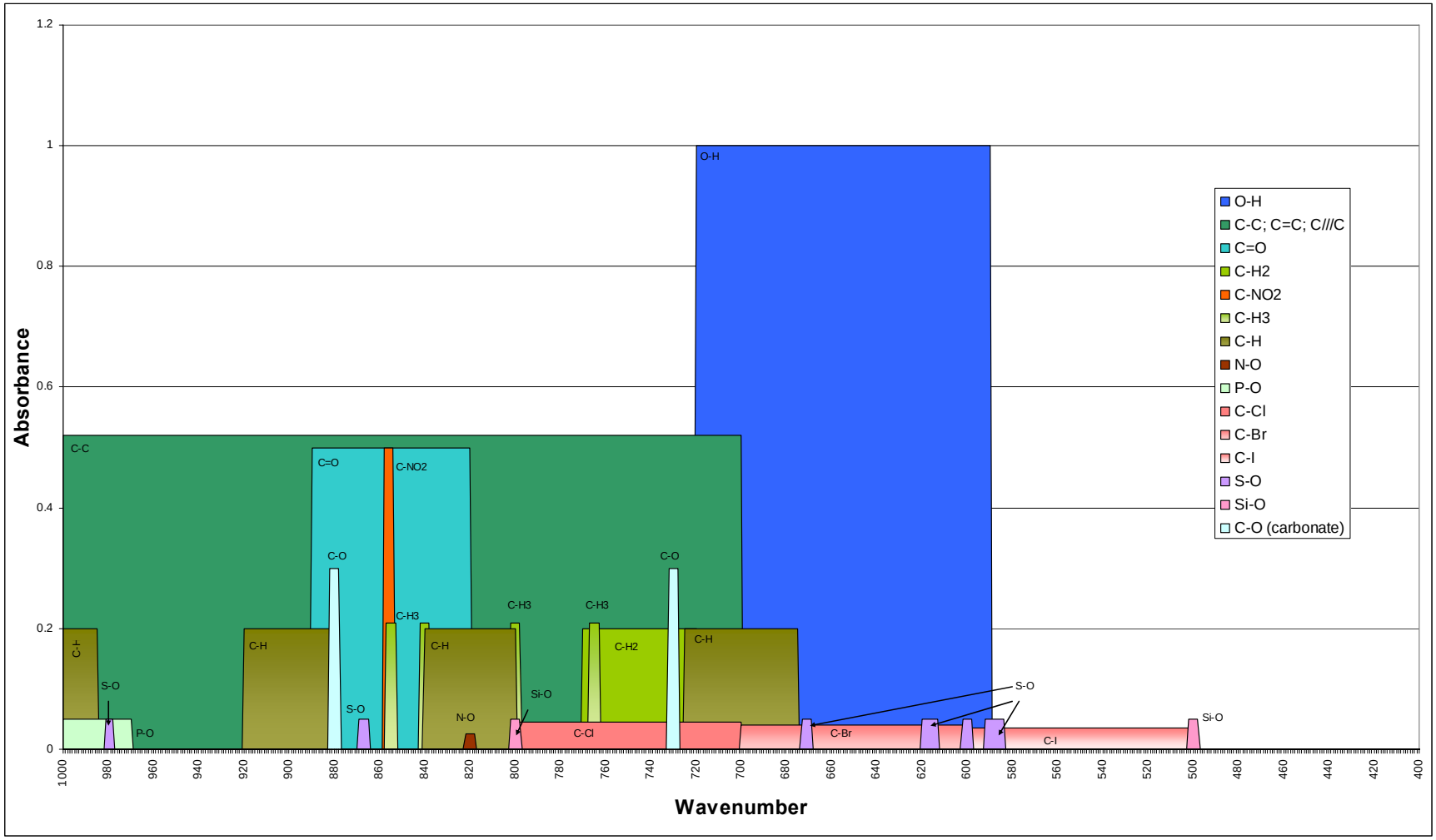

BIBLIOGRAPHY

CHAPTER 1

Allen, D., Palen, E., Haimov, M., Hering, S. and Young, J. (1994). Fourier Transform Infrared Spectroscopy of aerosol collected in a Low Pressure Impactor (LPI/FTIR): Method development and field calibration. Aerosol Science and Technology 21, 325-342.

Bolleter, W., Bushman, C., Tidwell, P. (1961). Spectrophotometric determination of ammonia as indophenol. Analytical Chemistry 33, 592-594.

Boudel, R., Fox, D., Turner, B. and Stern, A., 1994. Fundamentals of air pollution. Academic Press, 22-34.

Cahill, T. and Surovik, I. (1990). Visibility and Aerosols During the 1986 Carbonaceous Species Methods Comparison Study. Aerosol Science and Technology, 12(1): 149-160.

CAMNET, 2008. Real Time Air Pollution and Visibility Monitoring. http://www.hazecam.net/newark/gallery.htm

CCOHS, March 22 1999. How do particles enter the respiratory system? Canadian Center for Occupational Health and Safety. http://gala.ccohs.ca/oshanswers/chemicals/how_do.html

Dalluge, J., VanStee, L., Xu, X., Williams, J., Beens, J., Vreuls, R., Brinkman, U. (2002). Unraveling the composition of very complex samples by comprehensive gas chromatography coupled to time-of-flight mass spectrometry: Cigarette smoke. Journal of Chromatography A (974), 169-184.

Dekermenjian, M., Allen, D., Atkinson, R. and Arey, J. (1999). FTIR analysis of aerosol formed in the ozone oxidation of sesquiterpenes. Aerosol Science and Technology 30, 349-363.

Demerjian, K. (2004). EPA PM Supersite Final Report: $PM_{2.5}$ technology assessment and characterization study in New York state (PMTACS-NY).

Dzubay, T. and Stevens, R. (1975). Ambient Air Analysis with Dichotomus Sampler and X-Ray Fluorescence Spectrometer. Environmental Science and Technology 9, 663-667.

EPA. Particulate Matter ($PM_{2.5}$) Speciation Guidance Final Draft. October 7th, 1999.

EPA June 8th 2007. What is acid rain? www.epa.gov/acidrain/what/index.html

EPA March 6th 2008. Health and Environmental effects of Particulate Matter. http://www.epa.gov/ttn/oarpg/naaqsfin/pmhealth.html

EPA April 4th 2008. Module 3: Characteristcs of Particles-Particle size categories. www.epa.gov/air/oaqps/eog/bces/module3/category/category.htm

EPA, May 9th 2008. PM Standards. EPA. www.epa.gov/air/particlepollution/standards.html

EPA, June 19th, 2008. New York Designation Map. www.epa.gov/pmdesignations/1997standards/final/statemaps/New_York.htm

EPA, December 23 2009. NCore Networks and Site Information. http://www.epa.gov/ttn/amtic/ncore/networks.html

EPA, January 29th 2010. Air Pollution Control Orientation Course. http://www.epa.gov/apti/course422/ap7a.html

Gordon, R.J., Trivedi, N.J., Singh, B.P., Ellis, E.C. (1988). Characterization of aerosol organics by diffuse reflectance FTIR. Environmental Science and Technology 22, 672-677.

Hansen, A., Rosen, H., Novakov, T. (1984). The Aethalometer an instrument for the real-time measurement of optical absorption by aerosol particles. The Science of the Total Environment 36, 191-196.

Hildemann, L., Markowski, G., Cass, G. (1991). Chemical composition of emissions from urban sources of fine organic aerosol. Environmental Science and Technology 25, 744-759.

Holes, A., Eusebi, A., Grosjean, D. and Allen, D. (1997). FTIR analysis of aerosol formed in the photo-oxidation of 1,3,5-Trimethylbenzene. Aerosol Science and Technology 26, 516-526.

Kellner, R. (1978). Identification and determination of particulate compounds: infrared spectroscopy, extraction and chromatography. Analysis of Airborne Particles by Physical Methods (edited by Malissa H and Robinson JW). CRC Press, Boca Raton FL.

Krost, K. and McClenny, W. (1994). FTIR transmission spectroscopy for quantitation of ammonium bisulfate in fine particulate matter collected on Teflon filters. Applied Spectroscopy 48 (6), 702-705.

Lall, R., Kendall, M., Ito, K. and Thurston, G., 2004. Estimation of historical annual $PM_{2.5}$ exposures for health effects assessment. Atmospheric Environment 38, 5217-5226.

Lundanes, E., Greibrokk, T. (1985). Group separation of oil residues by supercritical fluid chromatography. Journal of Chromatography 349, 439-446.

Mansoori, B., Johnston, M., Wexler, A. (1996). Matrix assisted laser desorption/ionization (MALDI) size- and composition – selected aerosol particles. Analytical Chemistry 68, 3595-3601.

Mazurek, M., Simoneit, B., Cass, G., Gray, A. (1987). Quantitative high-resolution gas chromatography and high-resolution gas chromatography/mass spectrometry analyses of carbonaceous fine aerosol particles. International Journal of Environmental Analytical Chemistry 29, 119-139.

NYS Department of Environmental Conservation, 2008. Annual monitoring network plan: New York State ambient air monitoring program.

Paatero, P., 1997. Least squares formulation of robust non-negative factor analysis. Chemometrics and Intelligent Laboratory Systems 37, 23-35.

Palen, J., Allen, D., Pandis, S., Paulson, S., Seinfeld, J. and Flagan, R. (1992). Fourier Transform Infrared analysis of aerosol formed in the photo-oxidation of Isoprene and β-Pinene. Atmospheric Environment 26A (7), 1239-1251.

Schwab, J., Felton, H.D. and Demerjian, K., 2004. Aerosol chemical composition in New York State from integrated filter samples: urban/rural and seasonal contrasts. Journal of Geophysical Research 109, D16SO5 DOI: 1029/2003JDOO4078.

Seinfeld, J. and Pandis, S., 1998. Atmospheric Chemistry and Physics: From air pollution to climate change. US: John Wiley and Sons.

Solomon, P and Allen, D., 2004. Special Issue of Aerosol Science and Technology on findings from the fine particulate matter Supersites Programs. Aerosol Science and Technology 38 (S1), 1-4.

Stolzenburg, M. and Hering, S. (2000). Method for the automated measurement of fine particle nitrate in the atmosphere. Environmental Science and Technology 34, 907-914.

Thermo Nicolet, (2001). Introduction to Fourier transform infrared spectrometry. Thermo Nicolet Corporation. < http://mmrc.caltech.edu/FTIR/FTIRintro.pdf>

Wittig, A.E. and Allen, D., 2008. Improvement of the Chemical mass balance model for apportioning –sources of non-methane hydrocarbons using composite aged source profiles. Atmospheric Environment 42, 1319-1337.

CHAPTER 2

Blando, J., Procja, R. and Turpin, B., 2001. Issues in the quantitation of functional groups by FTIR spectroscopic analysis of impactor-collected aerosol samples. Aerosol Science and Technology 35, 899-908.

Carlton, A., Turpin, B., Johnson, W., Buckley, B., Simcik, M., Eisenreich, S. and Porcja, R., 1999. Microanalysis methods for characterization of personal aerosol exposures. Aerosol Science and Technology 31, 66-80.

Dekermenjian, M., Allen, D., Atkinson, R. and Arey, J., 1999. FTIR analysis of aerosol formed in the ozone oxidation of sesquiterpenes. Aerosol Science and Technology 30, 349-363.

Holes, A., Eusebi, A., Grosjean, D. and Allen, D., 1997. FTIR analysis of aerosol formed in the photooxidation of 1,3,5-Trimethylbenzene. Aerosol Science and Technology 26, 516-526.

Palen, E., Allen, D., Pandis, S., Paulson, S., Seinfeld, J. and Flagan, R., 1993. Fourier transform infrared analysis of aerosol formed in the photooxidation of 1-Octene. Atmospheric Environment 27A (9), 1471-1477.

CHAPTER 3

Allen, D. and Palen, E., 1989. Recent advances in aerosol analysis by infrared spectroscopy. Journal of Aerosol Science 20 (4), 441-455.

Cabada, J., Pandis, S., Subramanian, R., Robinson, A., Polidori, A. and Turpin, B., 2004a. Estimating the secondary organic aerosol contribution to $PM_{2.5}$ using the EC tracer method. Aerosol Science and Technology 38 (S1), 140-155.

Cabada, J., Rees, S., Takahama, S., Khlystov, A., Pandis, S., Davidson, C. and Robinson, A., 2004b. Mass size distribution and size resolved chemical composition of fine particulate matter at the Pittsburgh supersite. Atmospheric Environment 38, 3127-3141.

Carlton, A., Turpin, B., Johnson, W., Buckley, B., Simcik, M., Eisenreich, S. and Porcja, R., 1999. Microanalysis methods for characterization of personal aerosol exposures. Aerosol Science and Technology 31, 66-80.

EPA, January 17, 2006. 40 CFR Part 50: National Ambient Air Quality Standards for Particulate Matter; Propose Rule.

Gordon, R., Trivedi, N. and Singh, B., 1988. Characterization of aerosol organics by diffuse reflectance Fourier transform infrared spectroscopy. Environmental Science and Technology 22, 672- 677.

Krost, K. and McClenny, W., 1994. FTIR transmission spectroscopy for quantitation of ammonium bisulfate in fine-particulate matter collected on Teflon filters. Applied Spectroscopy 48 (6), 702-705.

Maria, S., Russel, L., Turpin, B. and Porcja, R., 2002. FTIR measurements of functional groups and organic mass in aerosol samples over the Caribbean. Atmospheric Environment 36, 5185-5196.

Reff, A., Turpin, B., Porcja, R., Giovennetti, R., Cui, W., Weisel, C., Zhang, J., Kwon, J., Alimokhtari, S., Morandi, M., Stock, T., Maberti, S., Colome, S., Winer, A., Shendell, D., Jones, J. and Farrar, C., 2005. Functional group characterization of indoor, outdoor, and personal $PM_{2.5}$: results from RIOPA. Indoor Air 15, 53-61.

Solomon, P., 2004. Special issue of Atmospheric Environment on findings from EPA's particulate matter Supersites Program. Atmospheric Environment 38, 3101-3106.

Subramanian, R., Khlystov, A., Cabada, J. and Robinson, A., 2004. Evaluation of Measurement Methods: Positive and negative artifacts in particulate organic carbon measurements with denuded and undenuded sampler configurations. Aerosol Science and Technology 38 (S1), 27-48.

Takahama, S., Wittig, B., Vayenas, D., Davidson, C. and Pandis, S., 2004. Modeling the diurnal variation of nitrate during the Pittsburgh air quality study. Journal of Geophysical Research 109, D16S06, doi: 10.1029/2003JD004149.

Turpin, B., Saxena, P. and Andrews, E., 2000. Measuring and simulating particulate organics in the atmosphere: problems and prospects. Atmospheric Environment 34, 2983-3013.

Wittig, B., Takahama, S., Khlystov, A., Pandis, S., Hering, S., Kirby, B. and Davidson, C., 2004. Semi-continuous $PM_{2.5}$ inorganic composition measurements during the Pittsburgh air quality study.

CHAPTER 4

Allen, D. and Palen, E., 1989. Recent advances in aerosol analysis by infrared spectroscopy. Journal of Aerosol Science 20 (4), 441-455.

Allen, D., Palen, E., Haimov, M., Hering, S. and Young, J., 1994. Fourier transform infrared spectroscopy of aerosol collected in a low pressure impactor (LPI/FTIR): Method development and field calibration. Aerosol Science and Technology 21, 325-342.

Blando, J., Procja, R. and Turpin, B., 2001. Issues in the quantitation of functional groups by FTIR spectroscopic analysis of impactor-collected aerosol samples. Aerosol Science and Technology 35, 899-908.

Carlton, A., Turpin, B., Johnson, W., Buckley, B., Simcik, M., Eisenreich, S. and Porcja, R., 1999. Microanalysis methods for characterization of personal aerosol exposures. Aerosol Science and Technology 31, 66-80.

EPA, February 3, 1995. Protocol for the use of Fourier transform infrared (FTIR) spectrometry for the analysis of gaseous emissions from stationary sources.

Farinas, K., Doh, L., Venkatraman, S. and Potts, R., 1994. Characterization of solute diffusion in a polymer using ATR-FTIR spectroscopy and bulk transport techniques.

Krost, K. and McClenny, W., 1994. FTIR transmission spectroscopy for quantitation of ammonium bisulfate in fine-particulate matter collected on Teflon filters. Applied Spectroscopy 48 (6), 702-705.

Reff, A., Turpin, B., Porcja, R., Giovennetti, R., Cui, W., Weisel, C., Zhang, J., Kwon, J., Alimokhtari, S., Morandi, M., Stock, T., Maberti, S., Colome, S., Winer, A., Shendell, D., Jones, J. and Farrar, C., 2005. Functional group characterization of indoor, outdoor, and personal $PM_{2.5}$: results from RIOPA. Indoor Air 15, 53-61.

Signorell, R., Kunzmann, M. and Suhm, M., 2000. FTIR investigation of non-volatile molecular nanoparticles. Chemical Physics Letters 329, 52-60.

Smith, B., 1996. Fundamentals of Fourier transform infrared spectroscopy. CRC Press, Inc. 1996 Corporate Blvd., N.W., Boca Raton, Florida.

CHAPTER 5

Allen, D., Palen, E., Haimov, M., Hering, S. and Young, J., 1994. Fourier transform infrared spectroscopy of aerosol collected in a low pressure impactor (LPI/FTIR): Method development and field calibration. Aerosol Science and Technology 21, 325-342.

Blando, J., Procja, R. and Turpin, B., 2001. Issues in the quantitation of functional groups by FTIR spectroscopic analysis of impactor-collected aerosol samples. Aerosol Science and Technology 35, 899-908.

Carlton, A., Turpin, B., Johnson, W., Buckley, B., Simcik, M., Eisenreich, S. and Porcja, R., 1999. Microanalysis methods for characterization of personal aerosol exposures. Aerosol Science and Technology 31, 66-80.

Coates, J., 2000. Interpretation of infrared spectra, a practical approach. Encyclopedia of Analysis Chemistry (Meyers, R., ed.), 10815- 10837. John Wiley & Sons Ltd, Chichester.

Dekermenjian, M., Allen, D., Atkinson, R. and Arey, J., 1999. FTIR analysis of aerosol formed in the ozone oxidation of sesquiterpenes. Aerosol Science and Technology 30, 349-363.

Dekermenjian, M., Allen, D., Atkinson, R. and Arey, J., 1999(a). FTIR analysis of aerosol formed in the photooxidation of napthtalene. Aerosol Science and Technology 30, 273-279.

Schwarzenbach, R., Gschwend, P., Imboden, D., 2003. Environmental Organic Chemistry, Second Edition. John Willey and Sons Inc., Hoboken, New Jersey.

Harris, D. and Bertolucci, M. (1978). Symmetry and Spectroscopy: An Introduction to Vibrational and Electronic Spectroscopy. Dover Publications, INC., New York.

Holes, A., Eusebi, A., Grosjean, D. and Allen, D., 1997. FTIR analysis of aerosol formed in the photooxidation of 1,3,5-Trimethylbenzene. Aerosol Science and Technology 26, 516-526.

Kellner, R. (1978). Identification and determination of particulate compounds: infrared spectroscopy, extraction and chromatography. Analysis of Airborne Particles by Physical Methods (edited by Malissa H and Robinson JW). CRC Press, Boca Raton FL.

Palen, E., Allen, D., Pandis, S., Paulson, S., Seinfeld, J. and Flagan, R., 1992. Fourier transform infrared analysis of aerosol formed in the photooxidation of Isoprene and β-Pinene. Atmospheric Environment 26A (7), 1239-1251.

Palen, E., Allen, D., Pandis, S., Paulson, S., Seinfeld, J. and Flagan, R., 1993. Fourier transform infrared analysis of aerosol formed in the photooxidation of 1-Octene. Atmospheric Environment 27A (9), 1471-1477.

Reff, A., Turpin, B., Porcja, R., Giovennetti, R., Cui, W., Weisel, C., Zhang, J., Kwon, J., Alimokhtari, S., Morandi, M., Stock, T., Maberti, S., Colome, S., Winer, A., Shendell, D., Jones, J. and Farrar, C., 2005. Functional group characterization of indoor, outdoor, and personal $PM_{2.5}$: results from RIOPA. Indoor Air 15, 53-61.